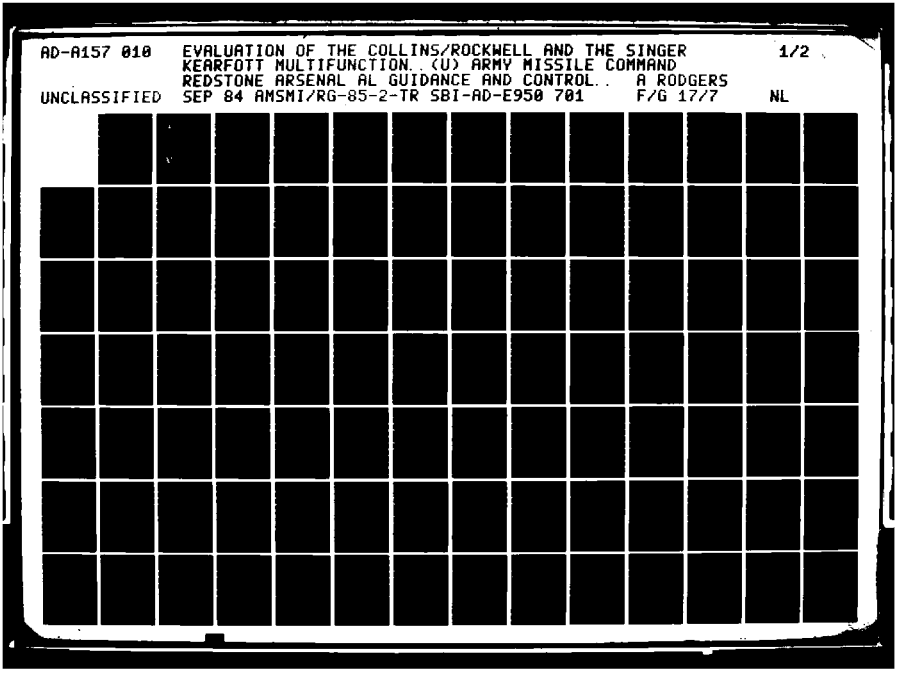
AD-A157 010 EVALUATION OF THE COLLINS/ROCKWELL AND THE SINGER KEARFOTT MULTIFUNCTION..(U) ARMY MISSILE COMMAND REDSTONE ARSENAL AL GUIDANCE AND CONTROL.. A RODGERS
1/2
UNCLASSIFIED SEP 84 AMSMI/RG-85-2-TR SBI-AD-E950 701 F/G 17/7 NL

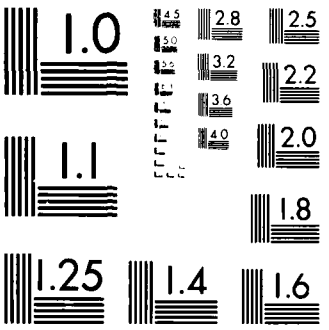

(2)

AD-A157 010

TECHNICAL REPORT RG-85-2

EVALUATION OF THE COLLINS/ROCKWELL AND THE SINGER KEARFOTT MULTIFUNCTION SENSORS (PHASE II)

Aubrey Rodgers
Guidance and Control Directorate
U. S. Army Missile Laboratory

SEPTEMBER 1984

U.S. ARMY MISSILE COMMAND
Redstone Arsenal, Alabama 35898-5000

Approved for public release; distribution is unlimited.

DISPOSITION INSTRUCTIONS

DESTROY THIS REPORT WHEN IT IS NO LONGER NEEDED. DO NOT RETURN IT TO THE ORIGINATOR.

DISCLAIMER

THE FINDINGS IN THIS REPORT ARE NOT TO BE CONSTRUED AS AN OFFICIAL DEPARTMENT OF THE ARMY POSITION UNLESS SO DESIGNATED BY OTHER AUTHORIZED DOCUMENTS.

TRADE NAMES

USE OF TRADE NAMES OR MANUFACTURERS IN THIS REPORT DOES NOT CONSTITUTE AN OFFICIAL INDORSEMENT OR APPROVAL OF THE USE OF SUCH COMMERCIAL HARDWARE OR SOFTWARE.

SECURITY CLASSIFICATION OF THIS PAGE (When Data Entered)

REPORT DOCUMENTATION PAGE

READ INSTRUCTIONS BEFORE COMPLETING FORM

1. REPORT NUMBER: RG-85-2	2. GOVT ACCESSION NO.: AD-A154 [illegible]
3. RECIPIENT'S CATALOG NUMBER:	
4. TITLE (and Subtitle): Evaluation of the Collins/Rockwell and the Singer Kearfott Multifunction Sensors (Phase II)	5. TYPE OF REPORT & PERIOD COVERED: Technical Report
	6. PERFORMING ORG. REPORT NUMBER:
7. AUTHOR(s): Aubrey Rodgers	8. CONTRACT OR GRANT NUMBER(s):
9. PERFORMING ORGANIZATION NAME AND ADDRESS: U. S. Army Missile Command, ATTN: AMSMI-RG, Redstone Arsenal, AL 35898-5254	10. PROGRAM ELEMENT, PROJECT, TASK AREA & WORK UNIT NUMBERS:
11. CONTROLLING OFFICE NAME AND ADDRESS: U. S. Army Missile Command, ATTN: AMSMI-RG, Redstone Arsenal, AL 35898-5254	12. REPORT DATE: September 1984 13. NUMBER OF PAGES: 172
14. MONITORING AGENCY NAME & ADDRESS (if different from Controlling Office):	15. SECURITY CLASS. (of this report): Unclassified 15a. DECLASSIFICATION/DOWNGRADING SCHEDULE:

16. DISTRIBUTION STATEMENT (of this Report)

Approved for public release; distribution is unlimited.

17. DISTRIBUTION STATEMENT (of the abstract entered in Block 20, if different from Report)

18. SUPPLEMENTARY NOTES

19. KEY WORDS (Continue on reverse side if necessary and identify by block number)

Multifunction sensors	Forcing function
Piezoelectric ceramic material	Suppressed carrier modulated signal
Angular Rate	Pulse generators
Linear Acceleration	Delta angle pulse
	Delta velocity pulse

20. ABSTRACT (Continue on reverse side if necessary and identify by block number)

The objective of this evaluation is to determine empirically the repeatable, non-repeatable and thermal error coefficients of the Collins/Rockwell and Singer Kearfott Multifunction gyro/accelerometer inertial reference units. The ultimate goal is to utilize these coefficients in error modeling algorithms in the effort of developing technology for cost efficient inertial sensors. The results of the evaluation support the postulate that the multifunction gyro/accelerometer concept, using appropriate error modeling coefficients is a technically sound method of improving performance characteristics and developing

DD FORM 1 JAN 73 1473 EDITION OF 1 NOV 65 IS OBSOLETE

SECURITY CLASSIFICATION OF THIS PAGE (When Data Entered)

cost efficient instruments.

ACKNOWLEDGEMENTS

Appreciation is expressed to Chris Roberts and Troy Hester for their profound help in data documentation and computer work.

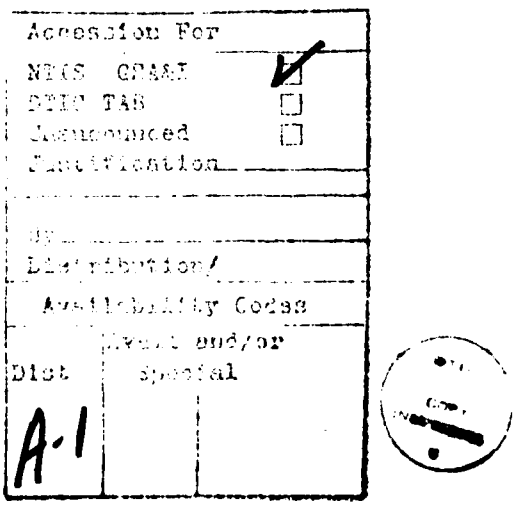

CONTENTS

LIST OF FIGURES

LIST OF FIGURES (Cont'd)

LIST OF TABLES

I. INTRODUCTION

Considerable progress has been made over the past several years in the development of a new strapdown three orthogonal axes (x, y, z) reference system. In the new technology, two multifunction sensors are used to obtain the required inertial measurement, each sensor providing two axes of angular rate and two axes of linear acceleration. The sensitive axes are arranged to utilize the redundant fourth axis information for system monitoring.

The multifunction sensor is designed for long life, mechanical simplicity, improved performance and improved reliability. In addition to these design features, the instrument offers significant advancements in weight, volume and cost reduction when compared with the array of conventional gyros and accelerometers which it replaces. The multifunction sensor design also eliminates all gimbal, gimbal bearings, requires no caging mechanism, no pivots and only two friction-sensitive components (spin bearings and sliprings). The instrument yields measurements equivalent to the output of four conventional single channel instruments. As a result, its complexity and initial maintenance costs are reduced to those of a single channel transducer. The efficiency of combined rate and acceleration sensing and the inherent simplicity of the design make the multifunction concept especially attractive for low cost guidance systems.

II. DESCRIPTION OF THE MULTIFUNCTION GYRO/ACCELEROMETER

The angular rate/linear acceleration sensor consists of a lightweight rotating structure which carries a number of piezoelectric transducers and electronic circuitry for signal conditioning and for coupling the transducer signals to the fixed frame. The spin bearing and sliprings for the rotating assembly are the only moving parts.

The transducer consists of layers of piezoelectric ceramic material. Piezoelectric ceramics are termed ferroelectric materials because they exhibit electric behavior physically analogous with the magnetic behavior of ferromagnetic material. Crystals of the material are nonsymmetric and have a built-in electric dipole. The ceramic consists of a mass of minute crystallities which are randomly oriented. After firing, the ceramic body is isotropic and exhibits no net piezoelectric effect because of the random orientation of the domain structures. The material is made piezoelectric by polarizing some of the domain structures at high temperature in a high electric field, analogous to polarizing a magnet. Once polarized, stress applied to the material causes a variation of the dipole moments and generates a voltage on the electrodes. The ceramic is permanently piezoelectric and can convert mechanical energy to electrical energy, and vice versa.

For illustration, when the cantilever-mounted transducer in Figure 1 is oriented horizontally, gravity (g) acting on the mass of the cantilever causes stress in the material and generates a voltage. If the unit is rotated 180°, the voltage polarity is reversed. For continuous rotation, the output voltage is a sine wave at the rotation frequency. The magnitude of the voltage is proportional to the ambient acceleration.

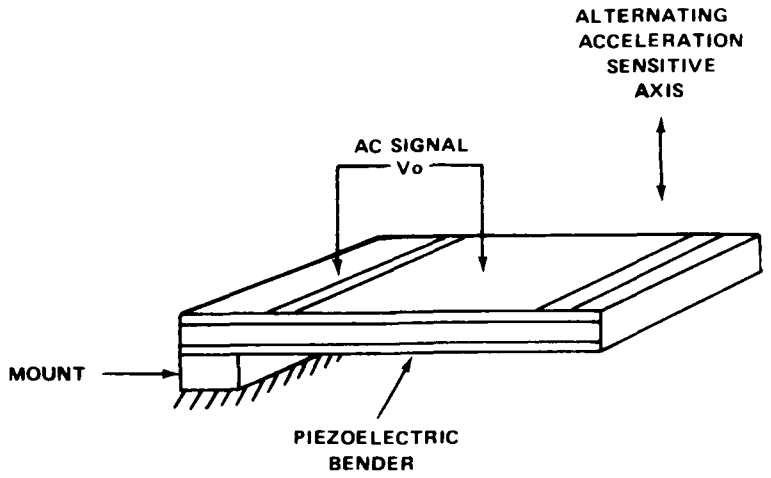

Figure 1. Typical functional configuration of piezoelectric ceramic accelerometer.

The multifunction gyro/accelerometer consists of two sets of transducers mounted on a common spin motor shaft (see Figure 2). The tranducers are constructed and mounted so that one set generates a voltage proportional to angular rate and the other to linear acceleration.

The operation of the angular rate transducer is based on the gyroscopic theory of an elastically restrained body which rotates about its spin axis at nominally 200 Hz. The cantilevered transducers are arranged in a 180 degree configuration for common mode rejection and signal enhancement. These transducers act both as the inetial members and the restoring spring. When an angular rate is applied in a plane orthogonal to the spin axis, the angular momentum of the rotating transducers generates a forcing function which is suppressed carrier modulated at the spin frequency. The amplitude of the output sinusoidal signal is proportional to the input rate magnitude and the phasing is such that maximum signal occurs when the sensing element is colinear with the input vector. The minimum signal occurs a quarter rotation away.

The acceleration sensor assembly consists of identical cantilevered transducers as shown for the rate gyro sensor assembly. The orientation of the acceleration sensitive axis is turned 90^{o} with respect to the gyro sensing elements so that its flexing axes are colinear with the spin axis. In this orientation, the transducers will react to linear acceleration in the plane perpendicular to the spin axis. The rotating transducers generate a suppressed-carrier-modulated spin frequency signal with amplitude proportional to the input acceleration magnitude. The amplitude is maximum when the beams sense the full force due to the acceleration and is minimum a quarter rotation away.

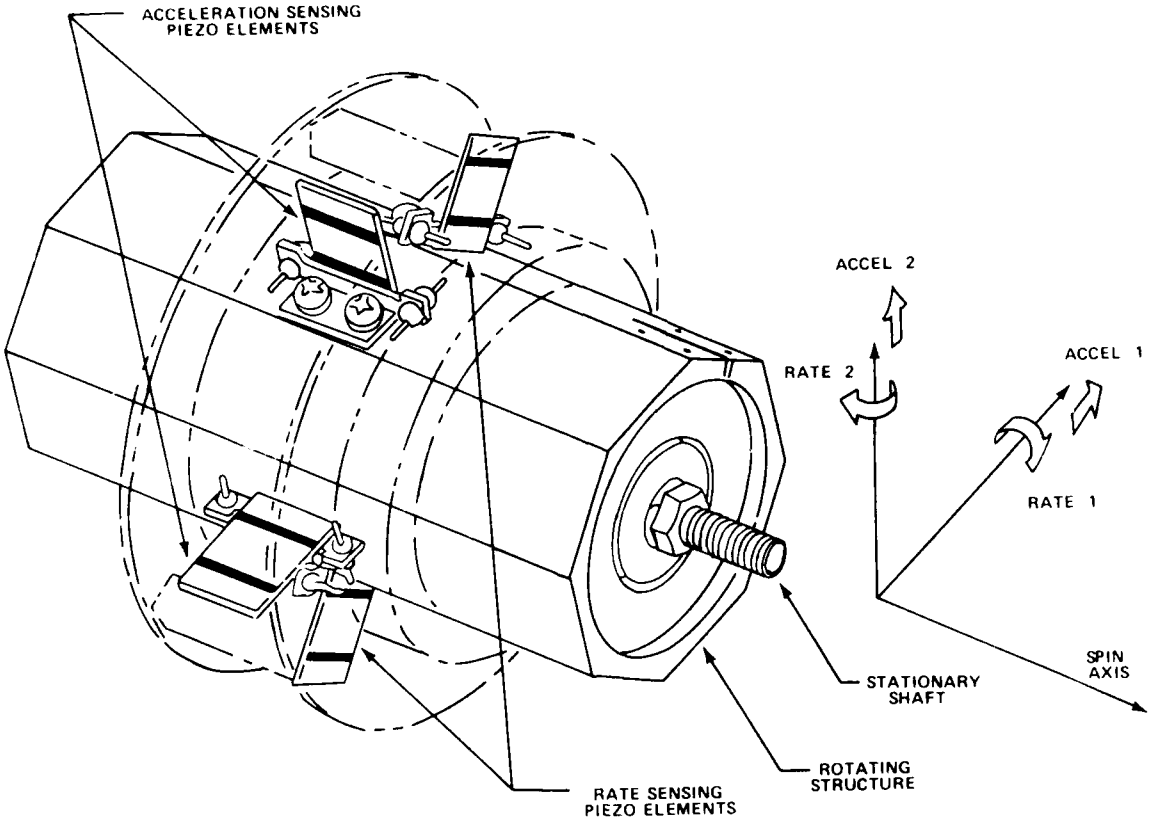

Figure 2. Combination angular rotation and linear acceleration sensor functional diagram.

Figure 3 is a signal flow block diagram of the multifunction gyro-accelerometer instrument. The angular rate/linear acceleration transducer circuits are time and synchronized from a stable clock. A hysteresis synchronous motor is driven by an inverter operating from a dc voltage. An inverter is used to transmit power to the wheel assembly through a transformer to drive the on-board circuits.

Signals from the angular rate and linear acceleration transducers (pickoffs) are routed down through the motor shaft to the slipring-brush block assembly and out to instrument mounted buffer pre-amplifiers. The buffers act as both an impedance matcher and a gain stage. The signals from the insrument mounted buffer amplifiers are summed appropriately to cancel undesired acceleration components. The signal voltages are sine waves at the spin frequency. The amplitude and phase of the sine waves define the respective rate vector or acceleration vector. These vectors are resolved into sine/cosine components by the demodulators. The demodulator circuits are digitally timed from an internal clocking circuit synchronized to the wheel. The precision timing establishes the orthogonality of the demodulated outputs and determines the alignment of the axes about the spin axis.

Table 15. Accelerometer Repeatability
(y Axis Down)(Cont'd)

Test No.	Accelerometer Axes (milli-g's)							
	AA_1		AB_1		AA_2		AB_2	
	μ	σ	μ	σ	μ	σ	μ	σ
Error Band	-128.5	1.59	-1119.6	5.68	-972.5	2.73	15.5	2.01
Turn-on	-151.9	0.82	-1110.4	5.18	-979.7	5.62	-42.6	2.67
y-Axis Up	-124.6	0.05	975.2	0.13	1030.2	0.10	35.6	0.29

Table 16. Accelerometer Repeatability
(z Axis Up)

Test No.	Accelerometer Axes (milli-g's)							
	AA_1		AB_1		AA_2		AB_2	
	μ	σ	μ	σ	μ	σ	μ	σ
1	-127.3	0.08	-77.9	0.07	20.9	0.08	1021.1	0.16
2	-128.3	0.11	-69.9	0.10	21.1	0.12	1022.8	0.16
3	-132.9	0.11	-67.1	0.07	20.3	0.11	1019.8	0.15
4	-129.2	0.09	-72.6	0.10	21.8	0.09	1023.3	0.21
5	-131.3	0.09	-68.1	0.11	19.7	0.09	1019.6	0.13
6	-127.6	0.07	-76.6	0.11	22.2	0.11	1022.1	0.12
Error Band	-129.4	2.25	-72.0	4.48	21.0	0.94	1021.5	1.50
Turn-on	-152.3	6.04	-75.2	5.12	15.9	2.81	972.7	10.46
z-Axis Down	-125.5	0.09	-70.1	0.12	37.7	0.17	-969.9	0.40

Table 14. Accelerometer Repeatability
(x Axis Down)

Test No.	Accelerometer Axes (milli-g's)							
	AA_1		AB_1		AA_2		AB_2	
	μ	σ	μ	σ	μ	σ	μ	σ
1	-1176.6	0.10	-80.2	0.08	29.4	0.11	-26.5	0.18
2	-1178.5	0.10	-71.8	0.12	30.4	0.09	-29.3	0.19
3	-1182.6	0.12	-71.5	0.13	28.7	0.08	-23.9	0.18
4	-1178.6	0.13	-73.3	0.09	31.1	0.09	-30.4	0.19
5	-1186.0	0.15	-69.1	0.09	29.9	0.09	-25.0	0.23
6	-1181.6	0.11	-71.0	0.08	32.6	0.06	-33.0	0.13
Error Band	-1180.6	3.43	-72.8	3.88	30.4	1.38	-28.0	3.48
Turn-on	-1198.6	4.46	-77.0	3.66	21.7	1.38	-33.8	2.83
x-Axis Up	920.6	0.08	-68.4	0.10	25.0	0.09	22.6	0.16

Table 15. Accelerometer Repeatability
(y Axis Down)

Test No.	Accelerometer Axes (milli-g's)							
	AA_1		AB_1		AA_2		AB_2	
	μ	σ	μ	σ	μ	σ	μ	σ
1	-125.6	0.09	-1111.9	0.12	-977.3	0.19	12.9	0.22
2	-128.1	0.09	-1122.3	0.12	-972.5	0.12	17.4	0.16
3	-128.9	0.06	-1122.9	0.12	-969.7	0.14	18.2	0.17
4	-130.0	0.06	-1122.9	0.14	-970.2	0.16	14.7	0.22
5	-129.7	0.08	-1124.7	0.10	-973.2	0.16	14.2	0.20
6	-128.9	0.15	-1112.8	0.16	-972.1	0.15	15.8	0.27

Table 12. Gyro Repeatability (y Axis Down) (Cont'd)

Test No.	Gyro Axes (degree/hr)							
	RA_1		RB_1		RA_2		RB_2	
	μ	σ	μ	σ	μ	σ	μ	σ
Error Band	1385.6	8.8	4194.6	10.5	1831.2	9.3	2754.2	49.3
Turn-on	1392.1	14.4	4183.1	55.8	1788.4	29.3	2793.8	41.2
y-Axis Up	-1704.1	2.7	-4553.1	6.7	-1177.4	2.3	2227.4	2.9

Table 13. Gyro Repeatability (z Axis Up)

Test No.	Gyro Axes (degree/hr)							
	RA_1		RB_1		RA_2		RB_2	
	μ	σ	μ	σ	μ	σ	μ	σ
1	-144.5	2.4	-185.4	2.1	585.6	2.1	951.3	3.6
2	-156.3	2.7	-177.2	3.6	569.9	3.1	961.8	3.2
3	-143.7	2.4	-193.1	2.5	596.2	2.7	1030.5	3.1
4	-154.2	1.8	-185.8	2.5	573.0	1.9	932.4	3.2
5	-150.2	2.9	-194.4	4.0	581.8	3.2	940.5	3.7
6	-146.8	3.7	-192.1	7.4	607.4	5.7	1047.0	2.1
Error Band	-149.3	5.2	-188.0	6.5	585.7	14.2	977.3	48.9
Turn-on	- 95.6	15.0	-270.4	20.8	496.0	30.7	960.6	43.7
z-Axis Down	-199.1	2.9	-168.1	11.2	54.4	2.8	3996.0	4.9

Table 11. Gyro Repeatability (x Axis Down)

Test No.	Gyro Axes (degree/hr)							
	RA_1		RB_1		RA_2		RB_2	
	μ	σ	μ	σ	μ	σ	μ	σ
1	4239.3	1.5	-1721.5	3.7	326.5	3.2	2492.9	2.3
2	4207.3	3.0	-1708.8	4.7	321.3	2.8	2470.8	2.8
3	4226.3	3.2	-1713.3	4.7	333.7	3.1	2518.8	2.6
4	4213.0	2.6	-1732.5	12.1	320.3	2.3	2413.0	2.5
5	4248.0	6.7	-1708.2	25.9	313.7	2.8	2410.5	2.8
6	4213.6	9.6	-1769.5	61.2	314.4	1.7	2434.6	2.4
Error Band	4224.6	16.3	-1706.4	27.2	321.6	7.6	2456.8	44.5
Turn-on	4355.9	25.7	-1769.5	15.0	194.3	9.0	2502.8	54.3
x-Axis Up	-4549.6	2.6	1376.3	3.9	329.4	2.8	2447.3	3.6

Table 12. Gyro Repeatability (y Axis Down)

Test No.	Gyro Axes (degree/hr)							
	RA_1		RB_1		RA_2		RB_2	
	μ	σ	μ	σ	μ	σ	μ	σ
1	1395.1	2.8	4212.6	4.5	1846.4	2.4	2705.3	2.9
2	1388.1	2.5	4194.5	2.5	1833.0	2.8	2816.6	3.0
3	1391.1	2.3	4190.7	2.9	1818.1	3.3	2710.3	3.2
4	1383.6	2.9	4180.1	2.5	1827.8	2.7	2809.8	2.4
5	1386.2	3.2	4193.3	4.1	1828.5	2.1	2758.5	3.7
6	1369.4	2.6	4196.2	2.0	1833.8	2.7	2725.1	3.0

The input axis misalignment error is expressed in milliradians. The error for each indicated accelerometer output axis is tabulated in Table 10.

Table 10. Accelerometer Axis Misalignment Error

αAA_1	-1.487 mrad
αAB_1	2.197 mrad
αAA_2	1.381 mrad
αAB_2	-1.193 mrad

E. Multifunction Gyro/Accelerometer Day-to-Day Repeatability - (Singer Kearfott)

The test setup and procedures described in paragraph B for the evaluation of the Rockwell Collins Phase II Unit were used to evaluate the Singer Kearfott Phase II Unit. The mean and the one sigma value of each gyro output are tabulated Tables 11, 12, and 13. Compare these results with Tables 1, 2, and 3.

The mean and the one sigma value for each accelerometer output are tabulated in Tables 14, 15, and 16. Compare these results with Tables 4, 5, and 6.

F. Gyro Static Drift Errors, G and Non-G - (Singer Kearfott)

Equivalent simultaneous equations, as shown in Table 7, were used to compute the g and non-g sensitive errors of the Phase II unit. The results are shown in Table 17. The results in Table 17 can be compared with the Rockwell Collins results shown in Table 8.

G. Accelerometer Static Evaluation (Bias and Axis Misalignment Errors)

The test setup and procedures described in paragraph D were used to evaluate the Singer Kearfott Phase II Unit. Equations (13) and (14) were used to compute the accelerometer bias and input misalignment errors. The results are tabulated in Tables 18 and 19. These results can be compared with the Collins results shown in Table 9 and 10.

After reviewing the data in Tables 11 through 17, Singer Kearfott decided to recall their Phase II unit in order to update it to a Phase III Inertial Measurement Unit.

D. Accelerometer Static Evaluation - Rockwell Collins

In evaluating accelerometer performance, it is necessary to investigate thoroughly certain basic requirements: (1) Accelerometers must possess a high degree of sensitivity and a minimum threshold value, even though they are required to operate under high acceleration inputs; (2) Accelerometers must transform these acceleration inputs into usable signals with a high degree of accuracy. To determine these basic performance characteristics, static testing is not only the most direct means of accelerometer evaluation but in this case it is the most practical approach.

In static testing, if an accelerometer had no internal forces acting upon it, its output would be exactly zero. Similarly, if the instrument was positioned in a one-g field, its output would indicate exactly one g. In the 180° one-g field, the accelerometer output would remain fixed in magnitude but would reverse in polarity. However, when internal forces are acting, the above relationships do not hold. These outputs may be broken down into the following components: (1) Bias, defined as an accelerometer output when no acceleration is applied and (2) Input axis misalignment, defined as the angular difference between an input axis and its associated input reference axis.

The multifunction accelerometer bias was determined by substituting the output measurements, made in the one-g fields, in the following equation:

$$\text{Bias} = \frac{(\text{positive 1-g}) + (\text{negative 1-g})}{2 \text{ scale factor}} \tag{13}$$

The unit of bias is expressed by an equivalent error in milli-g's. The bias for each accelerometer output axis is tabulated in Table 9.

Table 9. Accelerometer Bias

AA_1 Axis	2.863 mg
AB_1 Axis	-0.620 mg
AA_2 Axis	0.645 mg
AB_2 Axis	3.336 mg

The accelerometer input axis misalignment error was obtained by substituting the measured outputs at zero and one-g position in the following equation:

$$\alpha_{AA} = \tan^{-1} [(AA_0 - AAB) \div (AA_{90} - AAB)] \tag{14}$$

where AA_0 is the output at zero position,

AA_{90} is the output at one-g position and

AAB is the measured bias term.

Table 7. Simultaneous Equations

z-Axis Up	$RA_1 = + RA_1 (GSA) + R_{AAV} + W_v$	$RB_1 = - MU_{SA} + R_{AAV} - W_h$	(9)
z-Axis Down	$RA_1 = - RA_1 (GSA) + R_{AAV} - W_v$	$RB_1 = + MU_{SA} + R_{AAV} + W_h$	(10)
z-Axis Up	$RA_2 = + MU_B + R_{SAV} - W_h$	$RB_2 = - MU_A + R_{SAV} + W_O$	(11)
z-Axis Down	$RA_2 = - MU_B + R_{SAV} + W_h$	$RB_2 = + MU_A + R_{SAV} + W_O$	(12)

Terms Used:

GSA = On Axis g-sensitive drift.

MU = Mass unbalance along axis indicated (cross-axis g-sensitive drift).

R = Restraints (non-g sensitive) drift as determined from data in vertical position indicated.

W = Earth's rate component, horizontal, vertical, or east.

The computed g-sensitive and non-g sensitive drift rates for each indicated orientation of the gyros are tabulated in Table 8.

Table 8. G-Sensitive and Non G-Sensitive Errors

$RA_1 (R_{BAV})$	- 14.6°/hr	$RB_1 (R_{BAV})$	- 12.6°/hr
$RA_1 (R_{SAV})$	- 14.5°/hr	$RB_1 (R_{SAV})$	- 13.6°/hr
$RA_1 (R_{AAV})$	- 12.3°/hr	$RB_1 (R_{AAV})$	- 13.8°/hr
$RA_1 (MU_B)$	- 6.5°/hr/g	$RB_1 (MU_A)$	0.7°/hr/g
$RA_1 (MU_{SA})$	55.4°/hr/g	$RB_1 (MU_{SA})$	54.2°/hr/g
$RA_1 (GSA)$	- 38.5°/hr/g	$RB_1 (GSA)$	- 40.6°/hr/g
$RA_2 (R_{BAV})$	- 12.1°/hr	$RB_2 (R_{BAV})$	8.7°/hr
$RA_2 (R_{SAV})$	- 11.0°/hr	$RB_2 (R_{SAV})$	3.1°/hr
$RA_2 (R_{AAV})$	- 12.3°/hr	$RB_2 (R_{AAV})$	5.6°/hr
$RA_2 (MU_B)$	- 2.0°/hr/g	$RB_2 (MU_A)$	1.0°/hr/g
$RA_2 (MU_{SA})$	23.6°/hr/g	$RB_2 (MU_{SA})$	28.1°/hr/g
$RA_2 (GSA)$	- 54.2°/hr/g	$RB_2 (GSA)$	- 46.8°/hr/g

Table 6. Accelerometer Repeatability (z Axis Up) (Cont'd)

Test No.	Accelerometer Axes (Milli-g's)							
	AA_1		AB_1		AA_2		AB_2	
	μ	σ	μ	σ	μ	σ	μ	σ
Error Band	1008.1	0.24	1.1	0.81	0.8	0.47	-2.4	0.79
Turn-on	1009.9	0.26	-0.2	0.17	-0.3	0.42	-3.6	0.40
z-Axis Down	-1002.9	0.07	-1.9	0.07	0.2	0.02	0.4	0.03

C. Gyro Static Drift Errors, G and Non-G - Rockwell Collins.

The possible number of orientations in which the multifunction gyros may be tested are many. Using all of the combinations would result in unnecessarily excessive testing. Experience has shown that a six-position test can be used for complete evaluation and analysis. Knowing the earth's rate components and certain simultaneous equations as listed in Table 7, the g-sensitive and non-g sensitive errors can be computed.

Table 7. Simultaneous Equations

x-Axis Down	$RA_1 = -MU_B + RSav + W_0$	$RB_1 = +MU_A + RSav - W_h$	(1)
x-Axis Up	$RA_1 = +MU_B + RSav + W_0$	$RB_1 = -MU_A + RSav - W_h$	(2)
x-Axis Down	$RA_2 = -MU_{SA} + R_{BAV} - W_h$	$RB_2 = -RB_2\,(GSA) + R_{BAV} - W_v$	(3)
x-Axis Up	$RA_2 = +MU_{SA} + R_{BAV} - W_h$	$RB_2 = +RB_2\,(GSA) + R_{BAV} + W_v$	(4)
y-Axis Down	$RA_1 = --MU_{SA} + R_{BAV} - W_h$	$RB_1 = -RB_1\,(GSA) + R_{BAV} - W_v$	(5)
y-Axis Up	$RA_1 = +MU_{SA} + R_{BAV} - W_h$	$RB_1 = +RB_1\,(GSA) + R_{BAV} + W_v$	(6)
y-Axis Down	$RA_2 = -RA_2\,(GSA) + R_{AAV} - W_v$	$RB_2 = +MU_{SA} + R_{AAV} + W_0$	(7)
y-Axis Up	$RA_2 = +RA_2\,(GSA) + R_{AAV} + W_v$	$RB_2 = -MU_{SA} + R_{AAV} + W_0$	(8)

Table 5. Accelerometer Repeatability (y Axis Down)

Test No.	Accelerometer Axes (Milli-g's)							
	AA_1		AB_1		AA_2		AB_2	
	μ	σ	μ	σ	μ	σ	μ	σ
1	4.0	0.04	-1007.4	0.67	-1004.5	0.18	-2.9	0.08
2	2.6	0.04	-1007.7	0.20	-1004.0	0.68	-1.4	0.02
3	3.5	0.04	-1008.6	0.10	-1004.1	0.15	-3.6	0.03
4	2.4	0.04	-1007.8	0.10	-1005.0	0.15	-1.6	0.02
5	2.9	0.03	-1008.3	0.18	-1005.0	0.12	-2.0	0.04
6	3.4	0.06	-1008.7	0.15	-1004.2	0.15	-0.9	0.02
Error Band	3.1	0.58	-1008.1	0.51	-1004.5	0.45	-2.1	1.00
Turn-on	1.3	0.76	-1011.5	0.47	-1009.6	0.24	-2.9	0.62
y-Axis Up	0.1	0.05	1005.7	0.12	1004.6	0.19	6.2	0.08

Table 6. Accelerometer Repeatability (z Axis Up)

Test No.	Accelerometer Axes (Milli-g's)							
	AA_1		AB_1		AA_2		AB_2	
	μ	σ	μ	σ	μ	σ	μ	σ
1	1007.9	0.11	0.8	0.07	0.9	0.04	-1.7	0.03
2	1007.9	0.09	1.2	0.04	0.9	0.03	-3.3	0.03
3	1007.9	0.09	0.5	0.17	0.9	0.03	-1.8	0.02
4	1008.3	0.11	1.0	0.15	1.4	0.05	-1.6	0.02
5	1008.5	0.07	2.7	0.05	0.7	0.02	-3.2	0.01
6	1008.2	0.24	0.7	0.05	0.0	0.06	-2.8	0.01

Table 3. Gyro Repeatability (z Axis Up)
(Cont'd)

Test No.	Gyro Axes (degrees/hour)							
	RA_1		RB_1		RA_2		RB_2	
	μ	σ	μ	σ	μ	σ	μ	σ
Error Band	-46.3	4.1	-80.4	3.0	-25.4	2.5	2.1	1.1
Turn-on	5.9	4.7	-15.9	5.4	-19.1	1.9	-4.1	1.8
z-Axis Down	+21.8	0.2	52.7	0.4	3.3	0.8	4.2	0.4

Concurrently, the accelerometer day-to-day output data were recorded during the 4-day evaluation of the gyros. The mean and standard deviation of each test are tabulated in Tables 4 through 6. The unit of output data is expressed in milli-g's. The axes for accelerometer #1 are designated AA_1 and AB_1. The axes for accelerometer #2 are AA_2 and AB_2. Each set of test data is described by a 1σ value about its mean. An error band, utilizing the data of all six tests, is also tabulated in the tables. Turn-on data represents the accelerometer performance immediately upon instrument turn-on (cold start). All other data in the tables are accelerometer performance after thermal equilibrium.

Table 4. Accelerometer Repeatability (x Axis Down)

Test No.	Accelerometer Axes (Milli-g's)							
	AA_1		AB_1		AA_2		AB_2	
	μ	σ	μ	σ	μ	σ	μ	σ
1	2.0	0.07	-1.7	0.04	2.2	0.08	-1002.0	0.28
2	2.0	0.04	-2.6	0.04	0.5	0.09	-1003.3	0.34
3	2.0	0.03	-1.7	0.02	2.9	0.05	-1003.8	0.22
4	2.4	0.03	-1.6	0.02	1.4	0.08	-1004.1	0.12
5	2.1	0.02	-1.7	0.02	1.9	0.06	-1002.1	0.10
6	2.4	0.02	-1.6	0.02	0.8	0.03	-1003.6	0.09
Error Band	2.2	0.21	-1.8	0.41	1.6	0.87	-1003.1	0.90
Turn-on	1.6	0.32	-1.7	0.38	-0.6	0.55	-1009.5	0.91
x-Axis Up	2.4	0.03	0.9	0.05	-2.9	0.06	1006.9	0.38

Table 2. Gyro Repeatability (y Axis Down)

Test No.	Gyro Axes (degrees/hour)							
	RA_1		RB_1		RA_2		RB_2	
	μ	σ	μ	σ	μ	σ	μ	σ
1	-76.8	0.5	19.1	0.9	25.6	1.7	31.3	0.6
2	-85.7	0.5	17.3	0.5	33.5	0.3	33.8	0.4
3	-78.4	0.6	19.3	0.7	27.9	0.5	29.9	0.4
4	-82.6	0.5	11.1	0.8	33.8	0.7	34.5	0.3
5	-84.6	0.5	26.9	0.6	39.3	0.4	35.7	0.6
6	-85.7	0.5	23.2	0.4	39.6	0.4	37.1	0.2
Error Band	-82.3	3.9	19.5	5.4	33.3	5.7	33.7	2.7
Turn-on	-13.3	5.5	-21.5	5.4	-24.2	3.0	7.1	2.1
y-Axis Up	28.4	0.6	-44.6	0.4	-57.9	0.8	-22.5	0.4

Table 3. Gyro Repeatability (z Axis Up)

Test No.	Gyro Axes (degrees/hour)							
	RA_1		RB_1		RA_2		RB_2	
			μ	σ	μ	σ	μ	σ
1	[illegible]	[illegible]	-75.7	0.7	-26.3	0.6	1.8	0.8
[illegible]	[illegible]	[illegible]	-83.9	0.2	-21.8	1.3	1.1	0.2
[illegible]	[illegible]	[illegible]	-82.7	0.4	-24.1	0.7	4.2	0.3
[illegible]	[illegible]	[illegible]	-78.4	0.4	-24.2	1.0	2.2	0.5
[illegible]	[illegible]	[illegible]	[illegible]	0.2	-28.4	0.4	1.1	0.2
[illegible]	[illegible]	[illegible]	-81.3	0.8	-27.5	0.5	2.1	0.3

The data from six tests, each test consisting of 15 data points, were used in establishing the predictable mean drift error and the 1σ random behavior. The mean and the standard deviation of each test are tabulated in Tables 1 through 3. The unit of drift rate is expressed in degrees per hour. The axes for gyro #1 are identified as RA_1 and RB_1. The axes for gyro #2 are RA_2 and RB_2. Each set of test data is described by a 1σ value about its mean drift rate. Also, an error band, utilizing the data of all six tests, is described in the tables by a 1σ value about its mean. The error band contains the composite effects of all predictable errors and random uncertainties in the output data. Turn-on data were recorded immediately after instrument turn-on (cold start). All other data were recorded after thermal equilibrium.

Table 1. Gyro Repeatability (x Axis Down)

Test No.	Gyro Axes (degrees/hour)							
	RA_1		RB_1		RA_2		RB_2	
	μ	σ	μ	σ	μ	σ	μ	σ
1	-6.7	9.1	-20.0	0.2	-44.9	0.8	45.3	1.3
2	-8.2	1.1	-30.8	0.3	-54.6	1.4	56.3	1.4
3	-7.3	0.3	-21.5	0.4	-45.0	0.6	40.4	0.5
4	-7.5	0.3	-21.5	1.2	-47.2	1.2	44.3	0.4
5	-11.0	0.0	-29.2	0.3	-45.8	1.1	47.1	0.5
6	-7.5	0.3	-28.9	18.9	-50.9	0.7	48.2	0.6
Error Band	-8.0	1.5	-25.3	4.8	-48.1	3.9	46.9	5.3
Turn-on	4.1	3.9	-14.1	7.0	-21.1	4.8	-19.2	7.5
x-Axis Up	-21.1	0.3	-26.6	1.3	- 0.8	0.6	-29.6	0.5

The pulse generators provide incremental angle and velocity output signals in the form of TTL compatible pulses. Each delta angle pulse has a nominal weight of 0.024 degrees. Each delta velocity pulse has a nominal weight of 0.049 meters/sec. (Collins Unit).

A temperature sensor output is provided for temperature compensation of scale factor, if required, and for error modeling in critical applications.

III. EVALUATION

A. General.

The multifunction gyro/accelerometer considered in this report is an instrument that is being developed to potentially provide a reference for cost efficient navigational, guidance, or stabilization systems. A reference must be either inherently invariable or predicatably variable. An ideal instrument is invariable, however, actual instruments do deviate from the ideal. The objective of this task is to establish the predictable rate of deviation (drift errors) caused by design limitations or constructional deficiencies within the instrument.

In evaluating the instrument, it is necessary to investigate thoroughly the effect of operational temperature environment (-30 to 60°C) on performance. Because this temperature range exist in actual applications, it is mandatory that the instrument maintain its accuracy with a minimum of degradation.

The evaluation of the Rockwell Collins Phase II Unit was conducted in the following test sequence:

1. Day-to-day repeatability, ambient temperature.
2. Static drift errors.
3. Rate table tests (-30° to 60°C).
4. Rate table tests repeatability (-15° and 60°C).
5. Internal axis alignment tests.

B. Multifunction Gyro/Accelerometer Day-to-Day Repeatabiltiy - Rockwell Collins.

To determine the drift error repeatability and the random behavior at ambient temperature, the instrument was evaluated over a 4-day period with constant temperature, constant mounting pressure, and an unchanged axis orientation.

The most common statistical method, used to describe random behavior, is the random deviation identified by the Greek letter σ (sigma). The sigma (standard deviation) is a measure of the dispersion of the random drift rate about the mean, μ, and is expressed as the root mean square of the deviation of all the readings about the mean. The significance of standard deviation is that 68.3% of a large number of drift rate readings will not exceed this value.

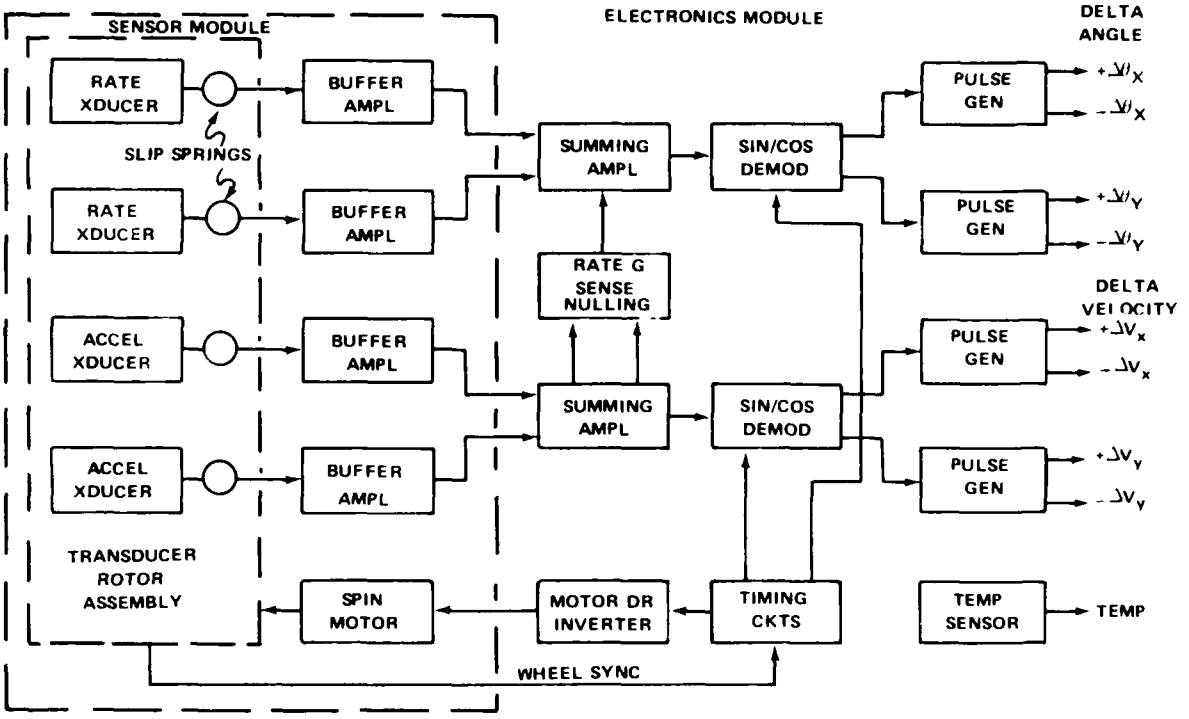

Figure 3. Block diagram of two-axis rotation/two-axis, acceleration sensor.

Table 17. G-Sensitive and Non-G Sensitive Errors

RA_1 (R_{BAV})	- 171.6°/hr	RB_1 (R_{BAV})	- 179.2°/hr
RA_1 (R_{SAV})	- 174.2°/hr	RB_1 (R_{SAV})	- 178.0°/hr
RA_1 (R_{AAV})	- 162.5°/hr	RB_1 (R_{AAV})	- 165.0°/hr
RA_1 (MU_B)	- 12.5°/hr/g	RB_1 (MU_A)	- 9.9°/hr/g
RA_1 (MU_{SA})	- 1554.8°/hr/g	RB_1 (MU_{SA})	- 1541.3°/hr/g
RA_1 (GSA)	- 4395.6°/hr/g	RB_1 (GSA)	- 4382.4°/hr/g
RA_2 (R_{BAV})	320.0°/hr	RB_2 (R_{BAV})	2486.6°/hr
RA_2 (R_{SAV})	325.5°/hr	RB_2 (R_{SAV})	2464.4°/hr
RA_2 (R_{AAV})	326.7°/hr	RB_2 (R_{AAV})	2490.8°/hr
RA_2 (MU_B)	- 3.9°/hr/g	RB_2 (MU_A)	- 4.7°/hr/g
RA_2 (MU_{SA})	265.6°/hr/g	RB_2 (MU_{SA})	263.4°/hr/g
RA_2 (GSA)	- 1512.8°/hr/g	RB_2 (GSA)	- 1517.9°/hr/g

Table 18. Accelerometer Bias

AA_1 Axis	- 0.124 mg
AB_1 Axis	- 0.069 mg
AB_2 Axis	+ 0.029 mg
AB_2 Axis	+ 0.026 mg

Table 19. Accelerometer Axis Misalignment Error

α AA_1	- 134.8 mrad
α AB_1	- 73.6 mrad
α AA_2	24.2 mrad
α AB_2	28.2 mrad

H. Gyro Rate Table Tests versus Temperature - Rockwell Collins Unit

1. Test setup and procedure

Gyro performance characteristics were determined by using a precision rate table that provided variable clockwise (CW) and counterclockwise (CCW) rates. First, the x, y, z axes of the multifunction gyro/accelerometer inertial reference unit were aligned to a six-sided reference mounting fixture prior to the rate tests. Secondly, the fixture was then secured to the rate table with the y-axis parallel to the rate table axis of rotation, which in turn was aligned with the local vertical. An environmental chamber, placed over the rate table, provided the mechanism for controlling the temperature environment.

The rate test sequence consisted of rotating the table CW and CCW at discrete rates up to 150 degrees per second. At each rate, the output data from both gyro input axes (A_2 and B_1) and cross axes (A_1 and B_2) were stored in the computer. The same procedure was repeated at eight different temperature setting (-22, 4, 24, 45, 79, 100, 120 and 140°F) to determine the thermal sensitivity of the gyroscopes. The rate tests at 4°F and 140°F were repeated to make sure that any effects of non-repeatability would be revealed.

Prior to each rate test, the accelerometer outputs, at zero rate input for each temperature setting, were stored in the computer. The data were used to establish the accelerometer thermal sensitivity.

2. Data Analysis and Results

For each rate test, a data sample of 63 discrete values for each gyro axes RA_1, RB_1, RA_2, and RB_2 was stored in the computer. Each discrete value of the data stored in the computer, is the average of a 4-second data sample. Using the 63 values, a best straight line curve fit was calculated. A one-sigma value, describing the dispersion of the random deviation about the best slope for each set of data, was also computed. This information was used to determine the scale factor, zero offset, linearity error, temperature sensitivity, resolution and rate alignment of axis B with respect to axis A.

Scale factor is defined as the ratio of a change in output to a change in the input. It is the slope of the straight line that can be best fitted by the method of least squares to the input-output data. Figure 4 is a line graph illustrating the best calculated straight line scale factor for gyro input axis RA_2 and a plot of the actual discrete data points. Figure 5 is a line graph of the dispersion of the actual composite data points about the calculated scale factor as shown in Figure 4. The composite errors are due to the composite effects of resolution, non-linearity, non-repeatability and other uncertainties in the output data. The large error deviations, plotted around zero input rates, are partially due to the rate table error caused by a slight difference in CW and CCW rotation.

Figure 6 is an expanded plot of the actual discrete data points for an input span of $\pm$ 1 deg/sec. The straight line slope is the calculated scale factor for the $\pm$ 150 deg/sec input span, not calculated for the $\pm$ 1 deg/sec input span.

Figures 7, 8 and 9 are similar line and data plots for gyro input axes RB_1.

Figure 10 is a calculated line and actual data plot for cross axis RA_1. Figure 11 is an expanded line graph of the random distribution of the actual data about the calculated best fit curve.

Figures 12 and 13 are similar plots for cross axis RB_2.

Figures 14 through 83 are similar gyro performance plots for each temperature setting. Figures 84 through 123 are the results of repeat tests conducted at 4°F and 140°F.

The data plotted in Figures 4 through 123 were obtained to determine the scale factor and zero offset (bias) thermal sensitivities. The data used to determine the scale factor, the one sigma value representing the dispersion of the scale factor random errors, the actual and calculated zero offsets for each figure are tabulated in Table 20.

Sensitivity is defined as the ratio of a change in output to a change in an undesirable or secondary input. For example, the drift rate thermal sensitivity of a gyro is the ratio of the change in scale factor to a change in temperture. Figure 124 presents line graphs illustrating the scale factor sensitivity data tabulated in Table 20 for gyro axes RA_2 and RB_1.

Zero offset is defined as the gyro output when the input rate is zero, generally expressed as an equivalent input rate. The line graphs in Figure 125 illustrate the thermal zero offset sensitivity of the data tabulated in Table 20 for gyro axes RA_2 and RB_1, both actual (A) and predicted (P) values.

The results of the rate tests, repeated at 4°F, are depicted in Figures 126 through 131. Figure 126 shows three calculated best straight line scale factors for gyro axes RA_2 at 4°F. The symbol R_0 represents the original test, R_1 and R_2 are repeat test symbols. Figure 127 is an expanded plot of the scale factors for an input span of $\pm$ 1 deg/sec. The plots for input axis RB_1 and cross axes RA_1 and RB_2 are depicted in Figures 128 through 131.

Similar plots at the repeat 140°F tests are depicted in Figures 132 through 137. Resolution is defined as the largest value of the minimum change in input, for inputs greater than the threshold, which produces a change in output equal to some specified percentage (at least 50%) of the change in output expected using the nominal scale factor. The results of the rate tests confirm that the multifunction gyros and its companion software have a resolution of 0.005 deg/sec. (Collins Unit).

The rate alignment of the multifunction gyros was obtained by using rate test and rotating the gyros about their sensitive axes in the CW and CCW directions. To determine the rate alignment of axis B with respect to axis A, the gyro was rotated in a CW and CCW direction about axis A and the rate alignment was calculated using the following equation:

$$\alpha\ RB = \tan^{-1}\left[(RB_{CW} - RB_{CCW}) \div (RA_{CW} - RA_{CCW})\right] \qquad (15)$$

The rate alignment errors for each gyro axis are tabulated in Table 21. The results are tabulated for vertical orientation, both up and down, as indicated. The error is expressed in milliradians.

I. Accelerometer Thermal Sensitivity - Rockwell Collins

The results of the accelerometer data, stored in the computer prior to each rate-temperature test, are shown in Figure 138. This figure illustrates both the best calculated straight line curve for accelerometer axes AA_2 and AB_1 and a plot of the actual discrete data points as a function of temperature. The data used to generate Figure 138 is tabulated in Tables 22 and 23. The calculated accelerometer output thermal sensitivities for axes AA_2 and AB_1 and the standard deviation of the errors for each set of data are also shown in these tables.

J. Rate Table Calibration and Results

The accuracy of the rate table was verified by precisely measuring the rotational period, both CW and CCW, for each nominal rate of interest. Column one, in Table 24, indicates the nominal rates used in calibrating the rate table. Column two affirms the actual measured rate for each nominal input rate. Column three verifies the error between the nominal rates and the actual measured rates. Column four presents the best straight line curve fit utilizing the data in columns one and three. Column five displays the error obtained by subtracting column four from column three. The calculated one sigma random deviation of the data in column five is equal to 0.1613°/sec.

A best straight line curve fit of the data in column four and a plot of the actual data in column three are illustrated in Figure 139. The slope of the computed line is 0.0197 with a bias of 0.0728°/sec.

A second calibration test was executed to confirm the repeatable accuracy. The results, displayed as ERROR 2 in Figure 139, are depicted as a best straight line fit and as a plot of the actual measured data.

The calibration of the rate table not only verifies the nominal/actual rate errors but also confirms the CW/CCW rotational errors. If required, these error coefficients can be used to remove the rate table uncertainties for the rate data depicted in the Input-Output Characteristics figures. For example, the corrected scale factors for gyro axes RA_2 and RB_1 in Figures 44 and 47 are -0.9678, -0.9945 in lieu of the nominal -0.9487, -0.9748, respectively. The corrected Input-Output characteristics of Figure 45 and 48 are illustrated in Figures 140 and 141. The line graphs in Figures 140 and 141 were obtained by removing the CW/CCW rotational error coefficients.

IV. CONCLUSIONS

The determination of the multifunction gyro/accelerometer repeatable, non-repeatable and thermal empirical errors was the primary objective of this evaluation. The synthesis of all these errors in conjunction with the inertial reference unit software computational capabilities allow for sophisticated error modeling algorithms at reasonable cost. This technique of

improving gyro/accelerometer performance by software error modeling will be very useful tool in the effort of addressing the long-term goal of developing technology for cost efficient inertial sensors.

A summary of the major empirical errors are:

Gyro Errors

	Collins	Singer
Scale factor	(See Fig. 124)	
g-sensitive error	55°/hr/g	44000°/hr/g
non-g sensitive error	15°/hr	325°/hr
non-repeatable day-to-day error	6°/hr (σ)	50°/hr (1σ)
linearity	0.2%	
RA_2 scale factor thermal sensitivity	0.069°/sec/°F	
RB_1 scale factor thermal sensitivity	0.112°/sec/°F	
axis alignment	1.0 mrad	

Accelerometer Errors

	Collins	Singer
Scale factor	(See Fig. 138)	
non-repeatable day-to-day error	1.0 mg (1σ)	5.7 mg (1σ)
bias	4 mg	0.125 mg
AA_2 output thermal sensitivity	0.651 mg/°F	
AB_1 output thermal sensitivity	0.637 mg/°F	
axis alignment	2.2 mrad	135 mrad

These test results, in general, support the opinion that the multifunction gyro/accelerometer develoment is a technically sound concept for cost efficient instruments.

V. RECOMMENDATIONS

Additional tests are needed to help isolate the source of non-repeatable gyro/accelerometer errors. Vibration, centrifuge and shock tests are needed to verify instrument performance characteristics in these environments.

It is recommended that software error modeling be explored utilizing the repeatable g sensitive, non-g sensitive and thermal error coefficients. Verification tests will be required to confirm the success of the modeling algorithms.

Table 20. Gyro Temperature-Sensitivity

Temp. °F	Scale Factor Sensitivity		Std. Deviation (1σ)(°/sec)		Zero Offset (Bias) Sensitivity (°/sec)			
					Actual		Calculated	
	RA_2	RB_1	RA_2	RB_1	RA_2	RB_1	RA_2	RB_1
-22	-.9916	-1.0402	.7790	.9350	.0155	.0155	-.0702	-.0730
5.5	-.9850	-1.0324	.1713	.3270	.0155	.0052	.0313	.0221
$4R_1$	-.9824	-1.0296	.1874	.3128	.0103	-.0052	.02667	-.0151
$4R_2$	-.9765	-1.0257	.4685	.4517	.0155	-.0052	.1237	.0825
24	-.9743	-1.0193	.1932	.1932	.0155	-.0103	.0352	.0063
45	-.9668	-1.0054	.2518	.2604	.0155	.0000	.0353	.0170
79	-.9487	- .9748	.1813	.2329	-.0155	.0000	-.0183	-.0419
100	-.9399	- .9623	.1728	.1696	-.0465	-.0155	-.0113	.0058
120	-.9198	- .9277	.4441	.4423	-.0724	-.0258	-.1675	-.1343
140	-.9168	- .9192	.3571	.3762	-.0724	-.0258	-.0792	-.0648
$140R_1$	-.9223	- .9269	.2322	.2276	.0000	-.0362	-.0296	-.0286
$140R_2$	-.9238	- .9311	.1833	.2013	-.0775	-.0310	-.0687	-.0340

R_1 and R_2 are repeat tests.

Table 21. Gyro Rate Alignment Errors

RA_1 (y-down)	-1.013 mrad	RB_1 (z-down)	1.089 mrad
RA_1 (y-up)	-0.635 mrad	RB_1 (z-up)	0.304 mrad
RA_2 (x-down)	-0.410 mrad	RB_2 (y-down)	0.174 mrad
RA_2 (x-up)	-0.926 mrad	RB_2 (y-up)	0.481 mrad

Table 22. Accelerometer Temperature Dependent Data for AA_2 Axis

Input (°F)	Actual (mg)	Predicted (mg)	Error (mg)
-22	1034.9100	1040.5651	-5.6551
4	1020.6600	1023.6360	-2.9760
4	1019.1800	1023.6360	-4.4560
5.5	1027.8400	1022.6590	5.1806
24	1011.3800	1010.6135	.7664
45	1001.7500	996.9400	4.8099
79	981.4000	974.8018	6.5981
100	968.3900	961.1283	7.2616
120	947.6700	948.1058	- .4358
140	931.3700	935.0834	-3.7134
140	931.8800	935.0834	-3.2034
140	933.5300	935.0834	-1.5534

Output Thermal Sensitivity = -0.6511 mg/°F.

Standard Deviation of Errors = 4.3061 mg.

Table 23. Accelerometer Temperature Dependent Data for AB_1 Axis

Input (°F)	Actual (mg)	Predicted (mg)	Error (mg)
-22	1032.9300	1039.2121	-6.2821
4	1020.7200	1022.6498	-1.9298
4	1018.7600	1022.6498	-3.8898
5.5	1024.4000	1021.6943	2.7056
24	1009.6200	1009.9096	- .2896
45	1000.1800	996.5323	3.6476
79	984.0400	974.8739	9.1660
100	974.4200	961.4966	12.9233
120	951.5700	948.7564	2.8135
140	931.5600	936.0162	-4.4562
140	929.3300	936.0162	-6.6862
140	933.6000	936.0162	-2.4162

Output Thermal Sensitivity = -0.6370 mg/°F.

Standard Deviation of Errors = 5.7947 mg.

Table 24. Rate Table Calibration

Nominal Rate °/s	Actual Rate °/sec	(Nominal-Actual) Rate °/sec	Predicted Rate °/sec	(Col. 3 - Col. 4) Error °/sec
-150	-147.4956	-2.5044	-2.8893	.3849
-140	-137.5668	-2.4332	-2.6918	.2586
-130	-127.5280	-2.4720	-2.4943	.0223
-120	-117.7329	-2.2671	-2.2968	.0297
-110	-107.9020	-2.0980	-2.0994	.0014
-100	- 98.1039	-1.8961	-1.9019	.0058
- 90	- 88.1359	-1.8641	-1.7044	-.1596

Table 24. Rate Table Calibration
(Cont'd)

Nominal Rate °/s	Actual Rate °/sec	(Nominal-Actual) Rate °/sec	Predicted Rate °/sec	(Col. 3 - Col. 4) Error °/sec
-80	- 78.4946	-1.5054	-1.5069	.0015
-70	- 68.5659	-1.4341	-1.3095	-.1245
-60	- 58.6867	-1.3133	-1.1120	-.2012
-50	-48.9212	-1.0788	- .9145	-.1642
-40	-39.0773	- .9227	- .7171	-.2056
-30	-29.2371	- .7629	- .5196	-.2432
-20	-19.4126	- .5875	- .3221	-.2653
-10	- 9.6597	- .3403	- .1246	-.2156
0	0.0000	0.0000	.0728	-.0728
10	9.6438	.3562	.2702	.0859
20	19.3859	.6141	.4677	.1463
30	29.1961	.8039	.6652	.1386
40	39.0031	.9969	.8627	.1342
50	48.8529	1.1472	1.0601	.0870
60	58.6173	1.3827	1.2576	.1250
70	68.4700	1.5300	1.4551	.0748
80	78.3810	1.6190	1.6525	-.0335
90	87.9544	2.0456	1.8500	.1955
100	97.9160	2.0840	2.0475	.0364
110	107.6822	2.3178	2.2450	.0727
120	117.4846	2.5154	2.4424	.0729
130	127.2233	2.7767	2.6399	.1367
140	137.1831	2.8169	2.8374	-.0205
150	147.2899	2.7303	3.0349	-.3046

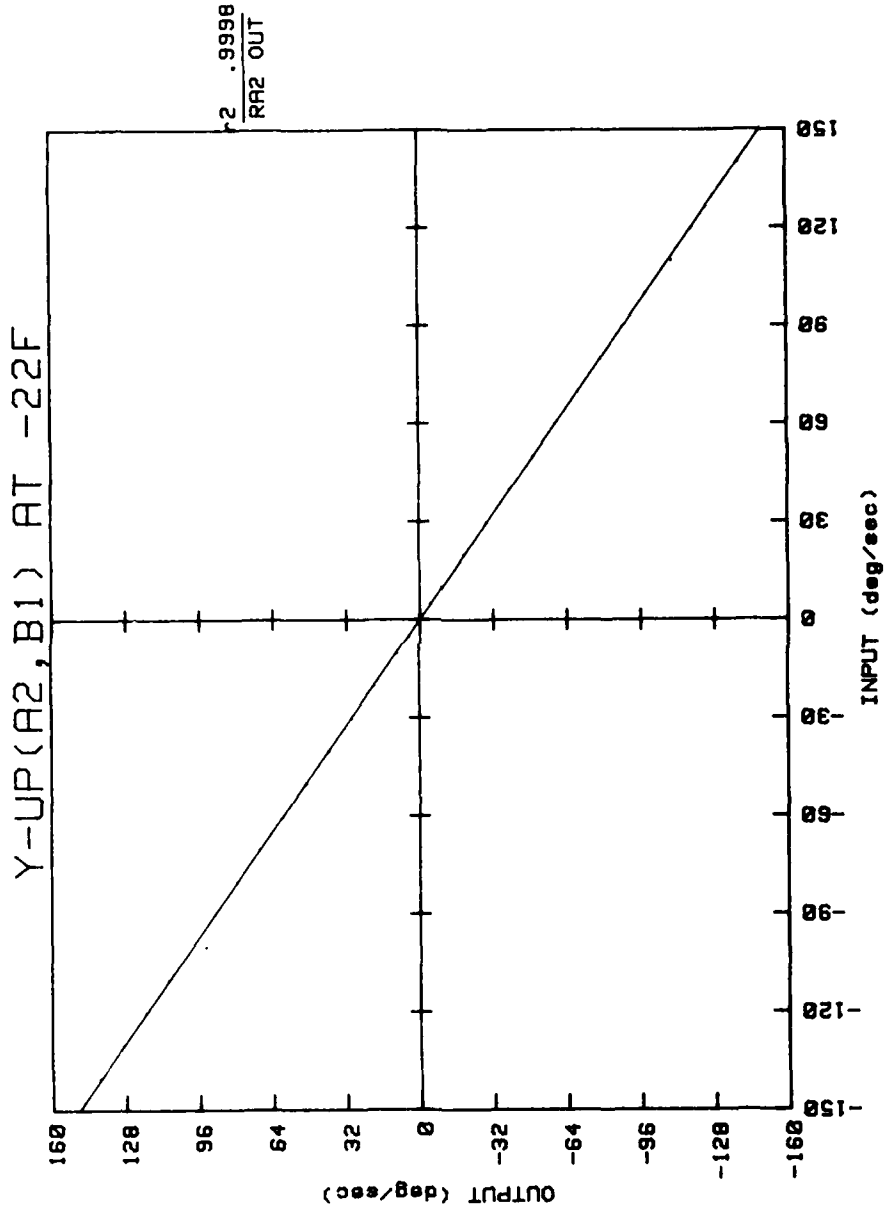

Figure 4. Input-output characteristics.

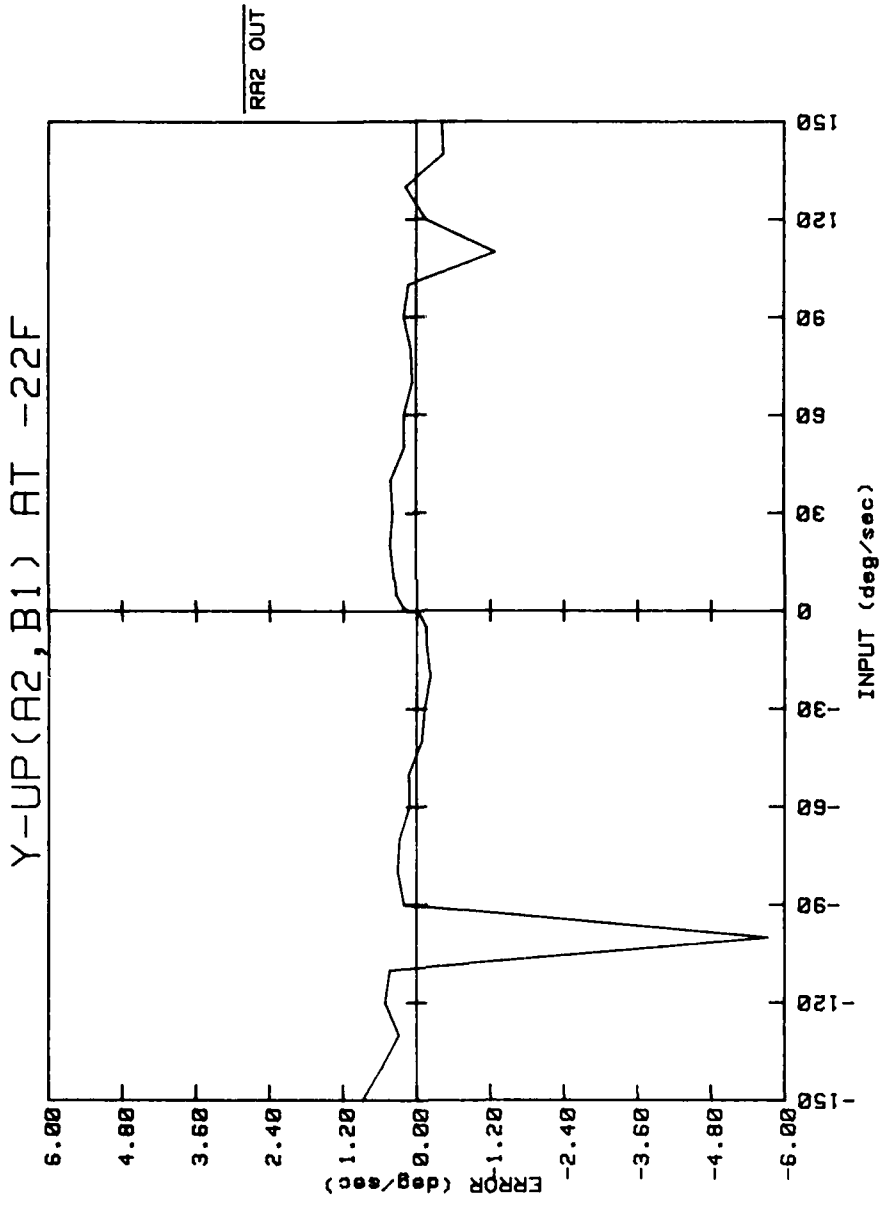

Figure 5. Input-output characteristics.

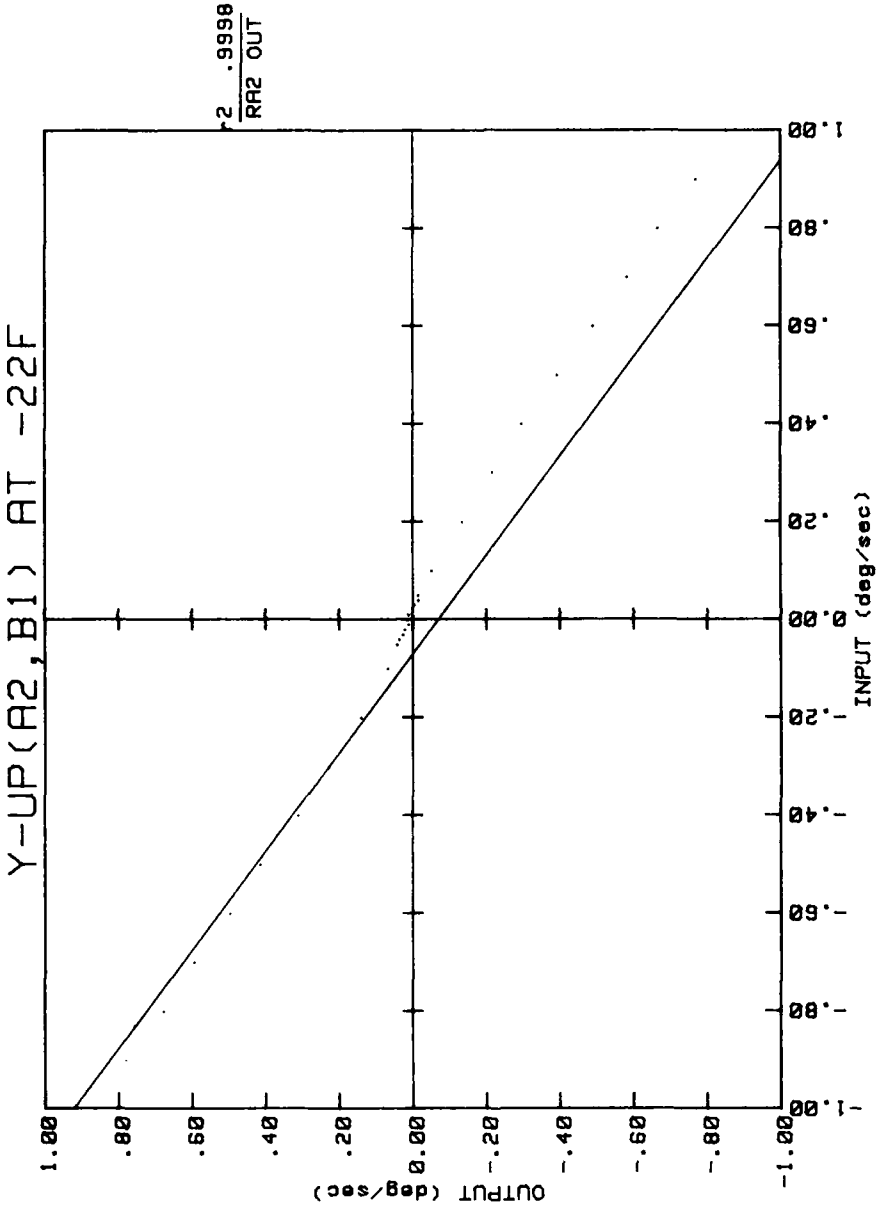

Figure 6. Input-output characteristics.

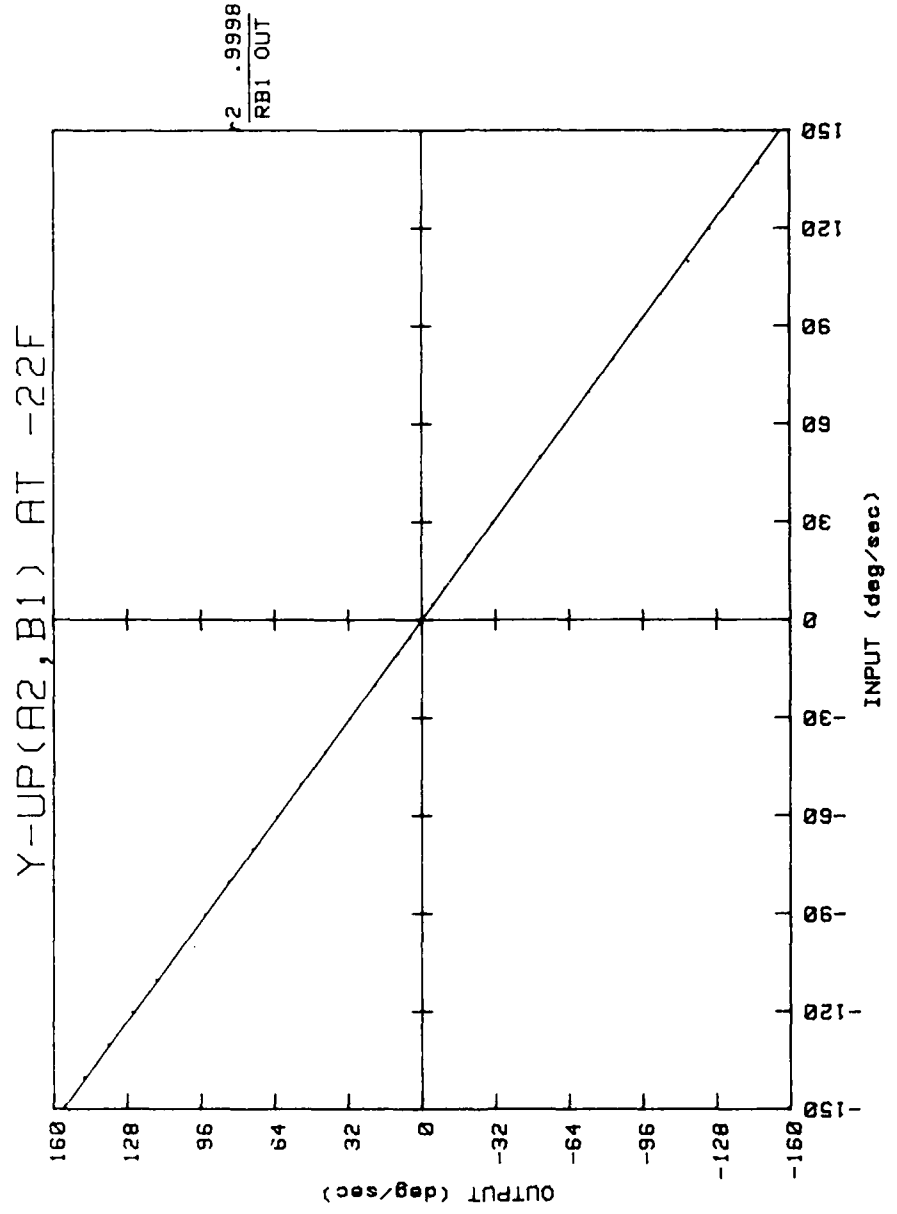

Figure 7. Input-output characteristics.

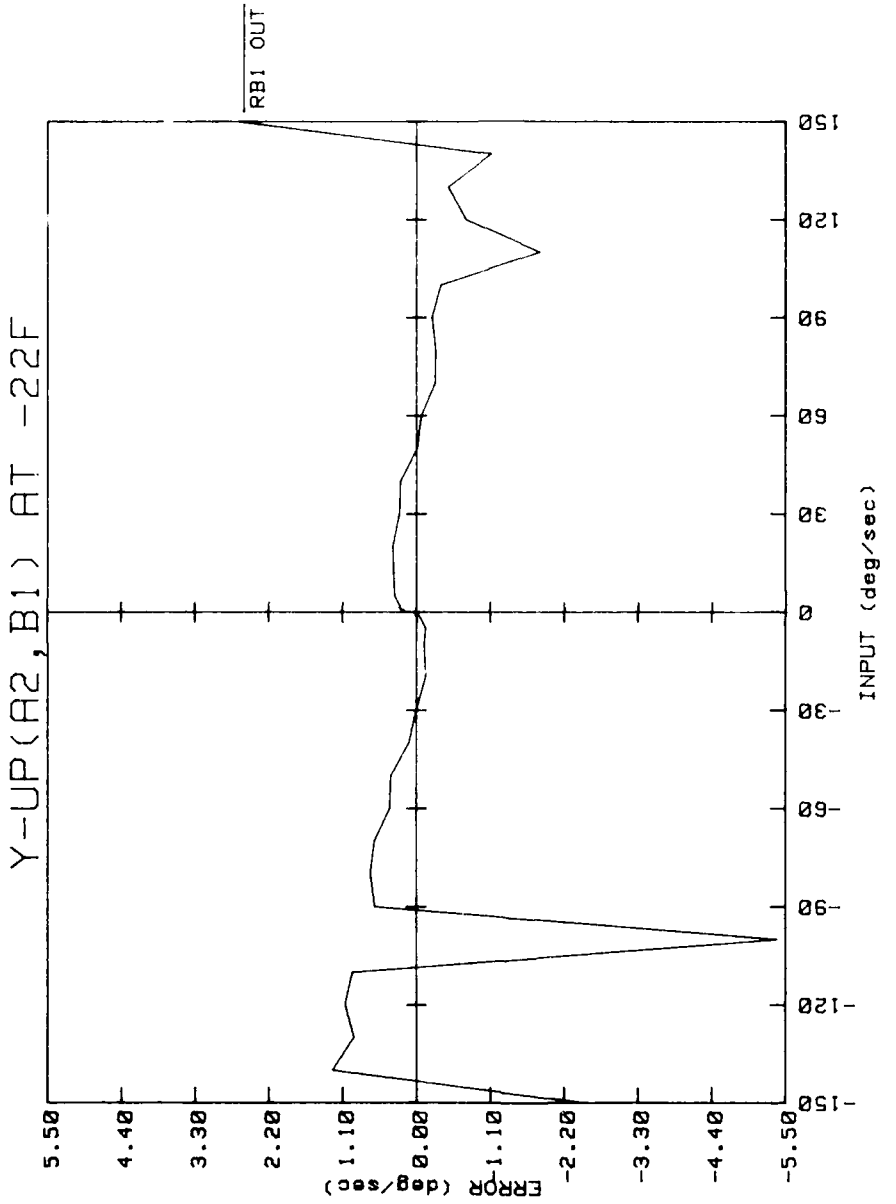

Figure 8. Input-output characteristics.

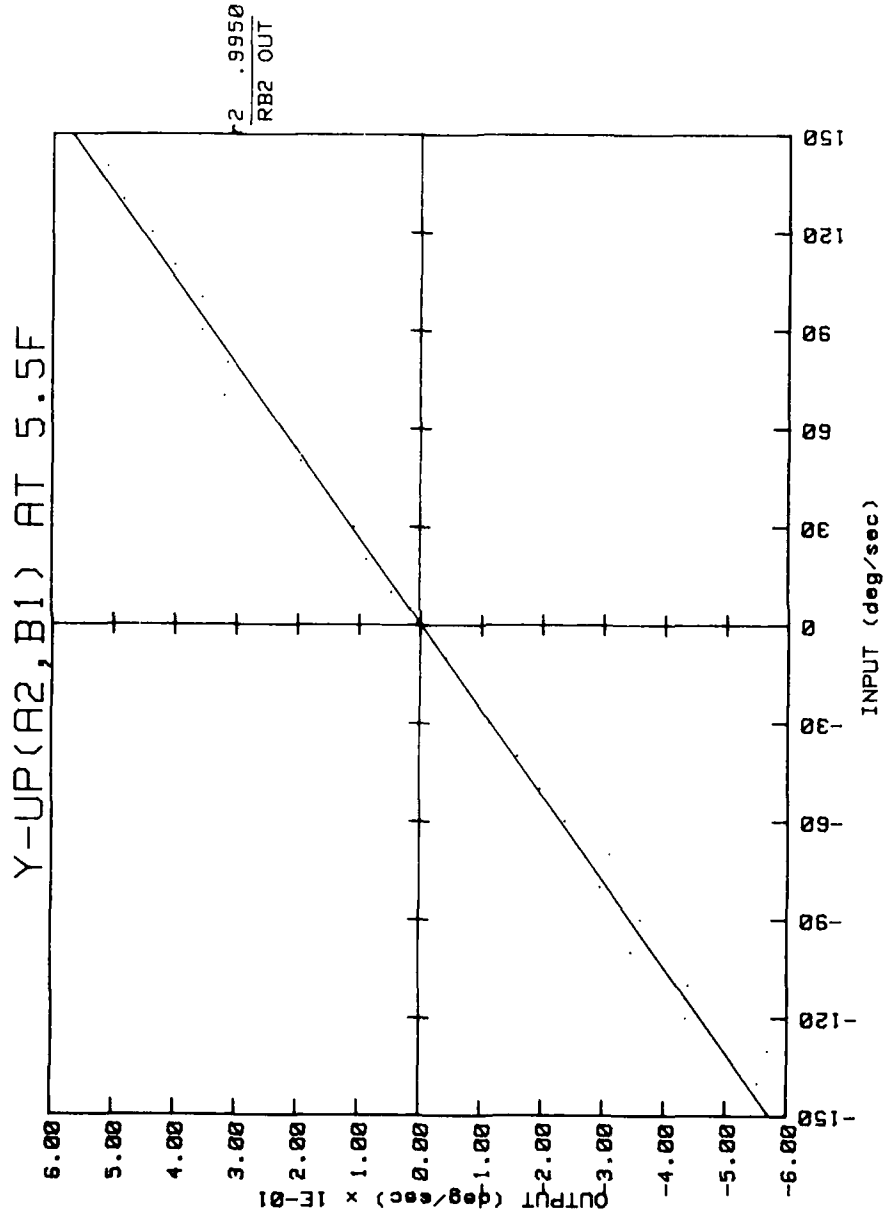

Figure 22. Input-output characteristics.

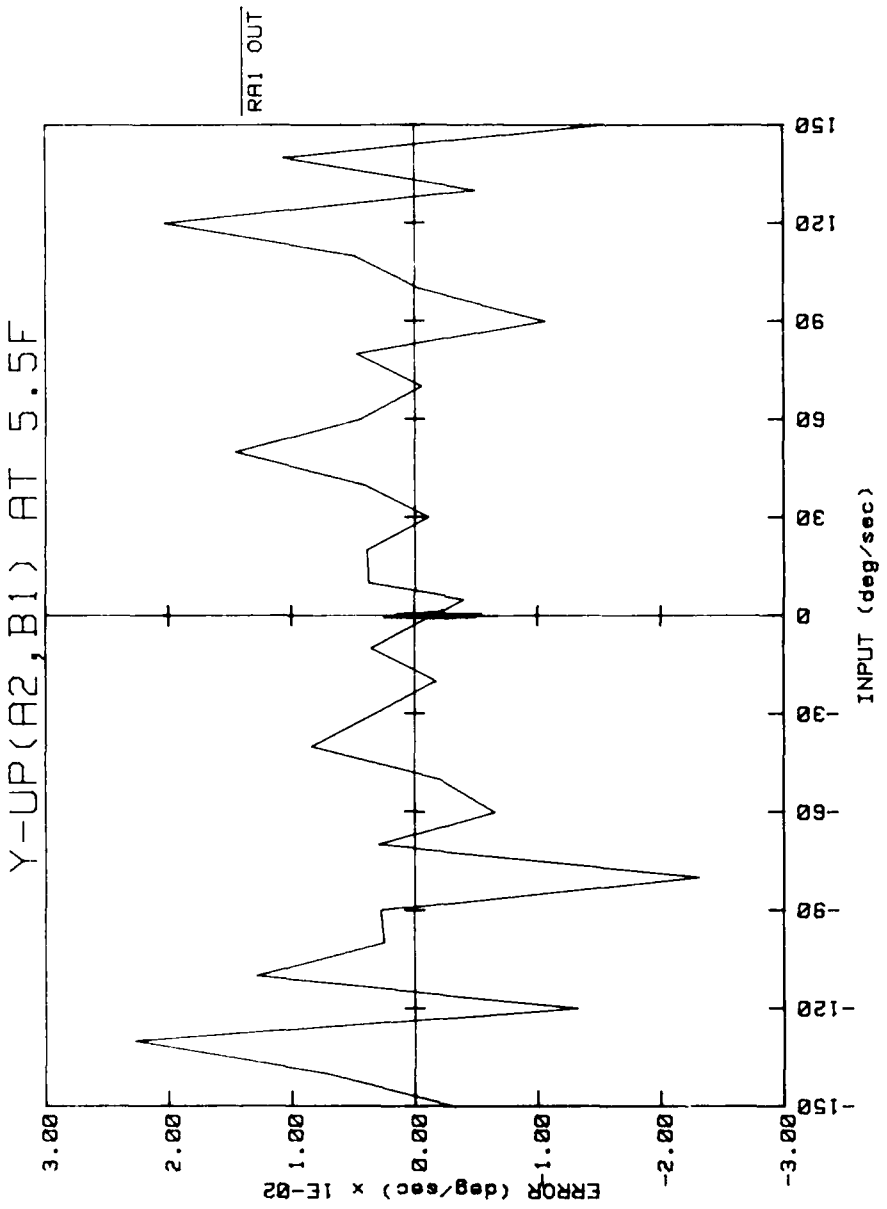

Figure 21. Input-output characteristics.

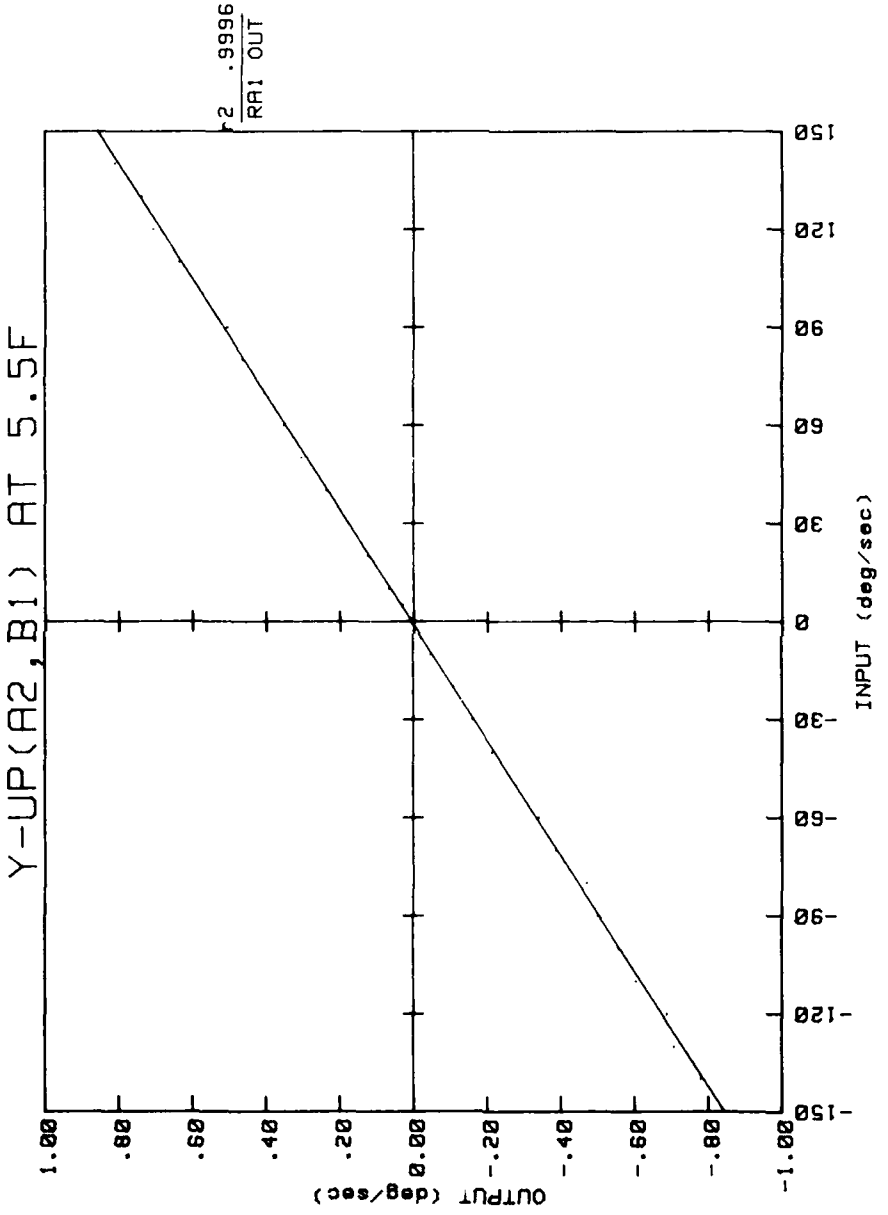

Figure 20. Input-output characteristics.

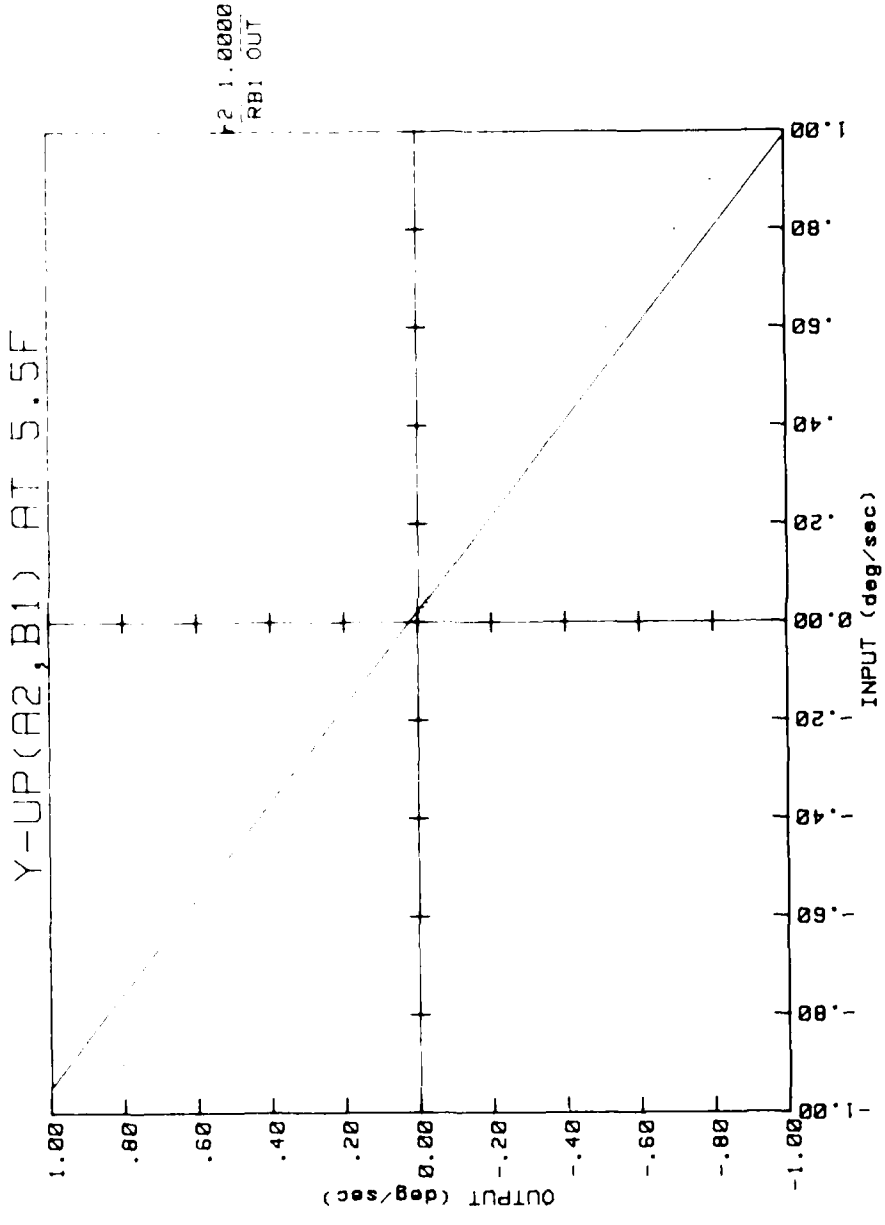

Figure 19. Input-output characteristics.

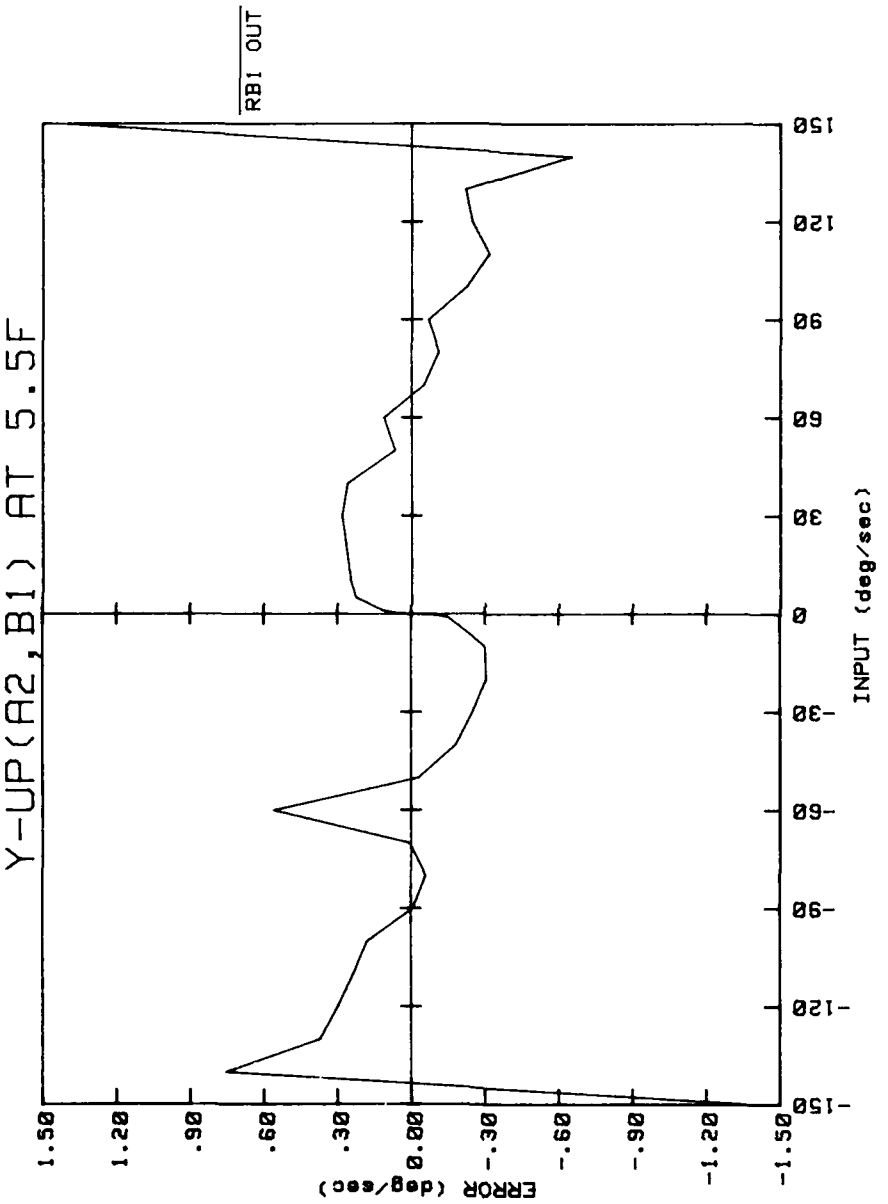

Figure 18. Input-output characteristics.

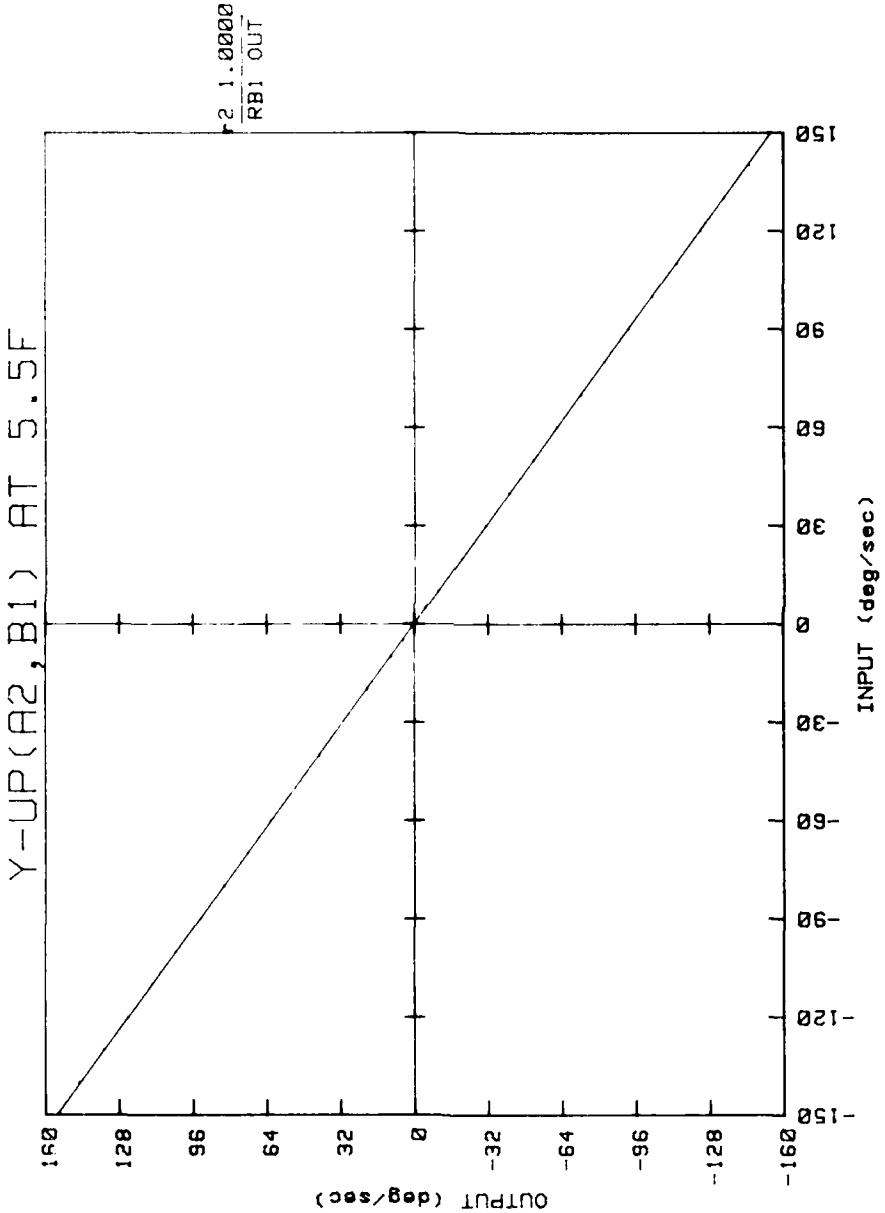

Figure 17. Input-output characteristics.

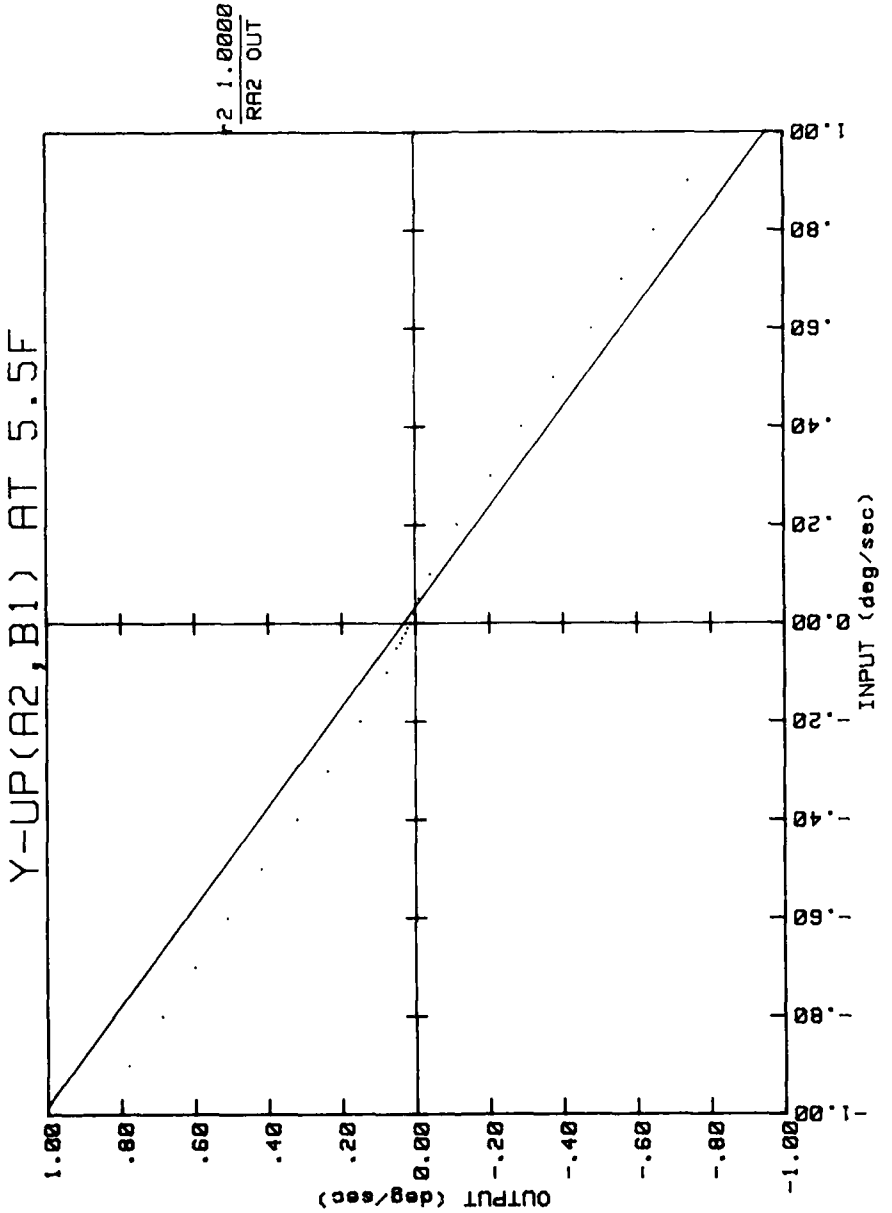

Figure 16. Input-output characteristics.

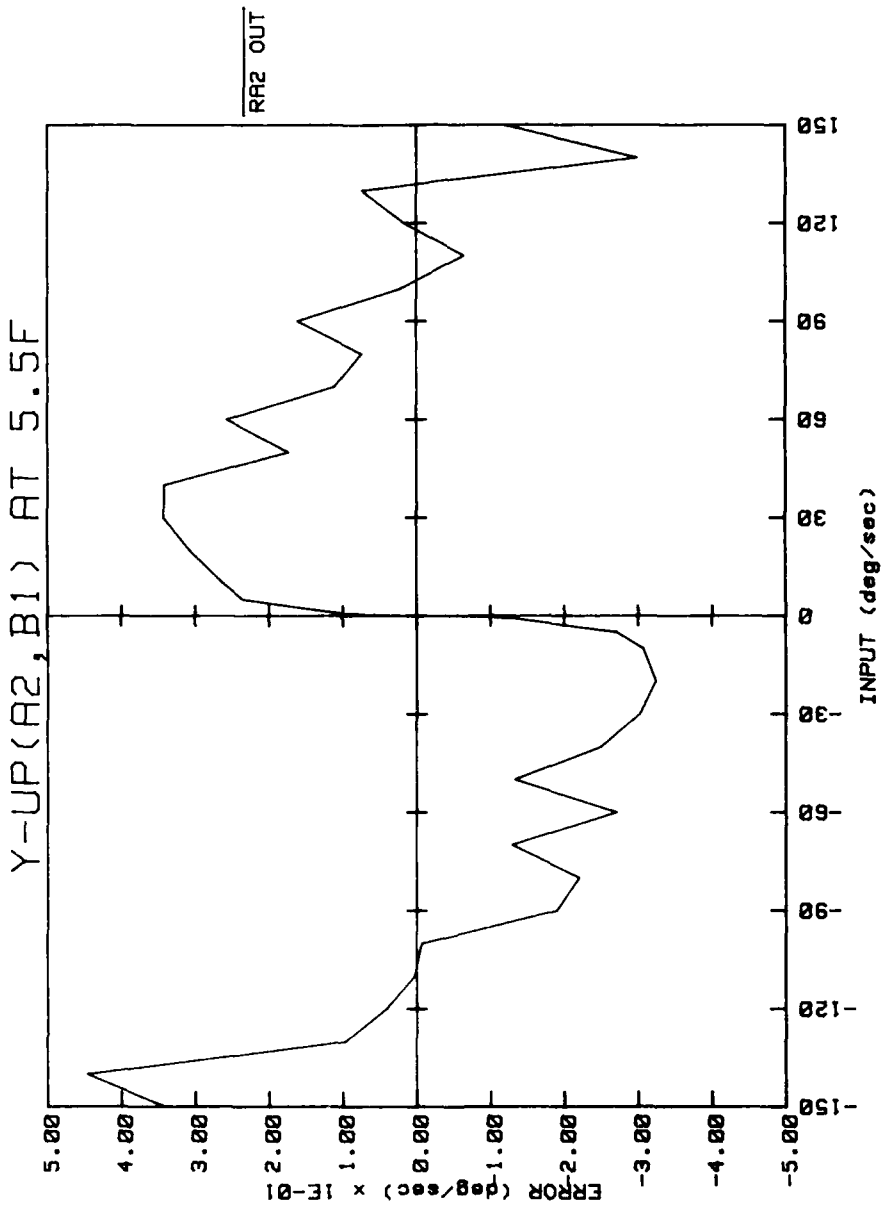

Figure 15. Input-output characteristics.

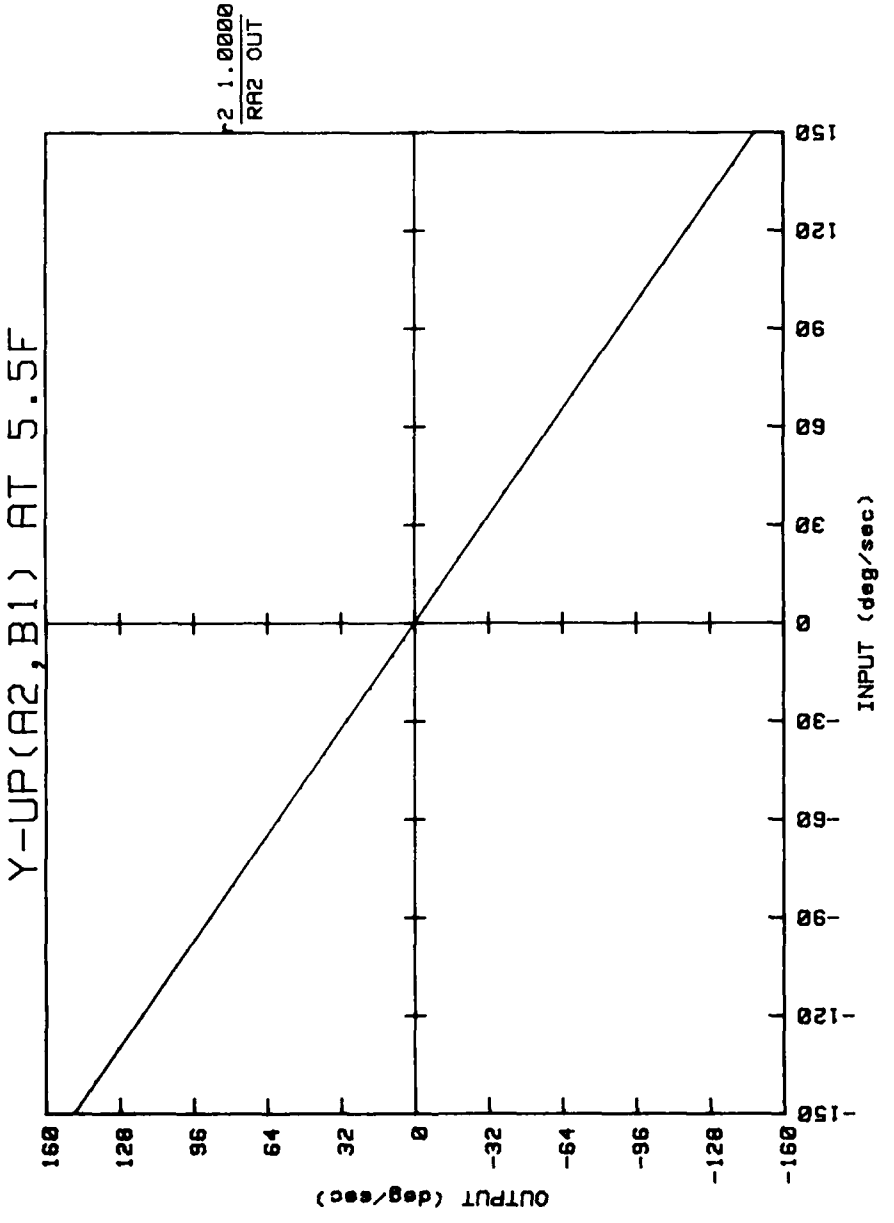

Figure 14. Input-output characteristics.

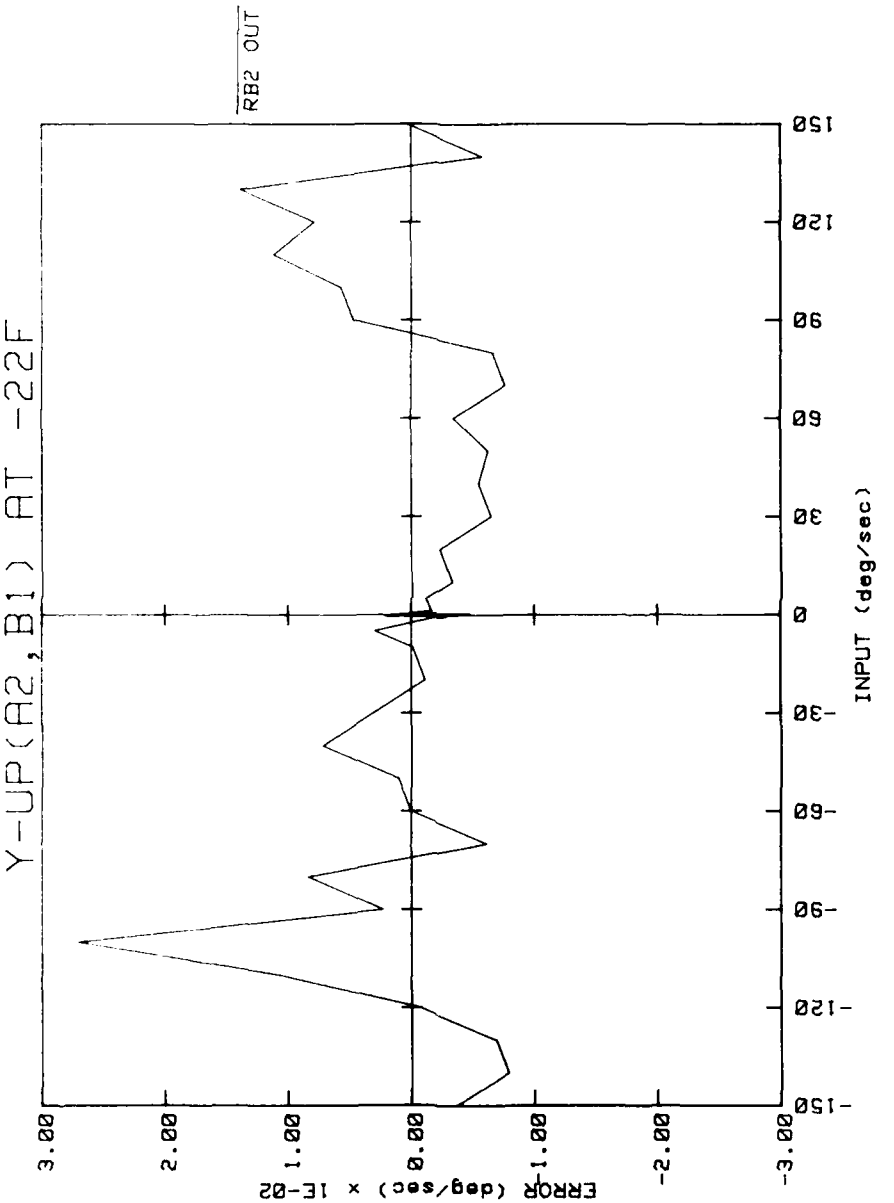

Figure 13. Input-output characteristics.

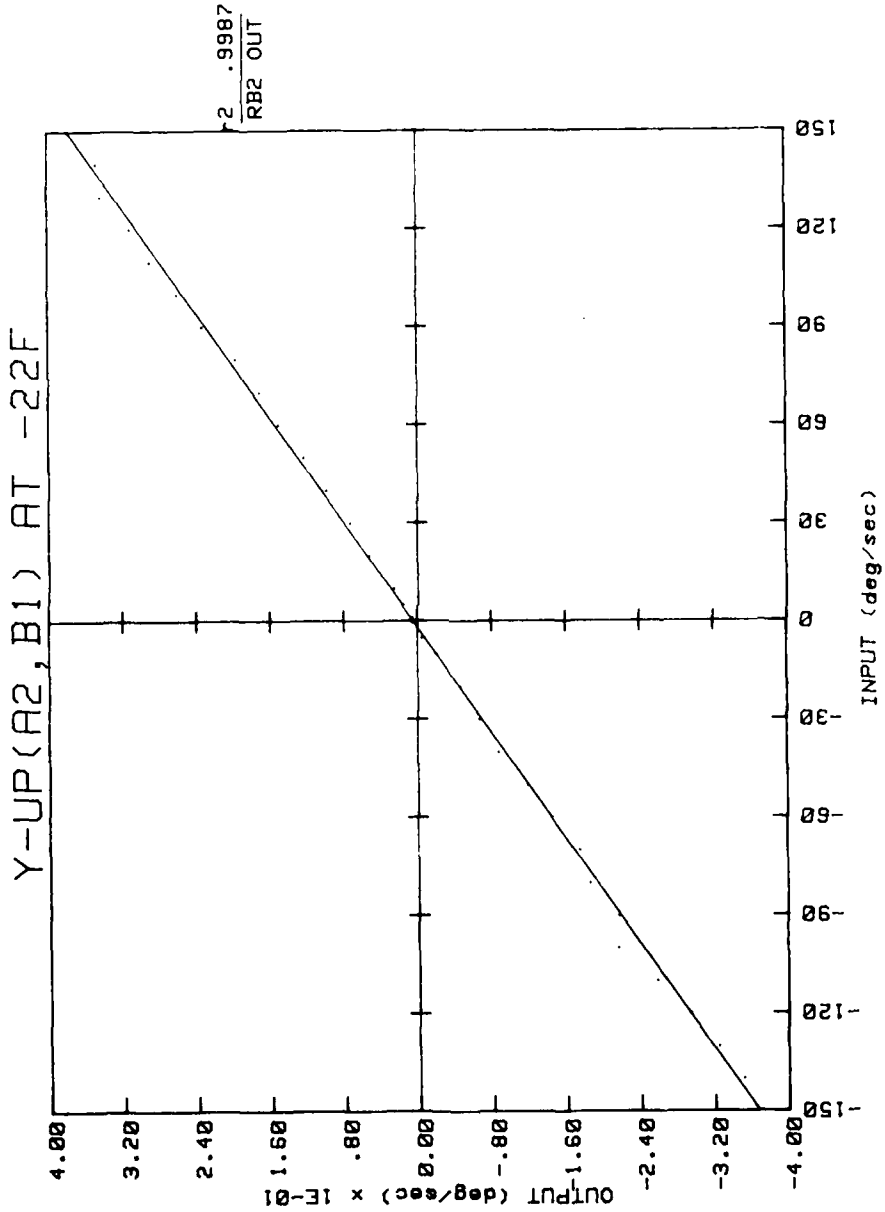

Figure 12. Input-output characteristics.

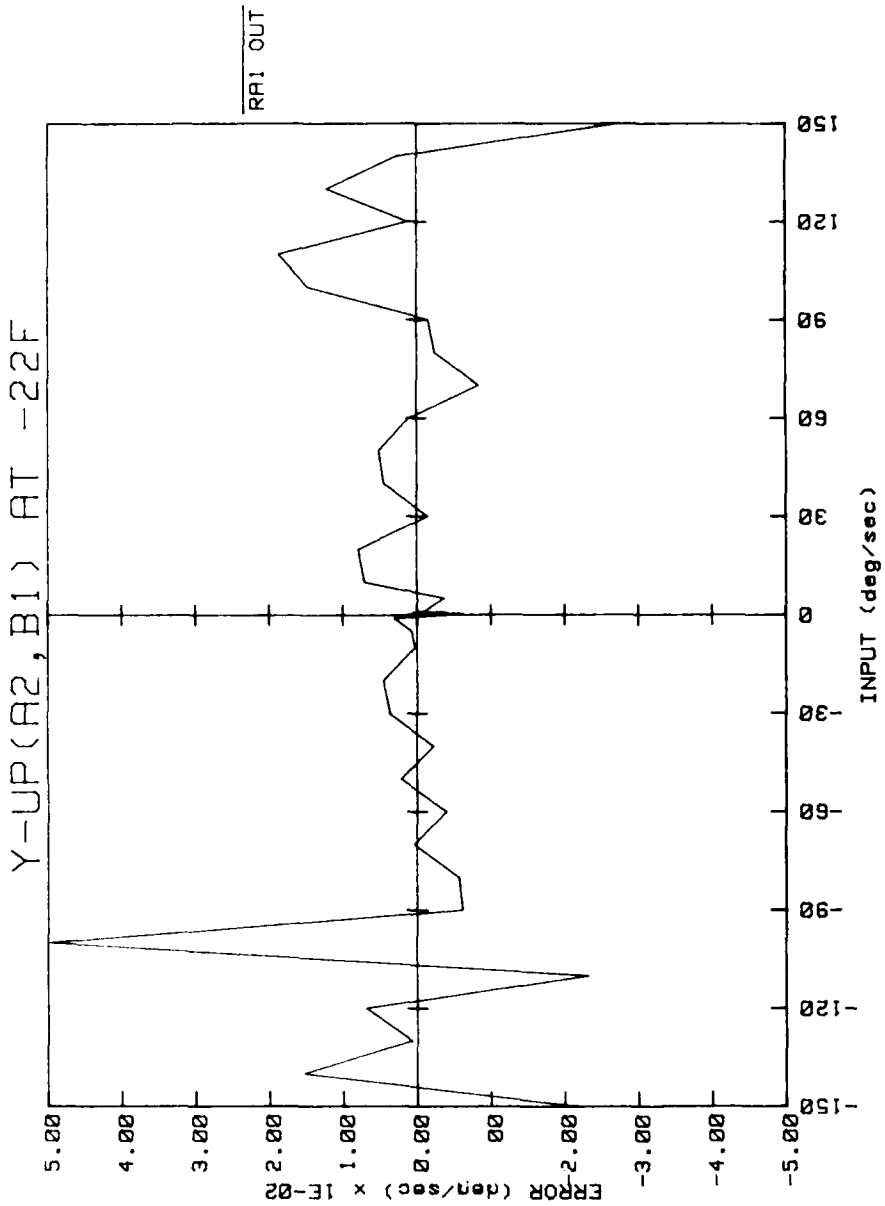

Figure 11. Input-output characteristics.

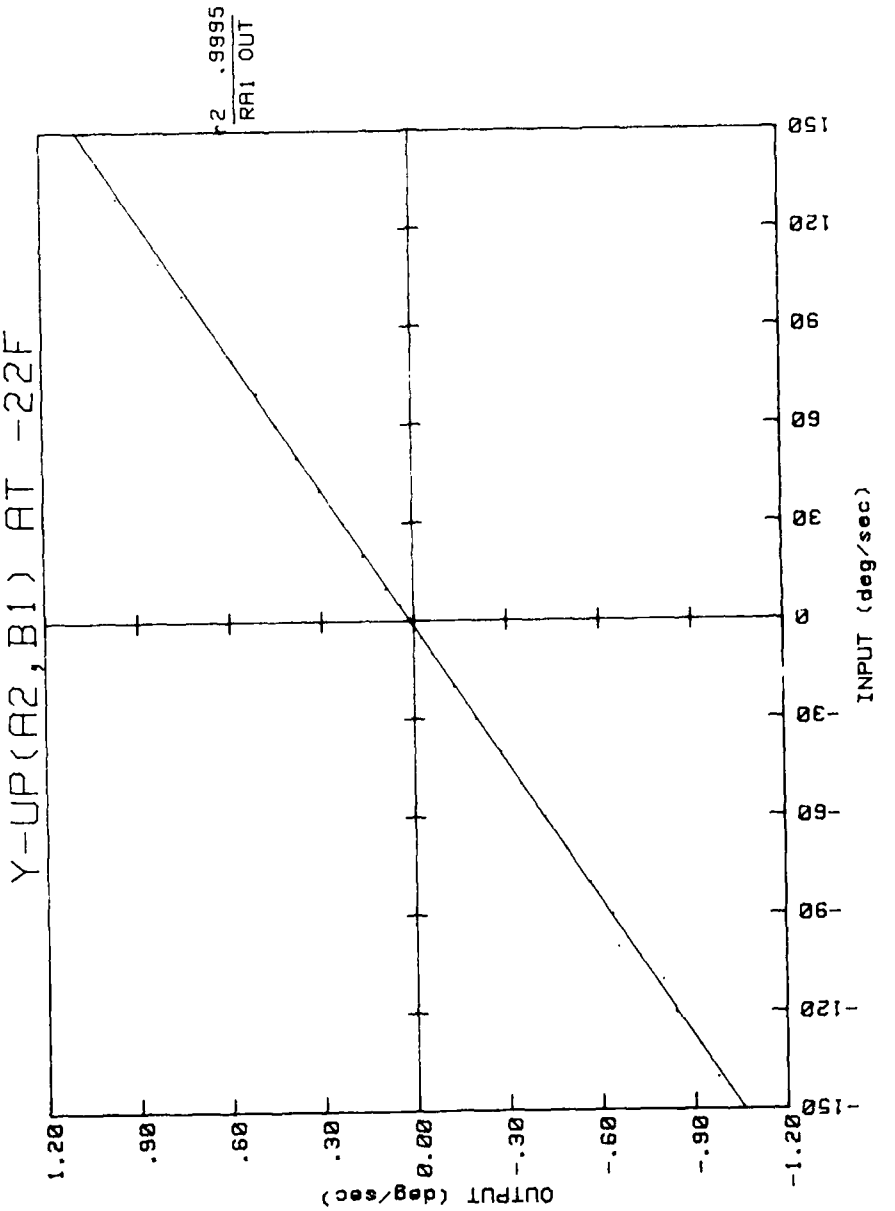

Figure 10. Input-output characteristics.

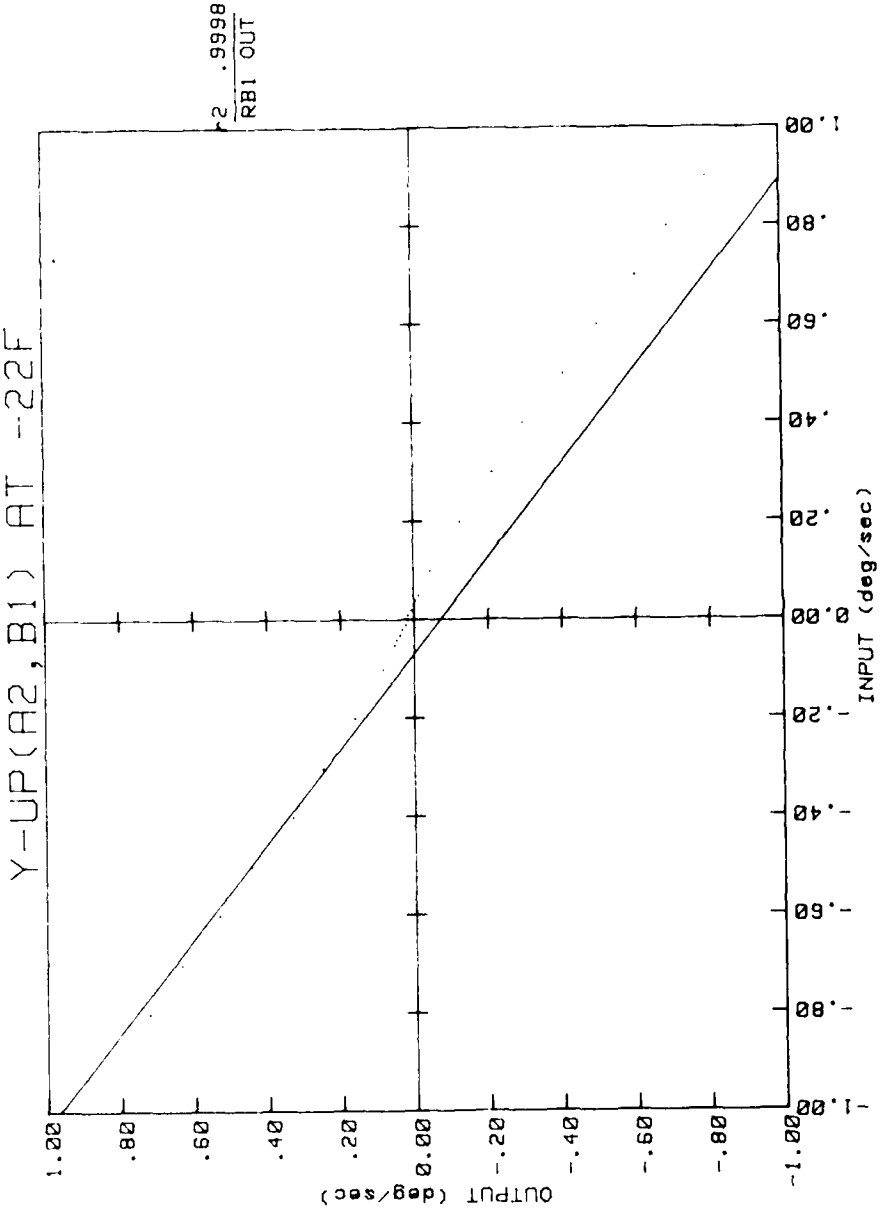

Figure 9. Input-output characteristics.

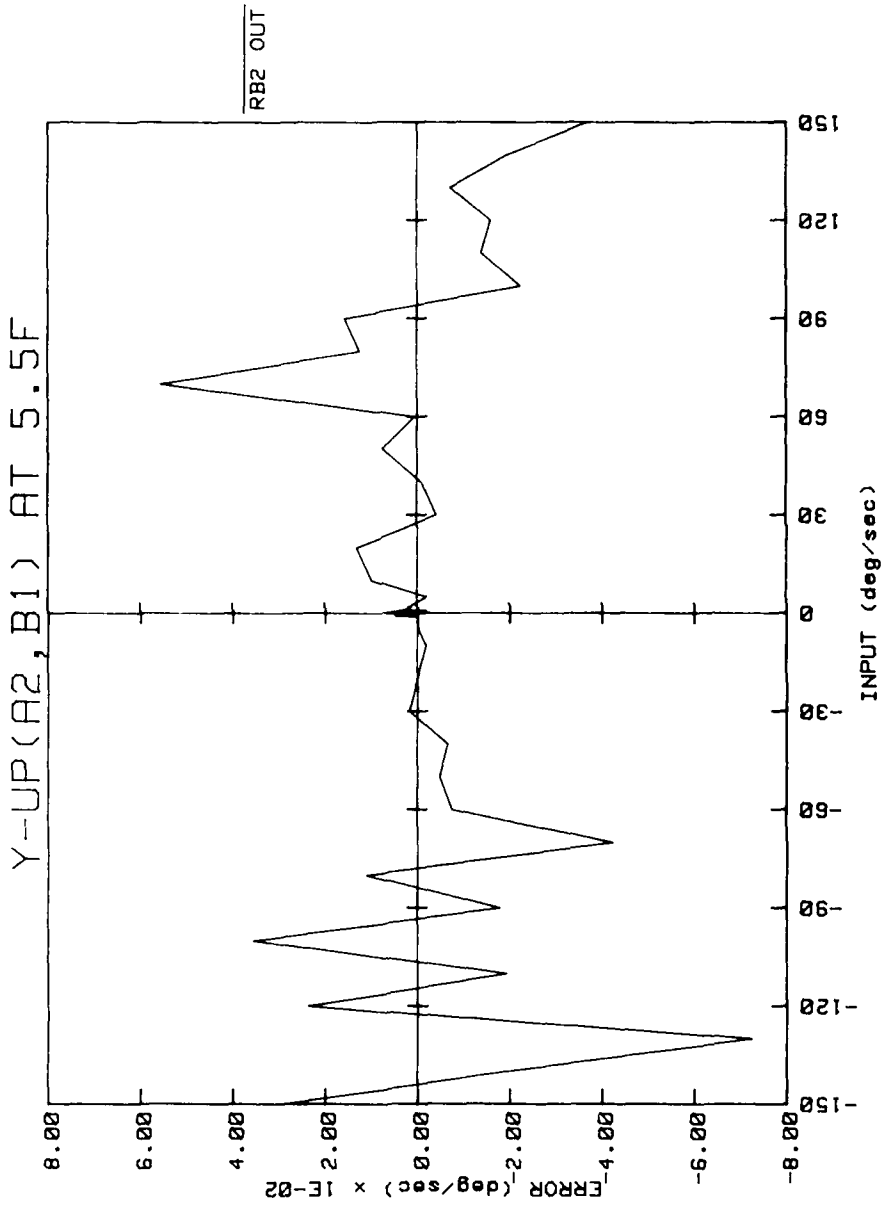

Figure 23. Input-output characteristics.

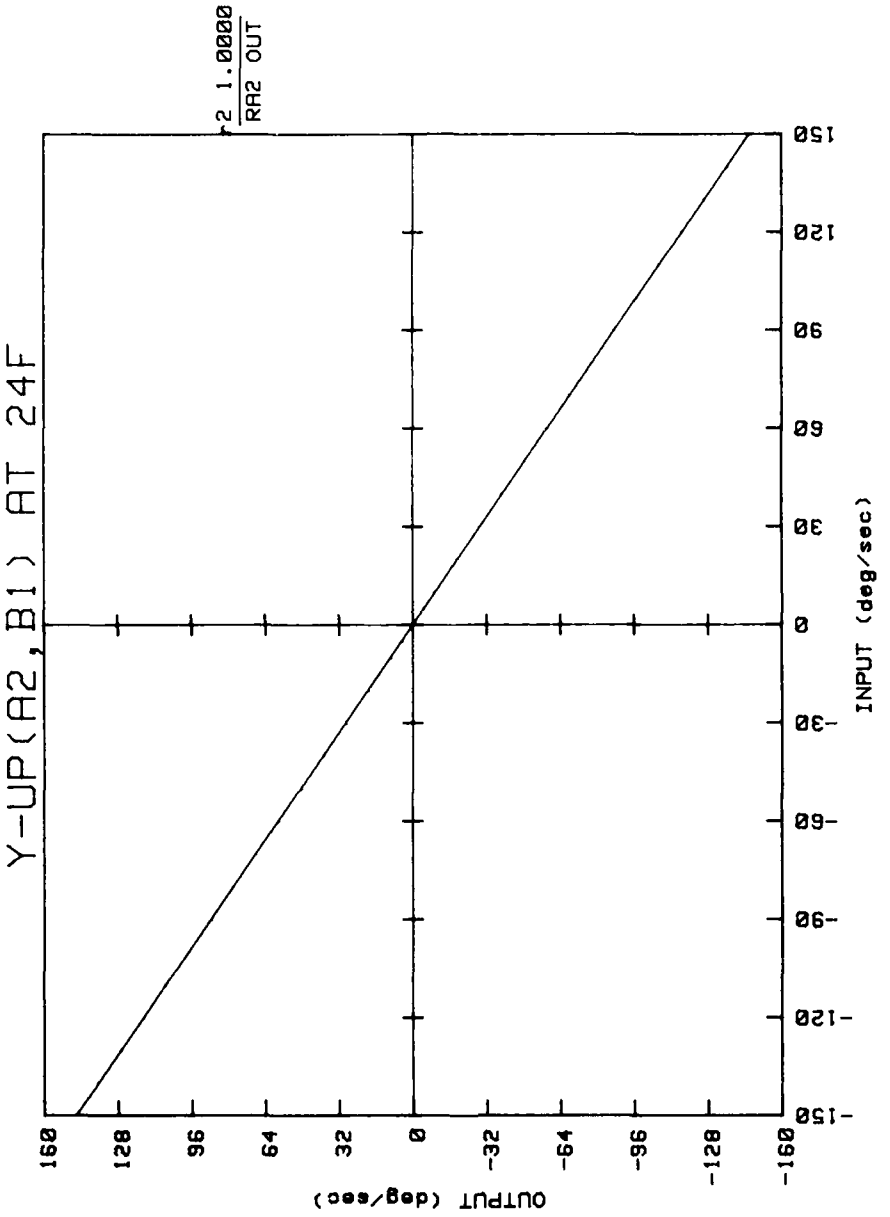

Figure 24. Input-output characteristics.

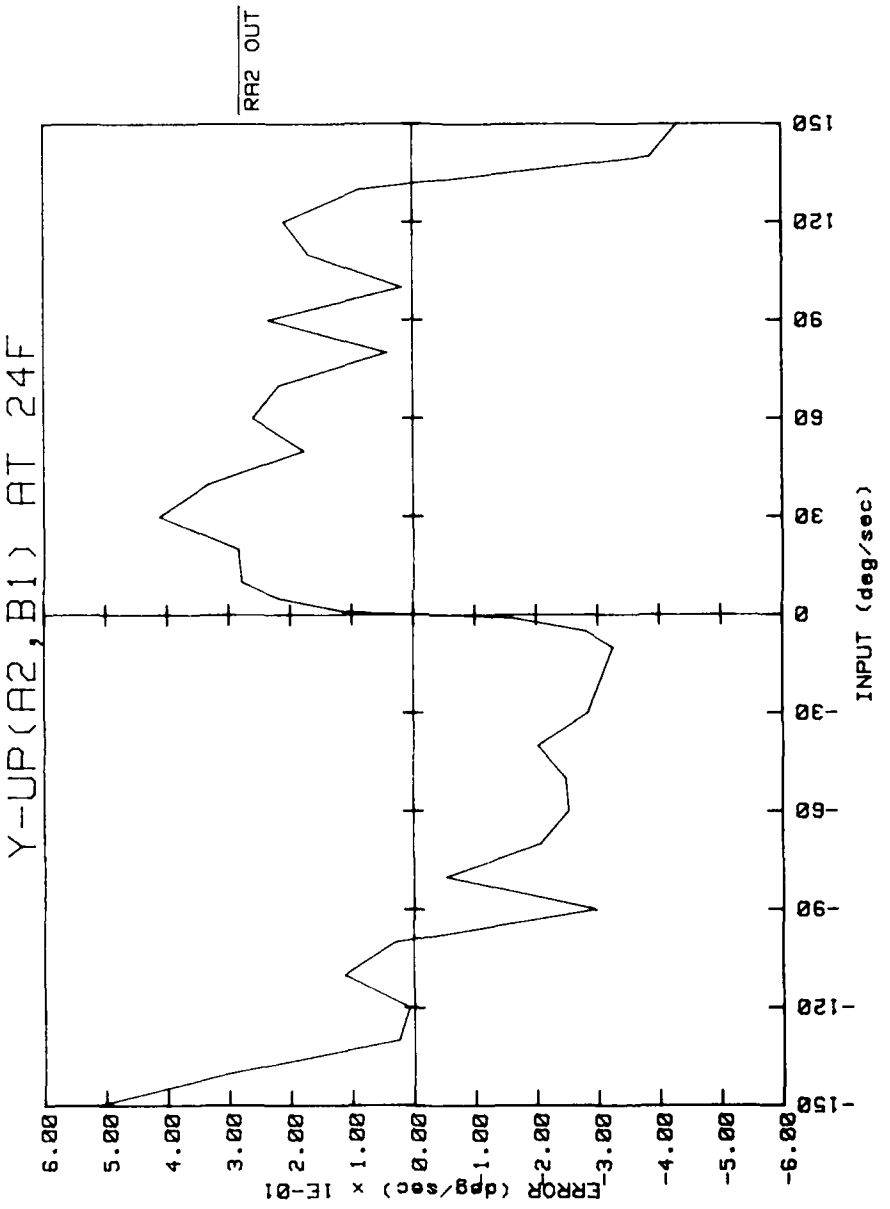

Figure 25. Input-output characteristics.

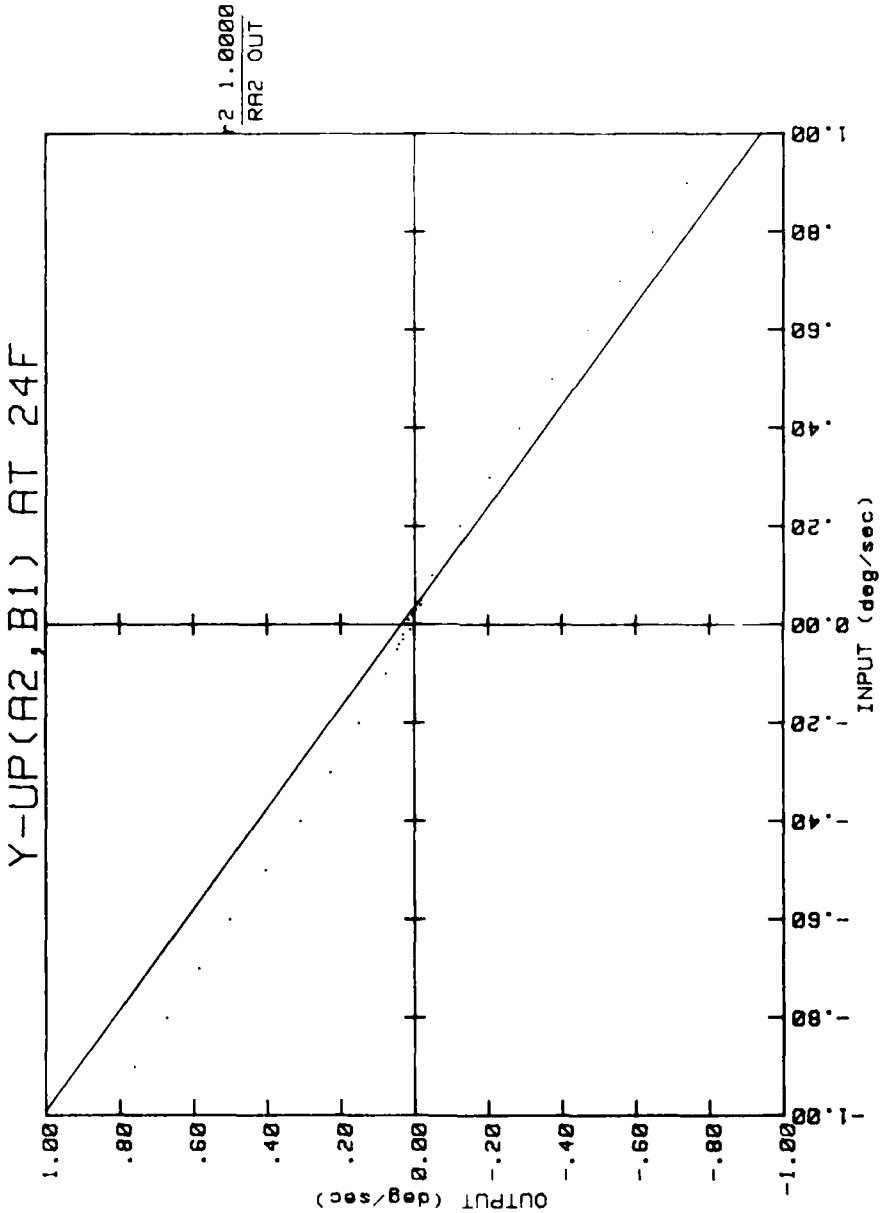

Figure 26. Input-output characteristics.

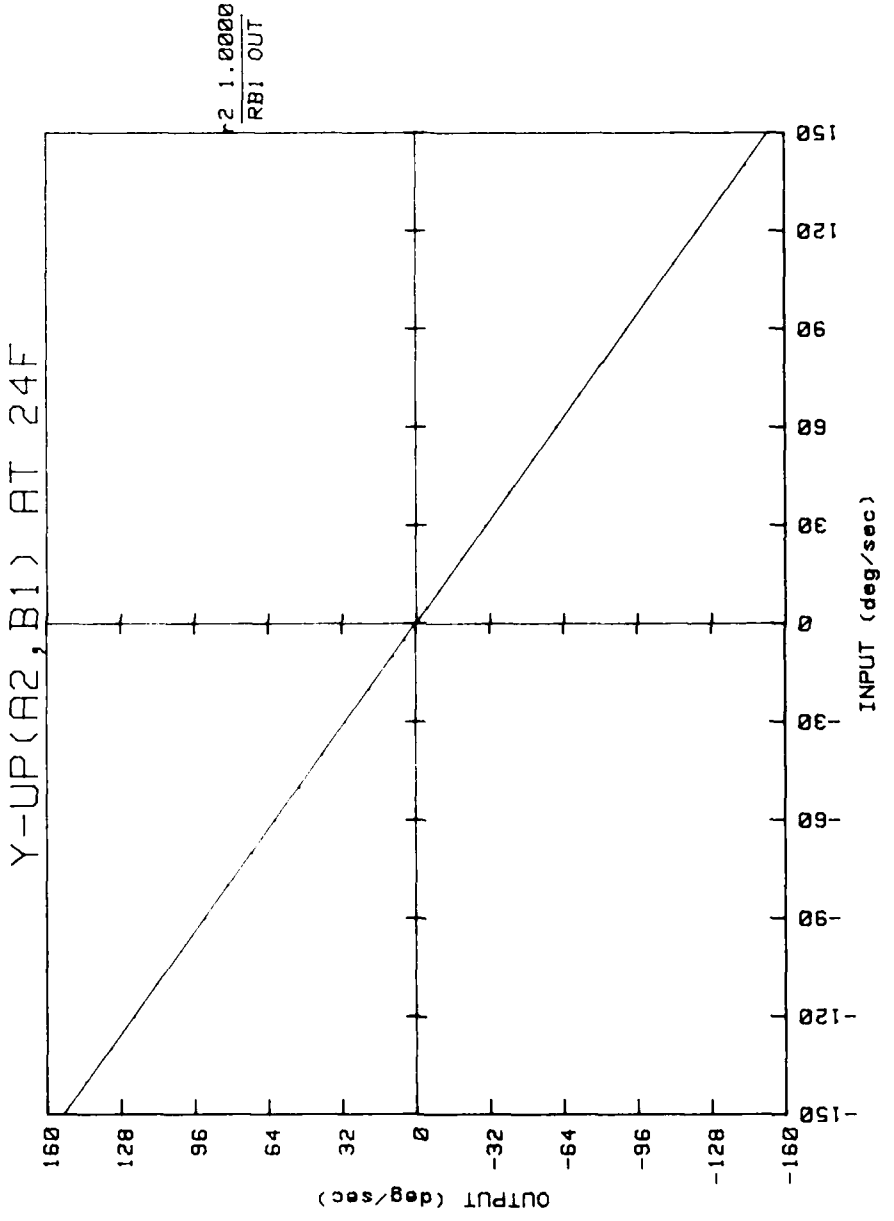

Figure 27. Input-output characteristics.

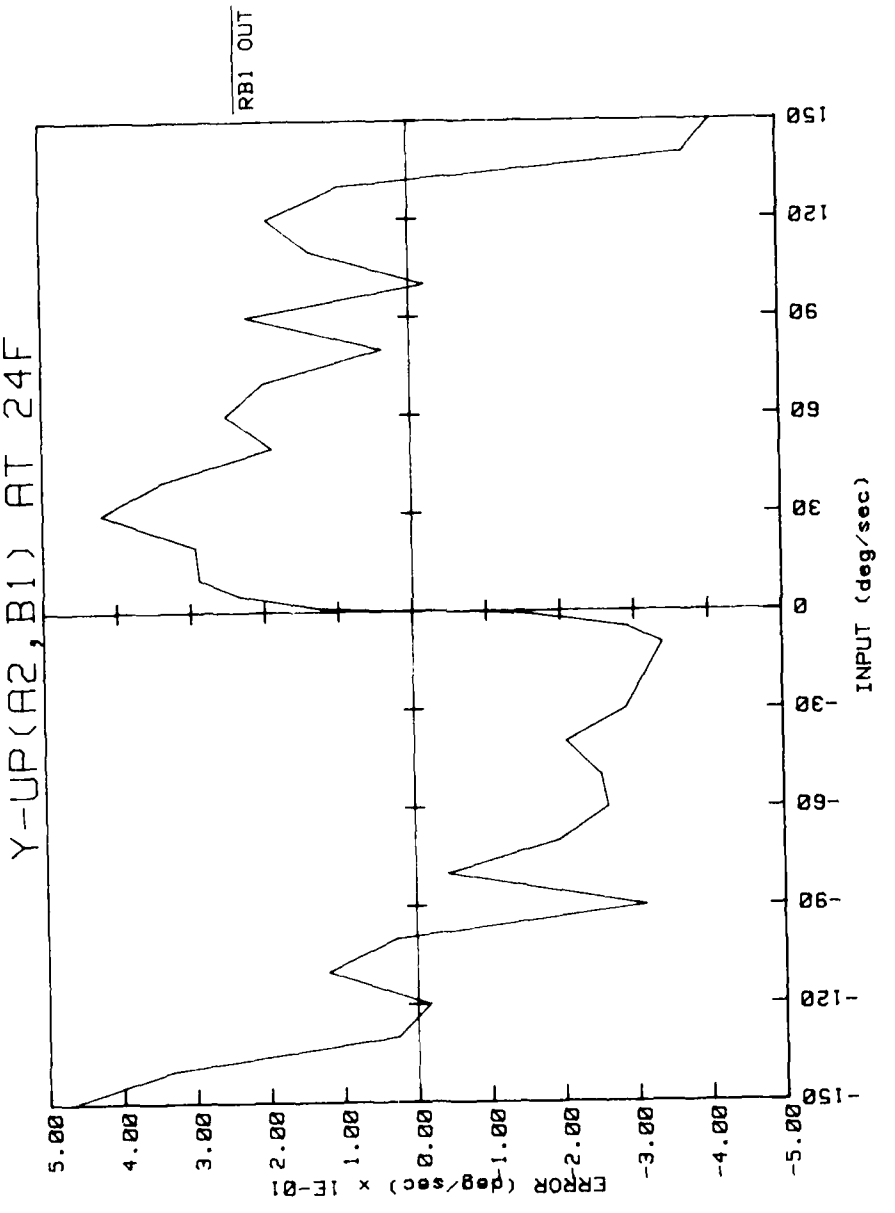

Figure 28. Input-output characteristics.

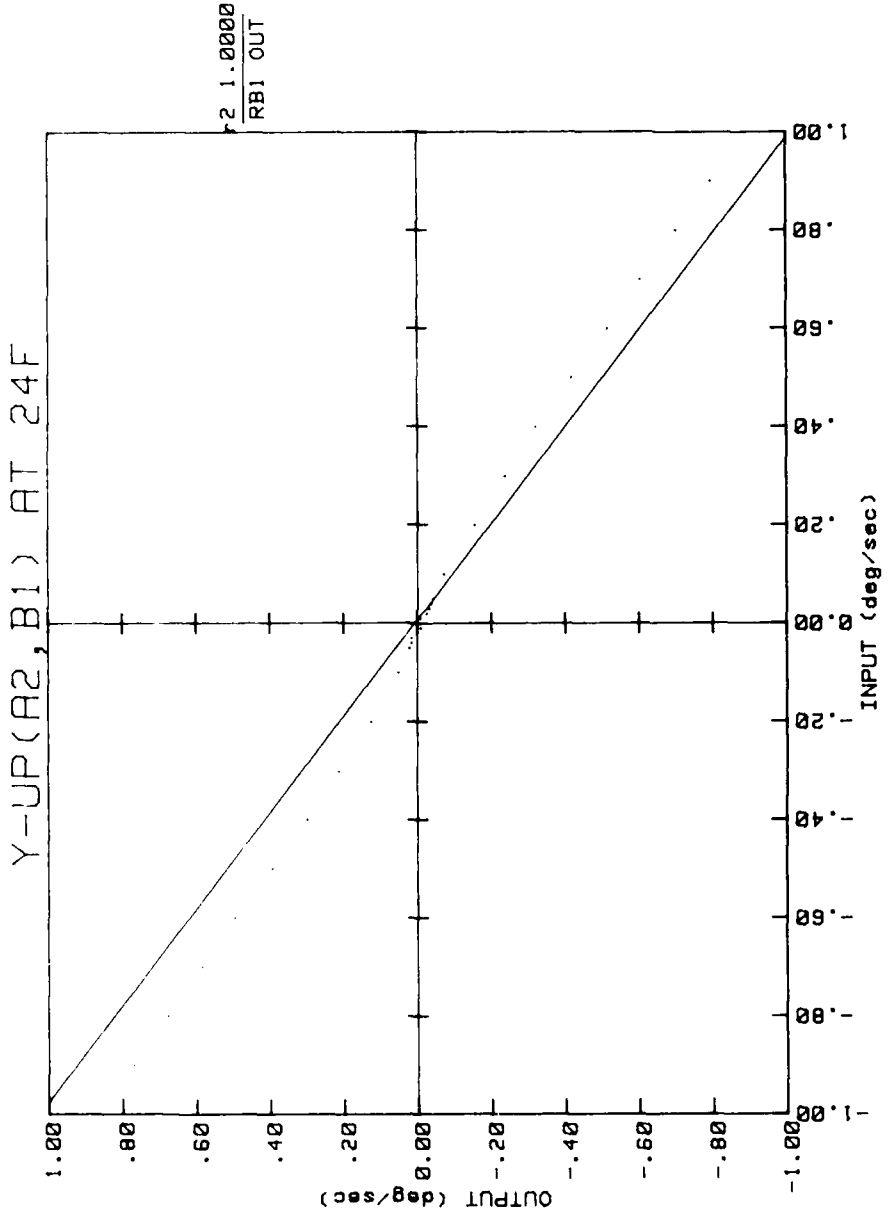

Figure 29. Input-output characteristics.

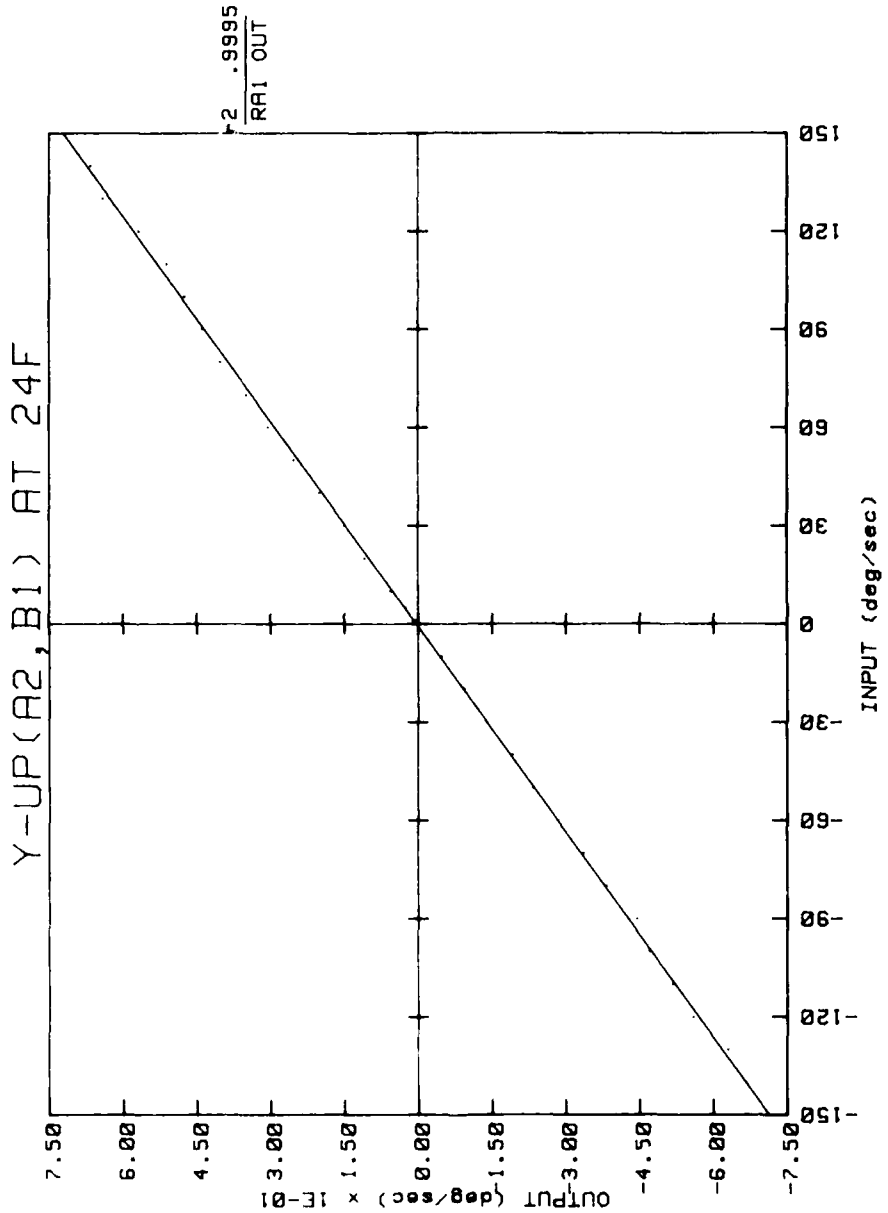

Figure 30. Input-output characteristics.

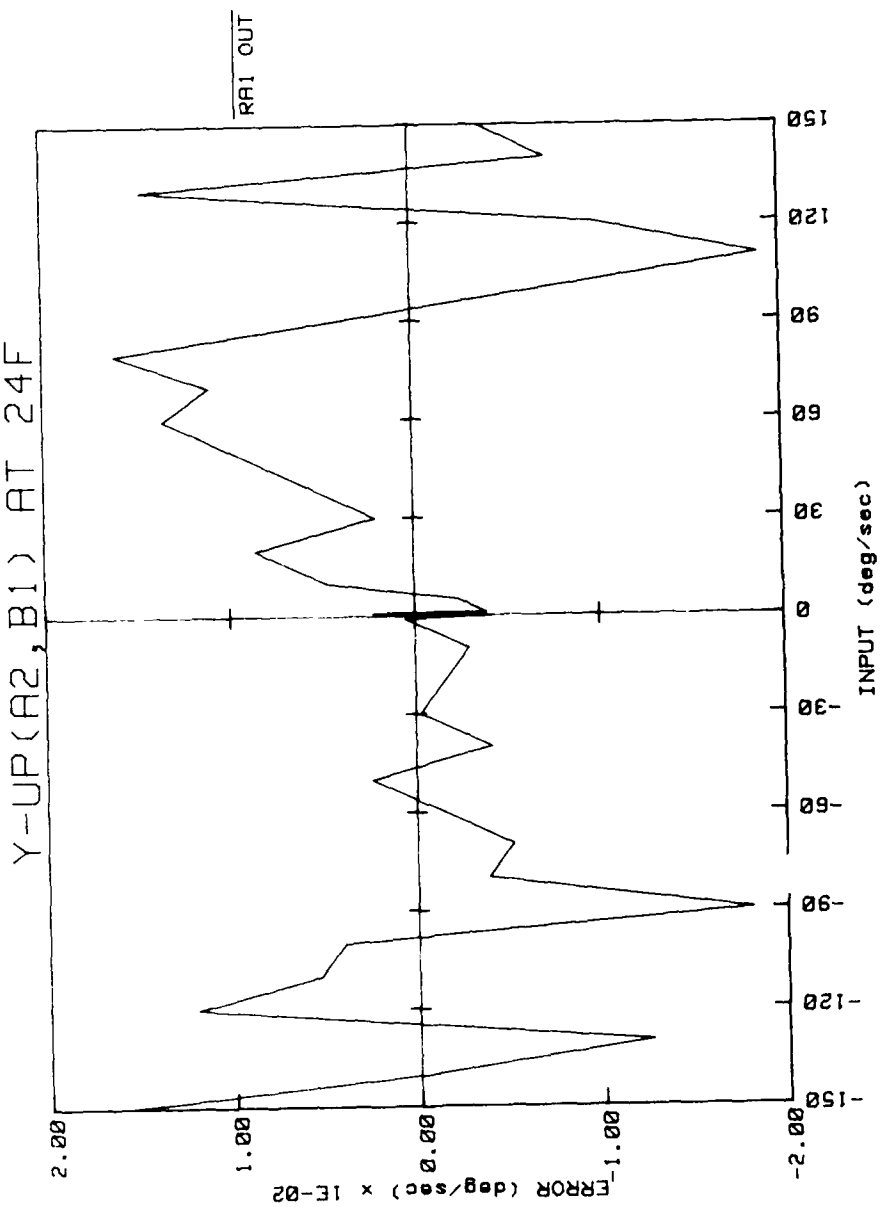

Figure 31. Input-output characteristics.

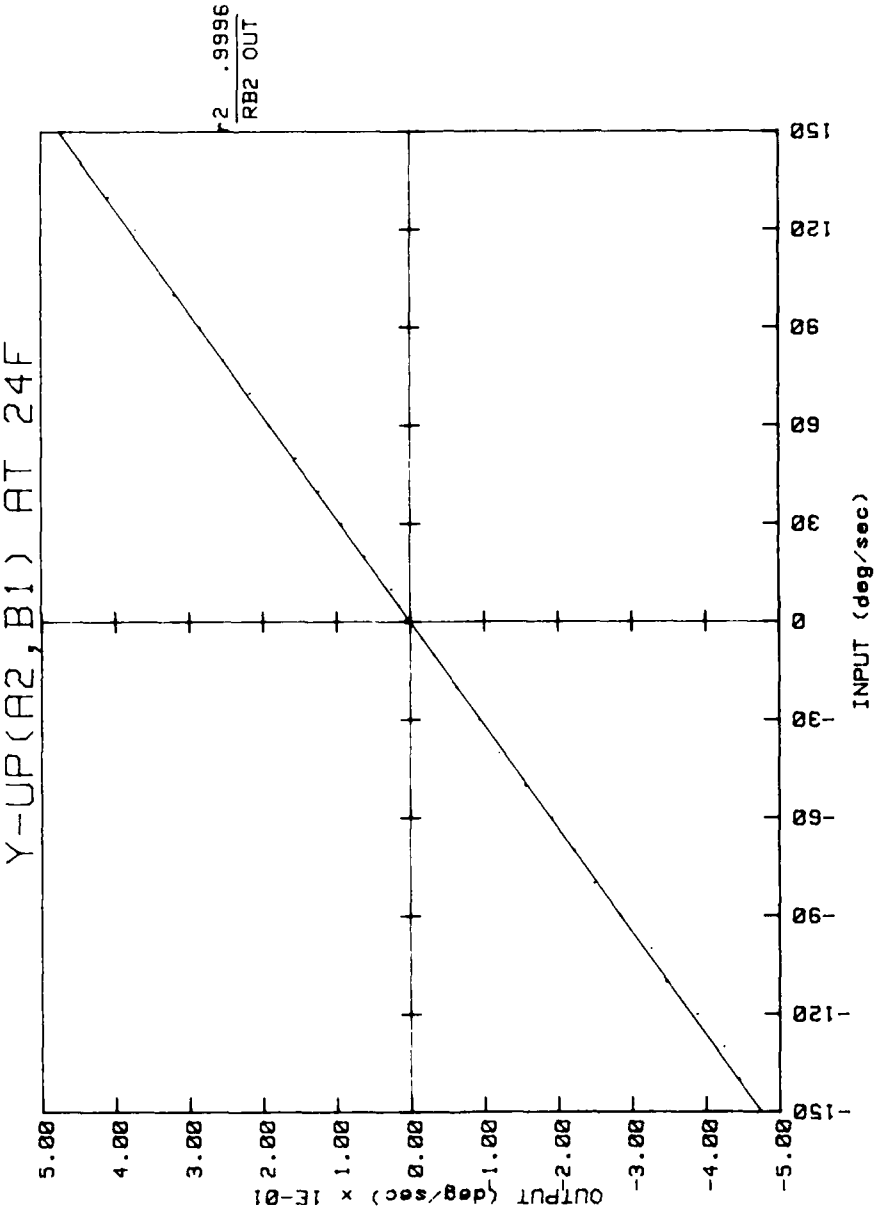

Figure 32. Input-output characteristics.

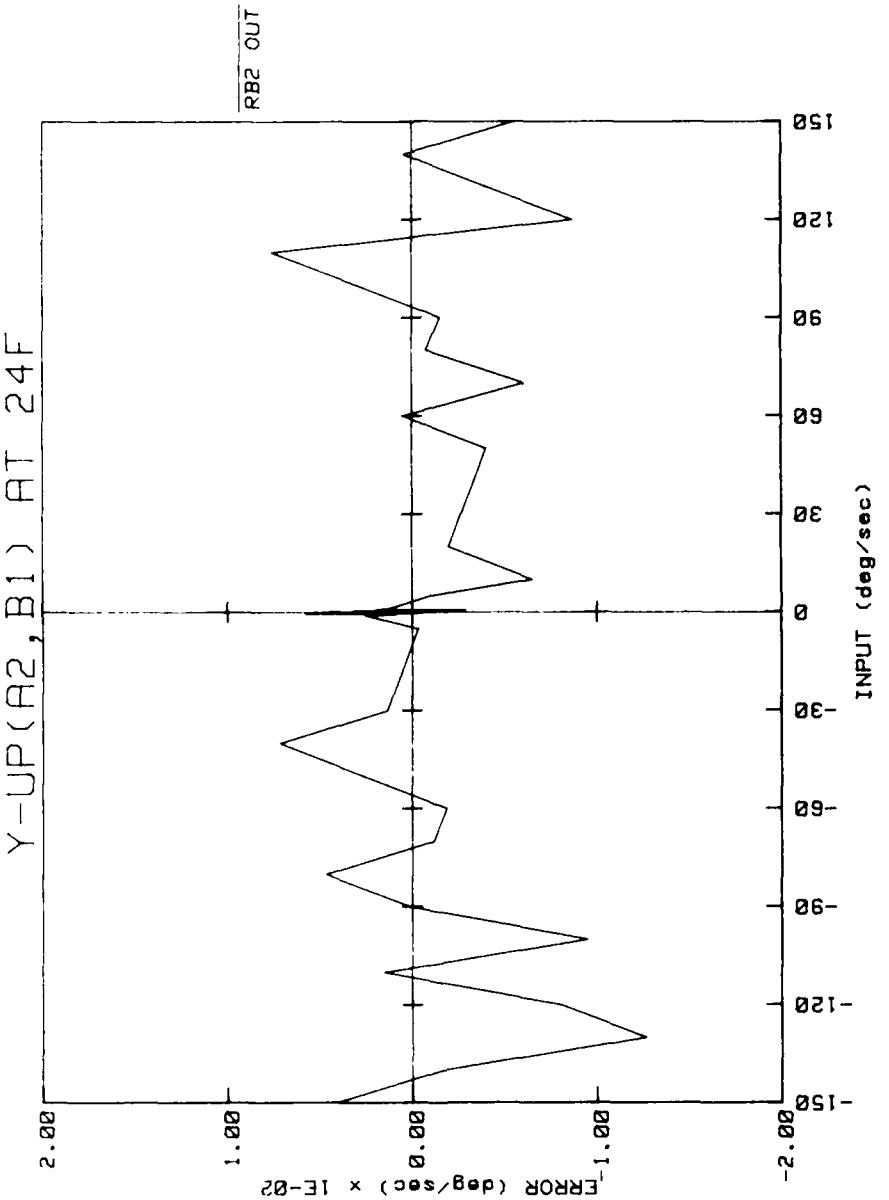

Figure 33. Input-output characteristics.

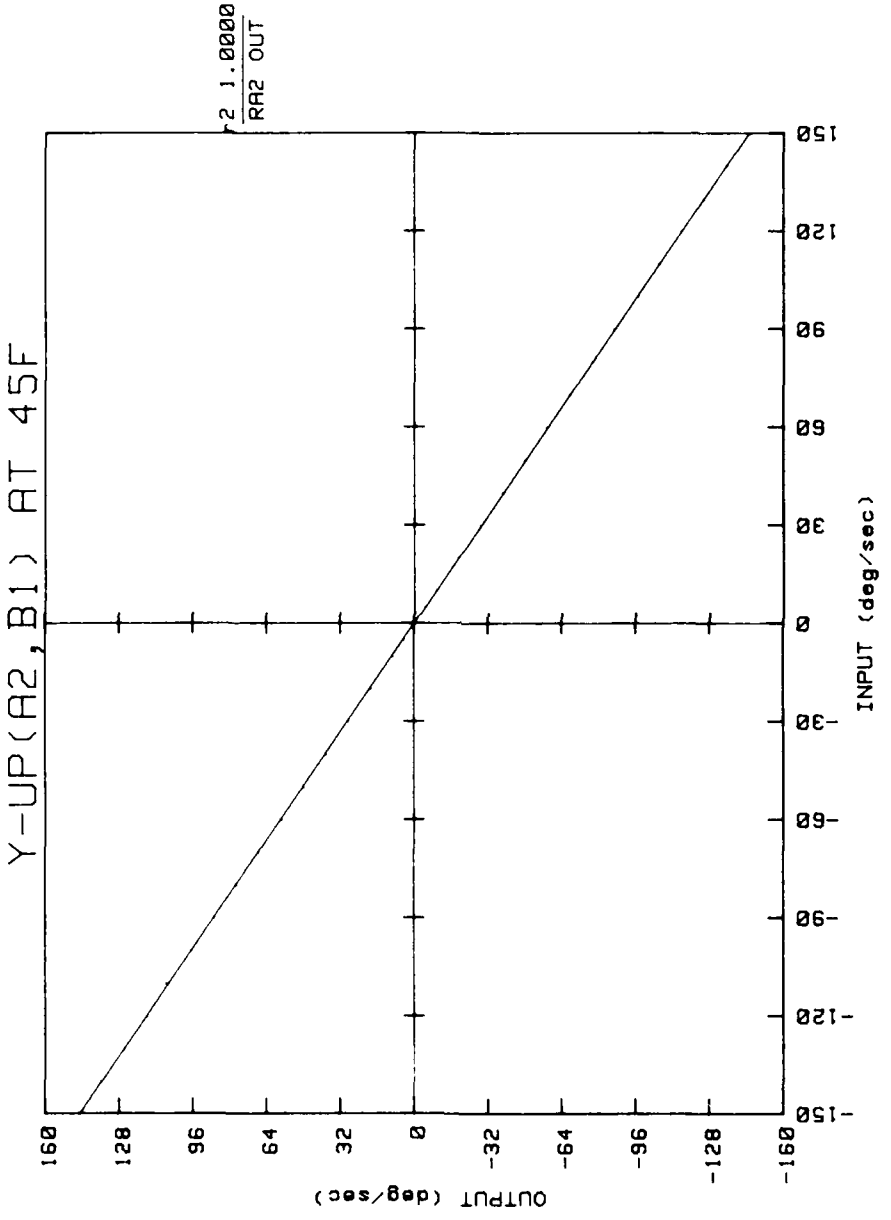

Figure 34. Input-output characteristics.

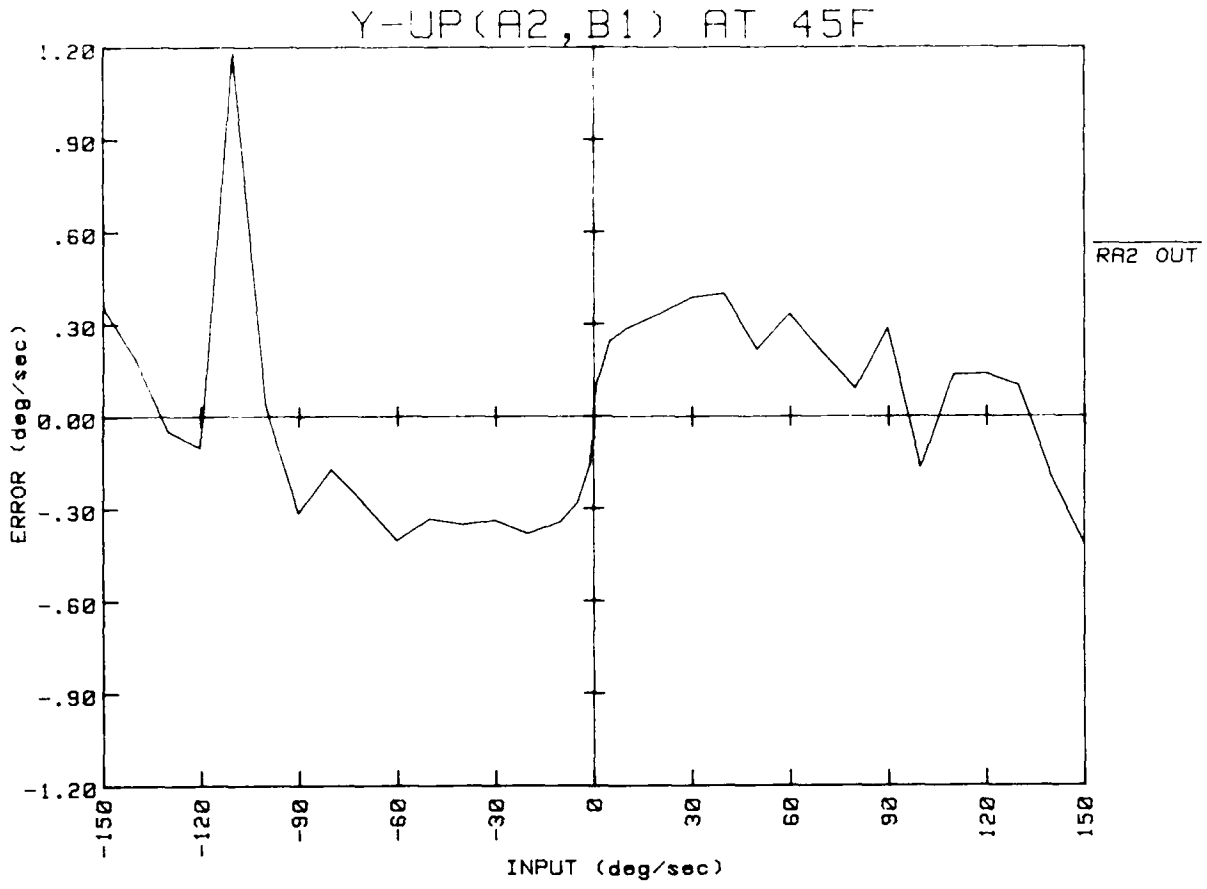

Figure 35. Input-output characteristics.

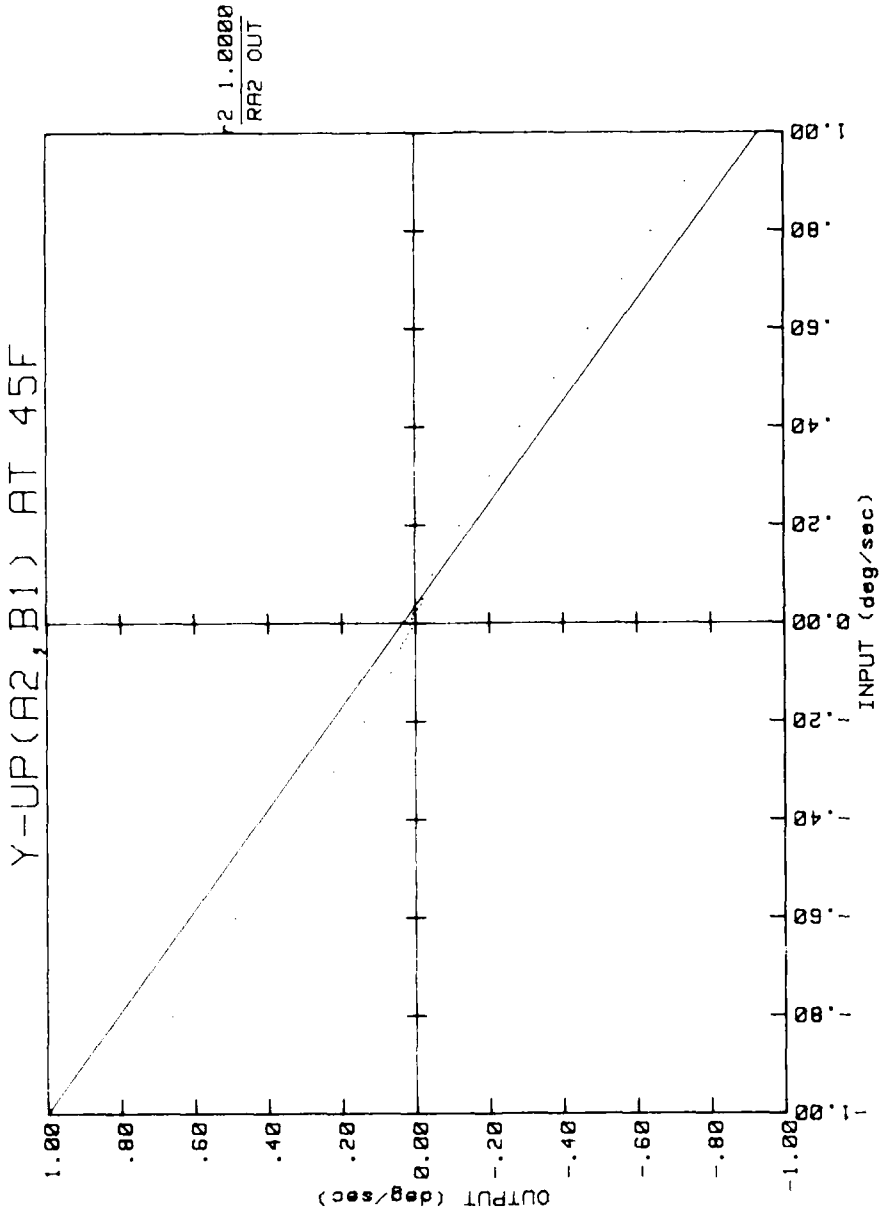

Figure 36. Input-output characteristics.

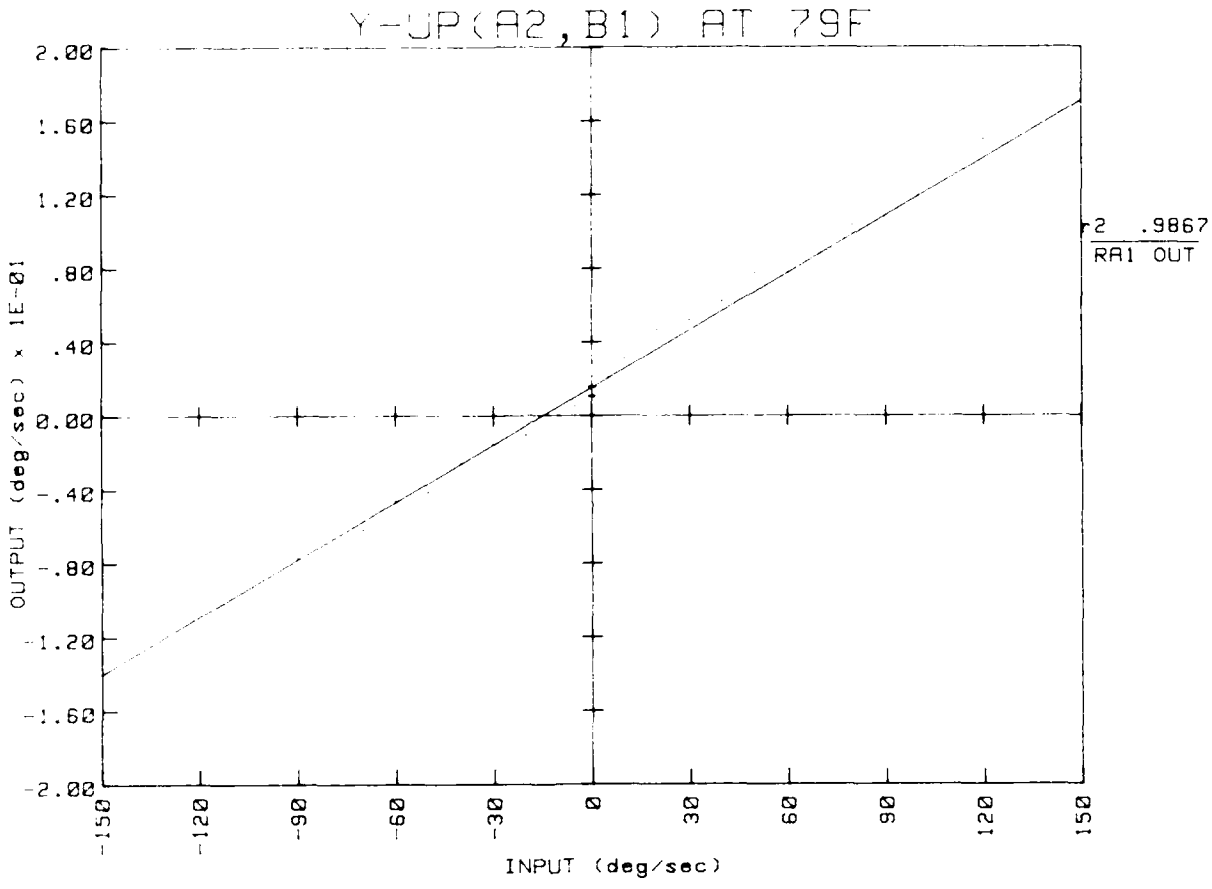

Figure 50. Input-output characteristics.

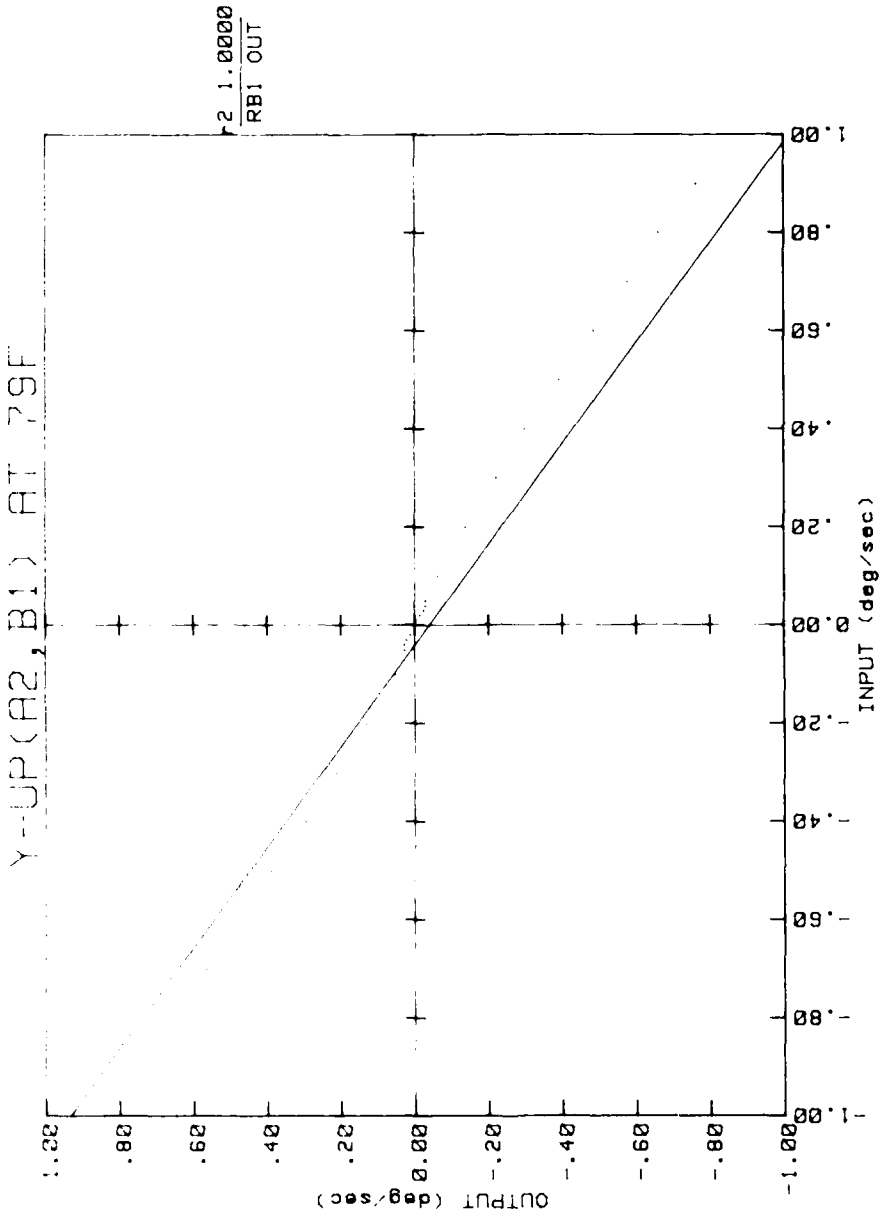

Figure 49. Input-output characteristics.

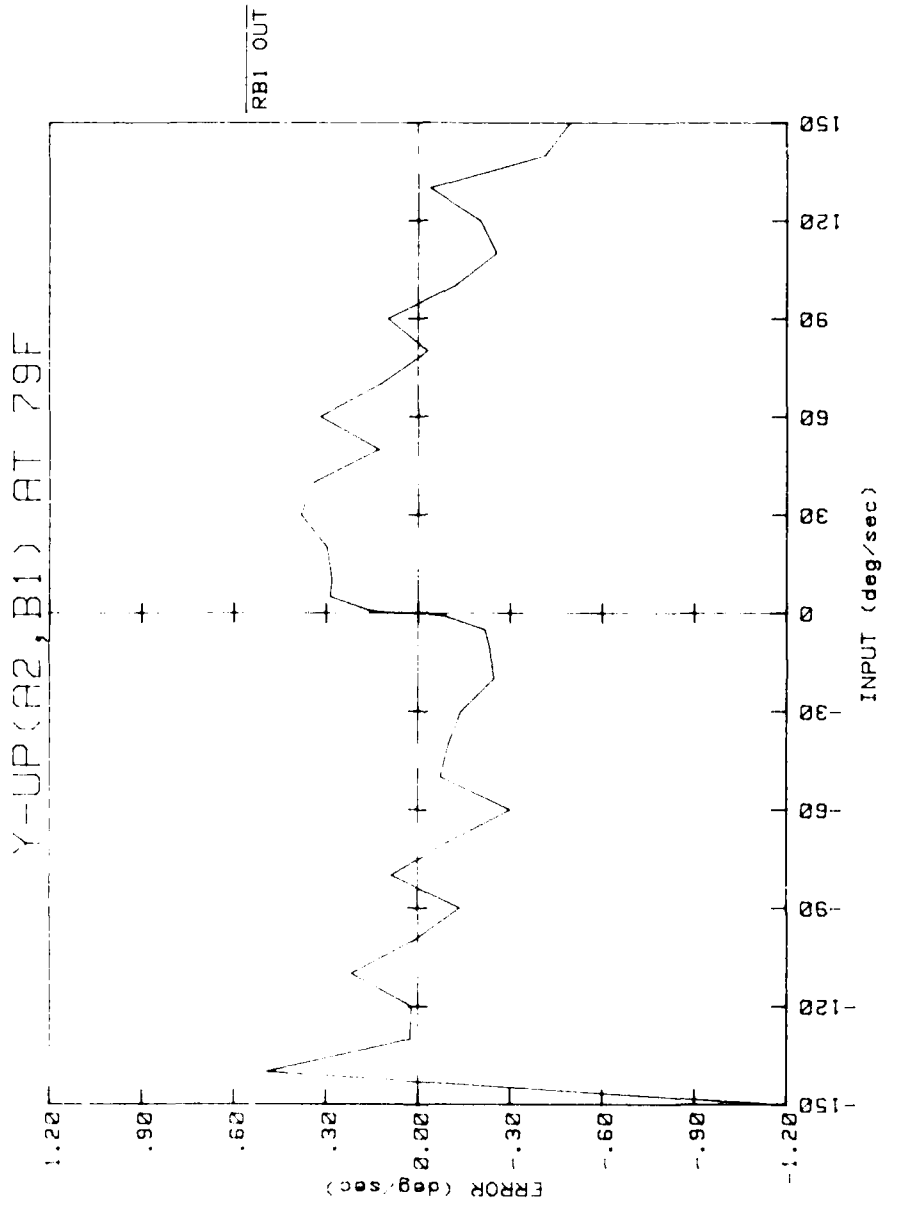

Figure 48. Input-output characteristics.

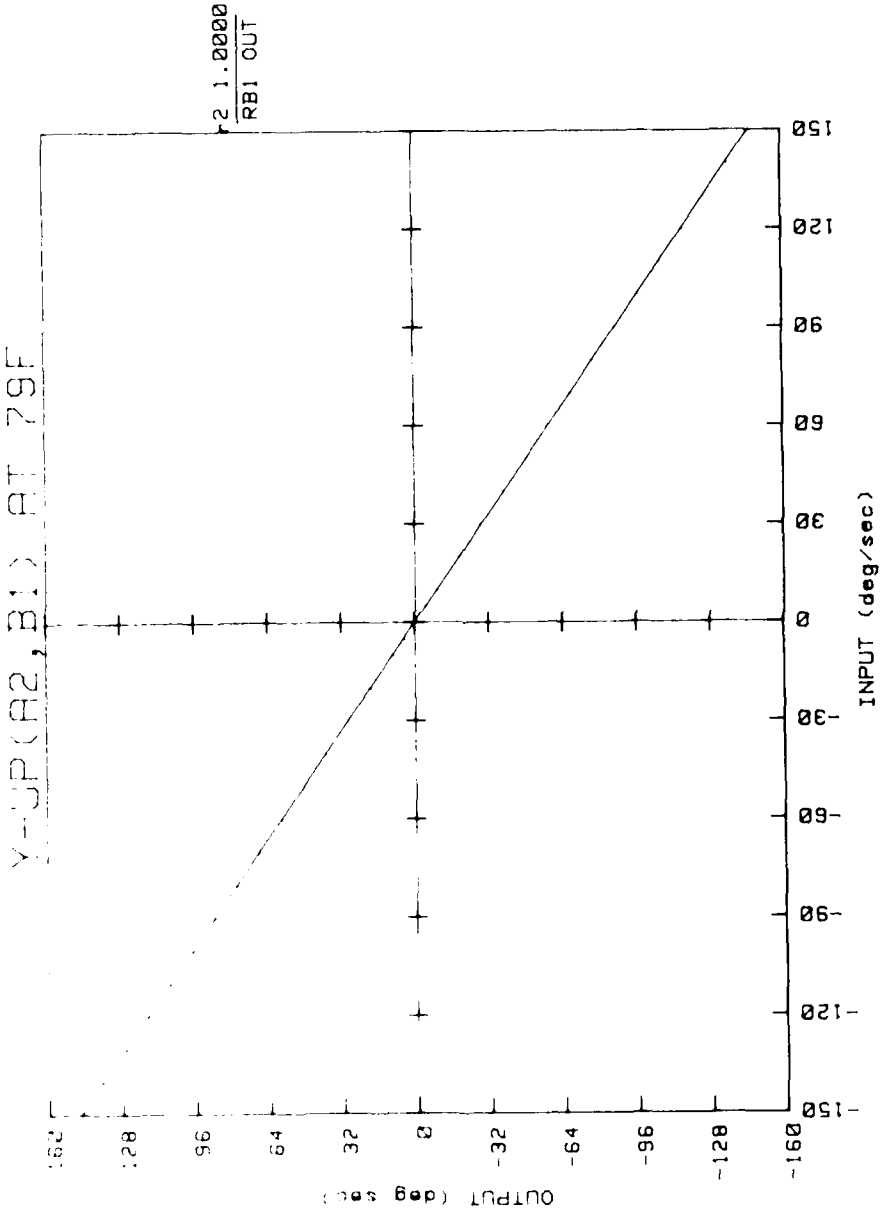

Figure 47. Input-output characteristics.

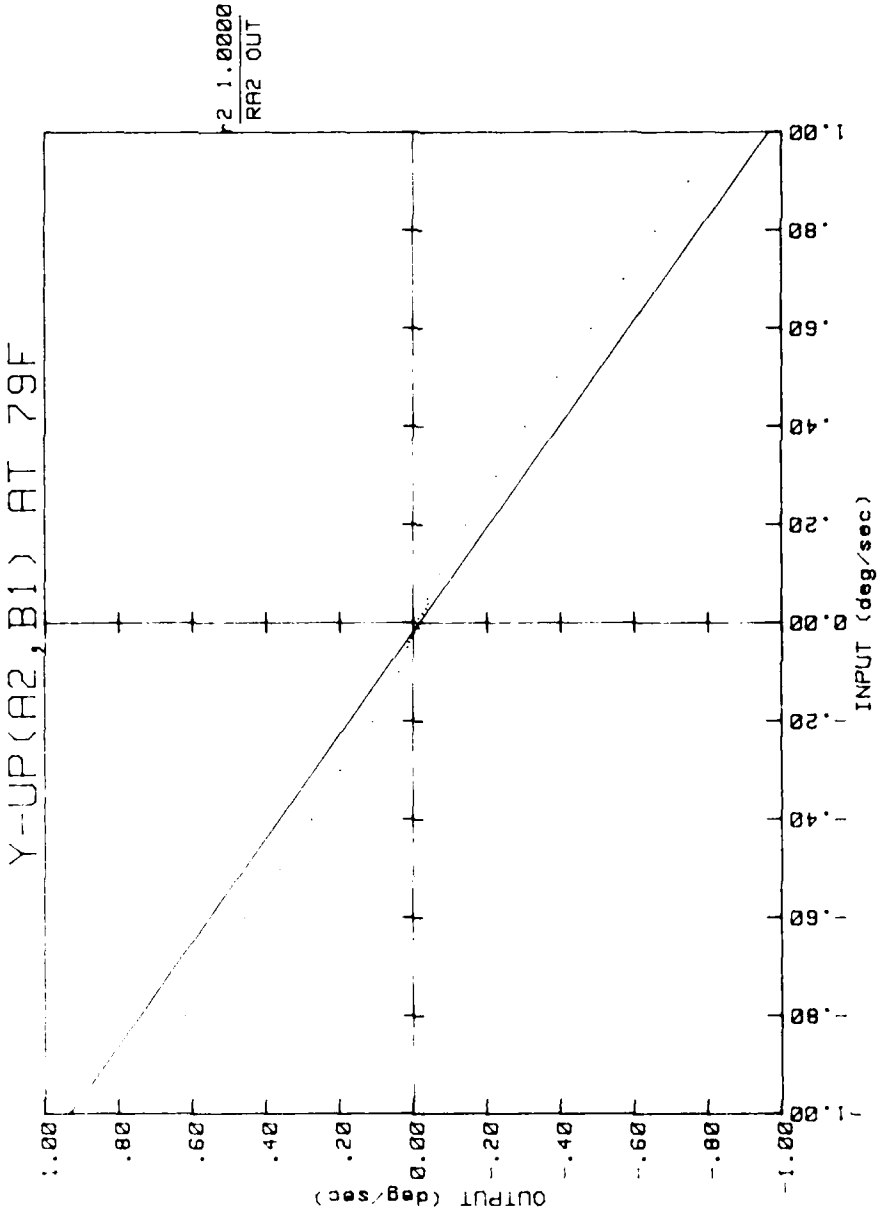

Figure 46. Input-output characteristics.

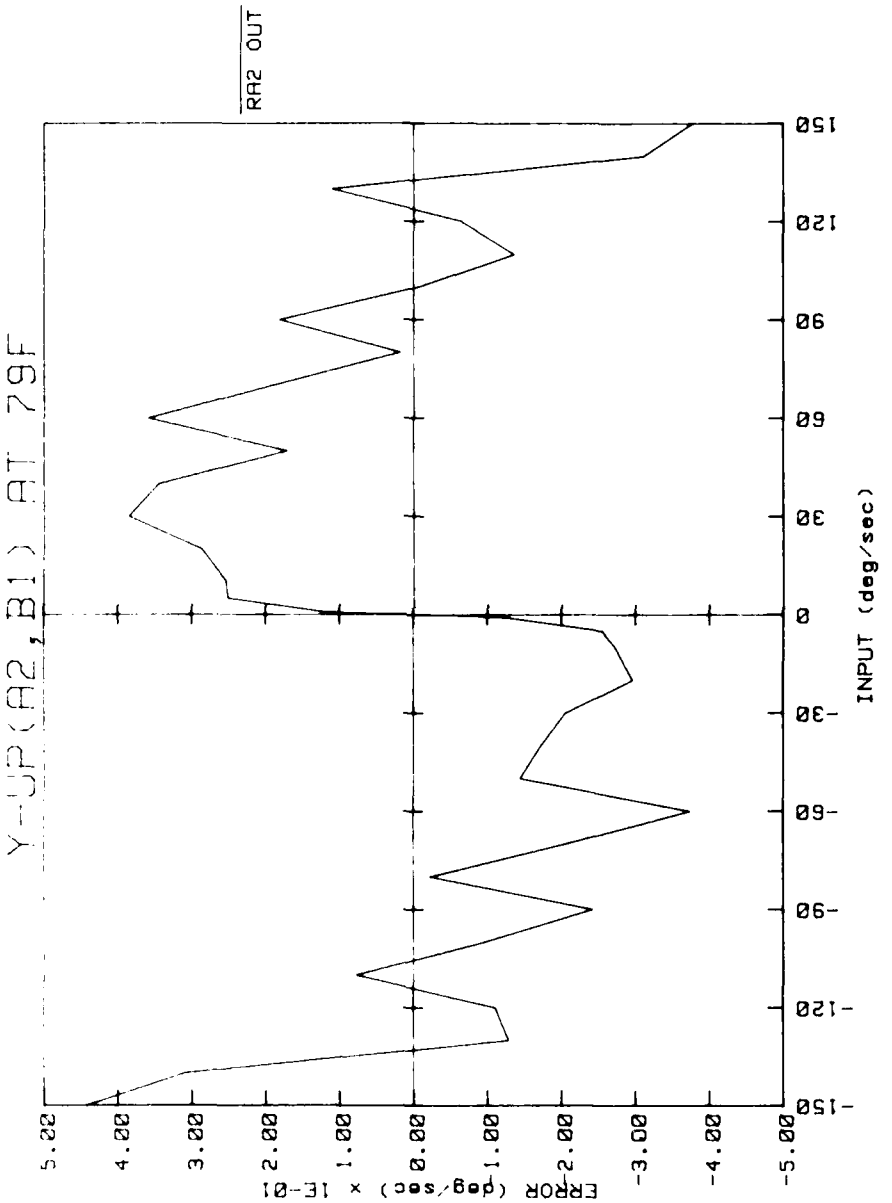

Figure 45. Input-output characteristics.

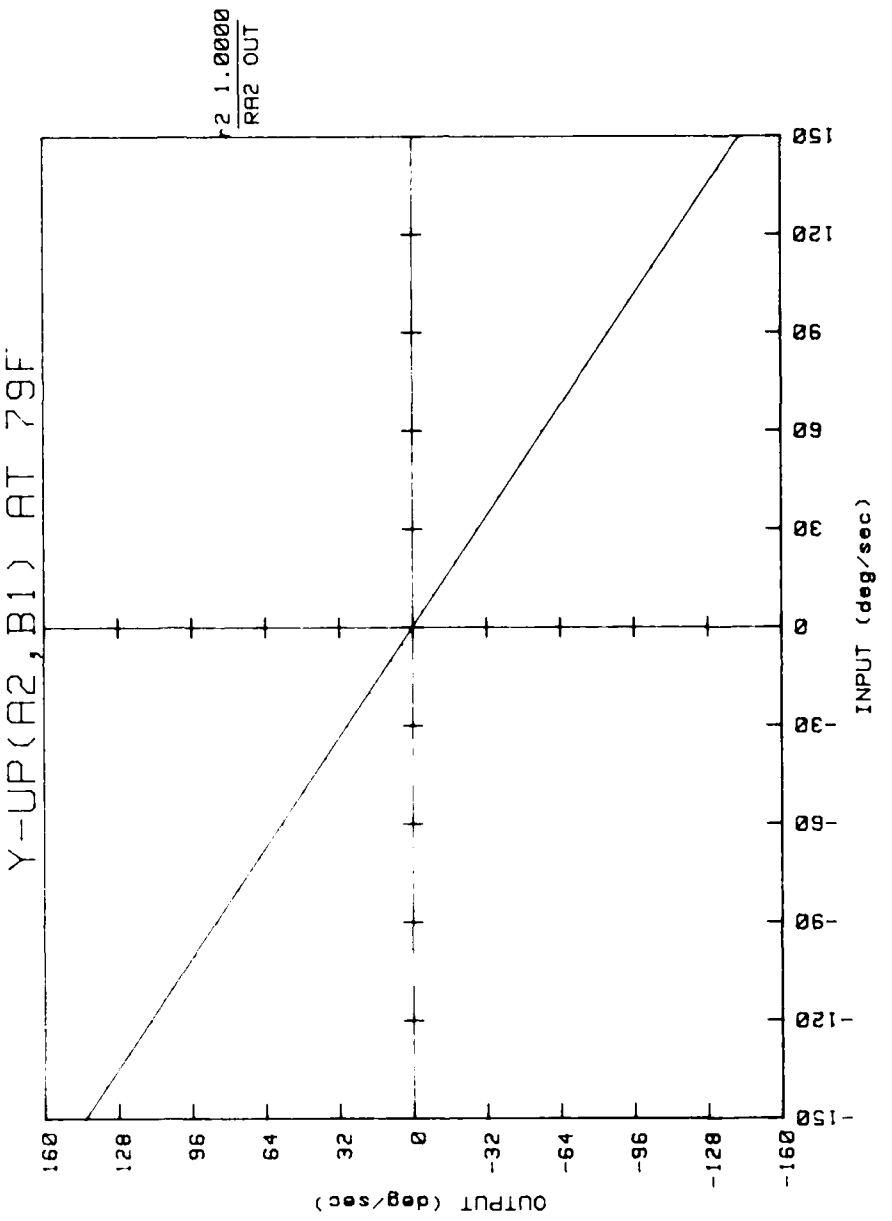

Figure 44. Input-output characteristics.

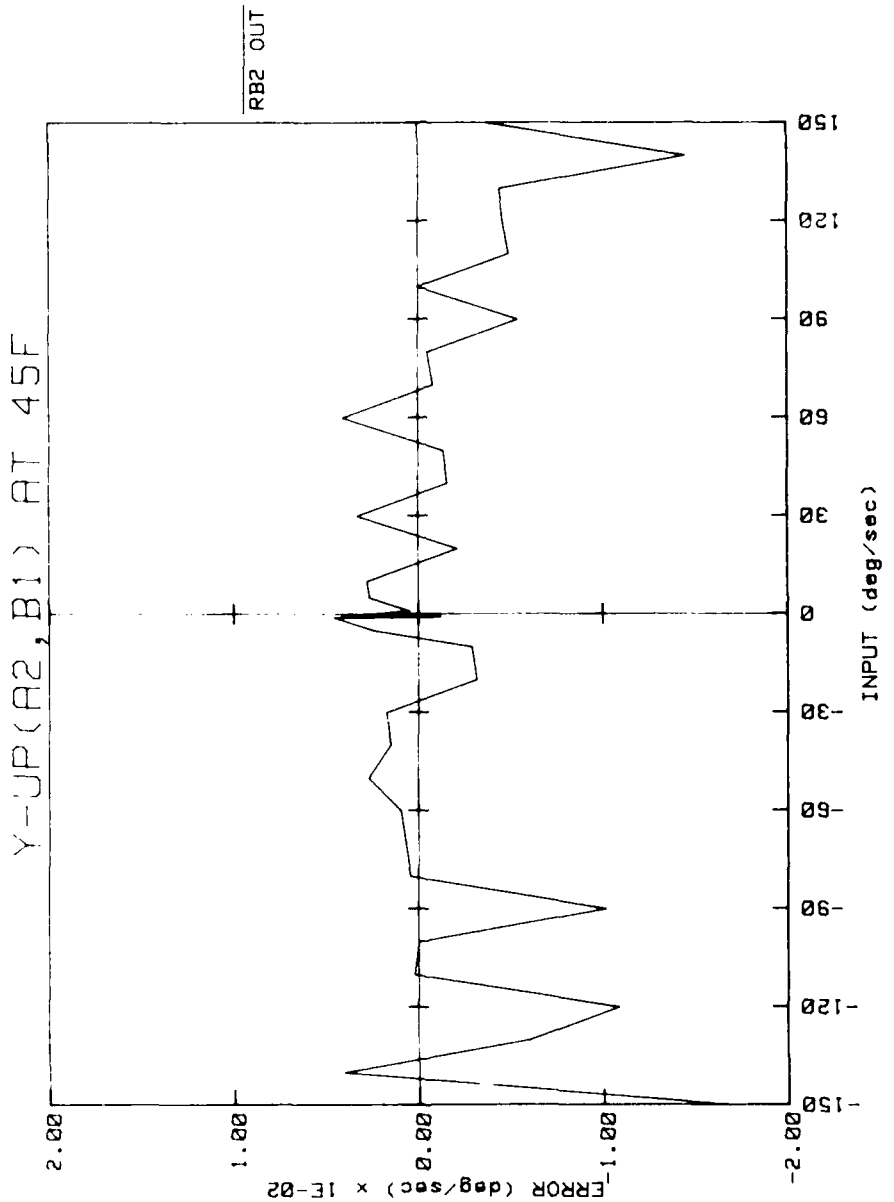

Figure 43. Input-output characteristics.

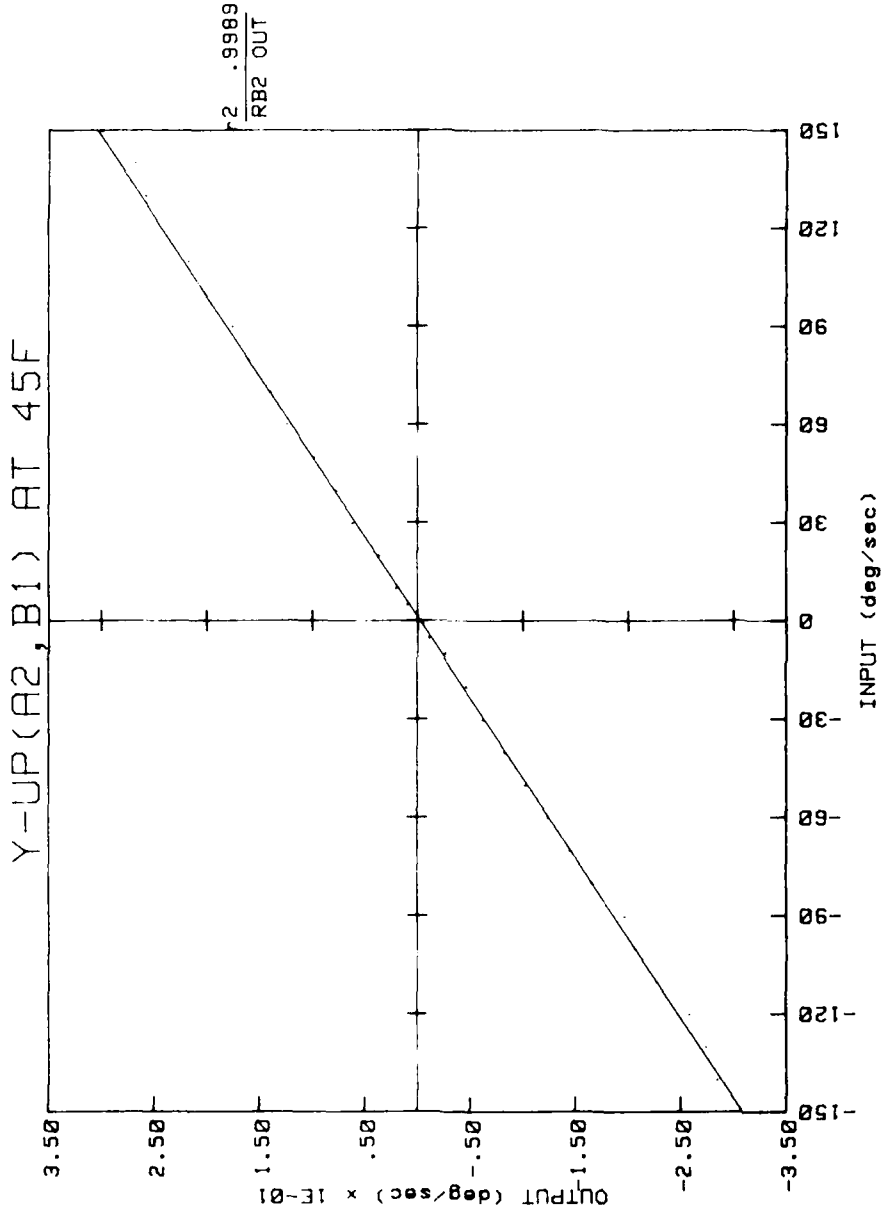

Figure 42. Input-output characteristics.

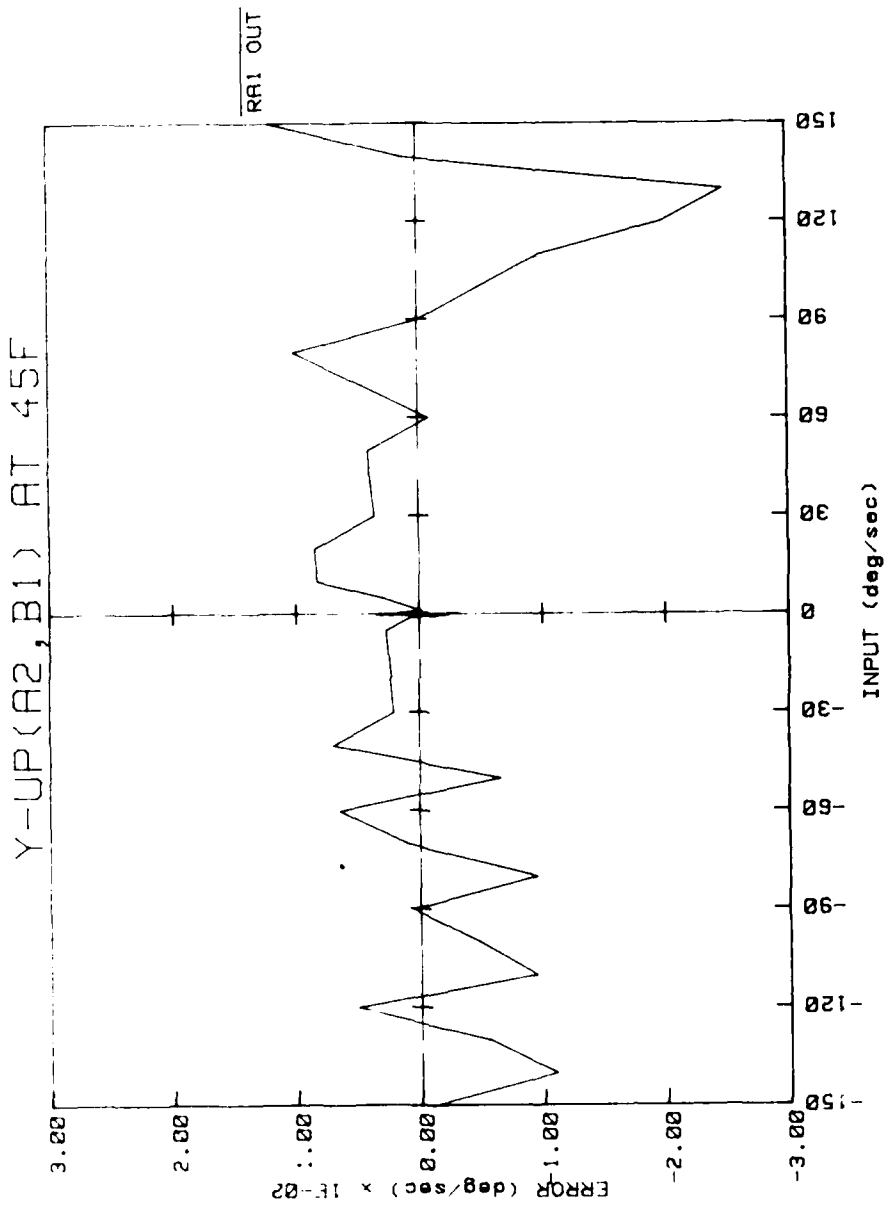

Figure 41. Input-output characteristics.

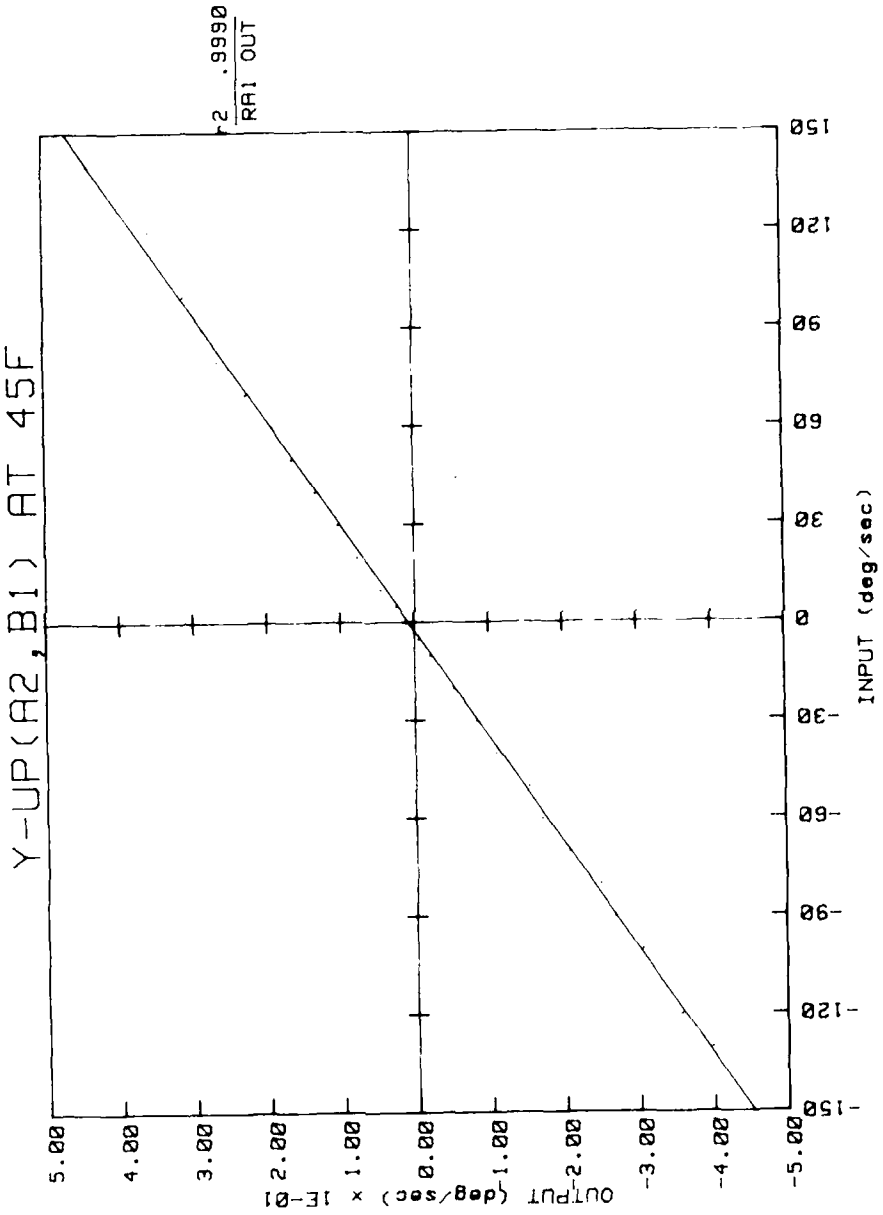

Figure 40. Input-output characteristics.

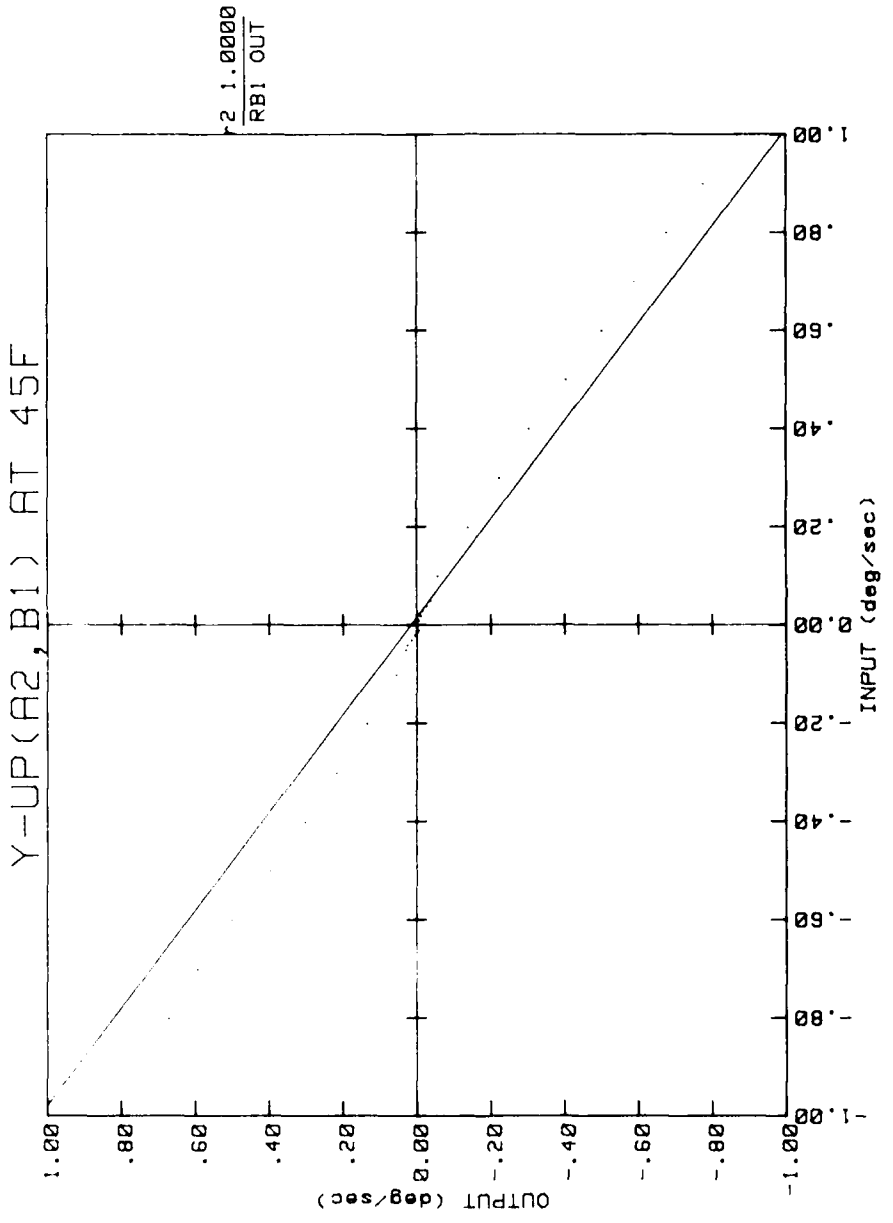

Figure 39. Input-output characteristics.

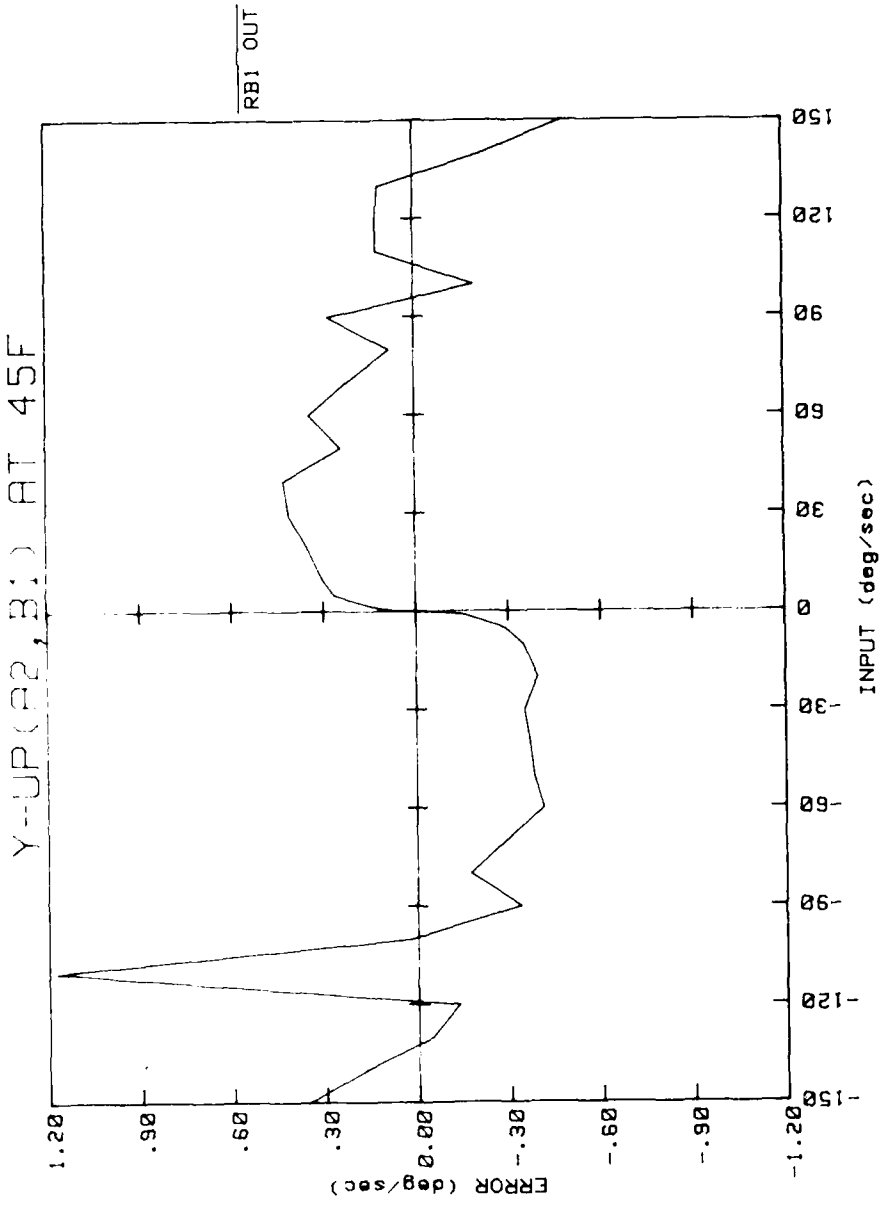

Figure 38. Input-output characteristics.

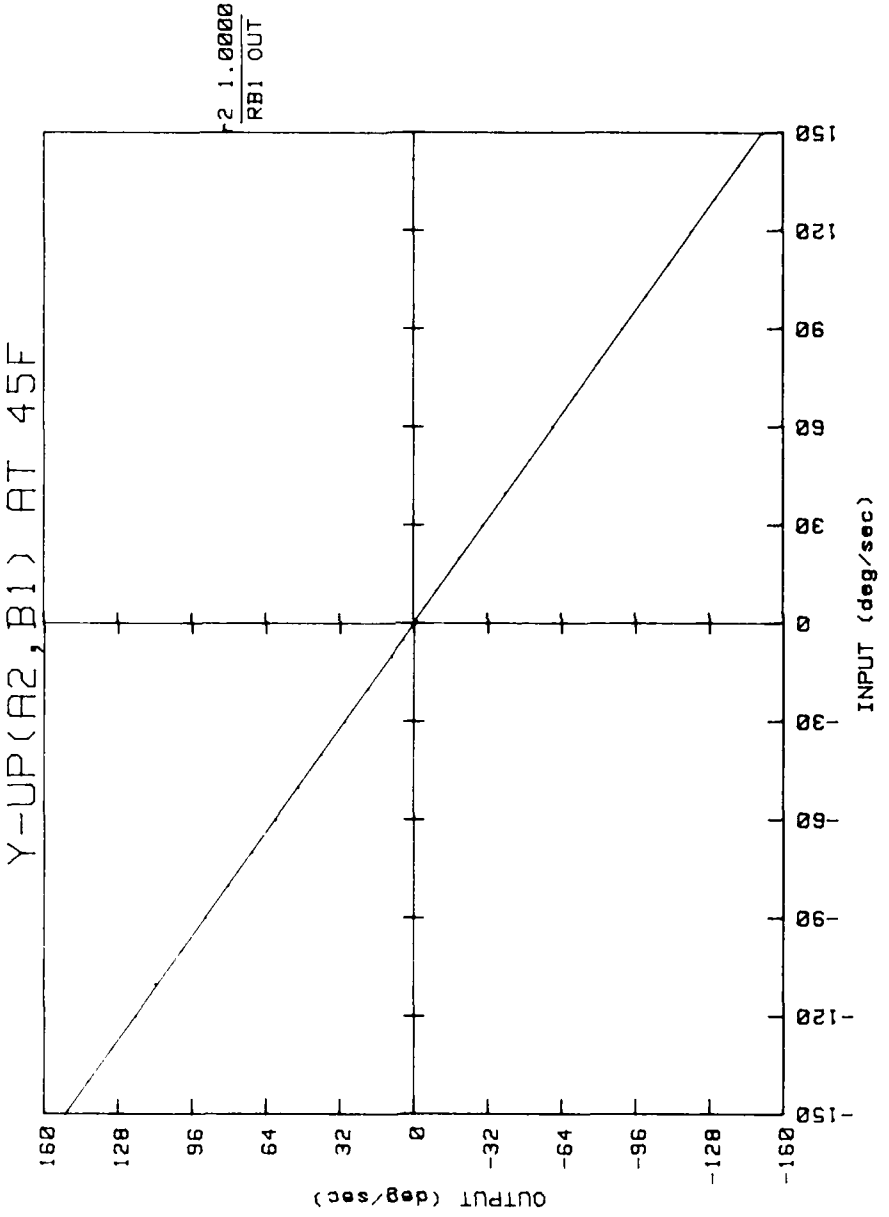

Figure 37. Input-output characteristics.

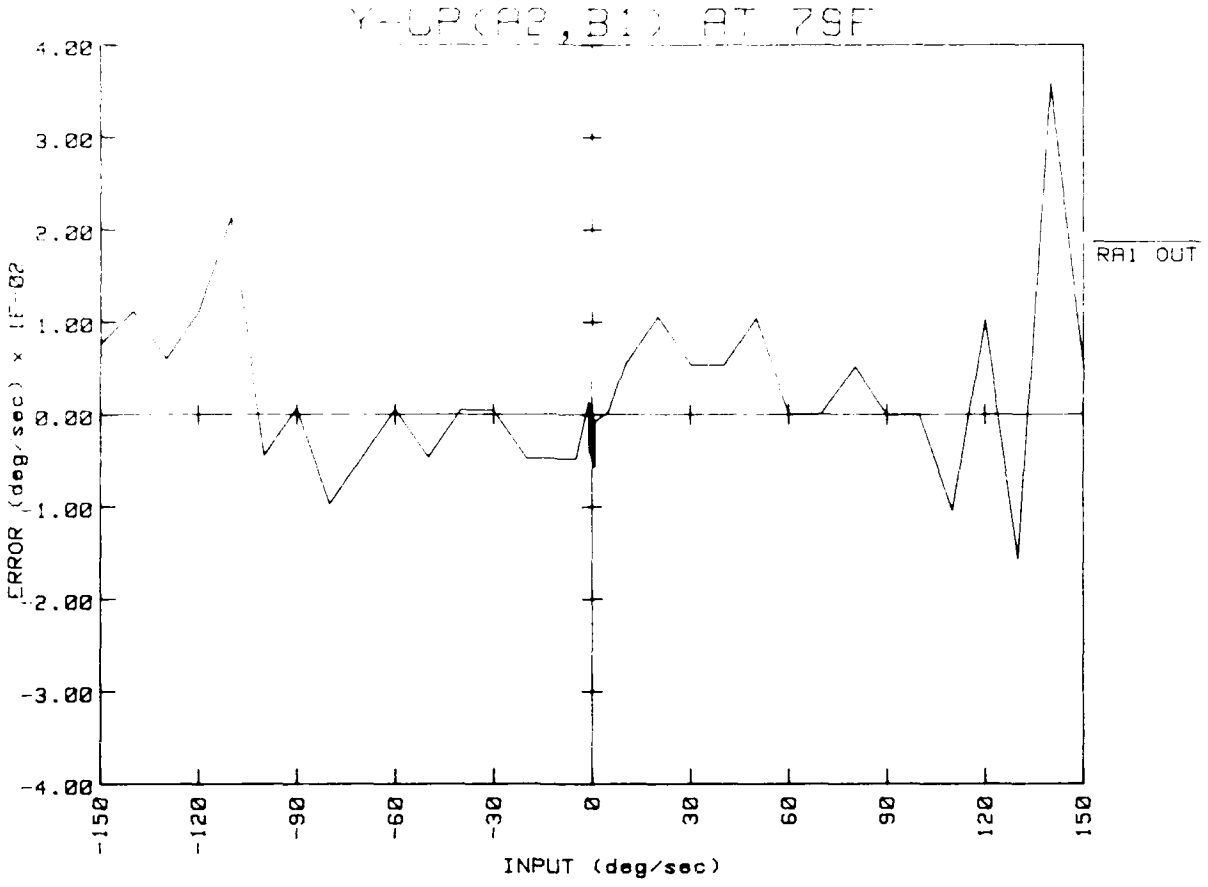

Figure 51. Input-output characteristics.

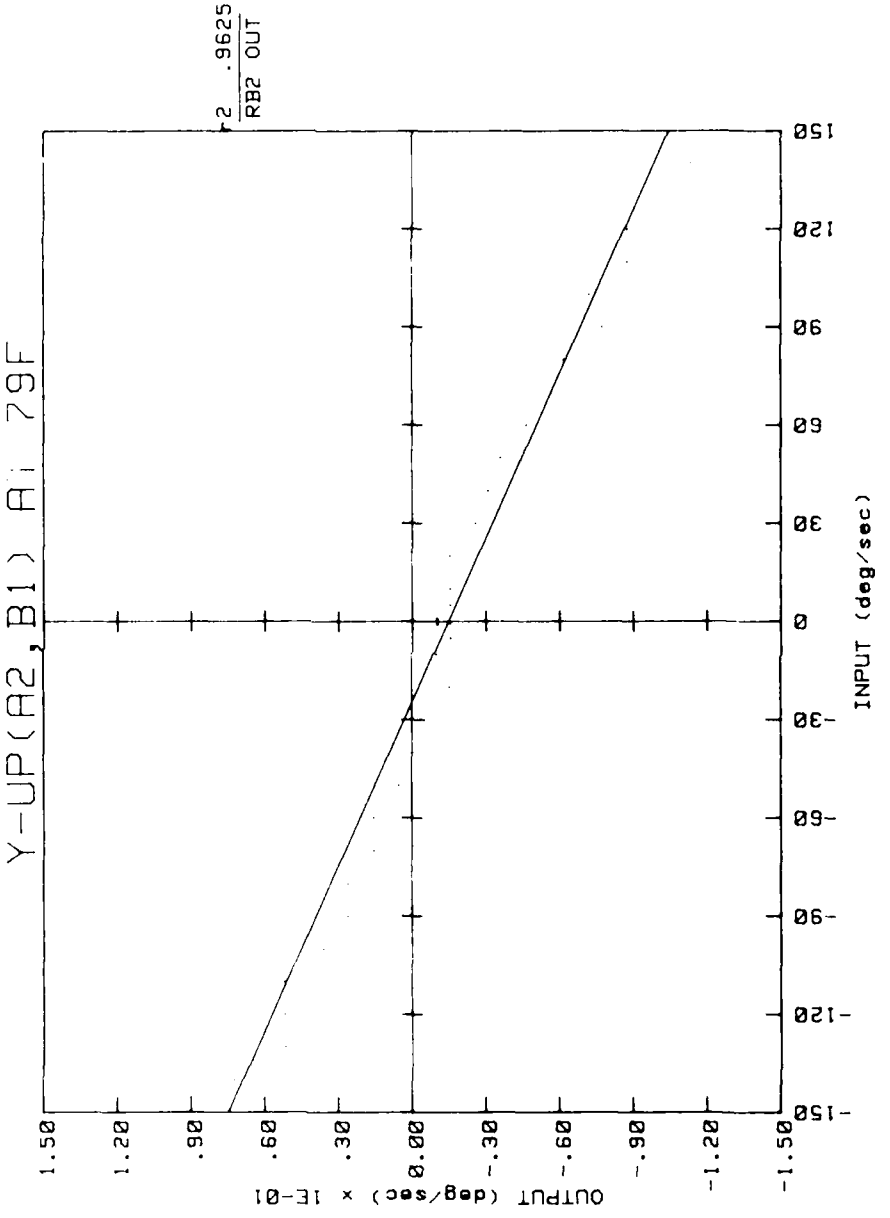

Figure 32. Input-output characteristics.

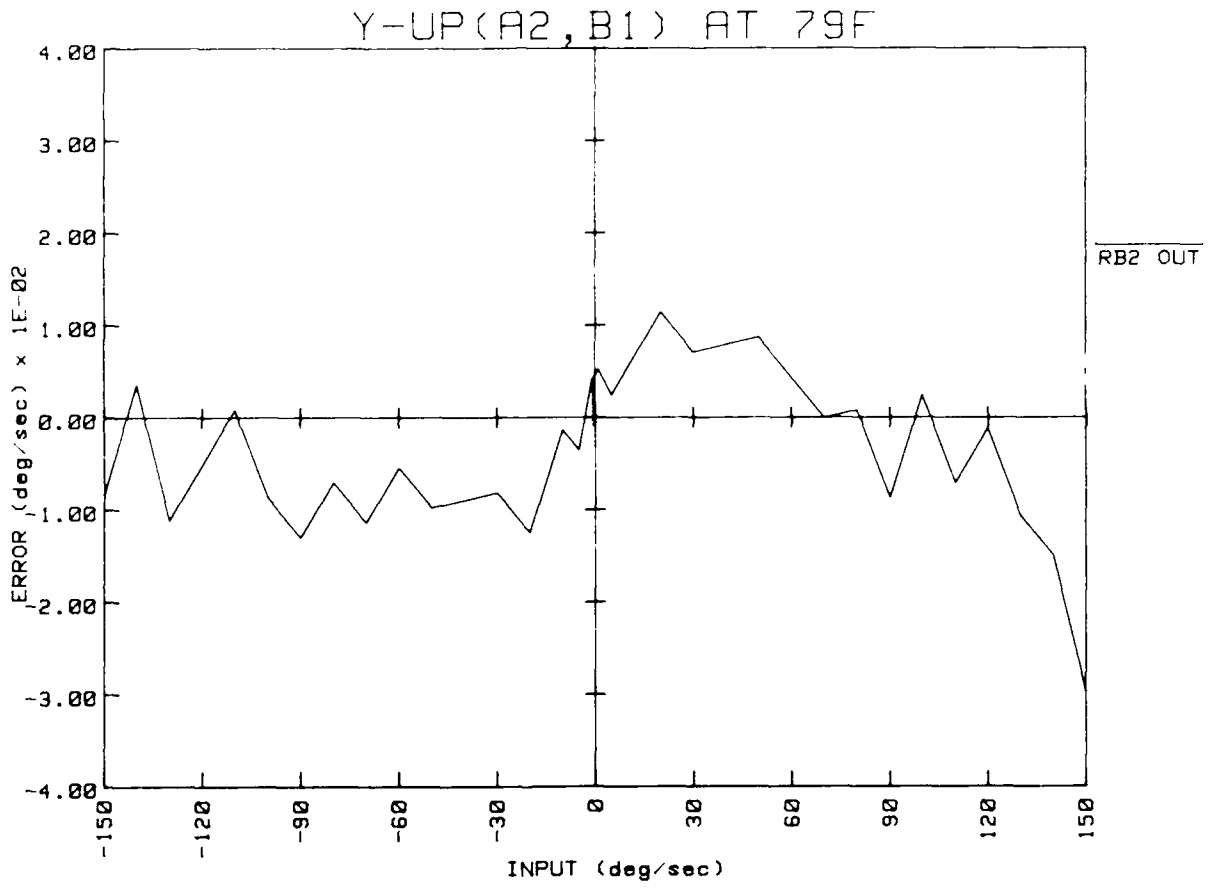

Figure 53. Input-output characteristics.

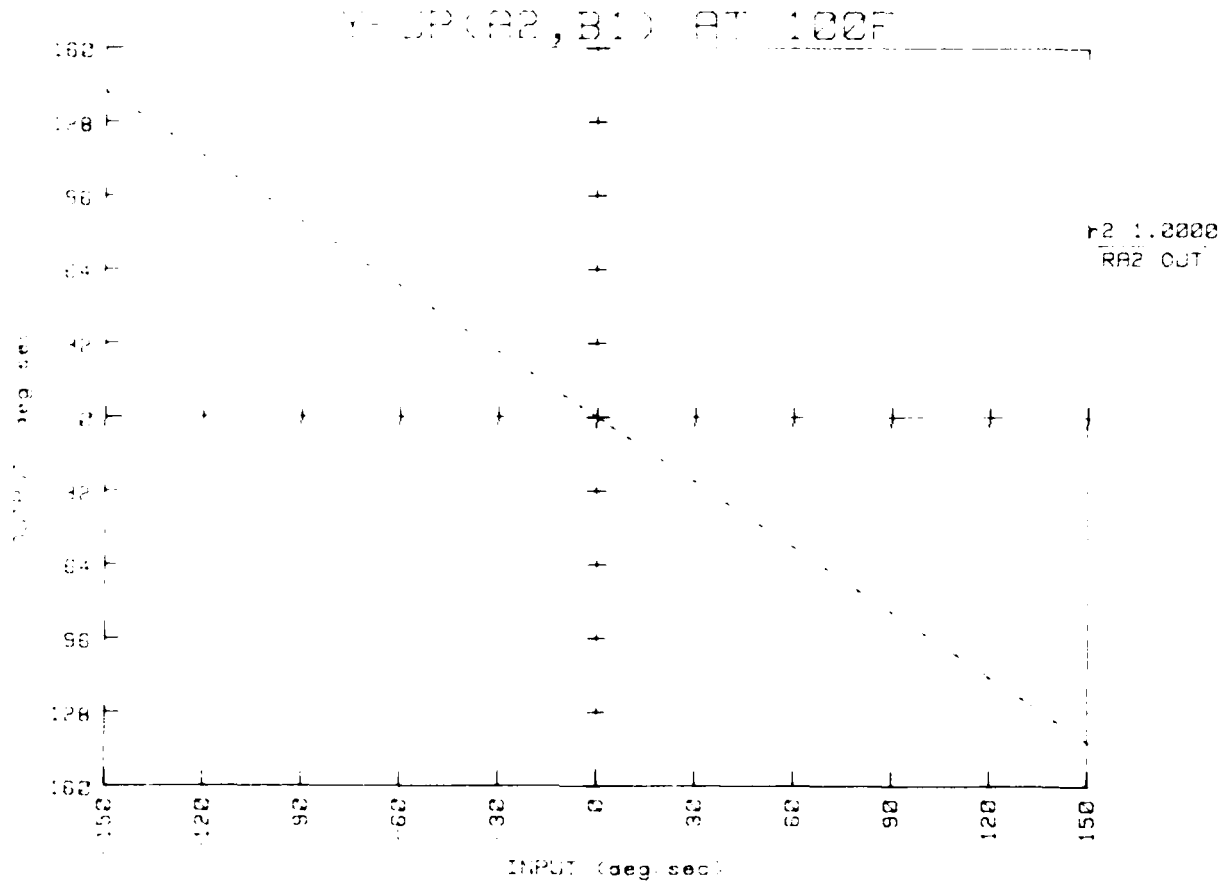

Figure 54. Input-output characteristics.

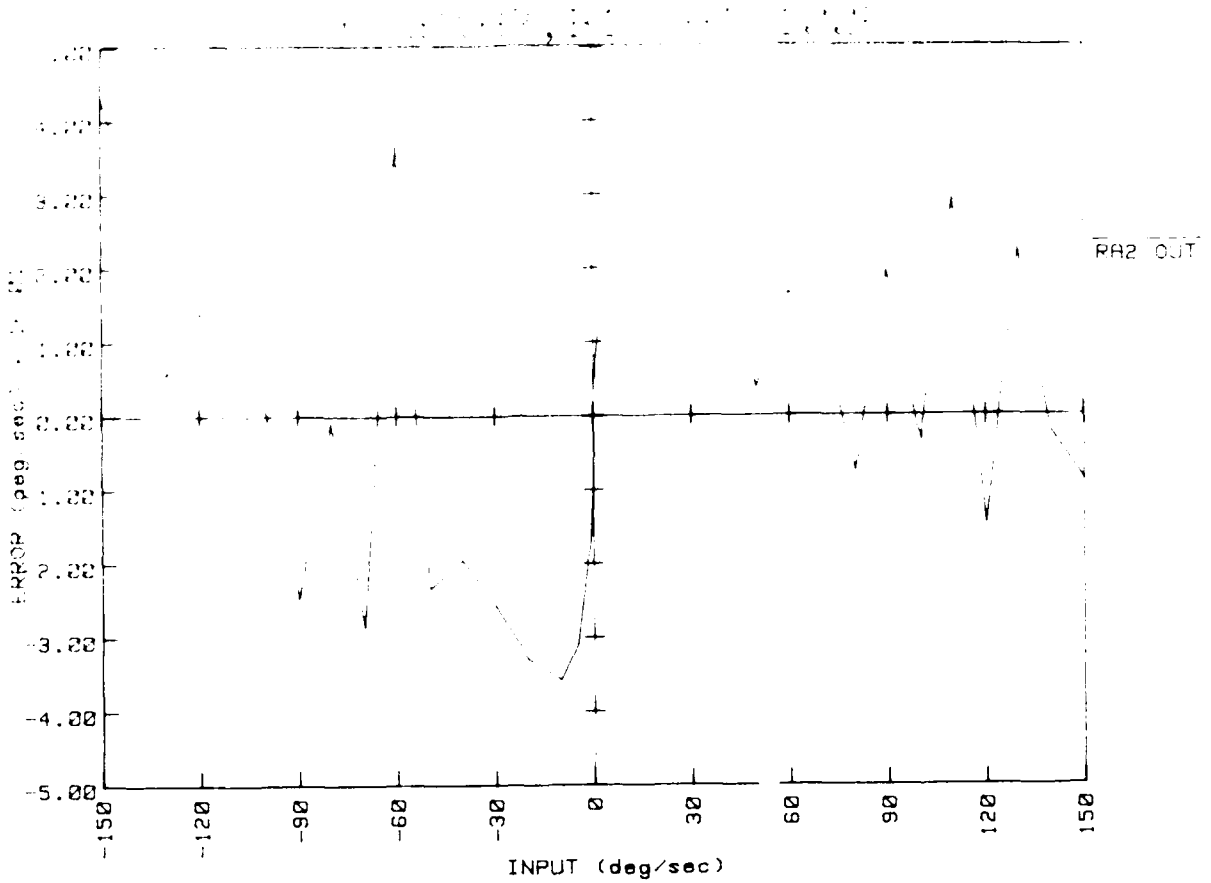

Figure 55. Input-output characteristics.

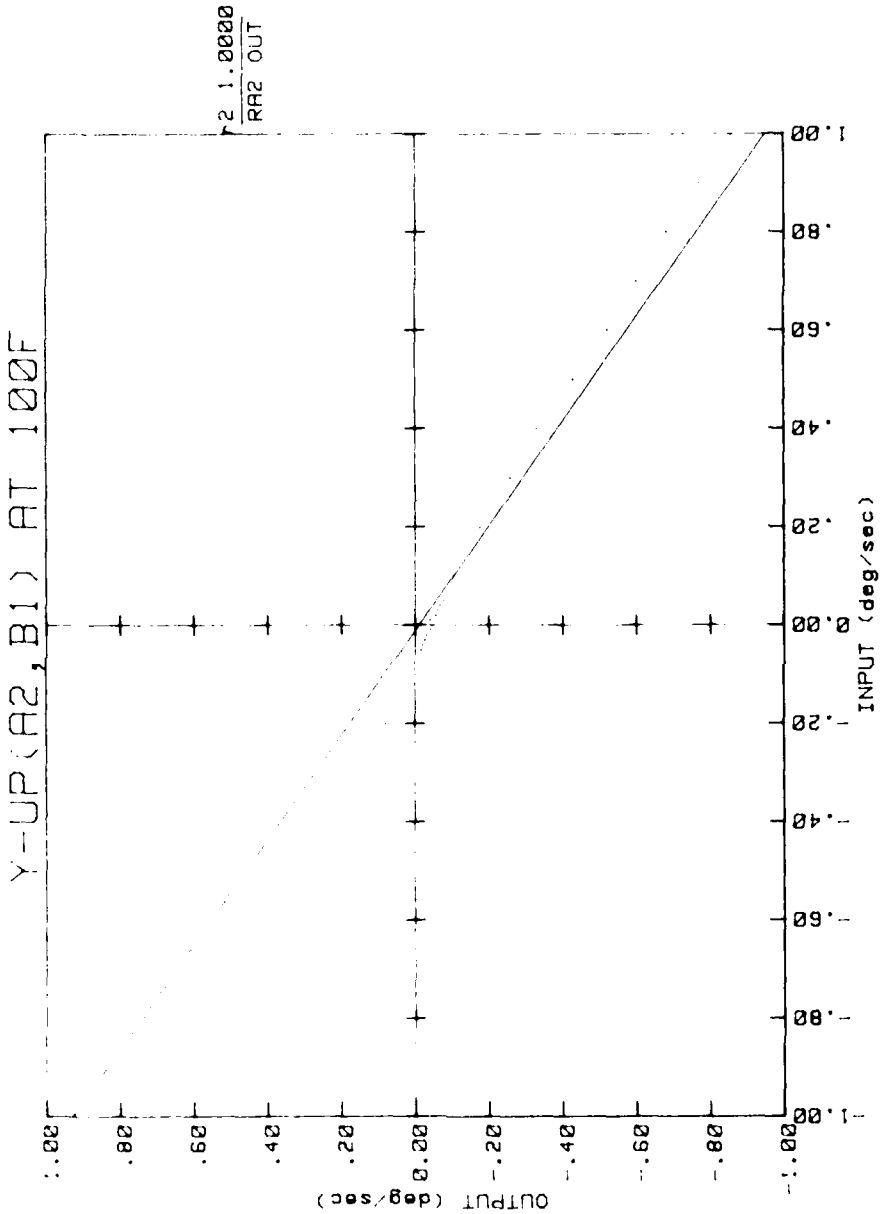

Figure 56. Input-output characteristics.

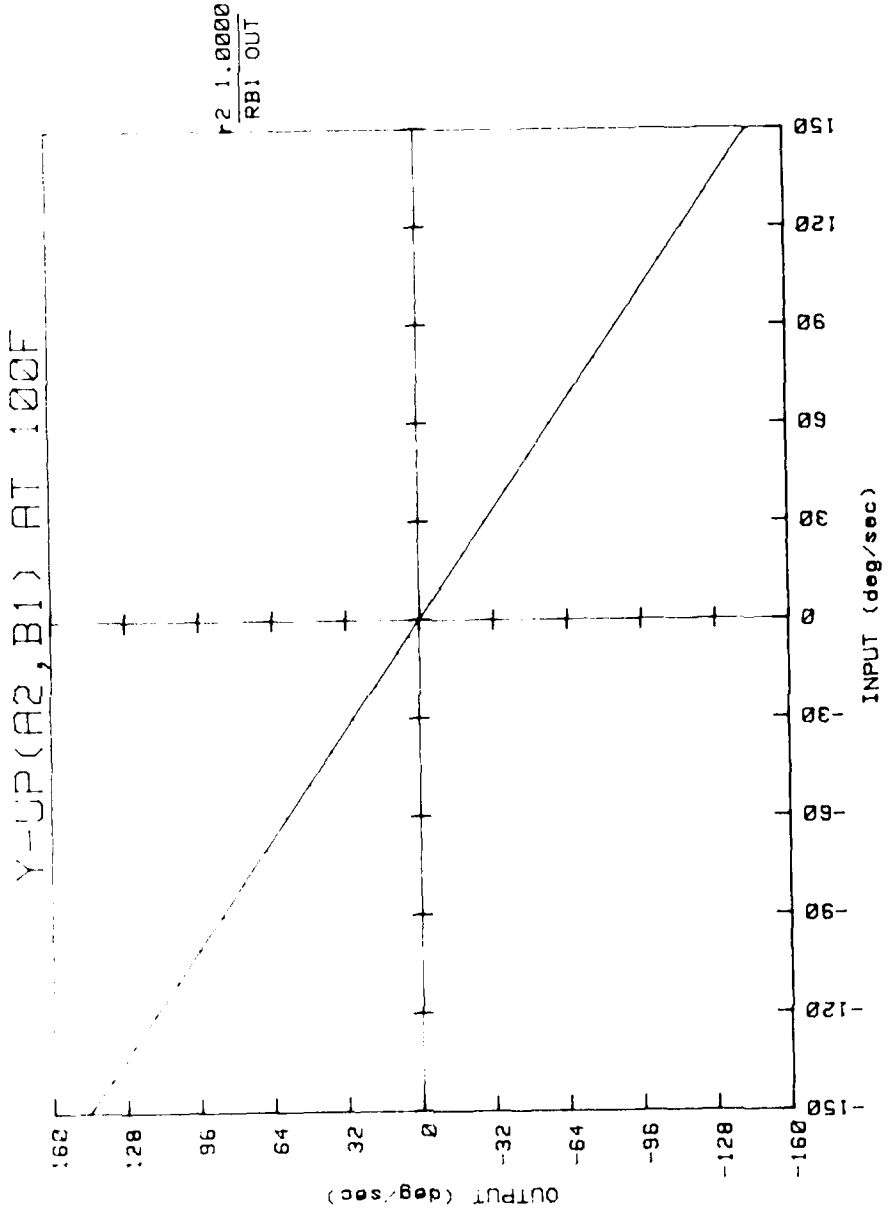

Figure 57. Input-output characteristics.

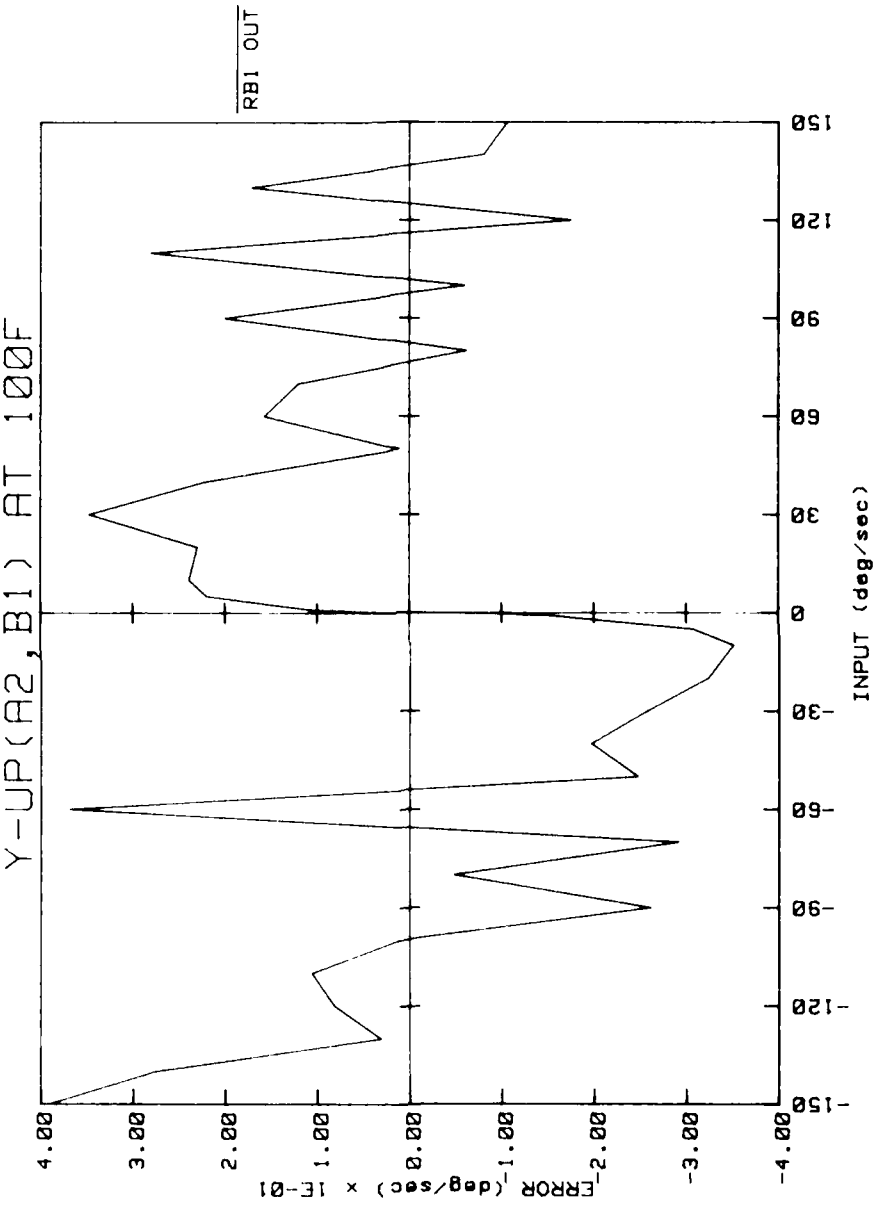

Figure 58. Input-output characteristics.

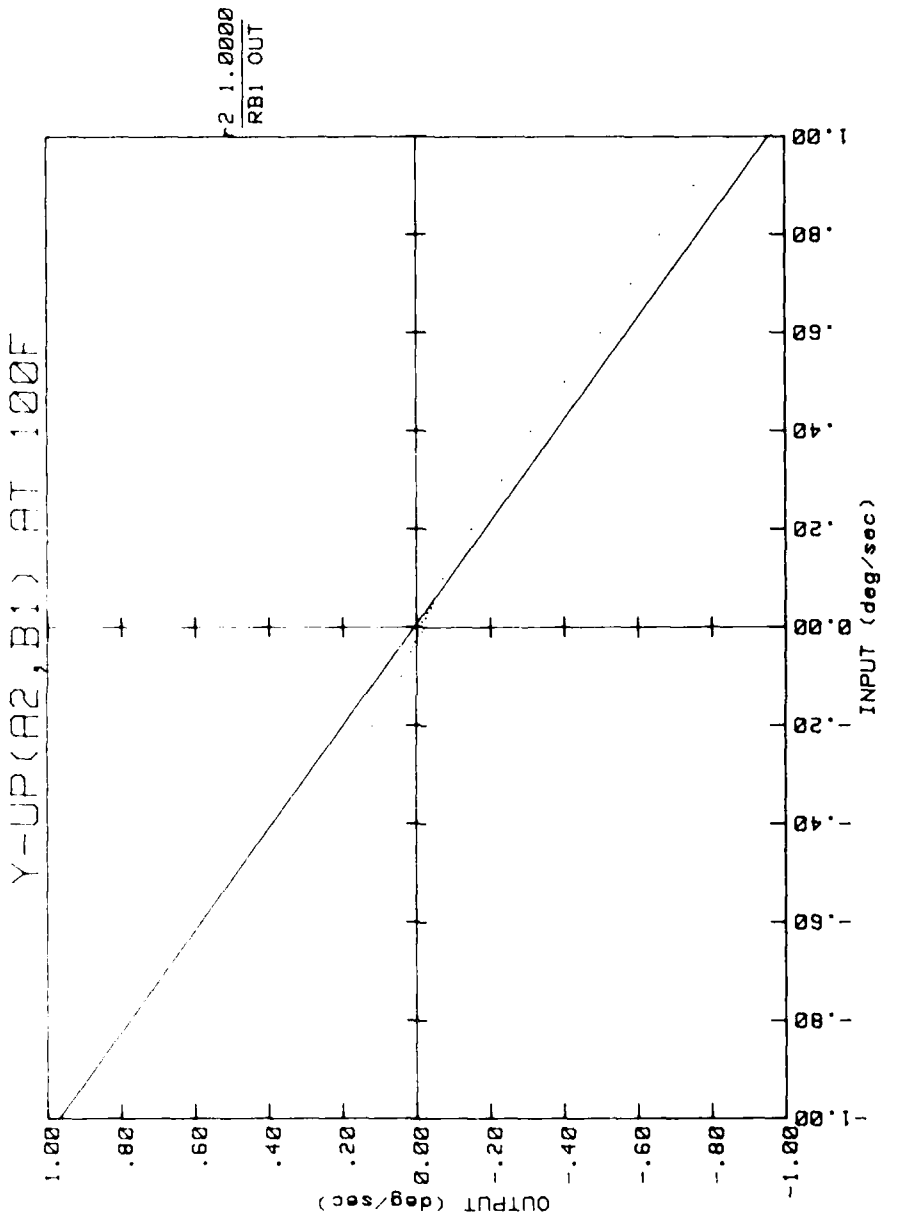

Figure 59. Input-output characteristics.

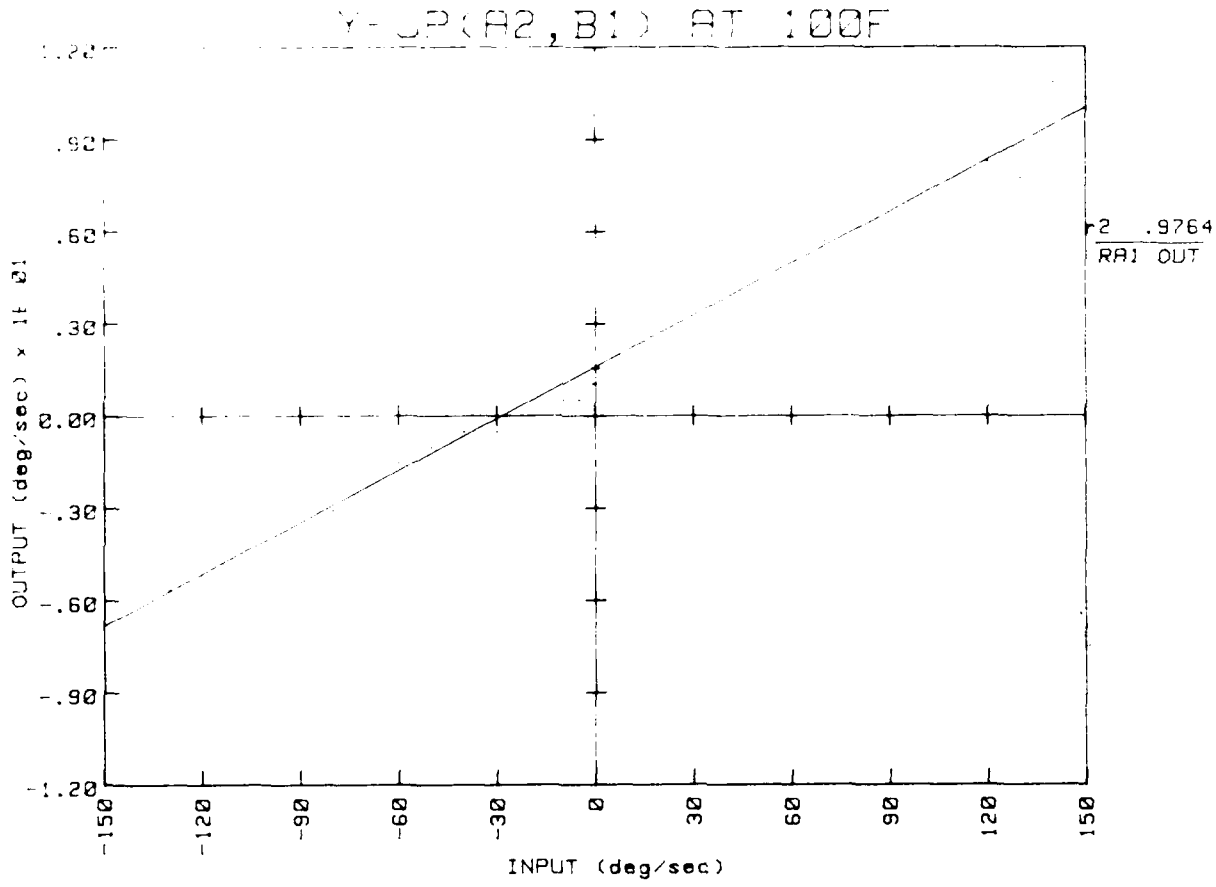

Figure 60. Input-output characteristics.

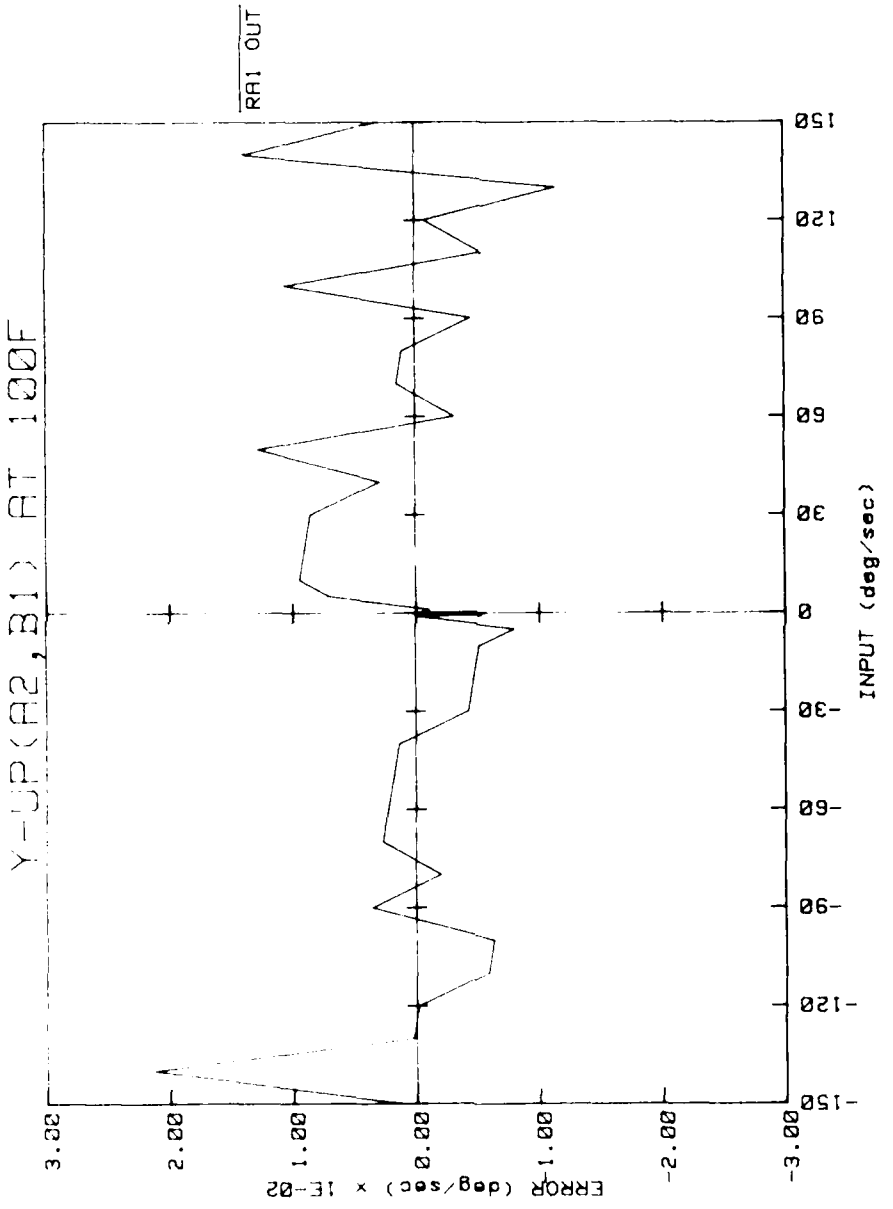

Figure 61. Input-output characteristics.

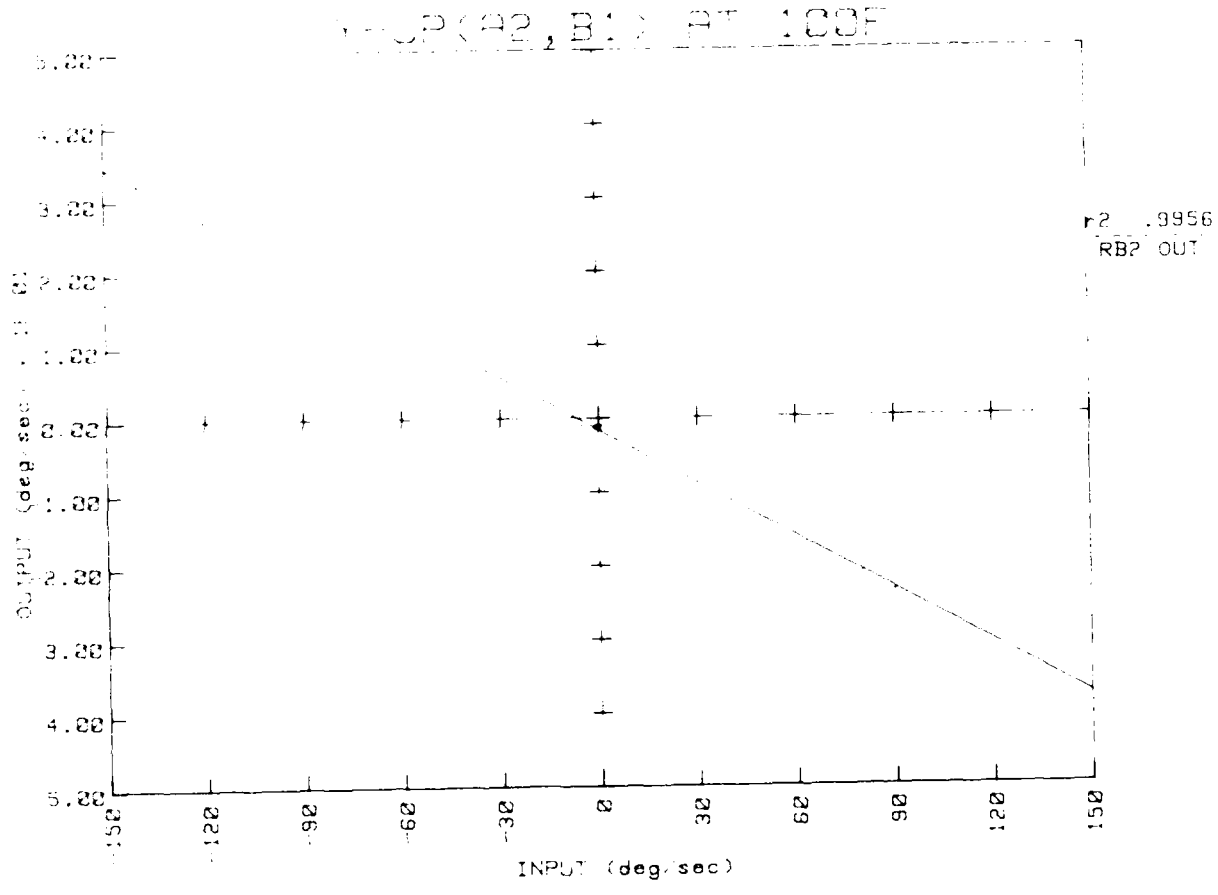

Figure 62. Input-output characteristics.

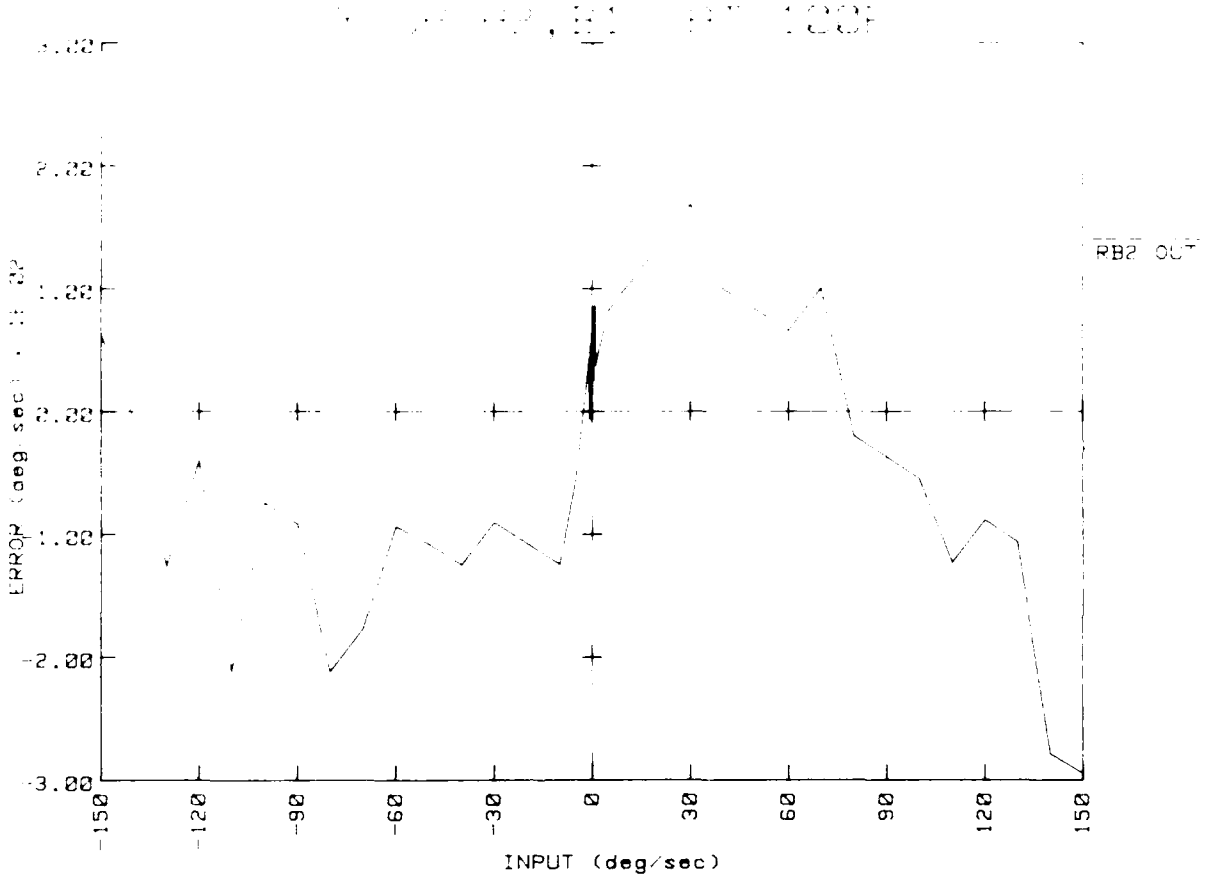

Figure 63. Input-output characteristics.

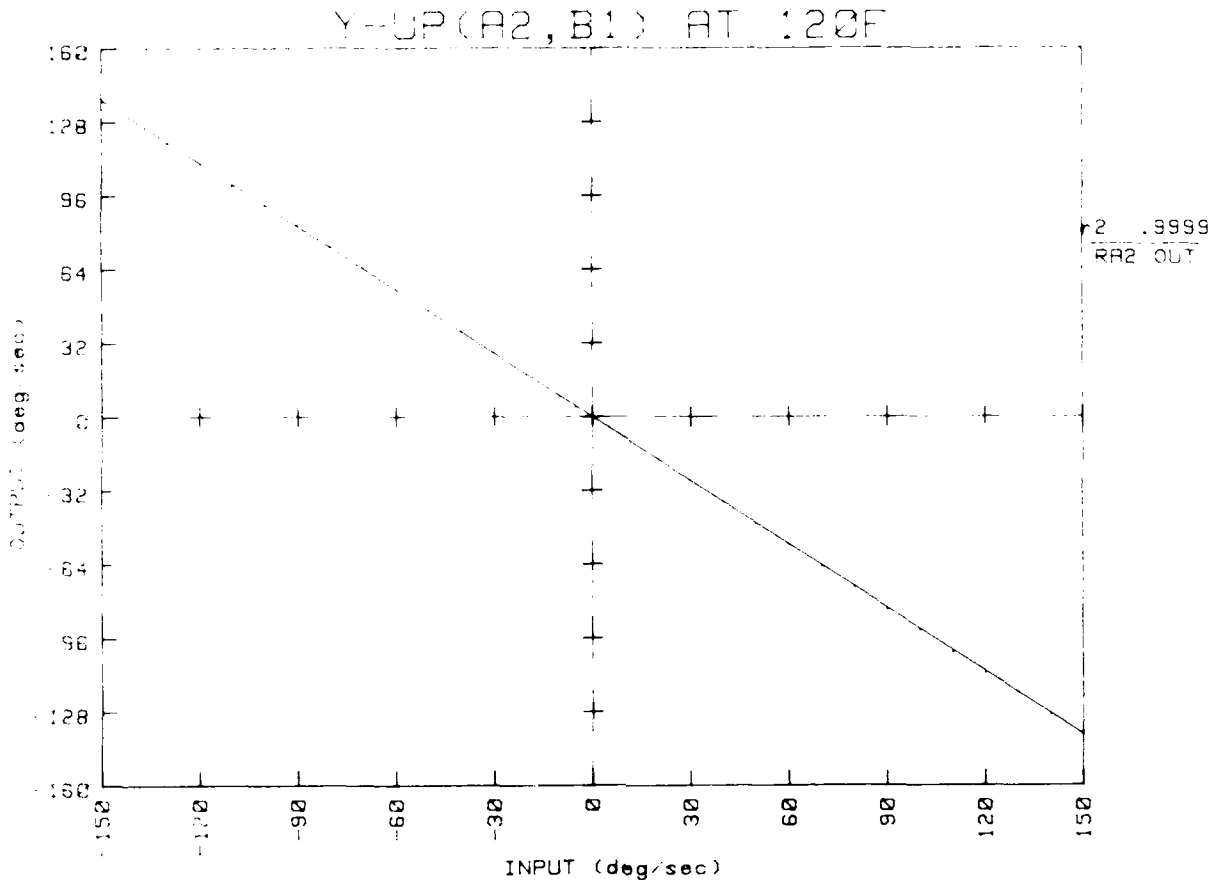

Figure 64. Input-output characteristics.

AD-A157 010 EVALUATION OF THE COLLINS/ROCKWELL AND THE SINGER KEARFOTT MULTIFUNCTION..(U) ARMY MISSILE COMMAND REDSTONE ARSENAL AL GUIDANCE AND CONTROL.. A RODGERS

UNCLASSIFIED SEP 84 AMSMI/RG-85-2-TR SBI-AD-E950 701 F/G 17/7 NL

2/2

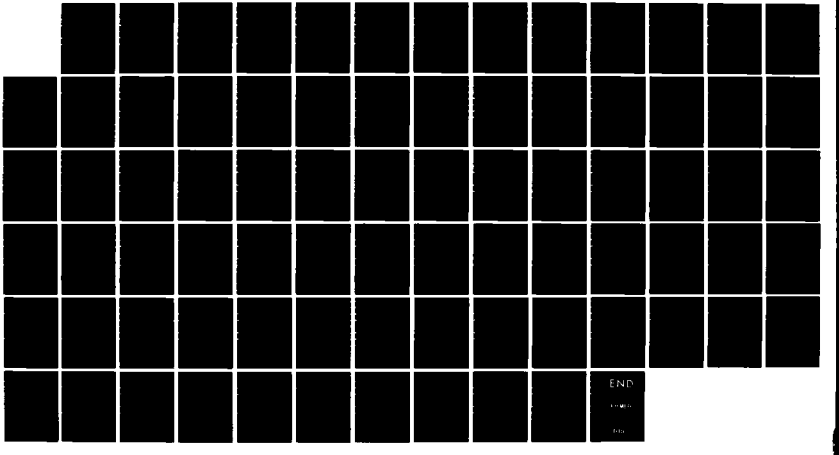

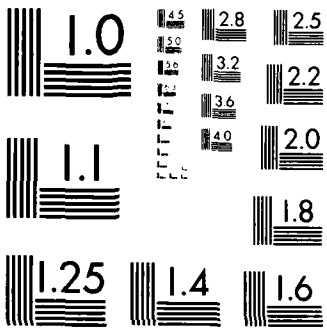

MICROCOPY RESOLUTION TEST CHART

NATIONAL BUREAU OF STANDARDS-1963-A

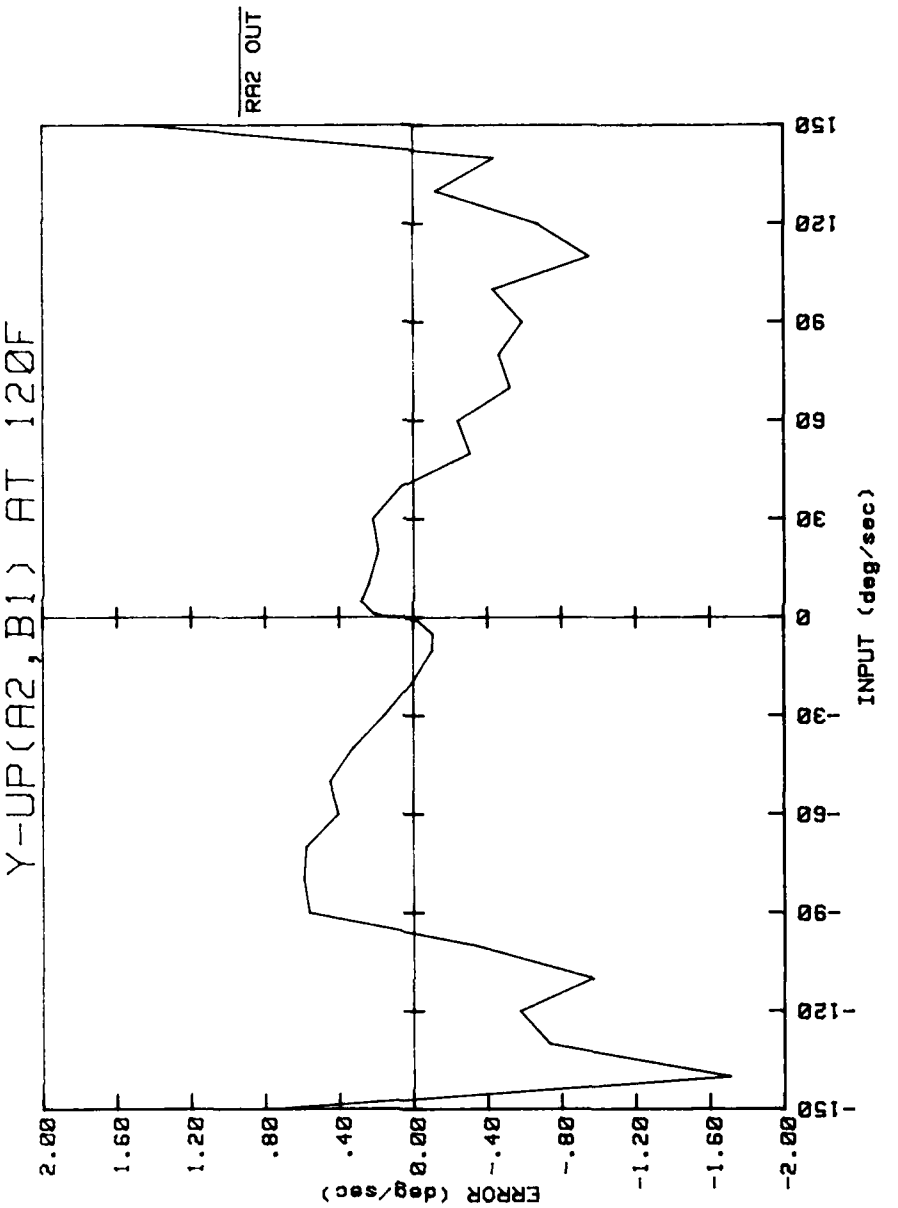

Figure 65. Input-output characteristics.

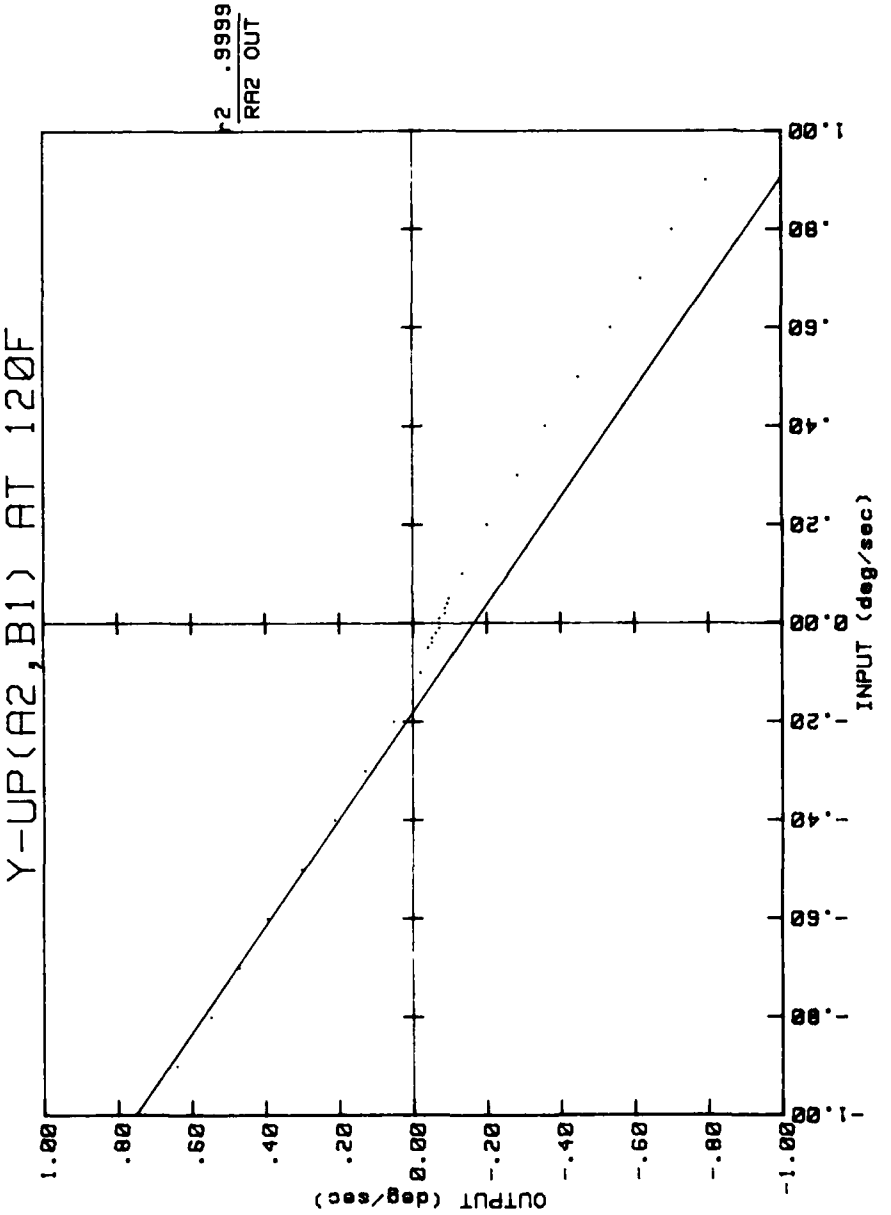

Figure 66. Input-output characteristics.

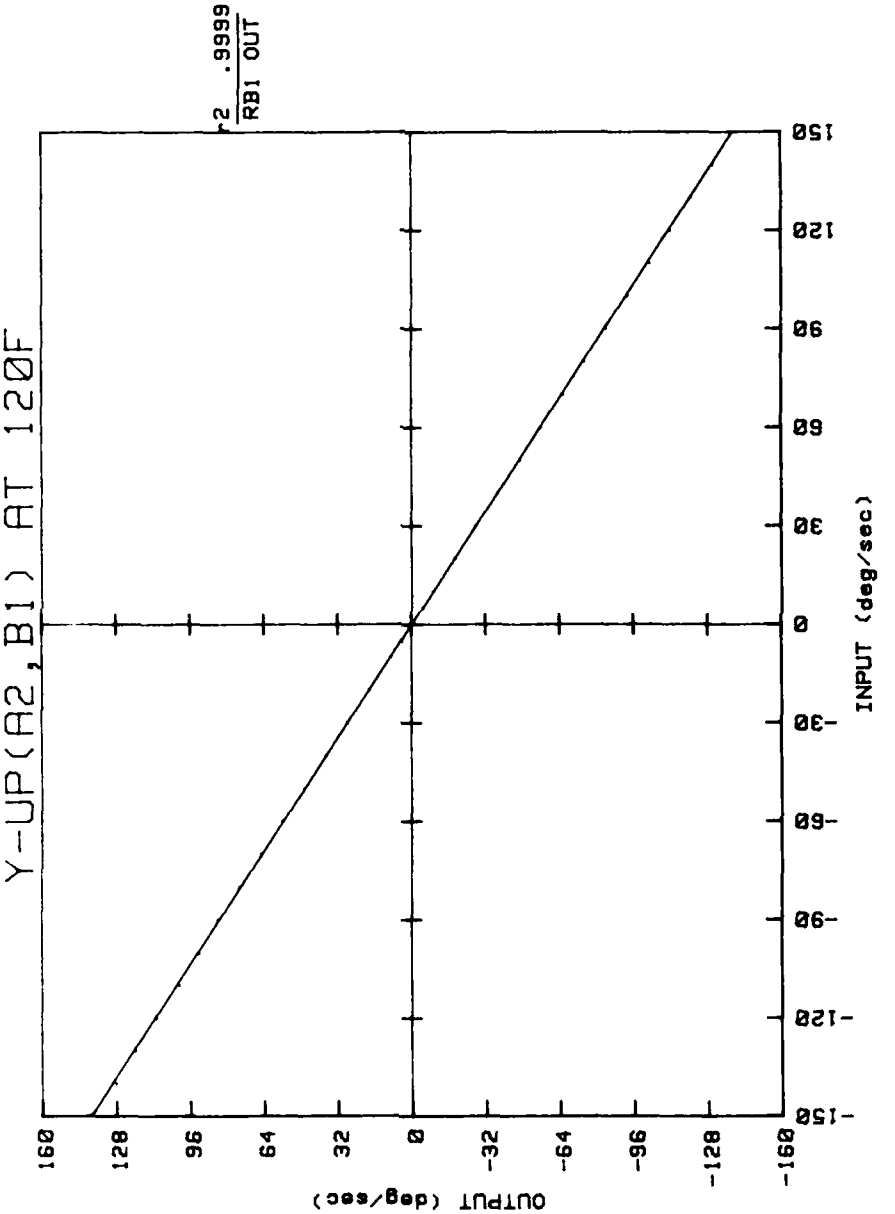

Figure 67. Input-output characteristics.

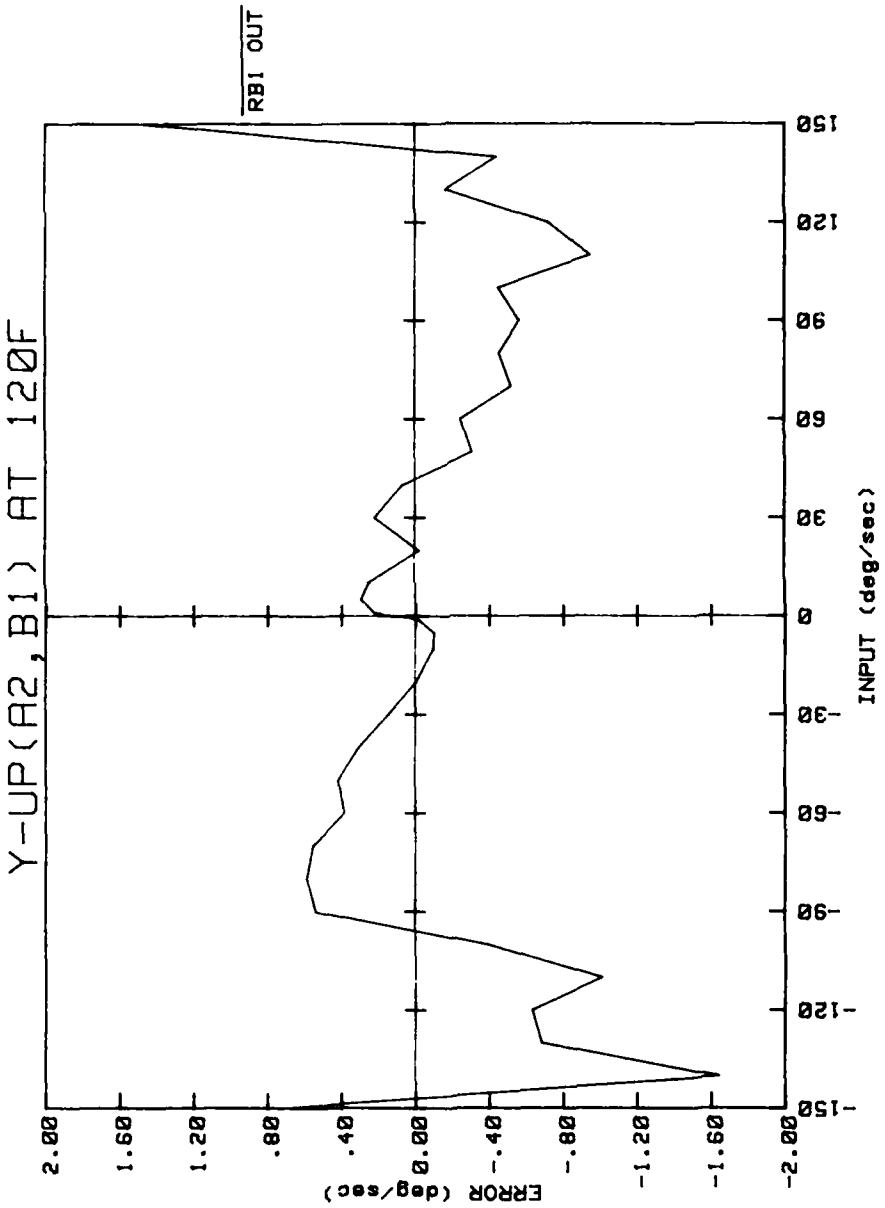

Figure 68. Input-output characteristics.

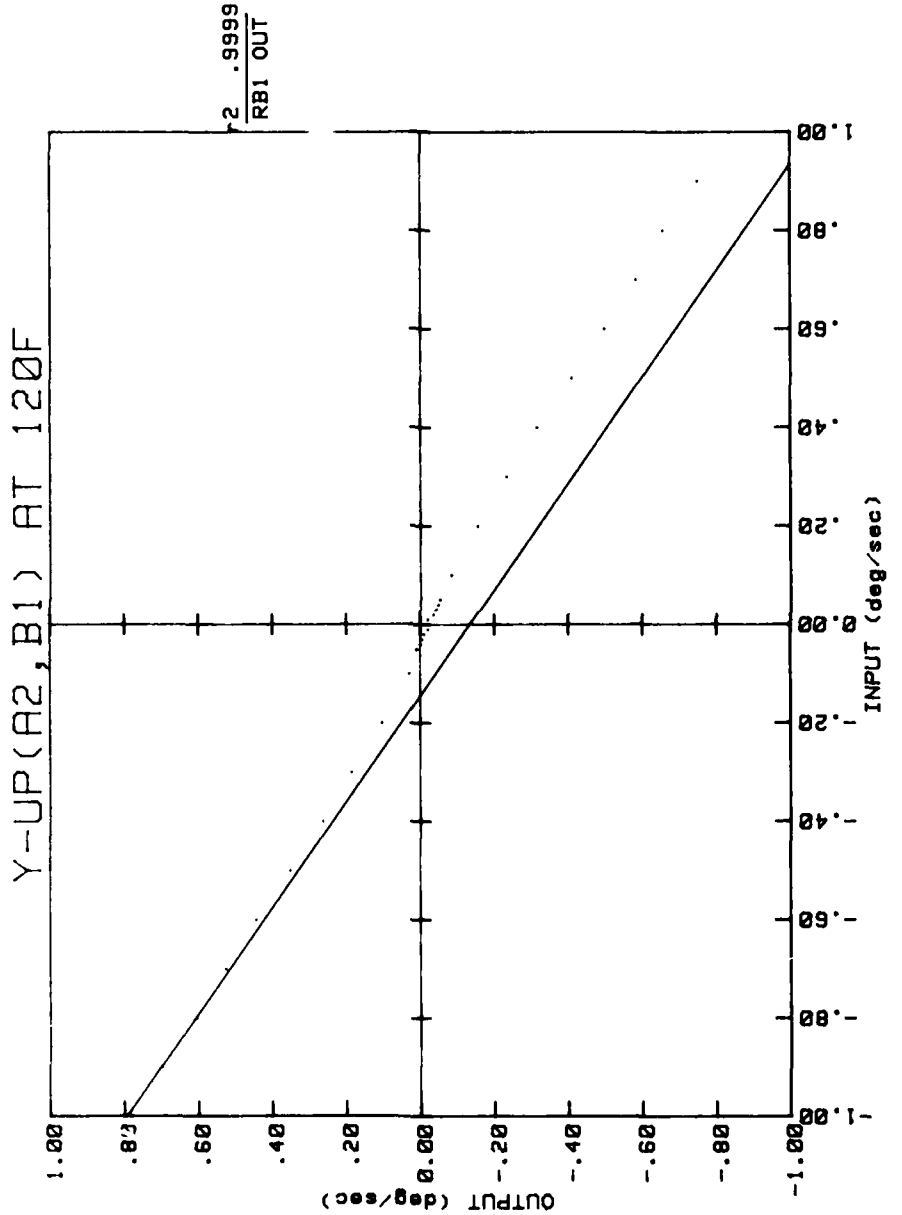

Figure 69. Input-output characteristics.

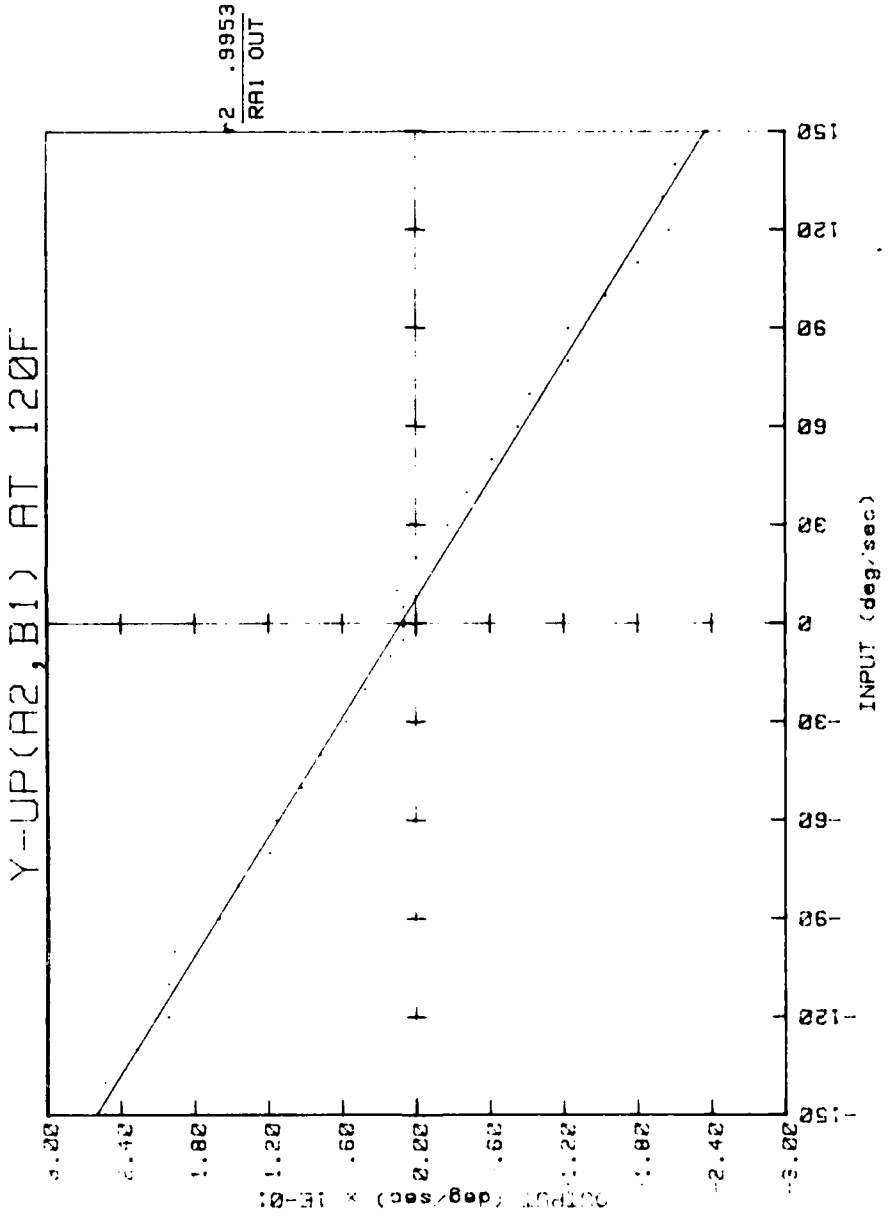

Figure 70. Input-output characteristics.

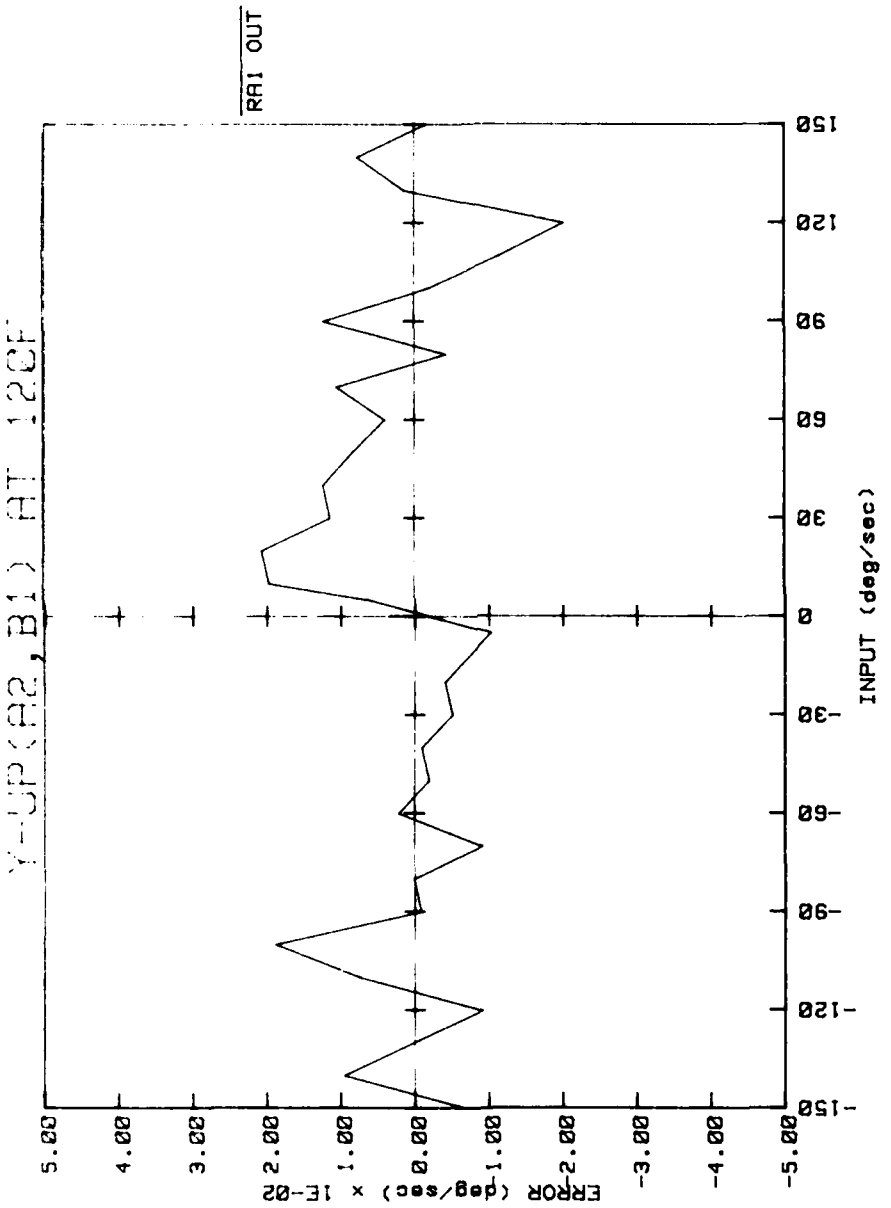

Figure 71. Input-output characteristics.

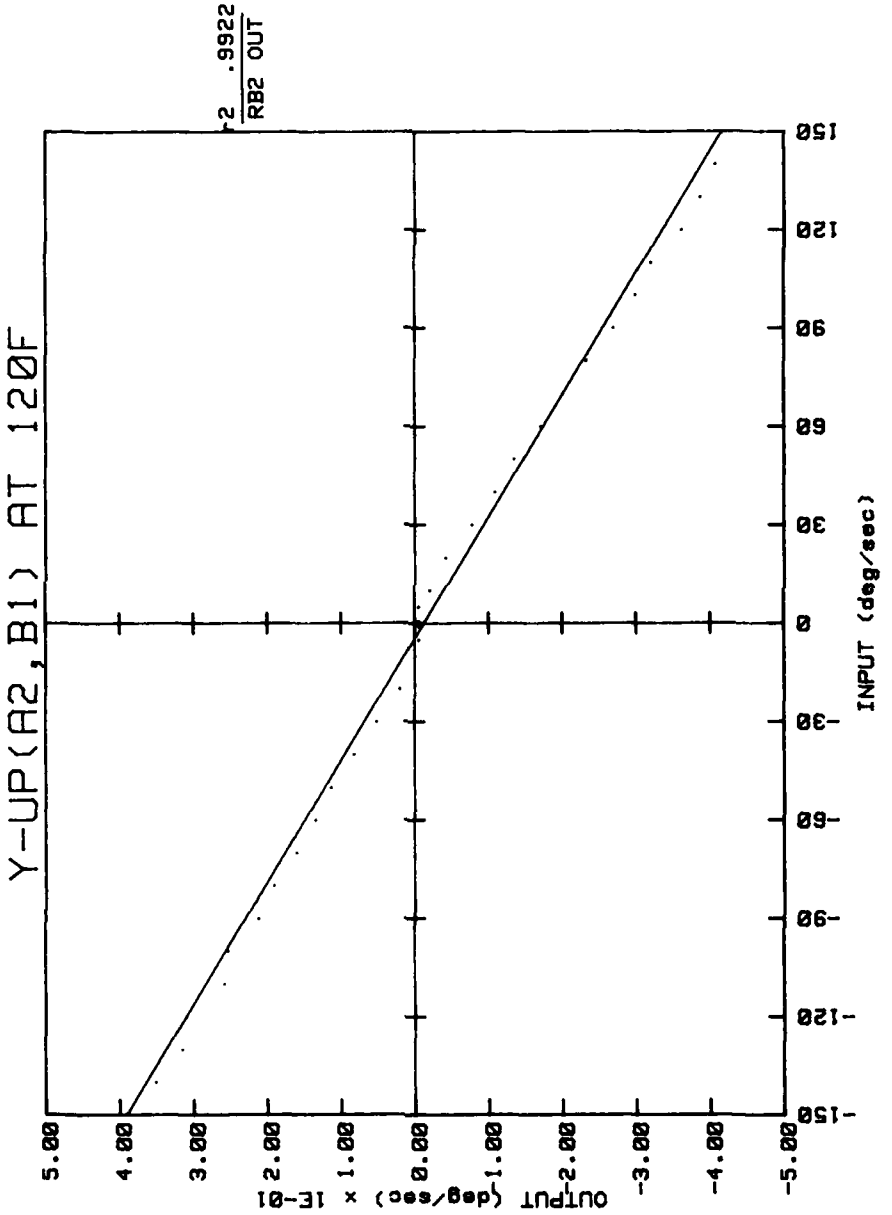

Figure 72. Input-output characteristics.

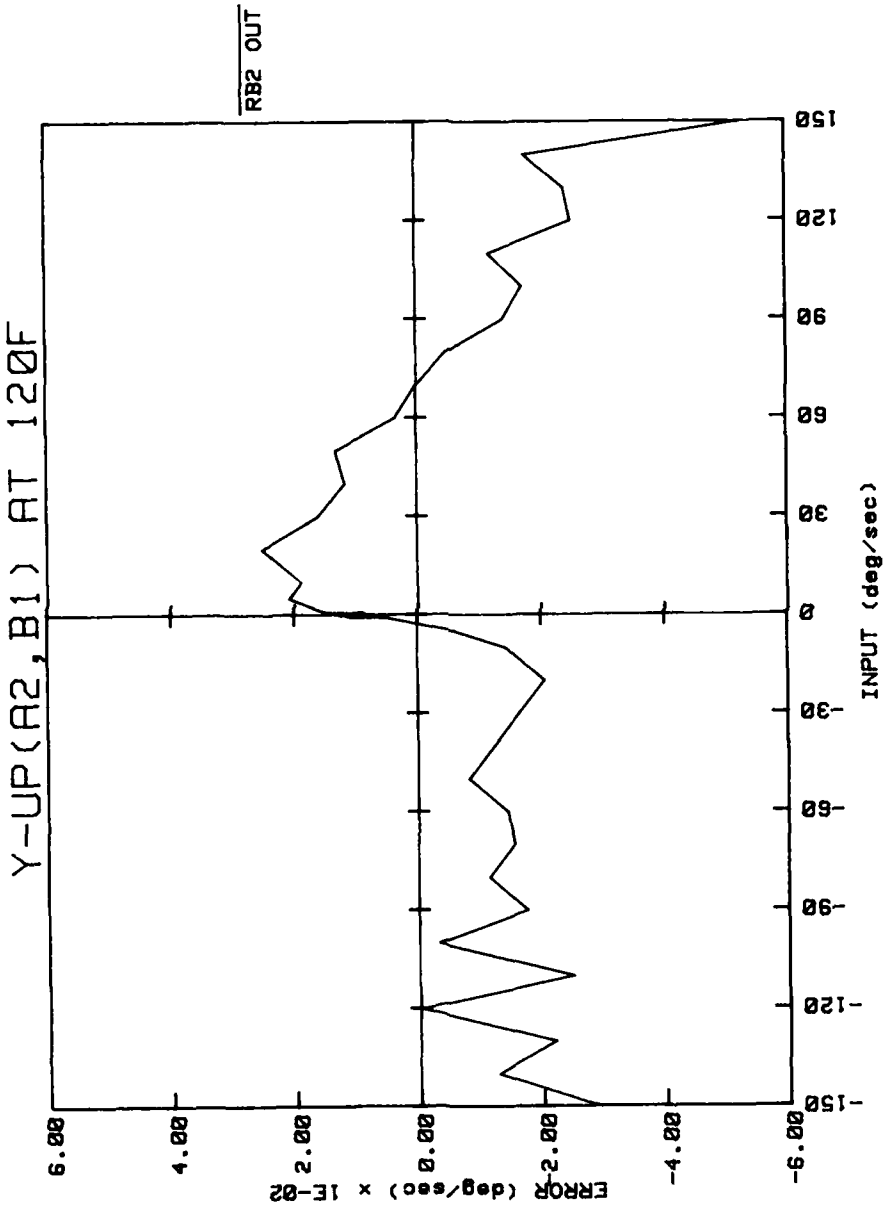

Figure 73. Input-output characteristics.

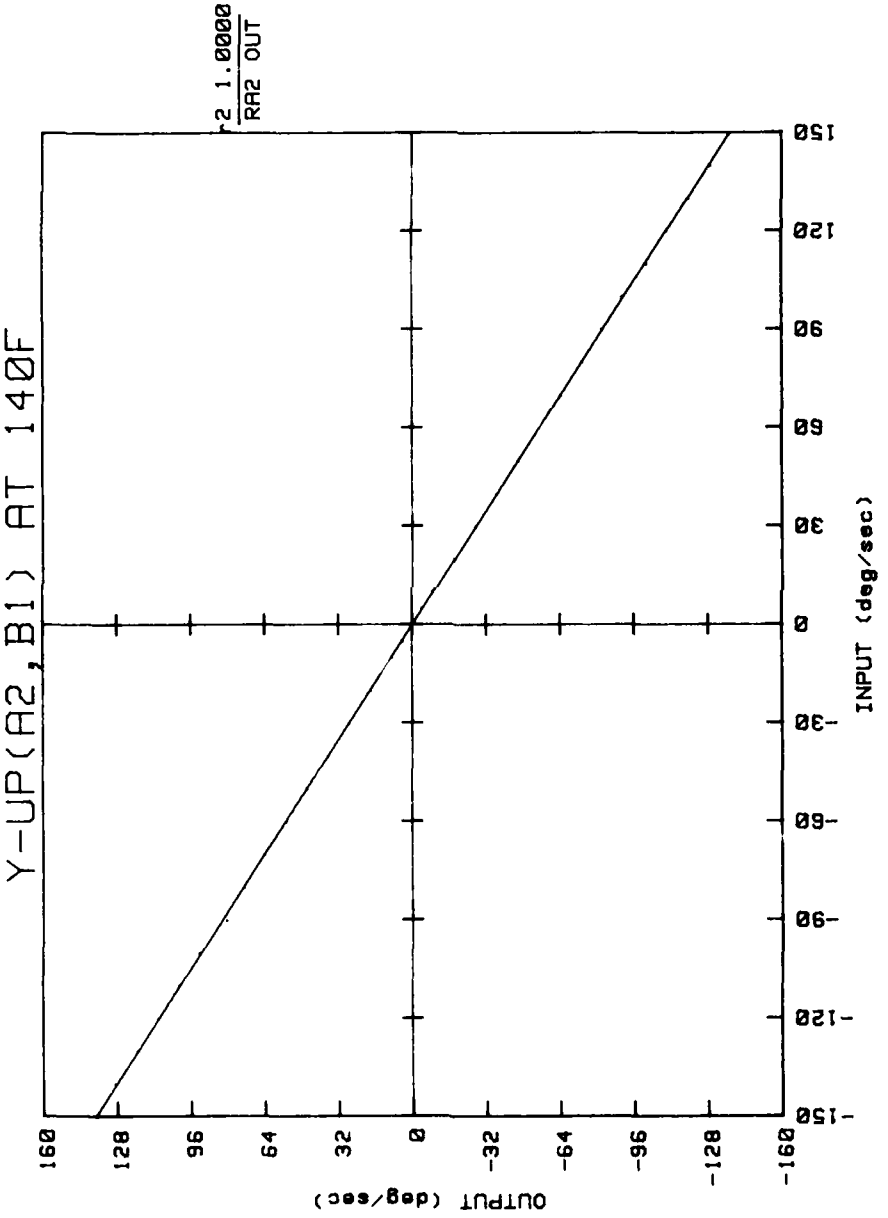

Figure 74. Input-output characteristics.

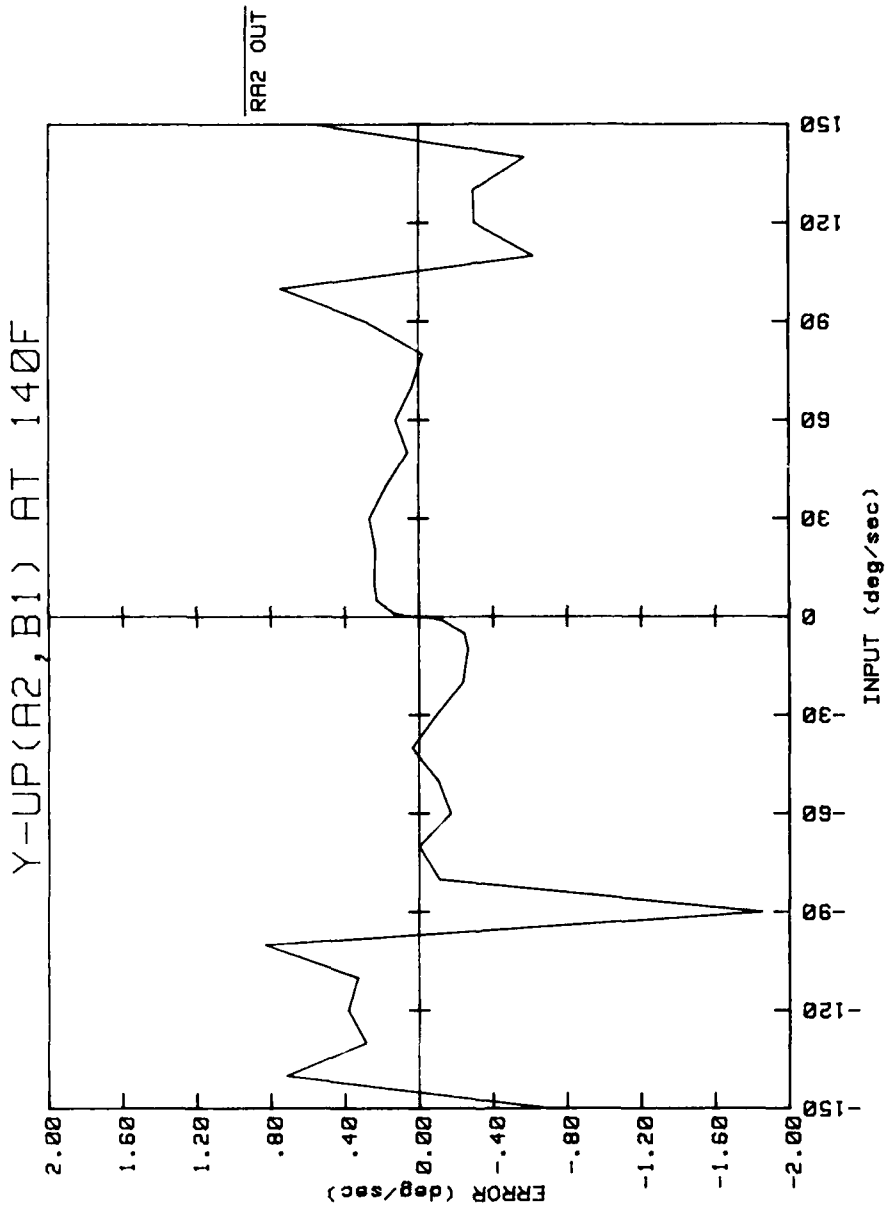

Figure 75. Input-output characteristics.

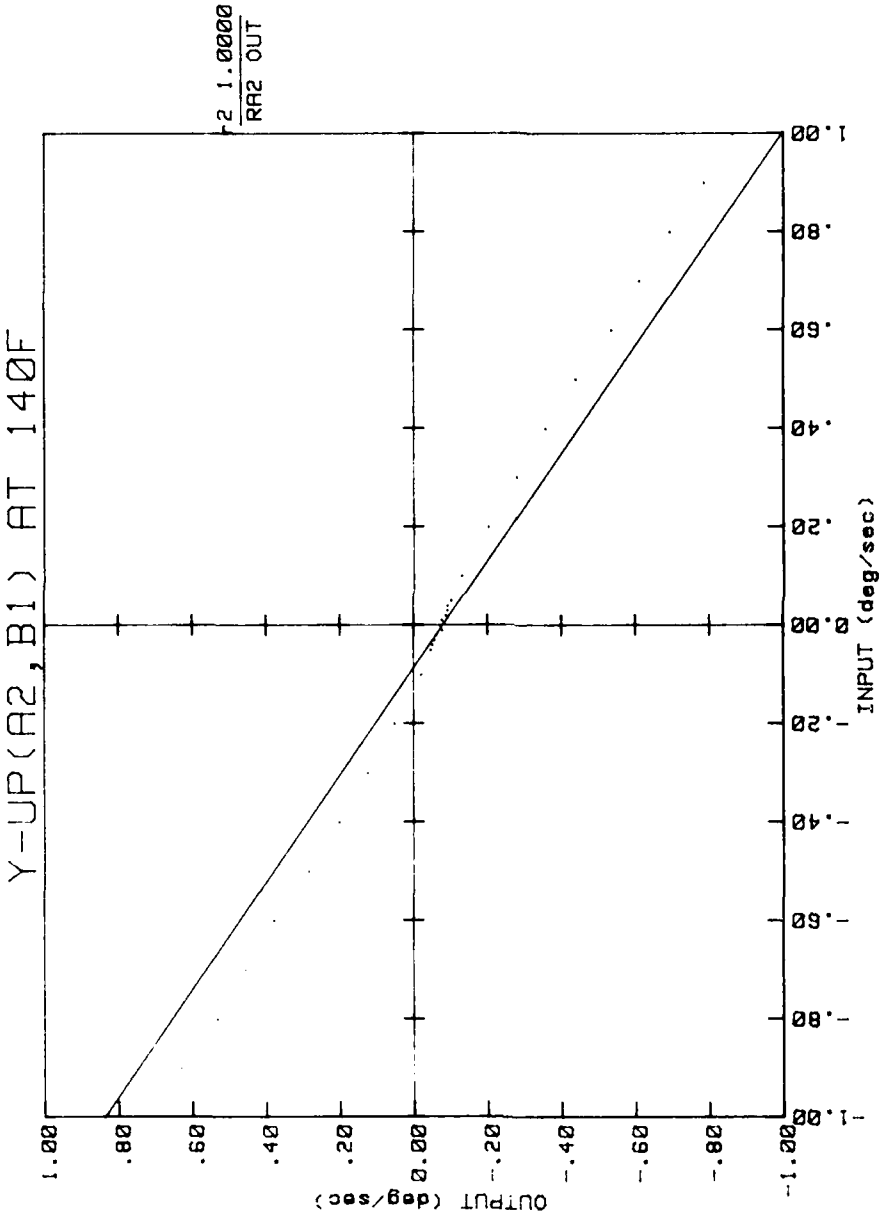

Figure 76. Input-output characteristics.

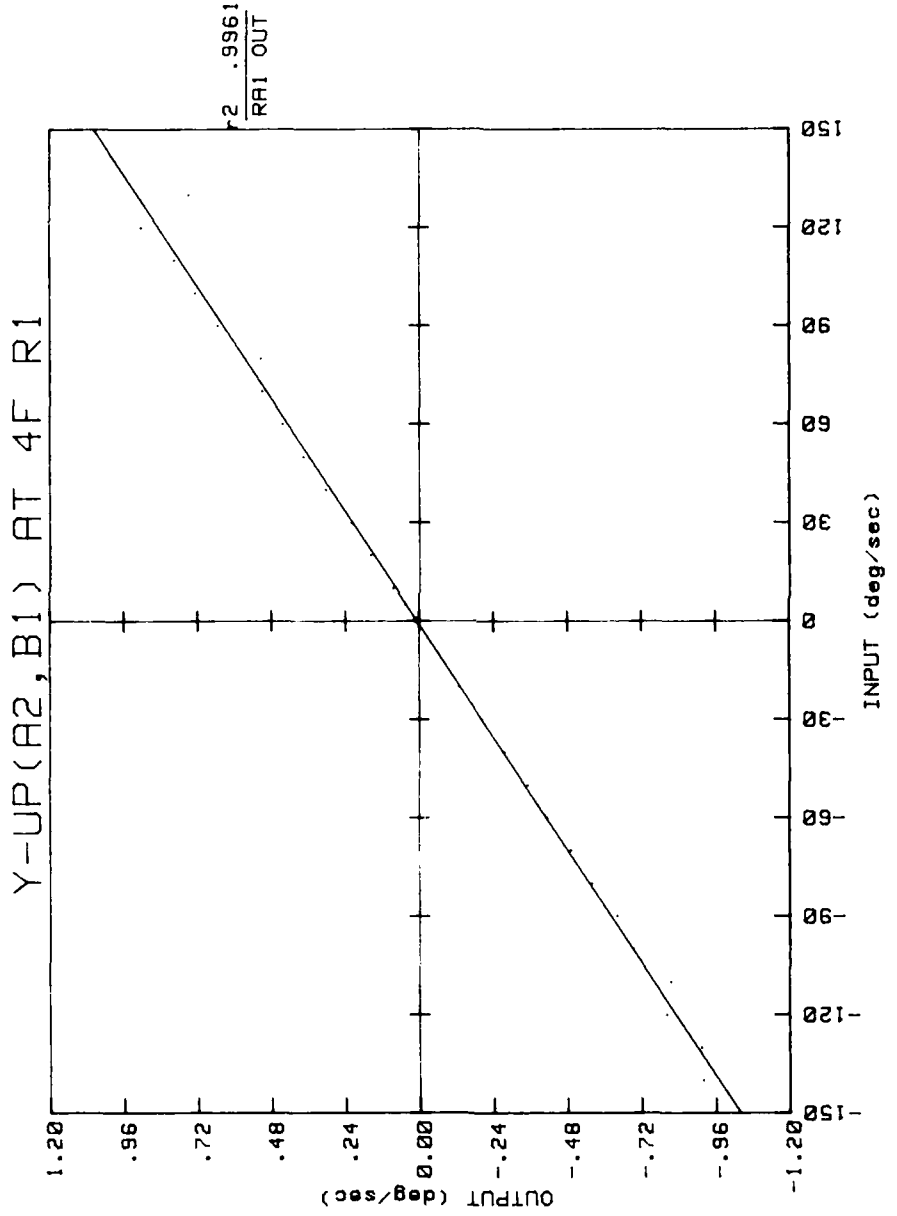

Figure 90. Input-output characteristics for repeat test R1.

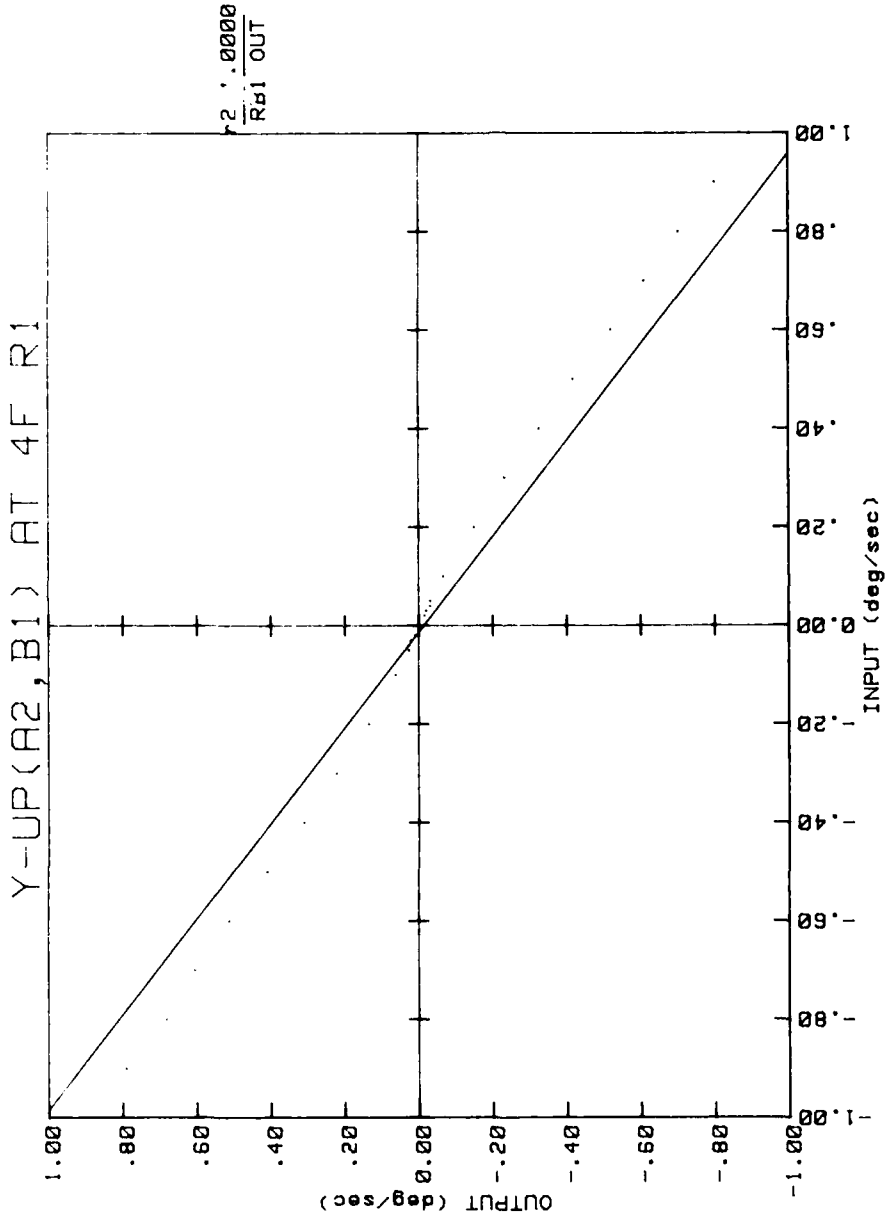

Figure 89. Input-output characteristics for repeat test R1.

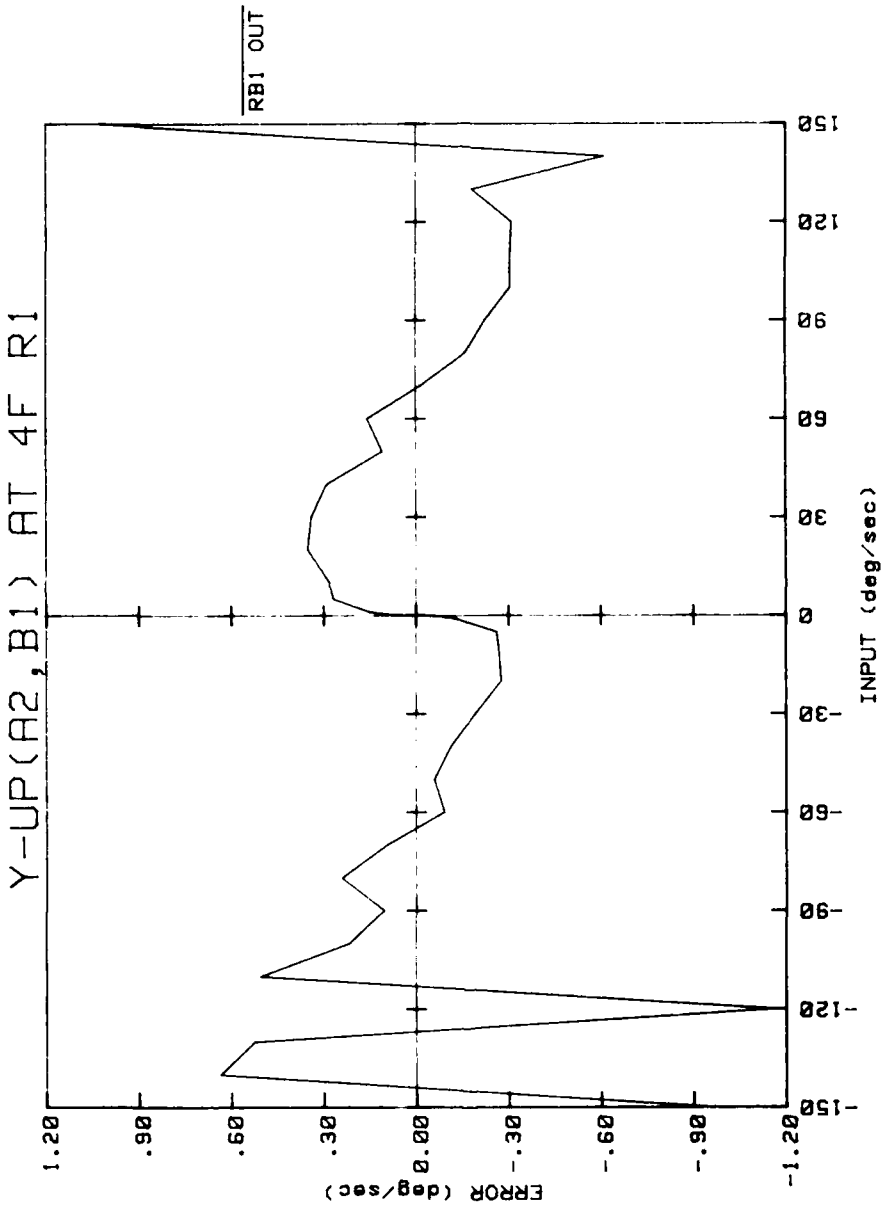

Figure 88. Input-output characteristics for repeat test R1.

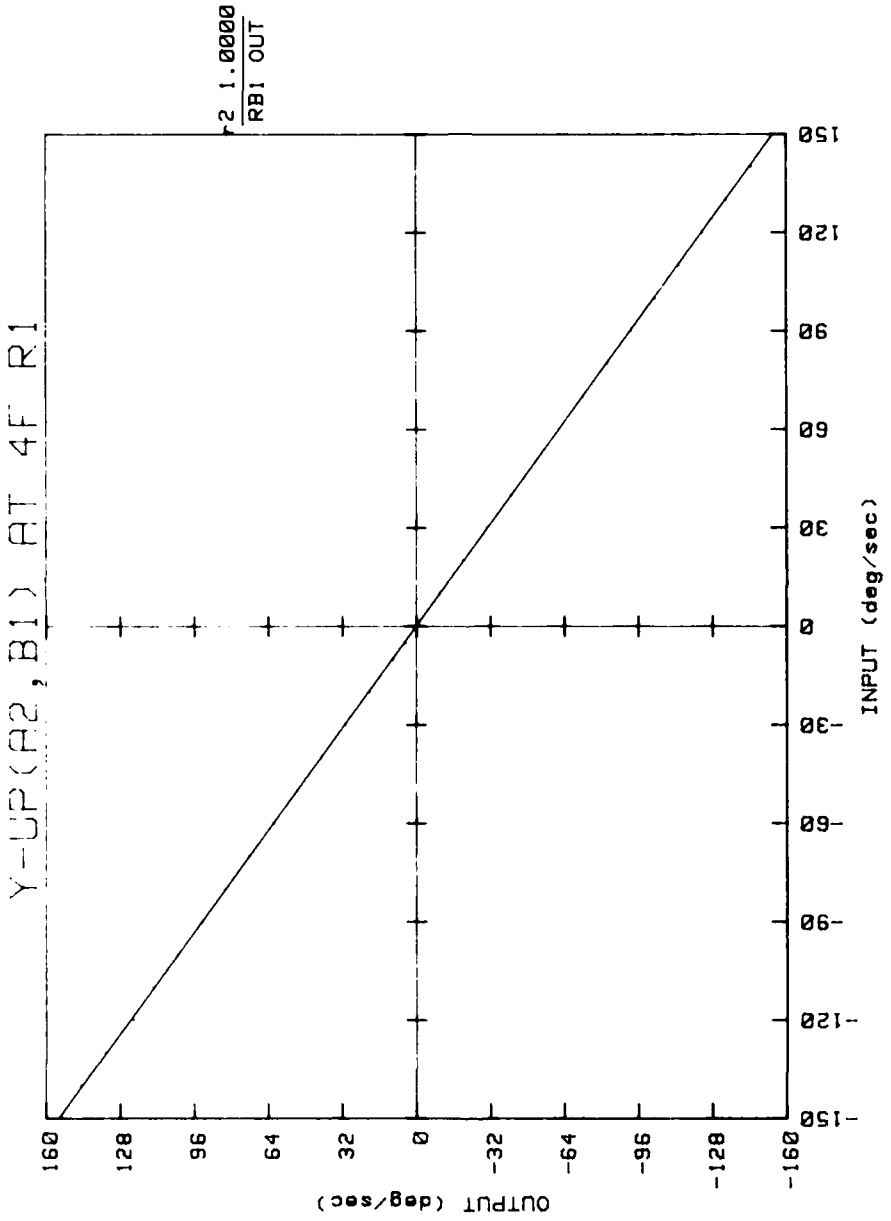

Figure 87. Input-output characteristics for repeat test R1.

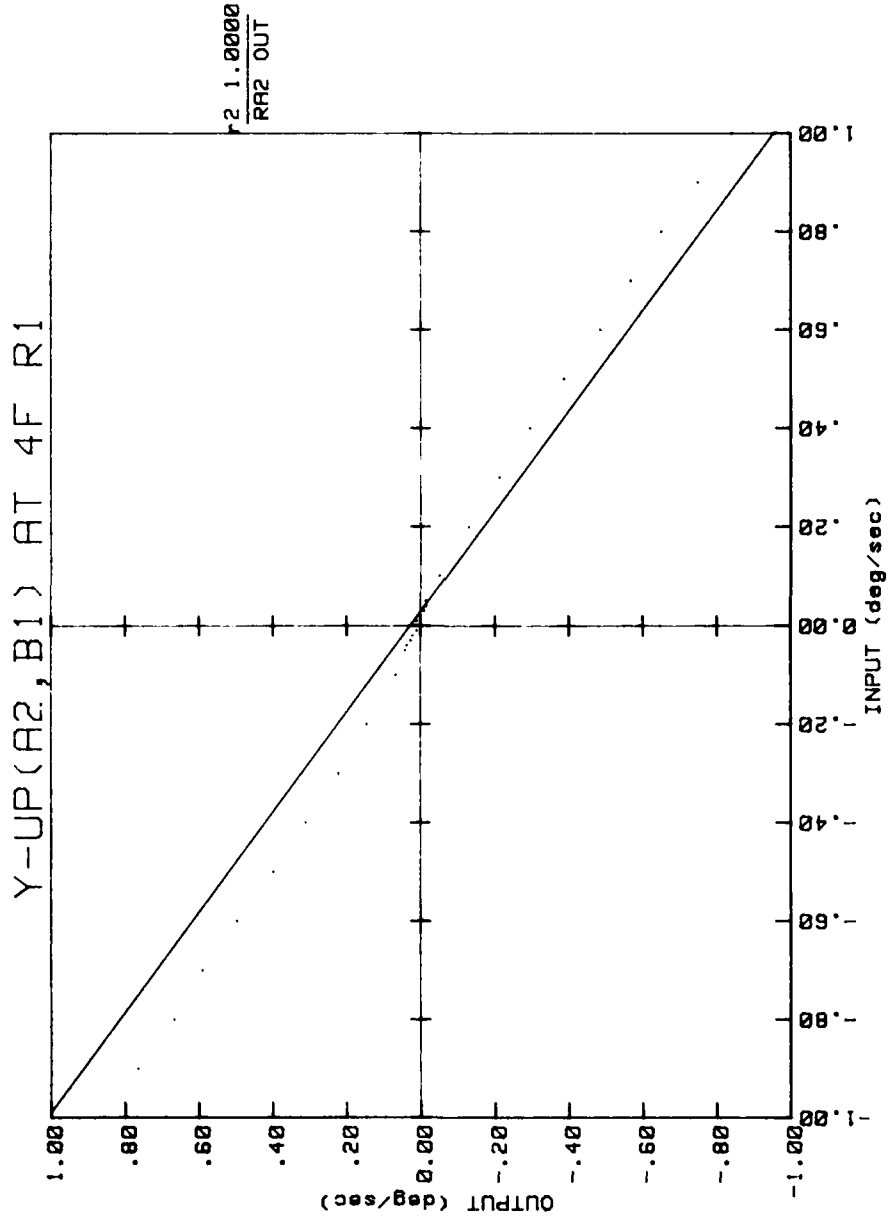

Figure 86. Input-output characteristics for repeat test R1.

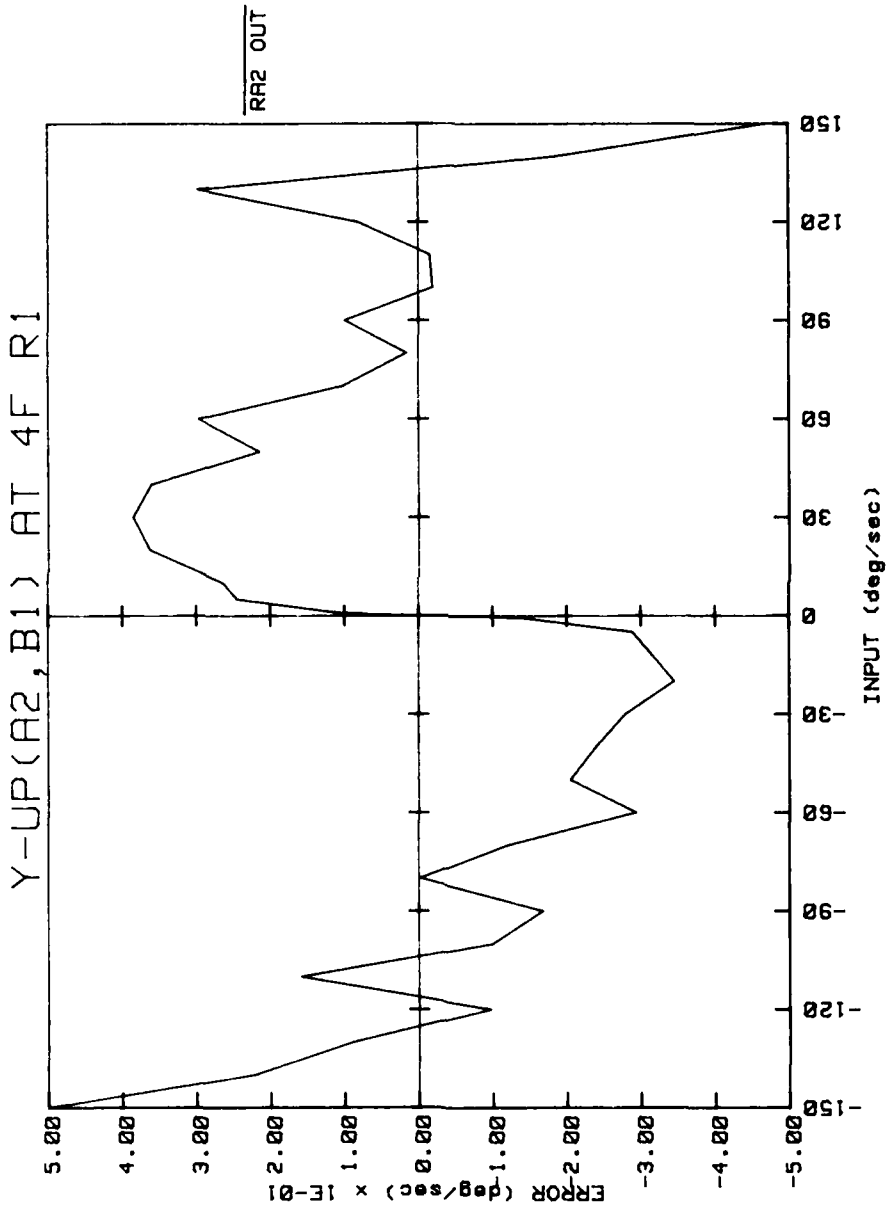

Figure 85. Input-output characteristics for repeat test R1.

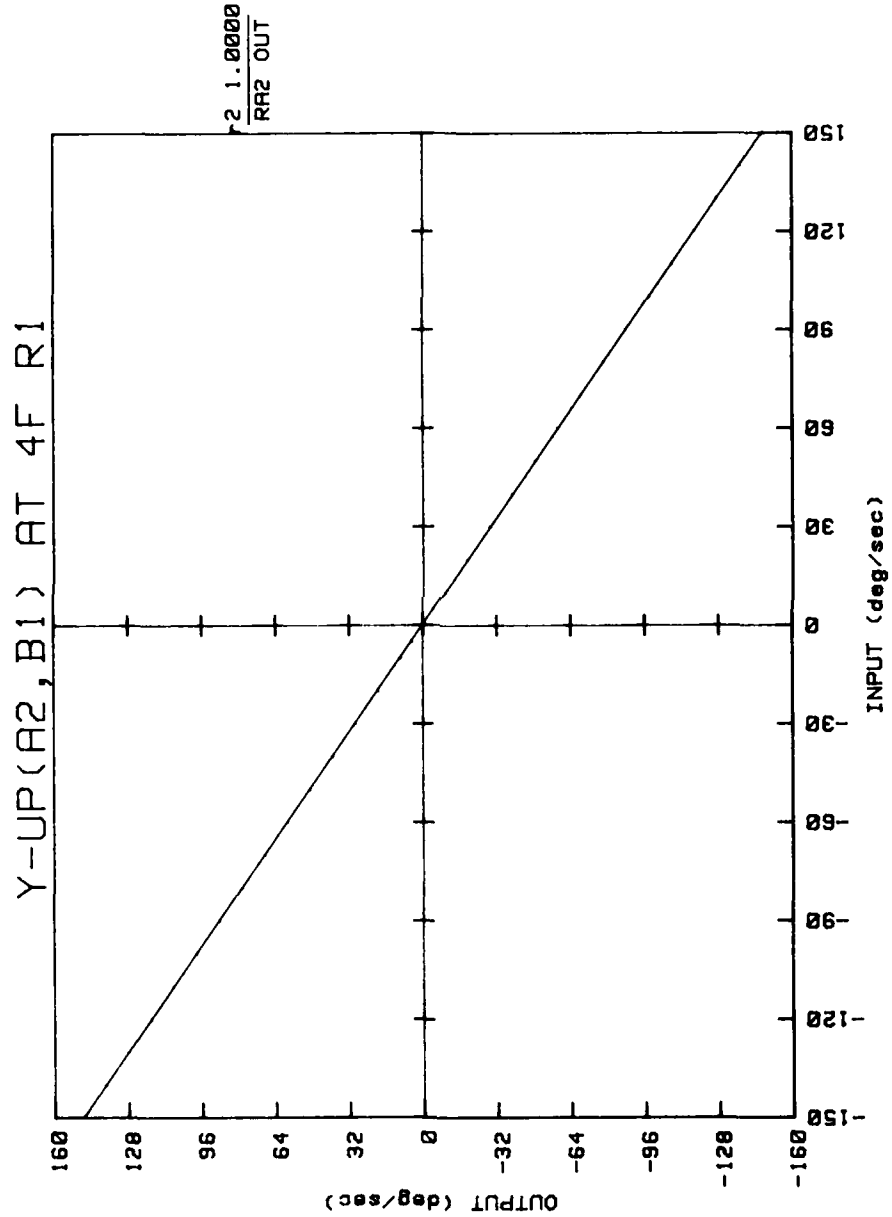

Figure 84. Input-output characteristics for repeat test R1.

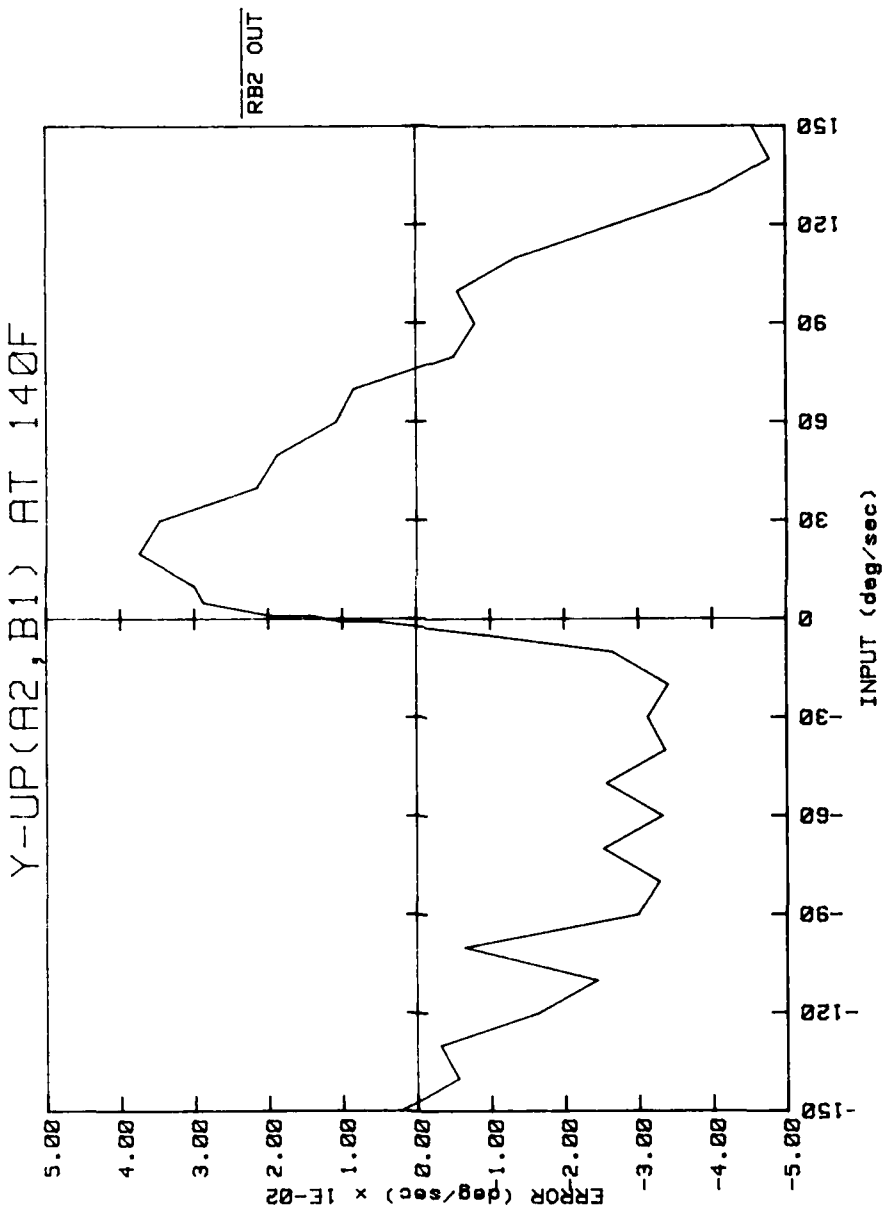

Figure 83. Input-output characteristics.

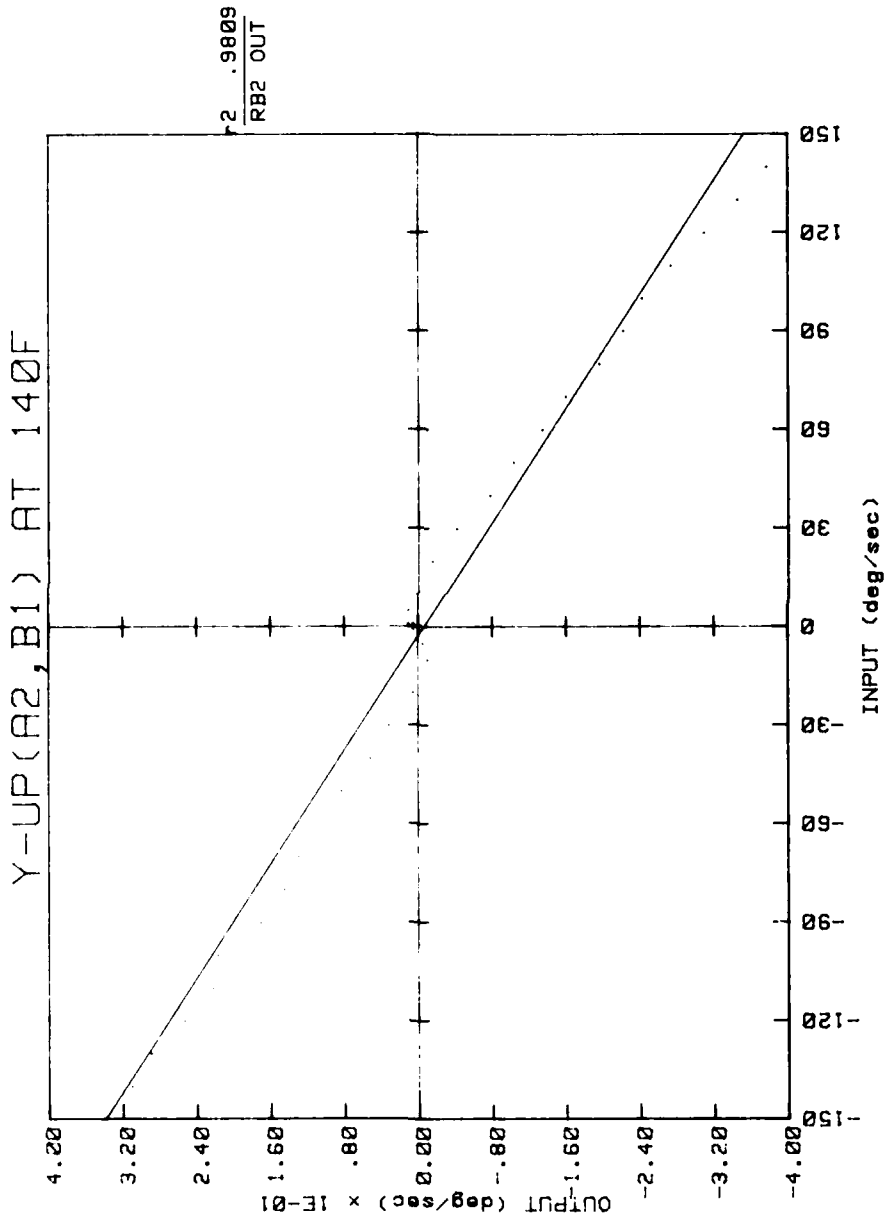

Figure 82. Input-output characteristics.

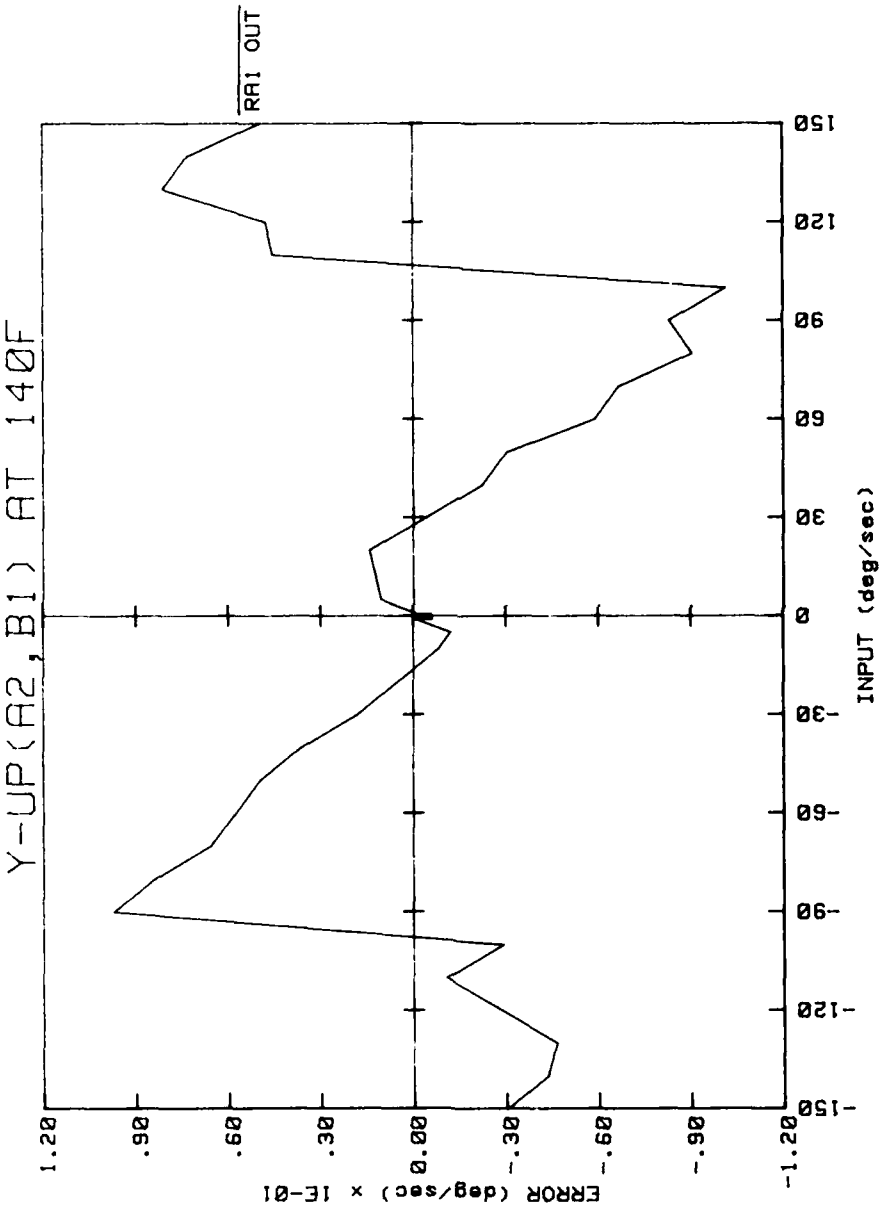

Figure 81. Input-output characteristics.

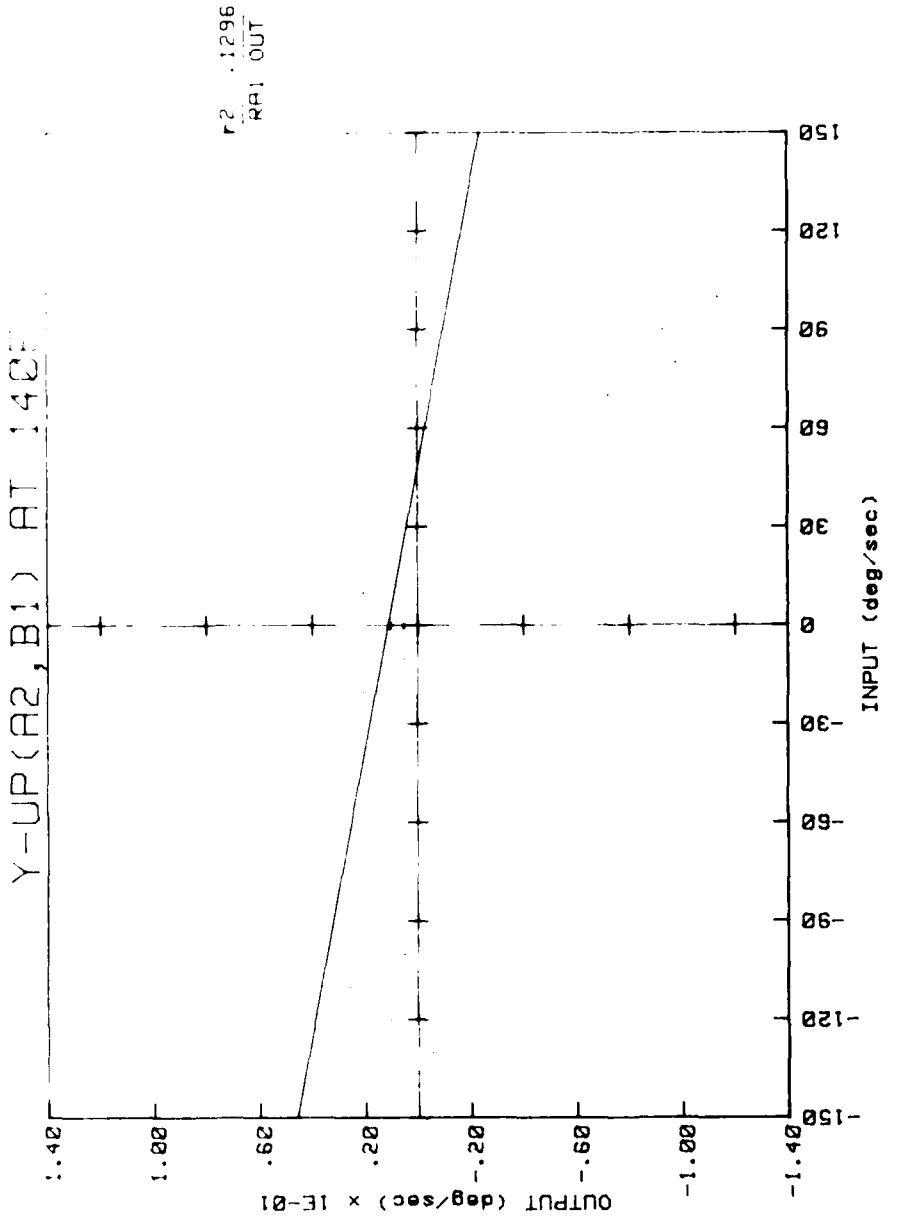

Figure 80. Input-output characteristics.

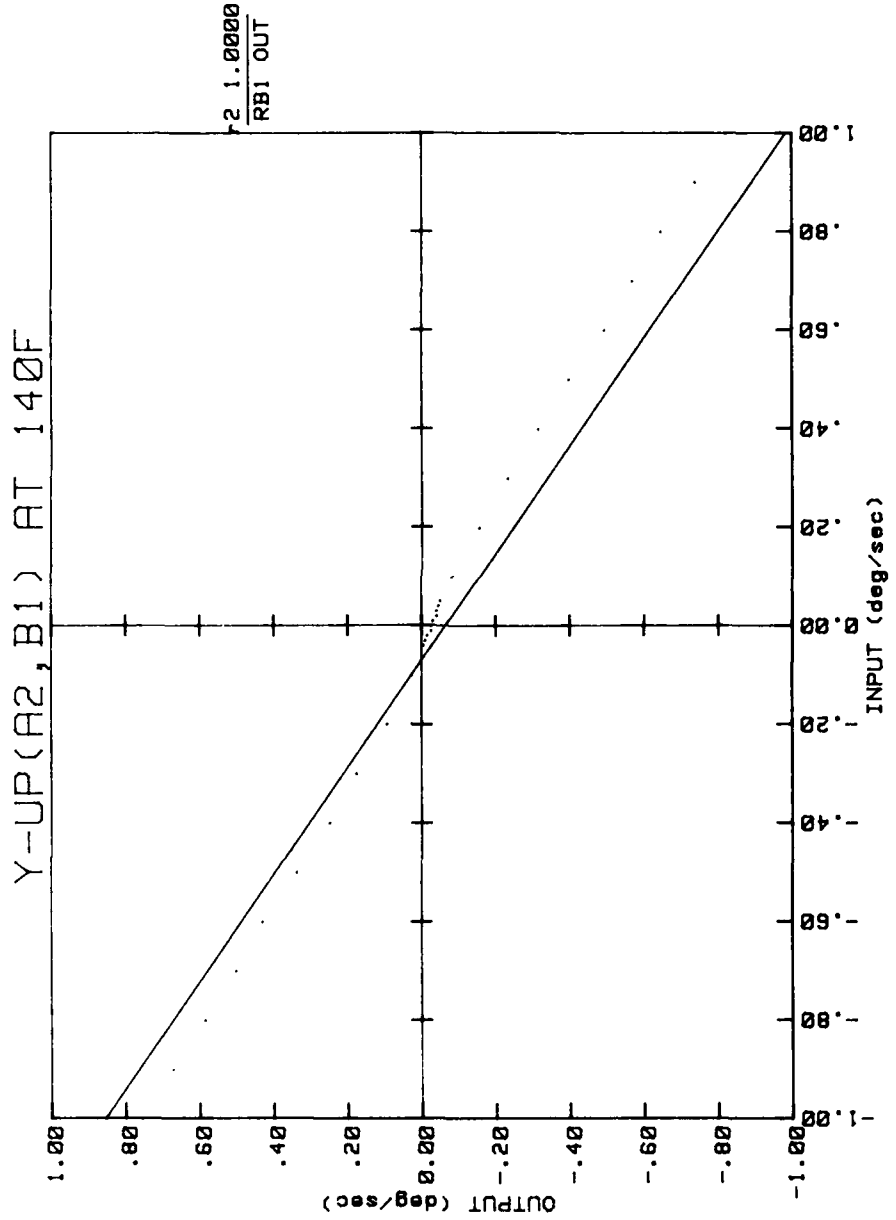

Figure 79. Input-output characteristics.

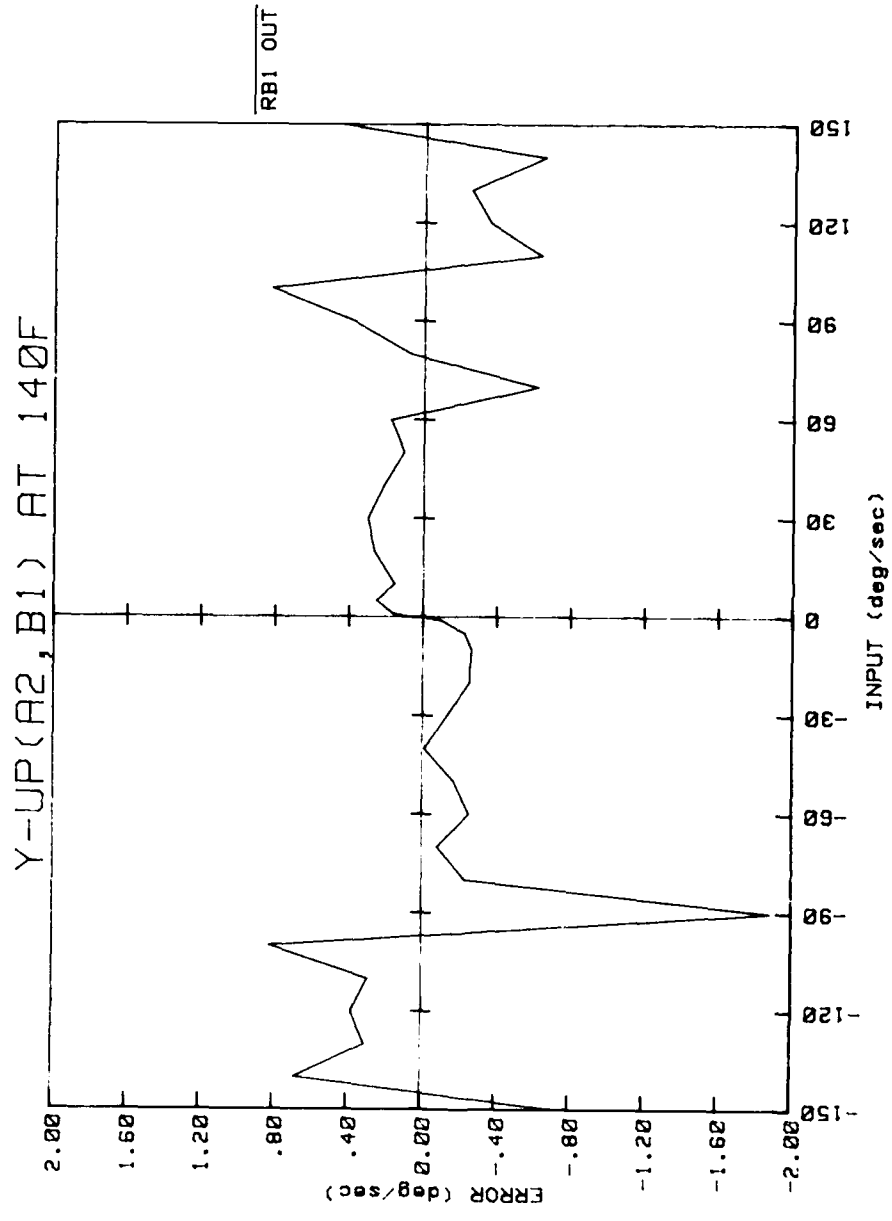

Figure 78. Input-output characteristics.

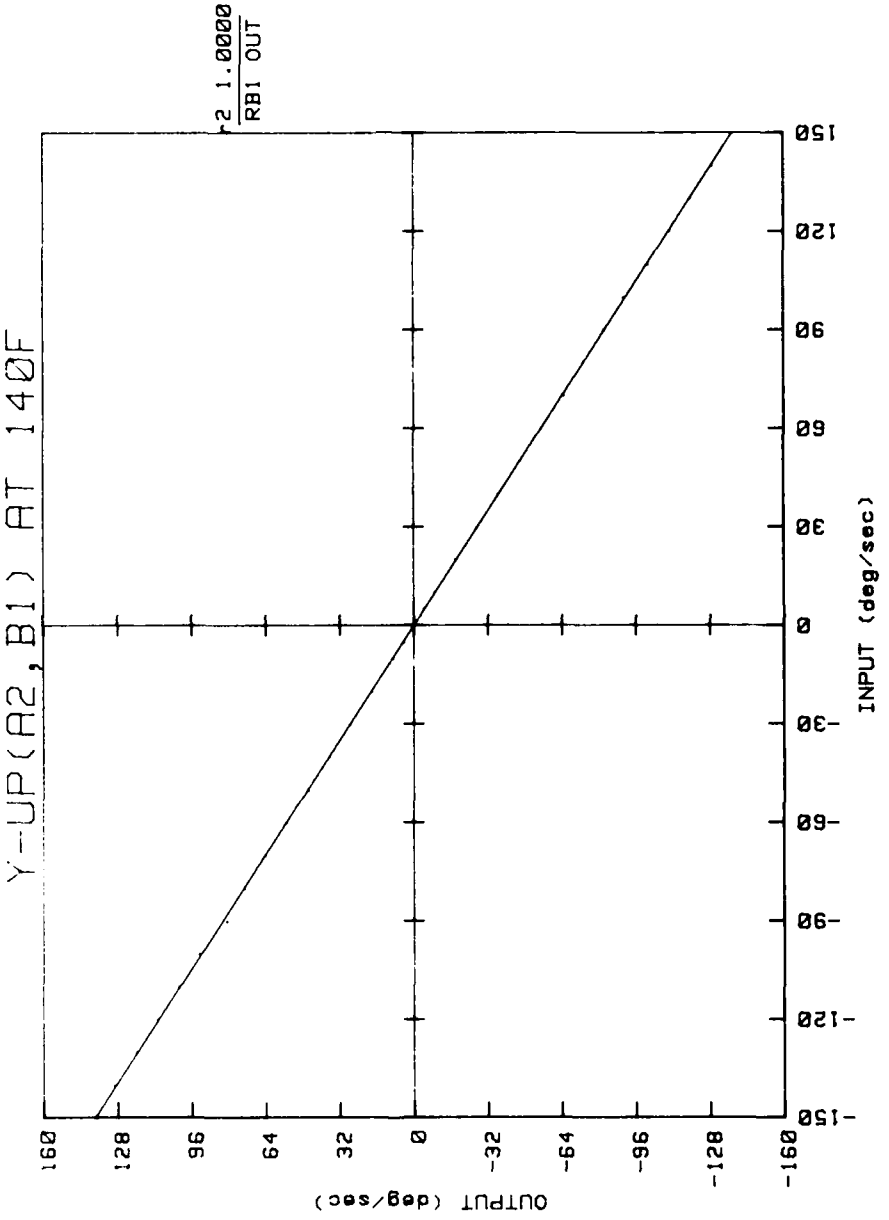

Figure 77. Input-output characteristics.

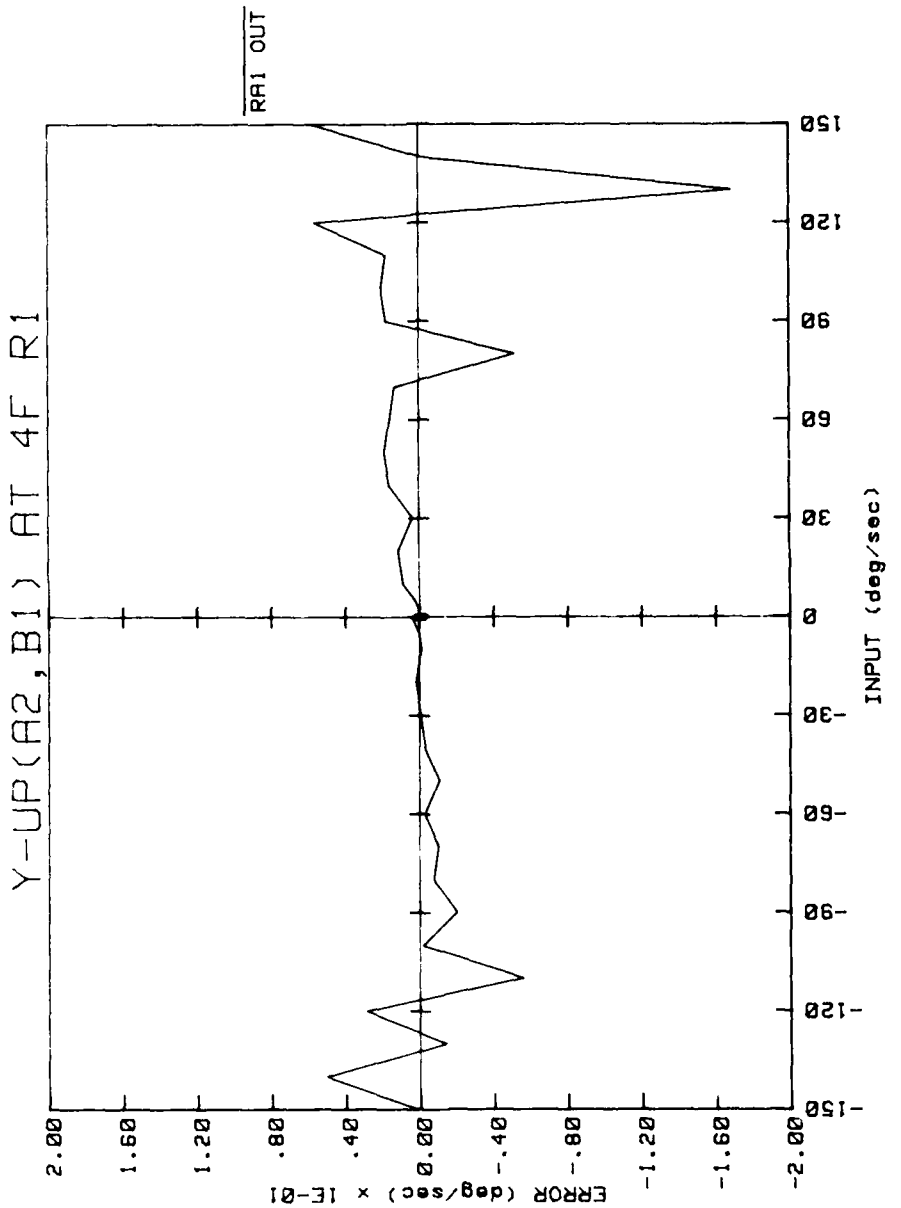

Figure 91. Input-output characteristics for repeat test R1.

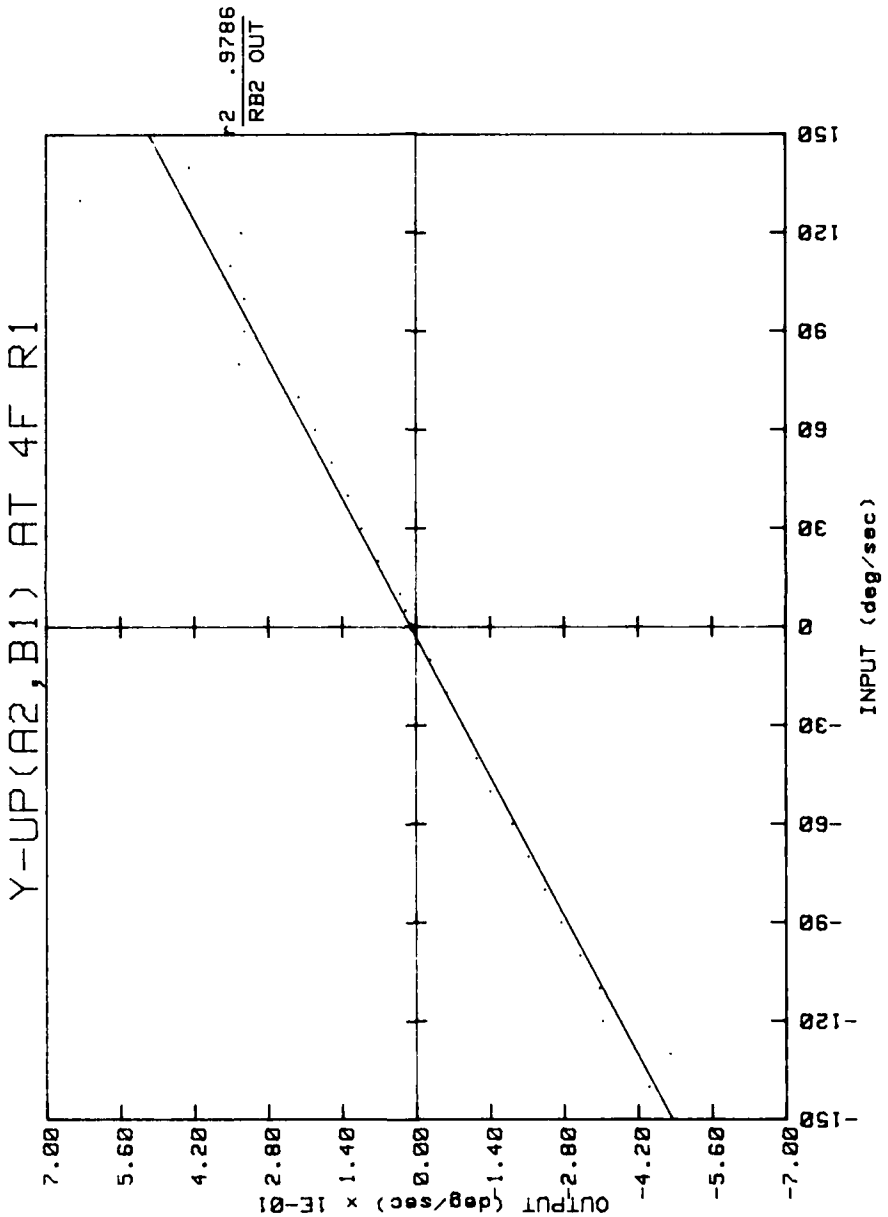

Figure 92. Input-output characteristics for repeat test R1.

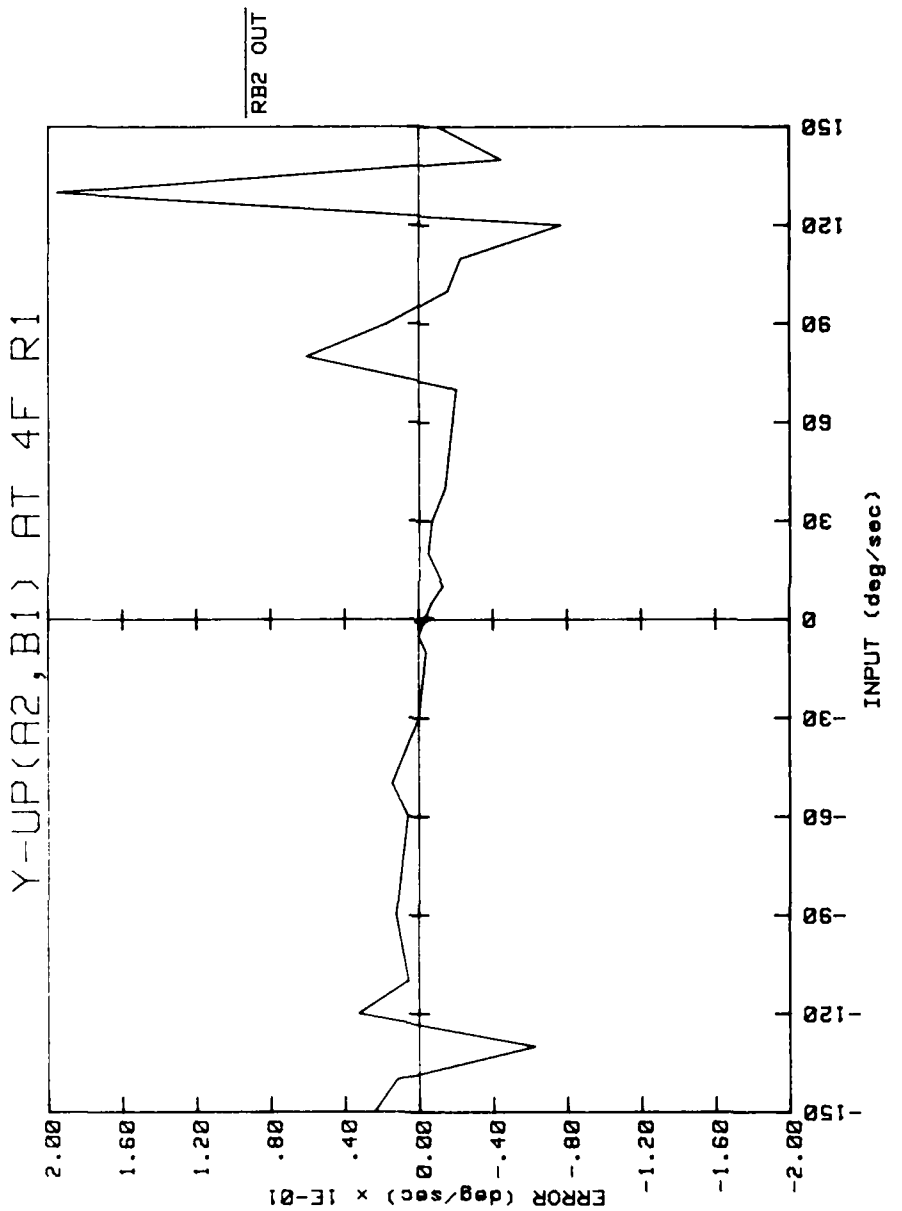

Figure 93. Input-output characteristics for repeat test R1.

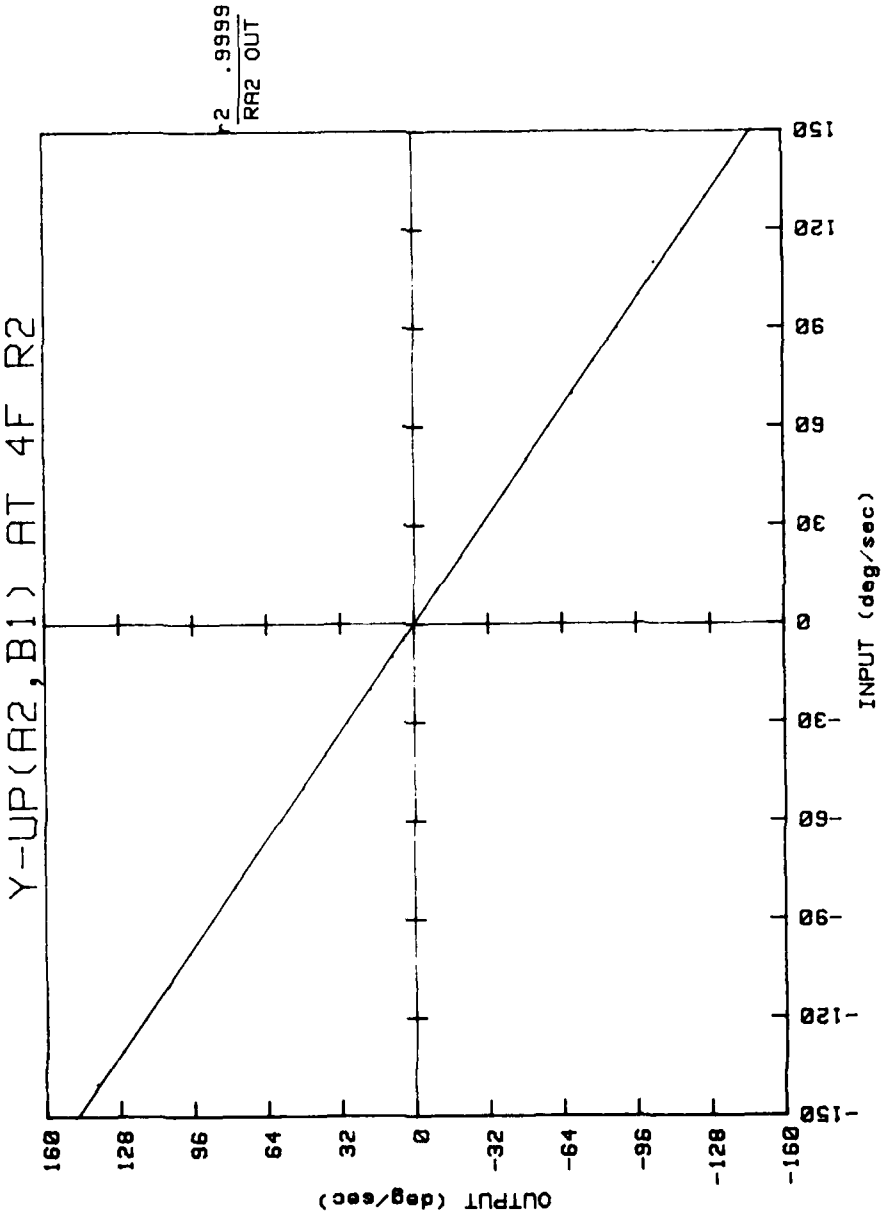

Figure 94. Input-output characteristics for repeat test R2.

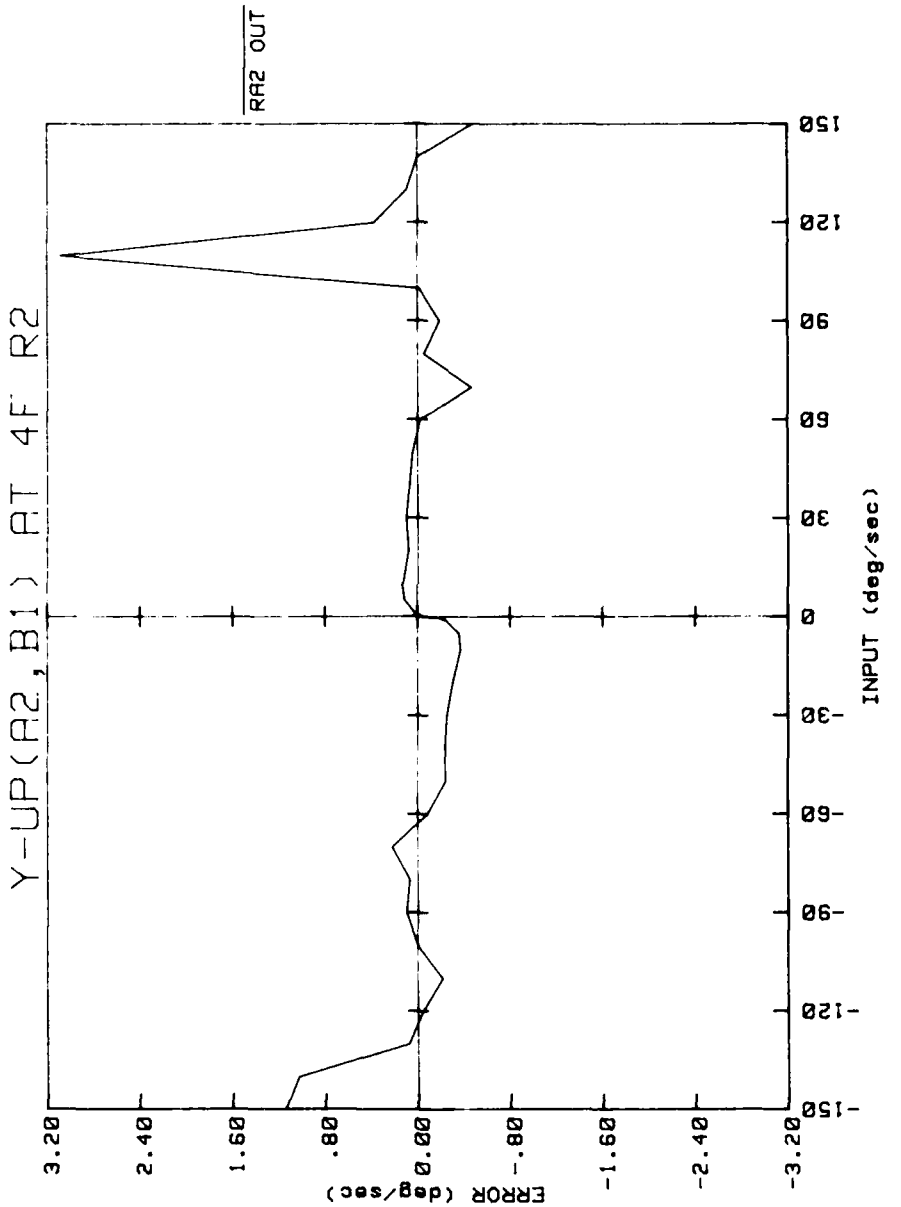

Figure 95. Input-output characteristics for repeat test R2.

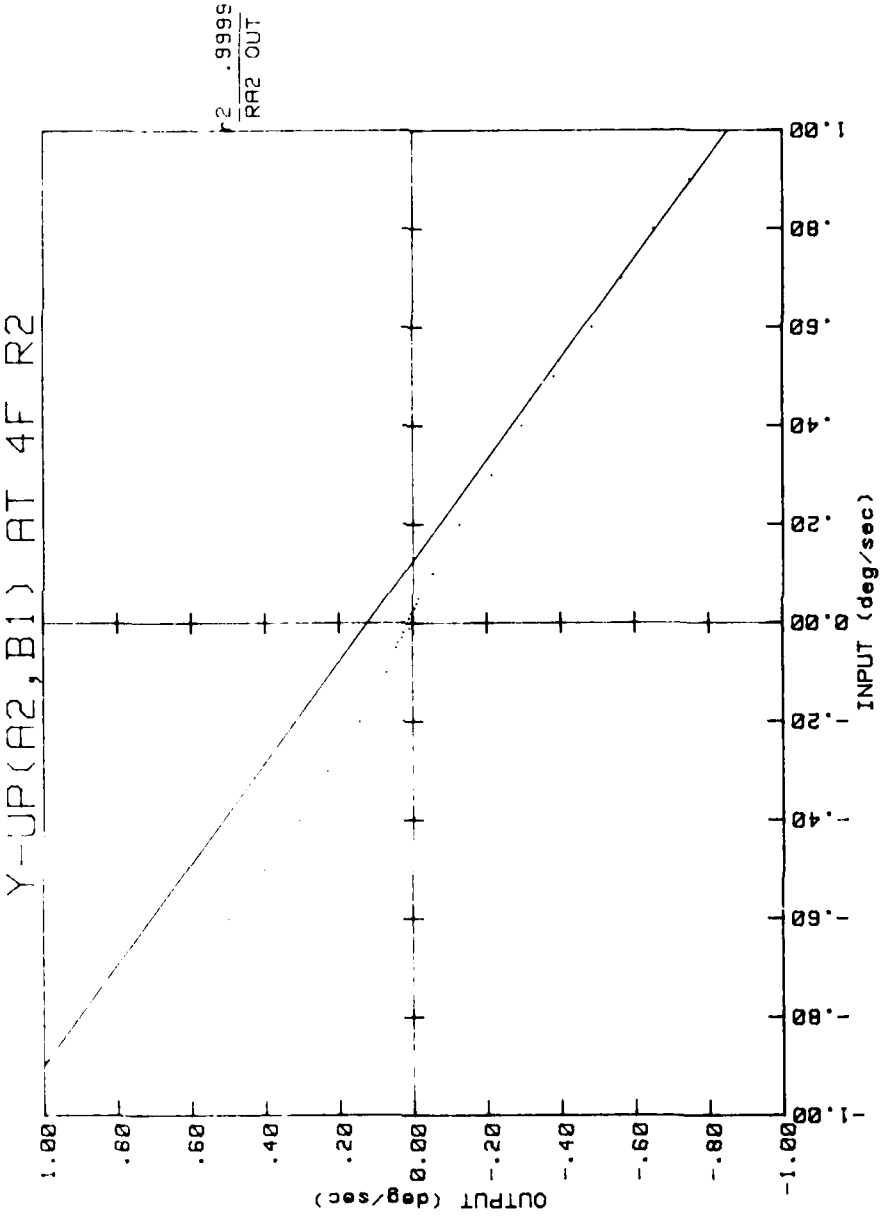

Figure 96. Input-output characteristics for repeat test R2.

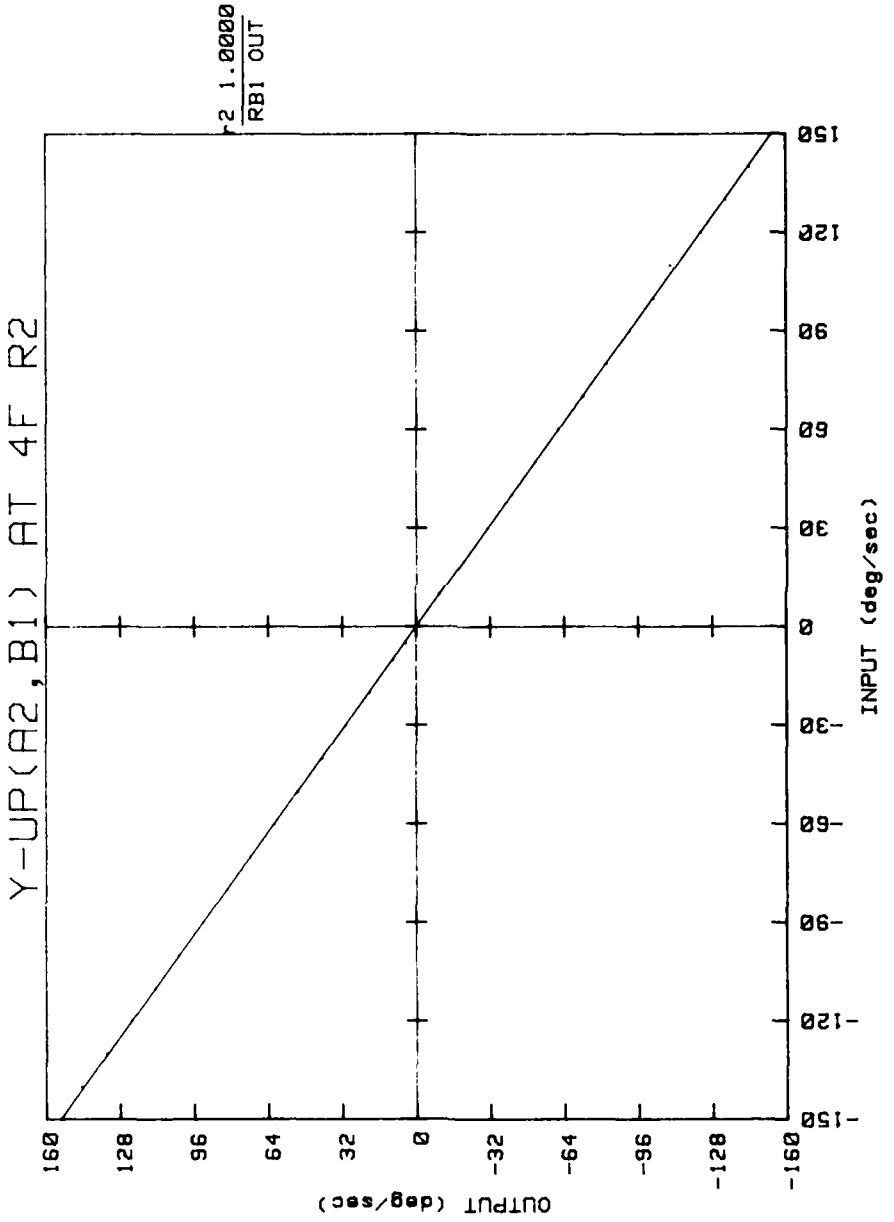

Figure 97. Input-output characteristics for repeat test R2.

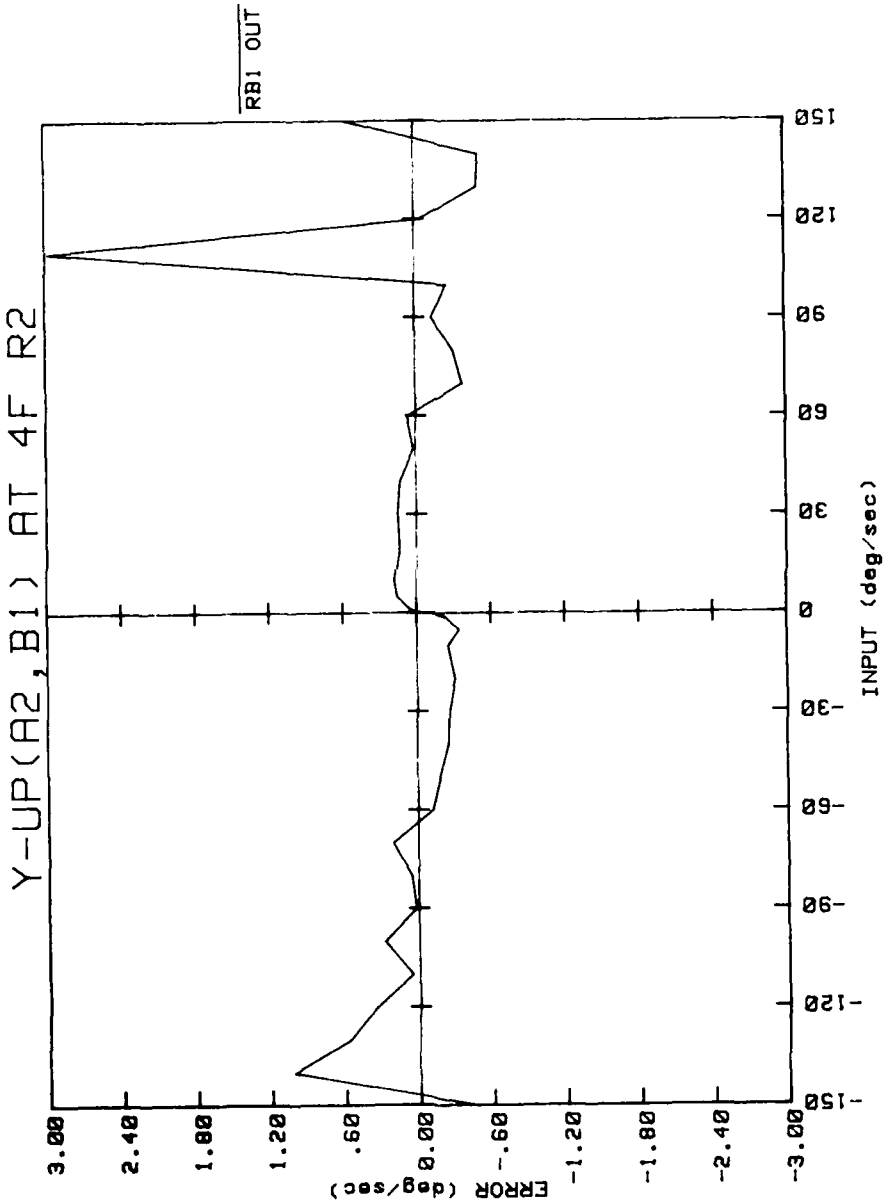

Figure 98. Input-output characteristics for repeat test R2.

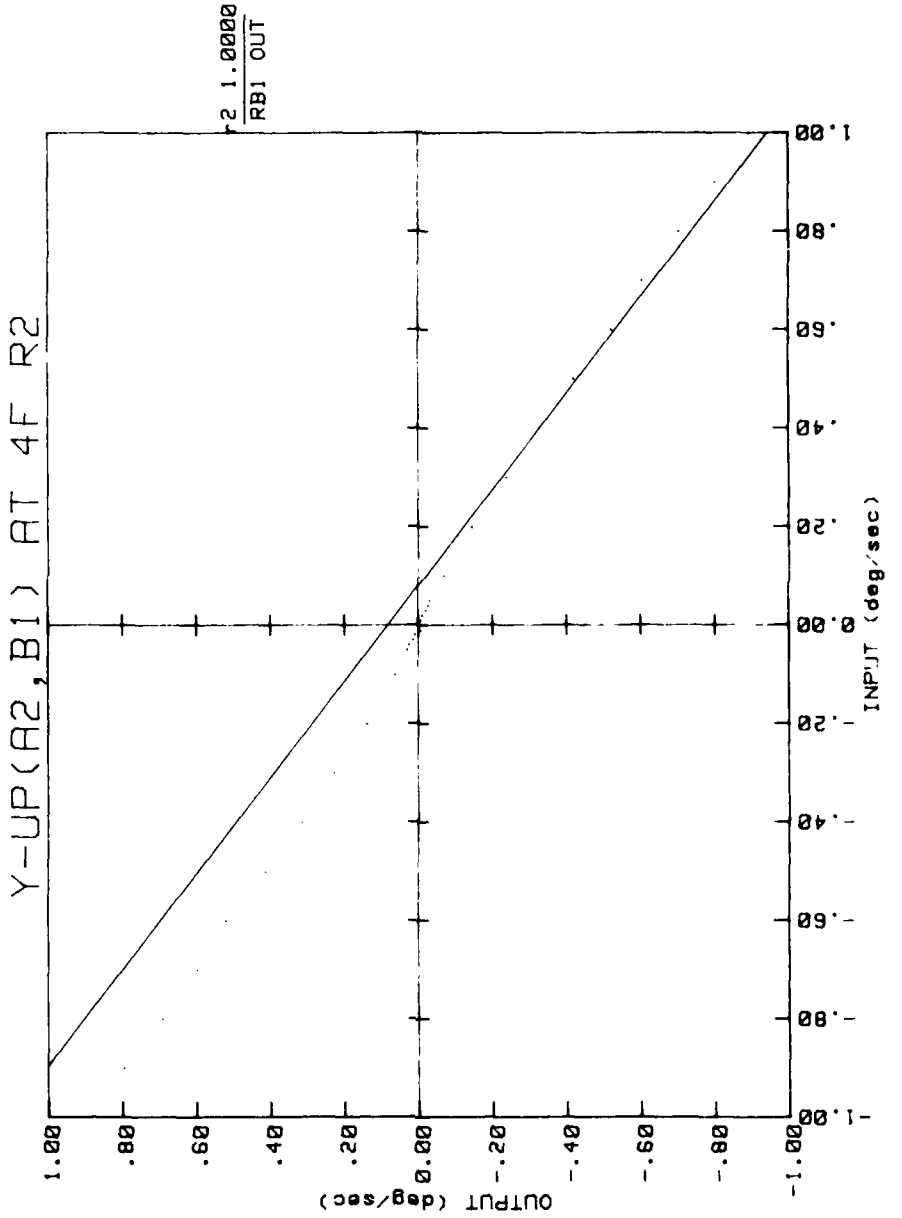

Figure 46. Input-output characteristics for repeat test R2.

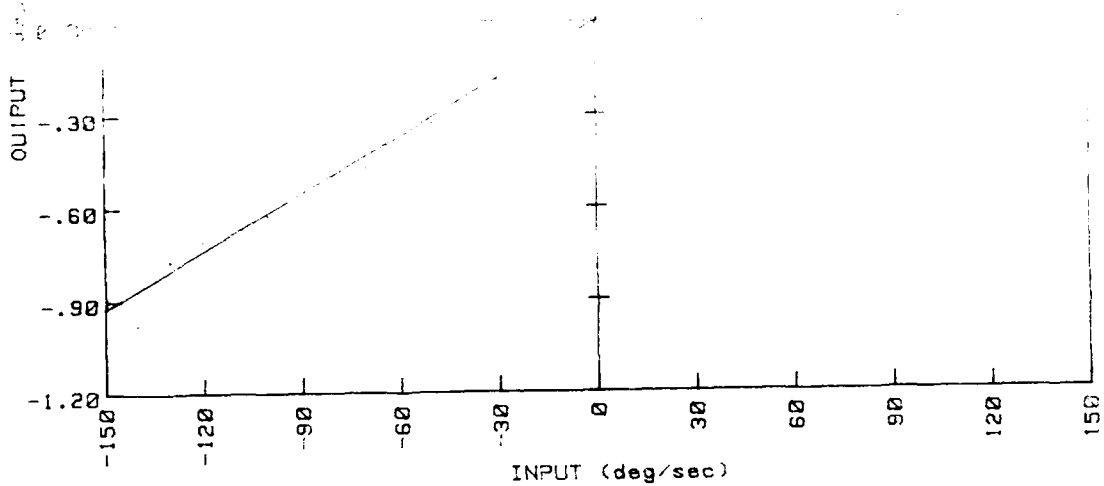
OUTPUT
-.30
-.60
-.90
-1.20
-150
-120
-90
-60
-30
0
30
60
90
120
150
INPUT (deg/sec)

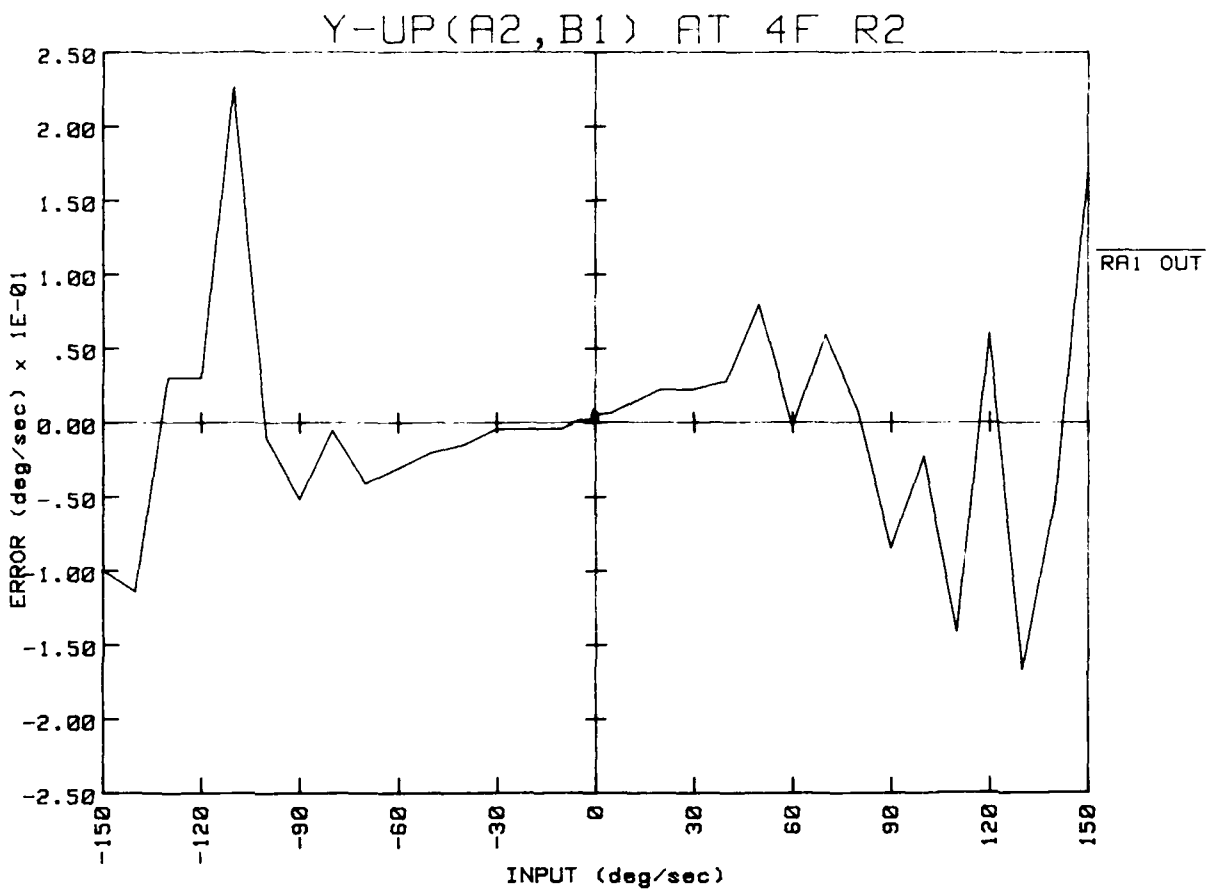

Figure 101. Input-output characteristics for repeat test R2.

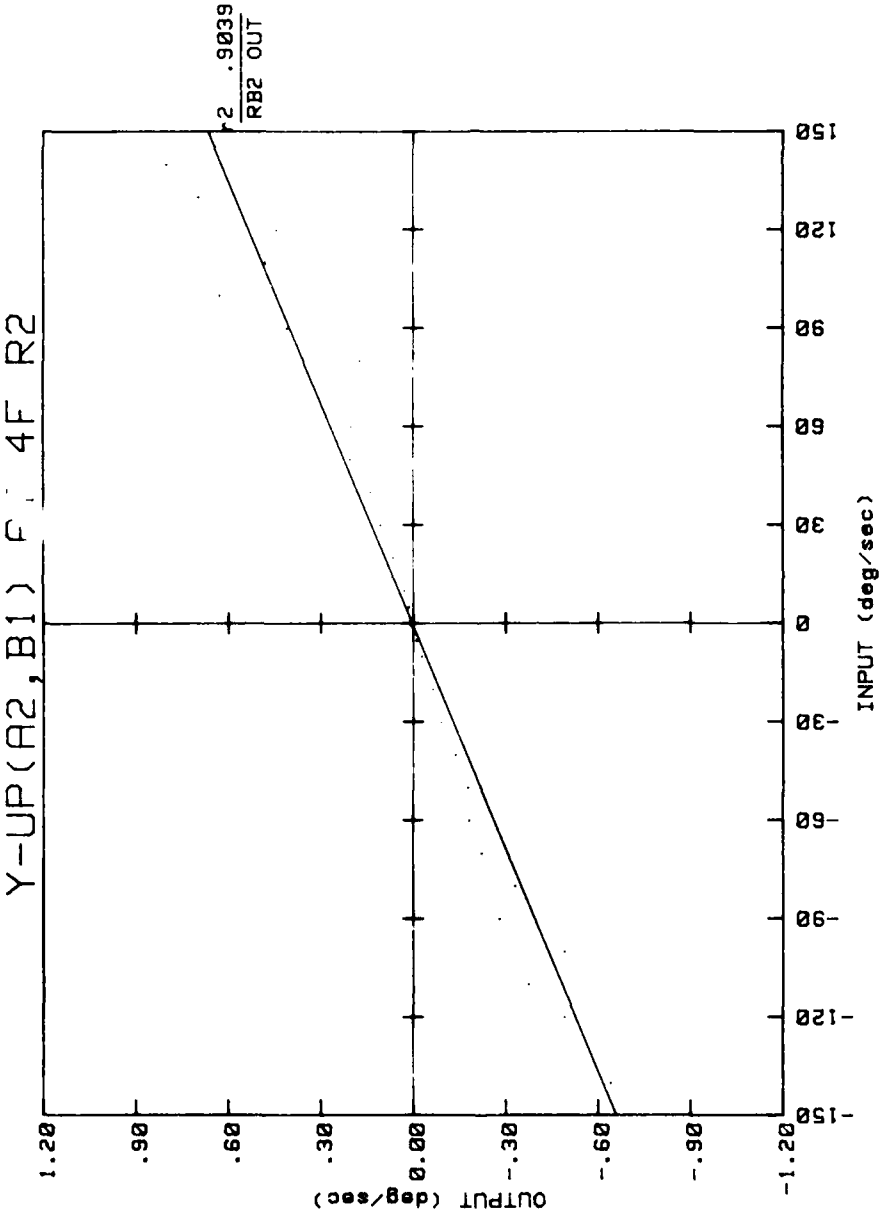

Figure 102. Input-output characteristics for repeat test R2.

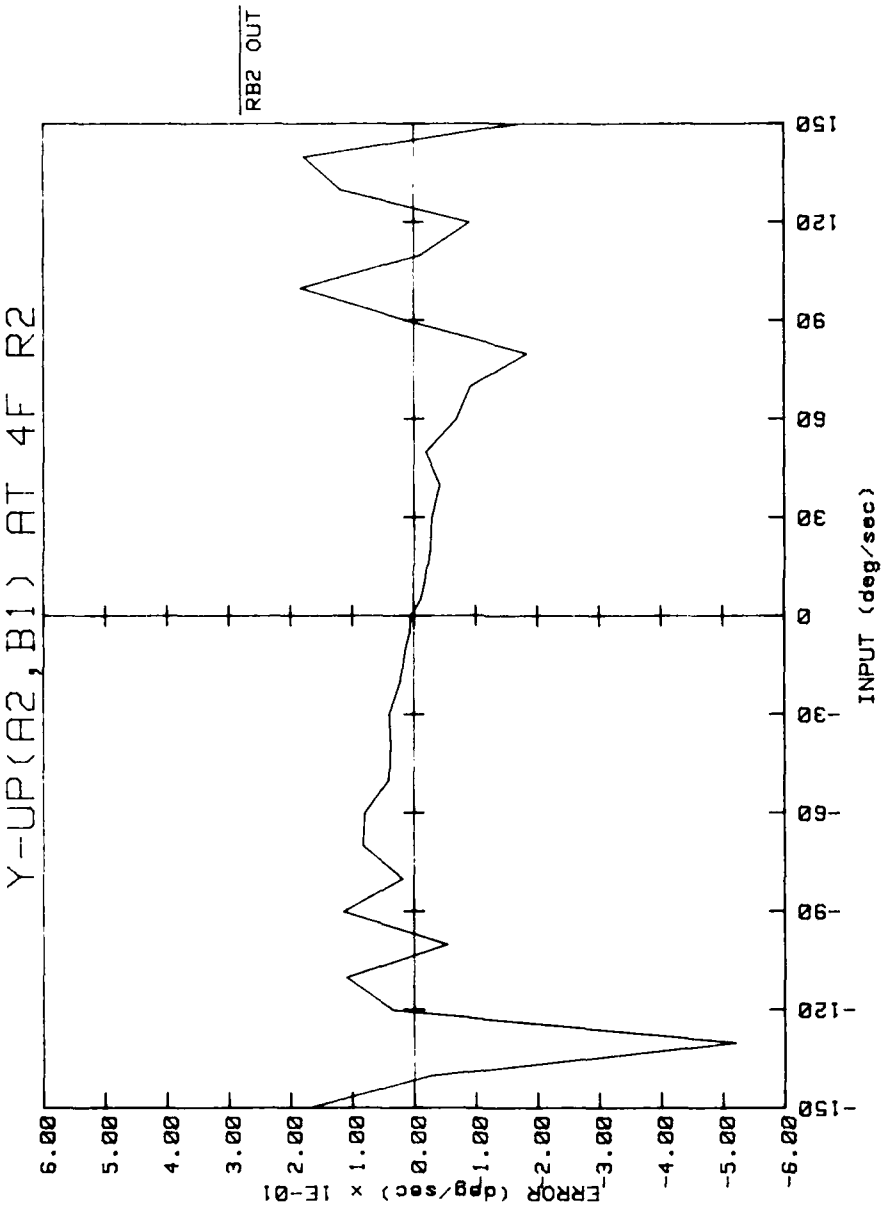

Figure 103. Input-output characteristics for repeat test R2.

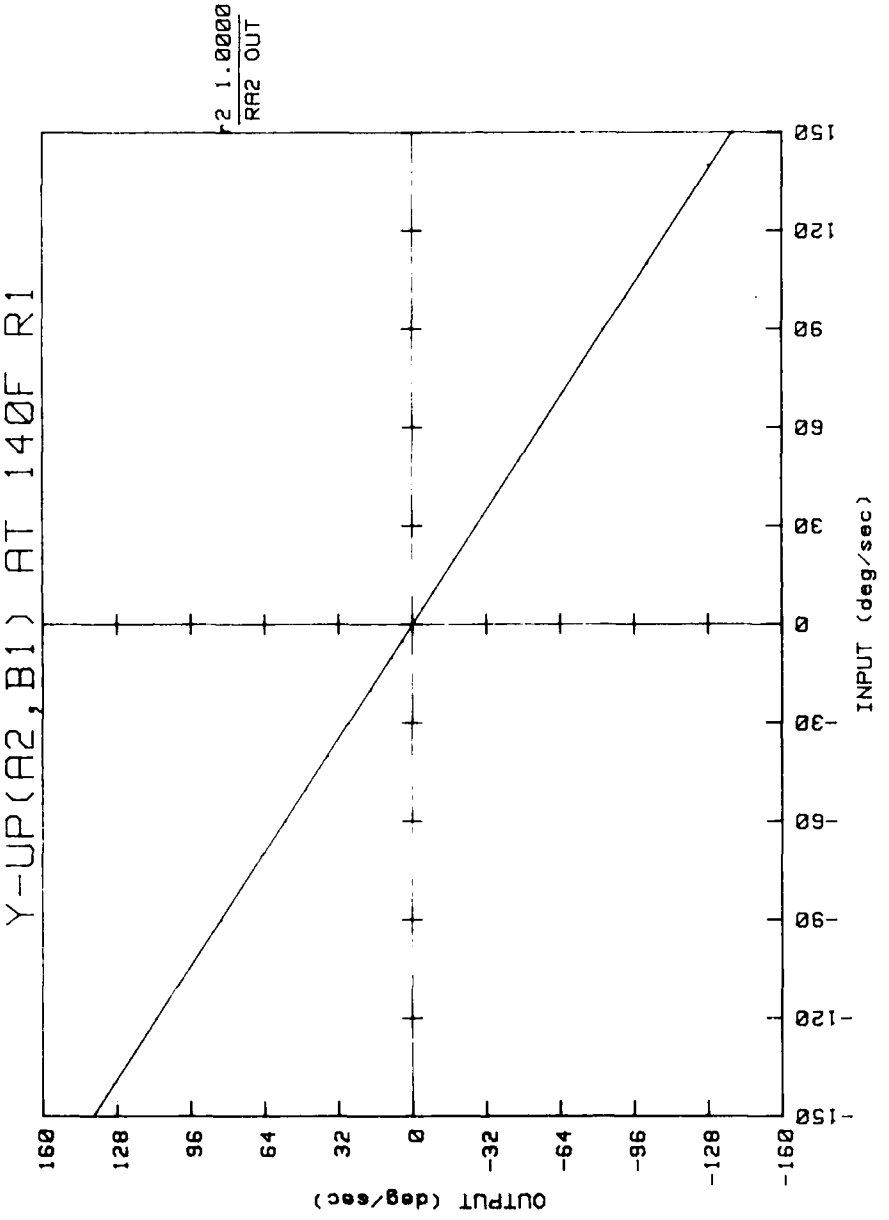

Figure 104. Input-output characteristics for repeat test R1.

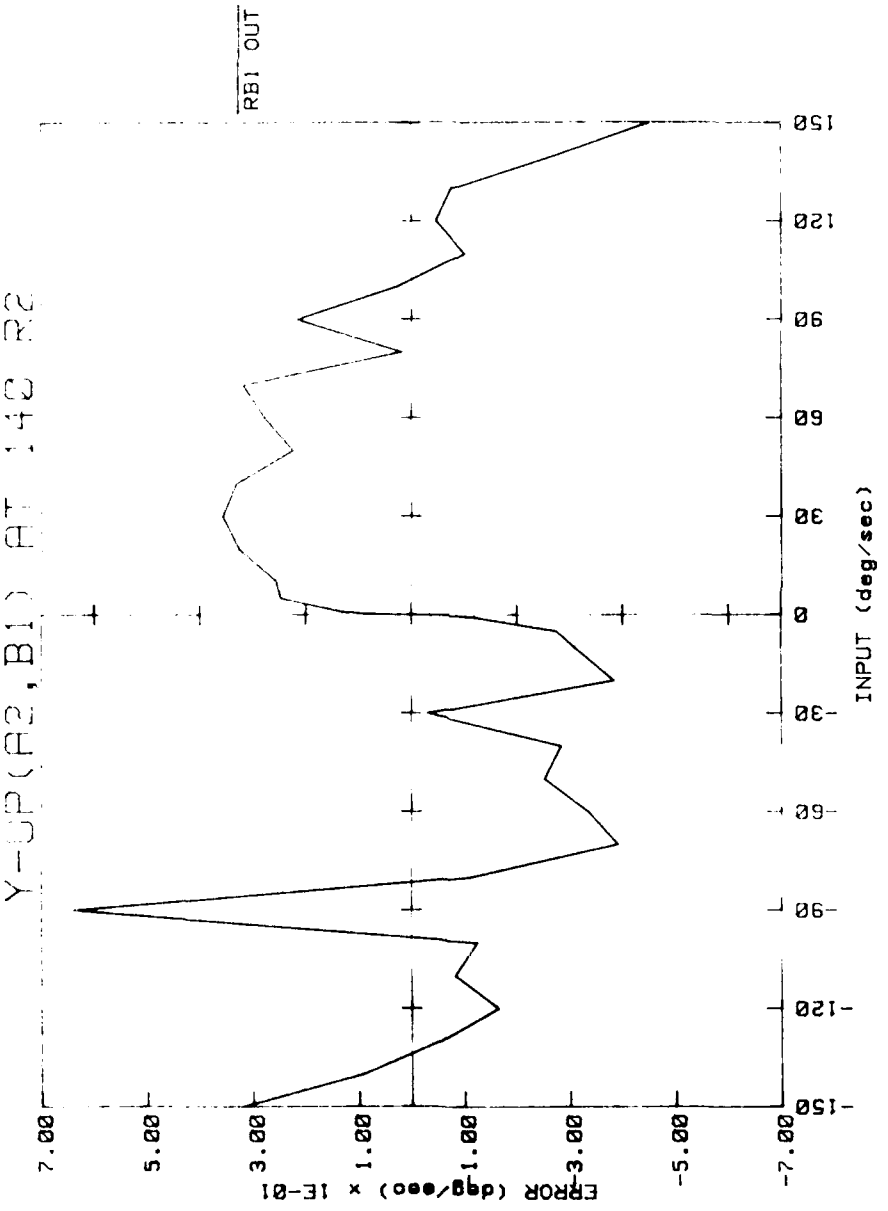

Figure 118. Input-output characteristics for repeat test R2.

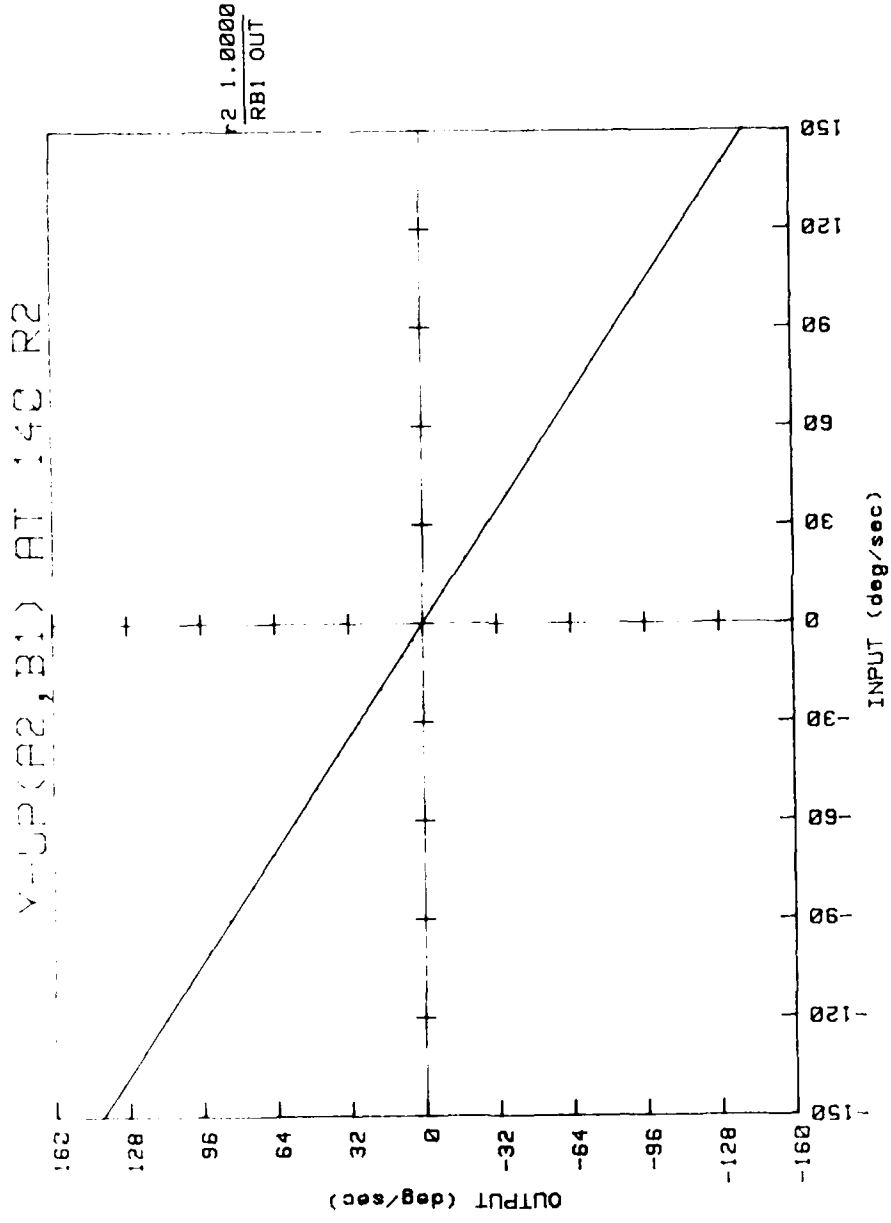

Figure 117. Input-output characteristics for repeat test R2.

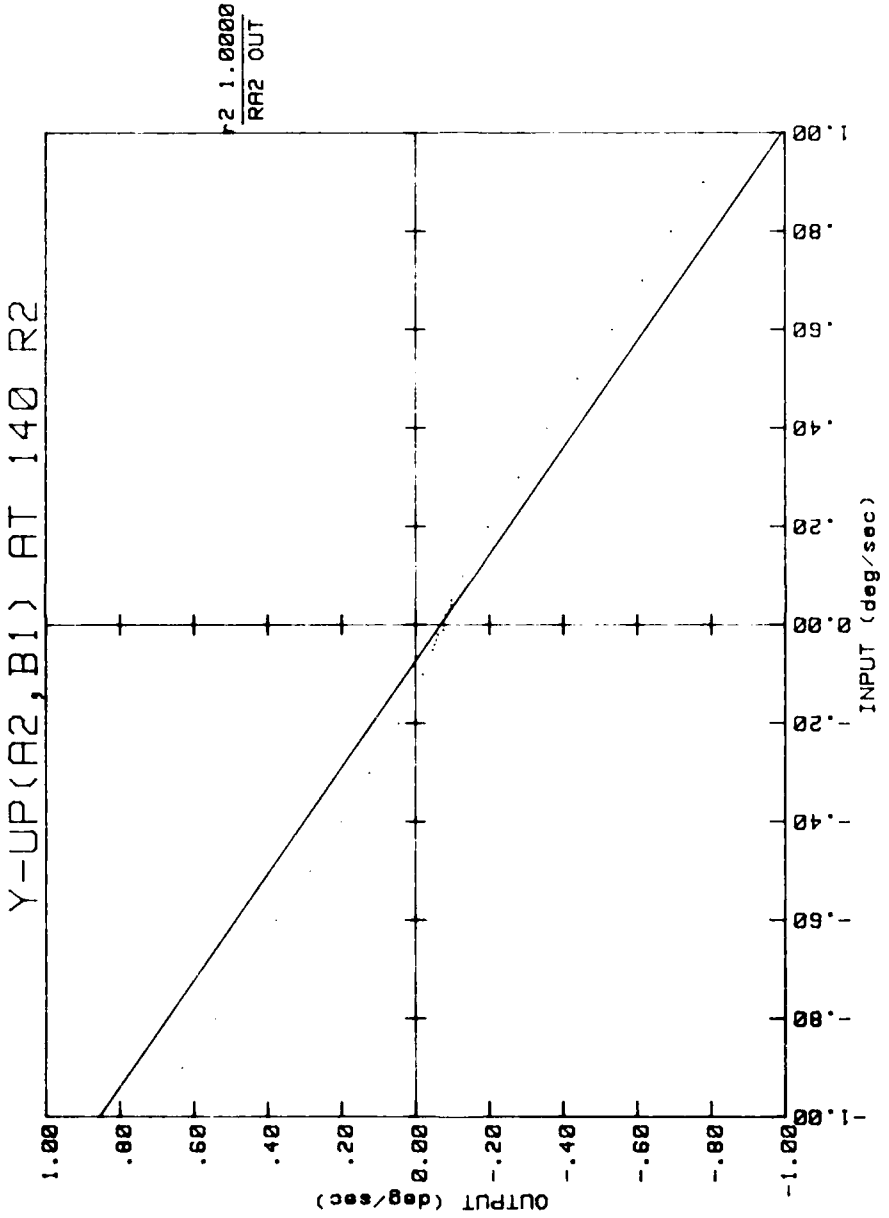

Figure 116. Input-output characteristics for repeat test R2.

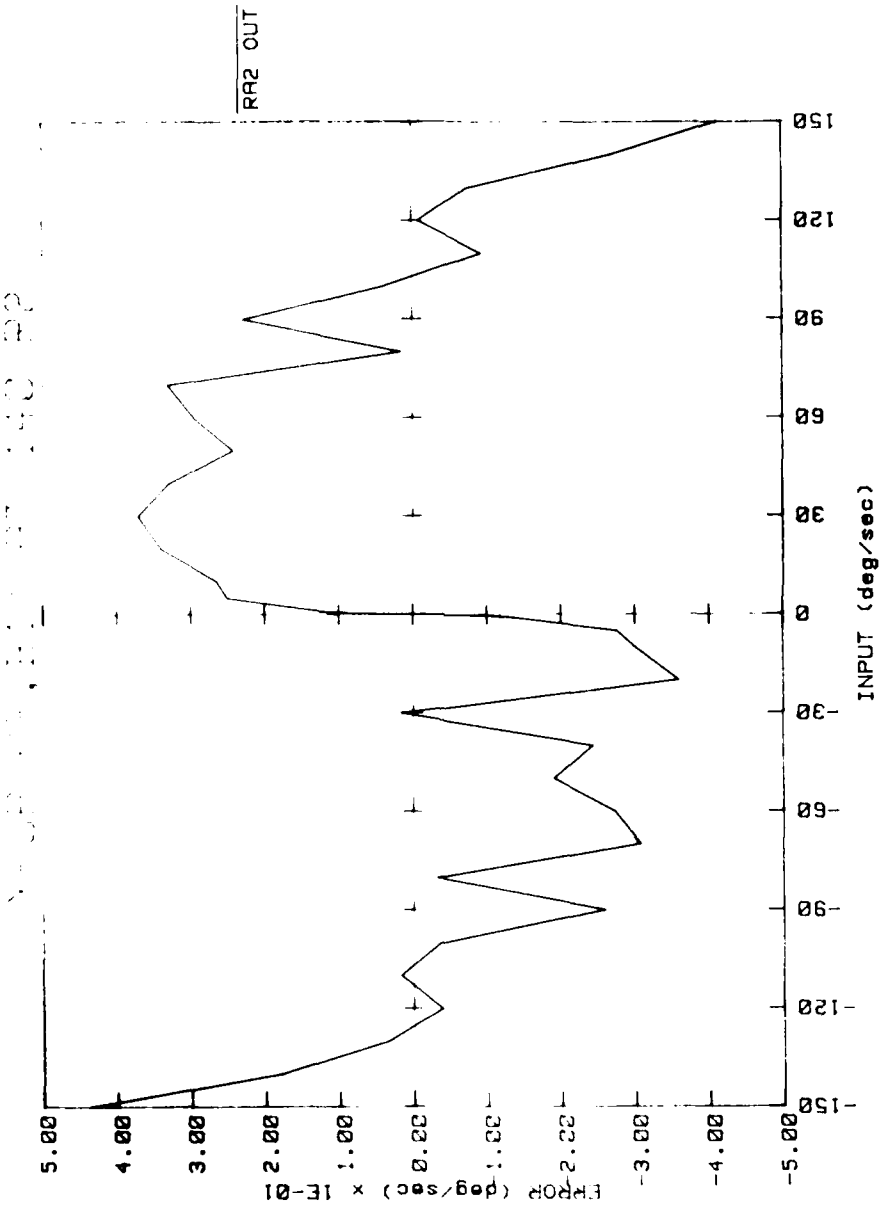

Figure 115. Input-output characteristics for repeat test R2.

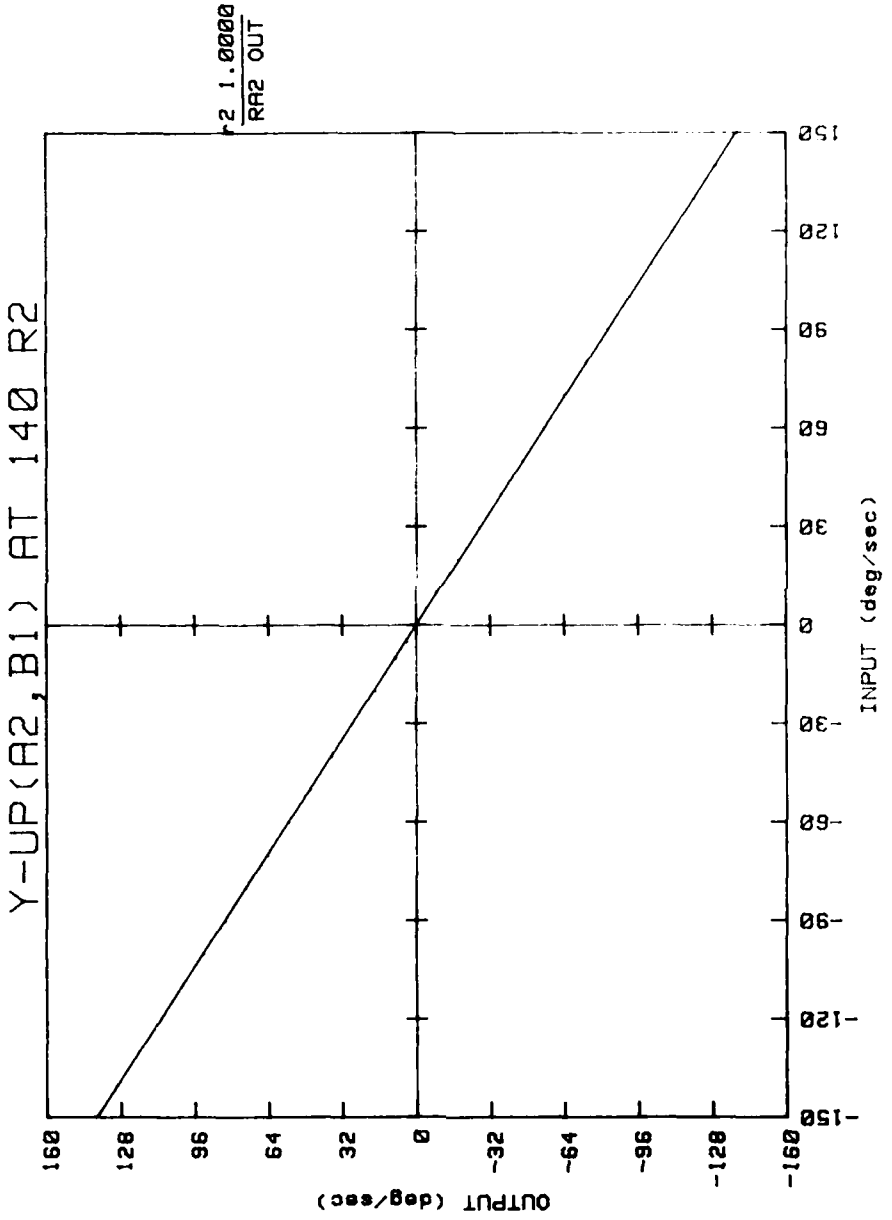

Figure 114. Input-output characteristics for repeat test R2.

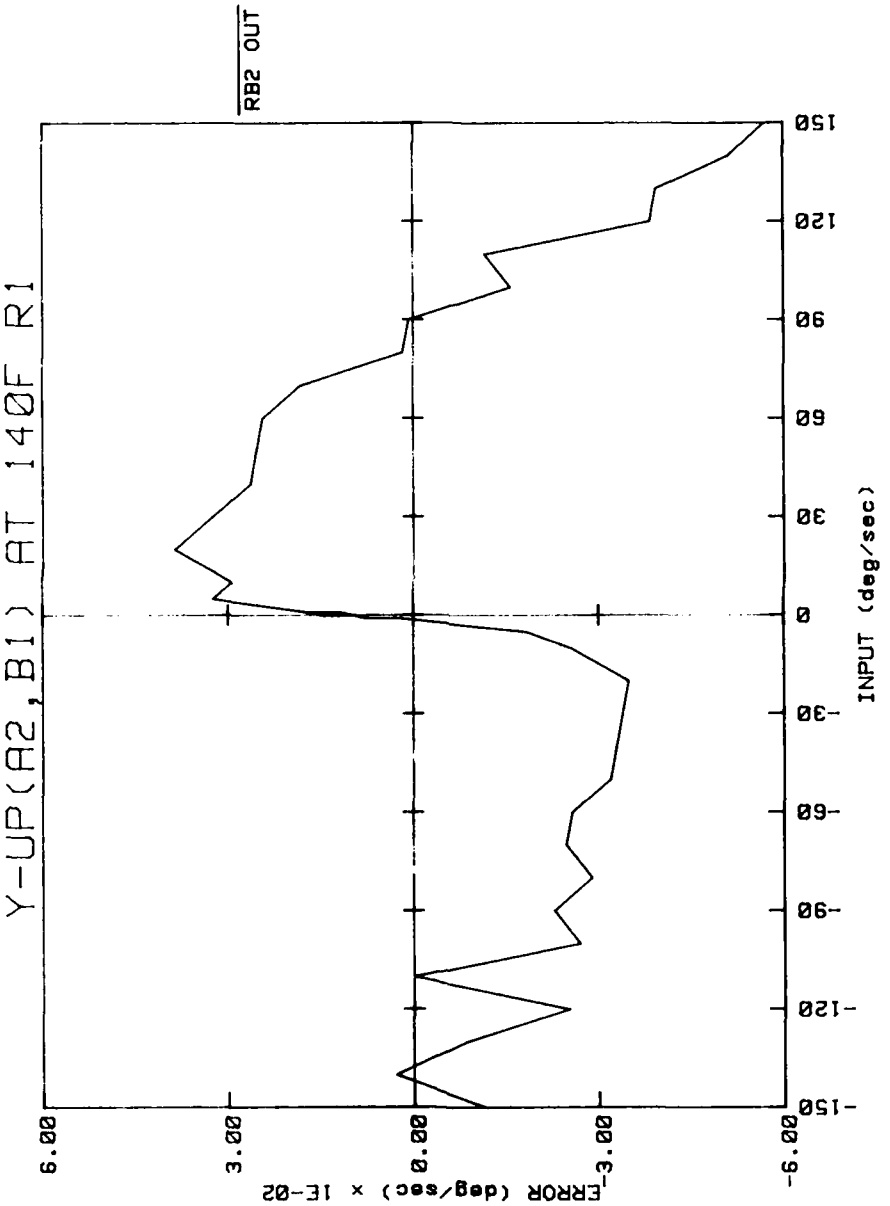

Figure 113. Input-output characteristics for repeat test R1.

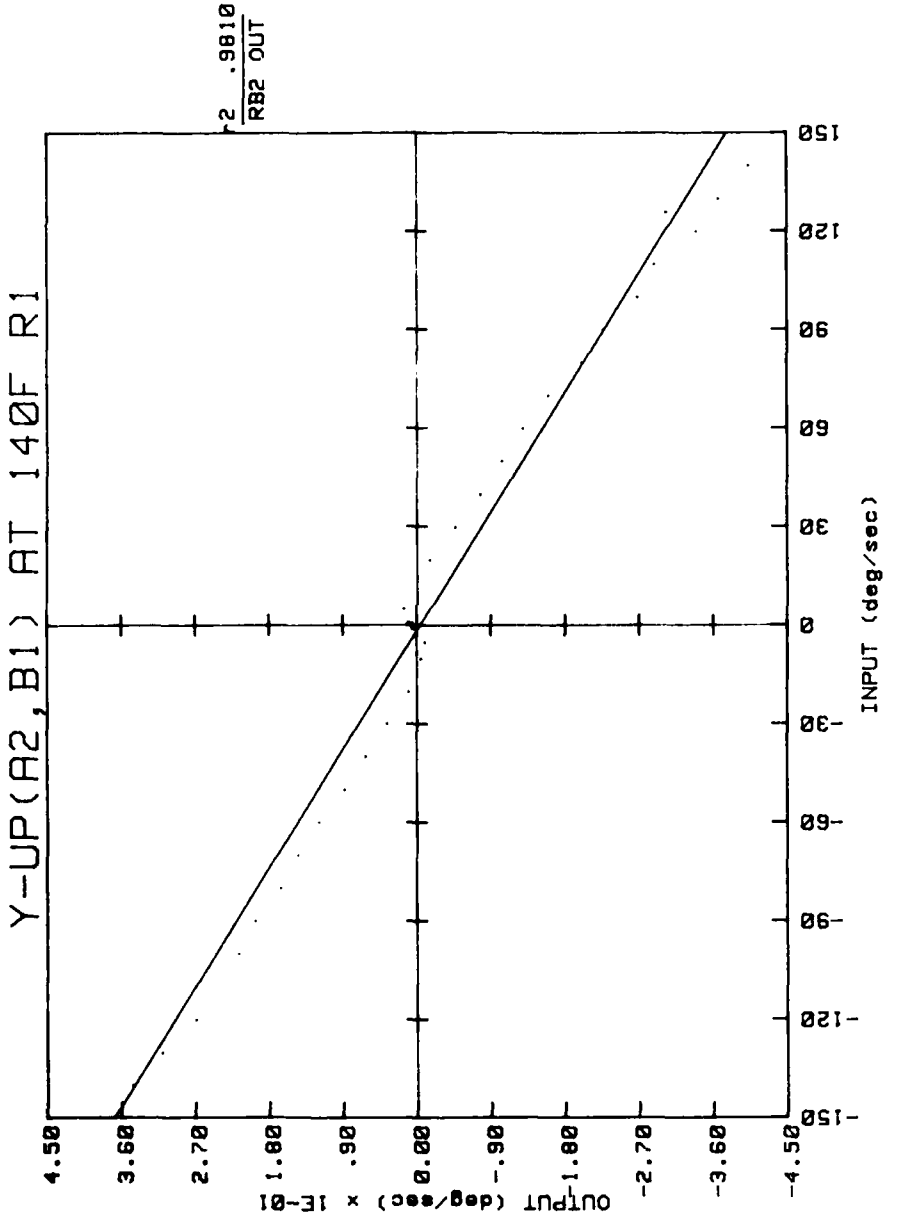

Figure 112. Input-output characteristics for repeat test R1.

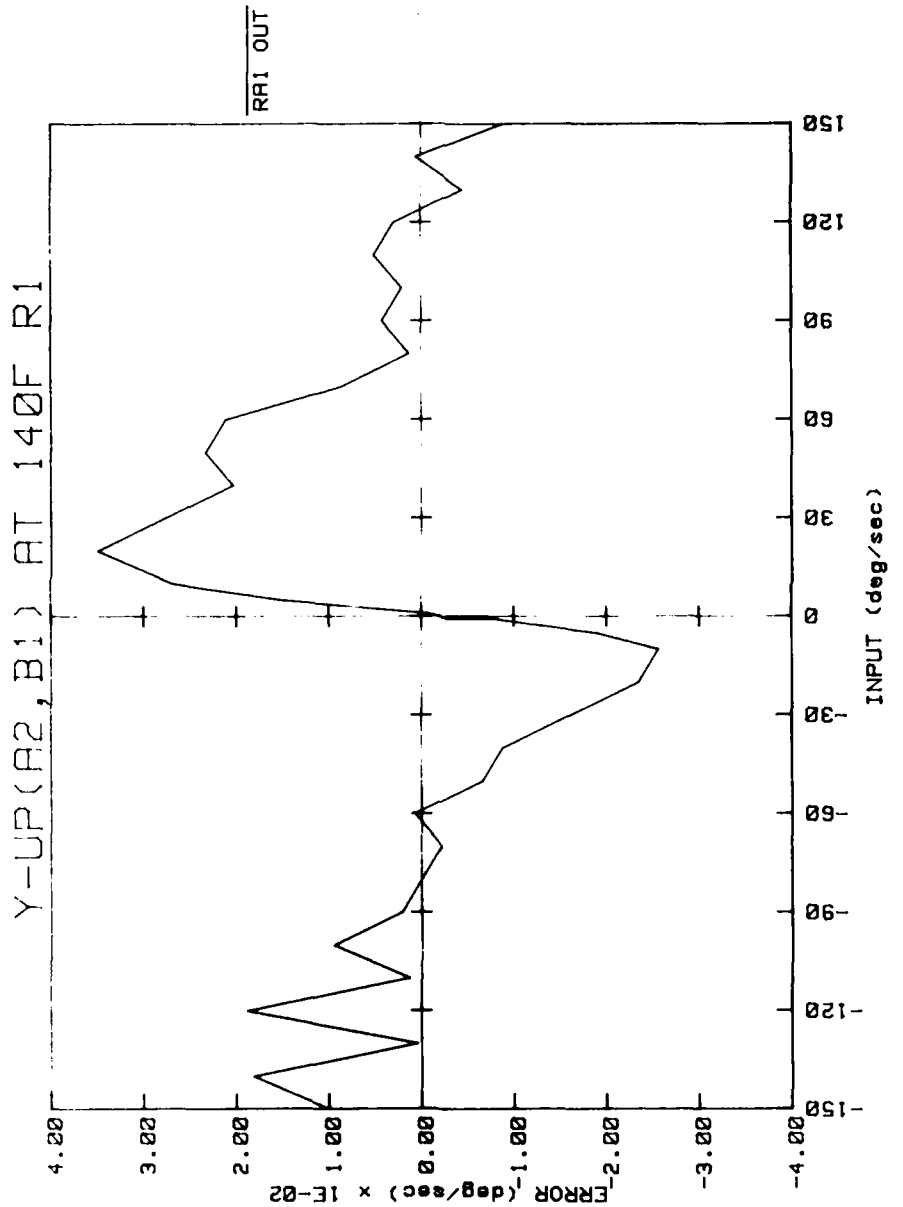

Figure 111. Input-output characteristics for repeat test R1.

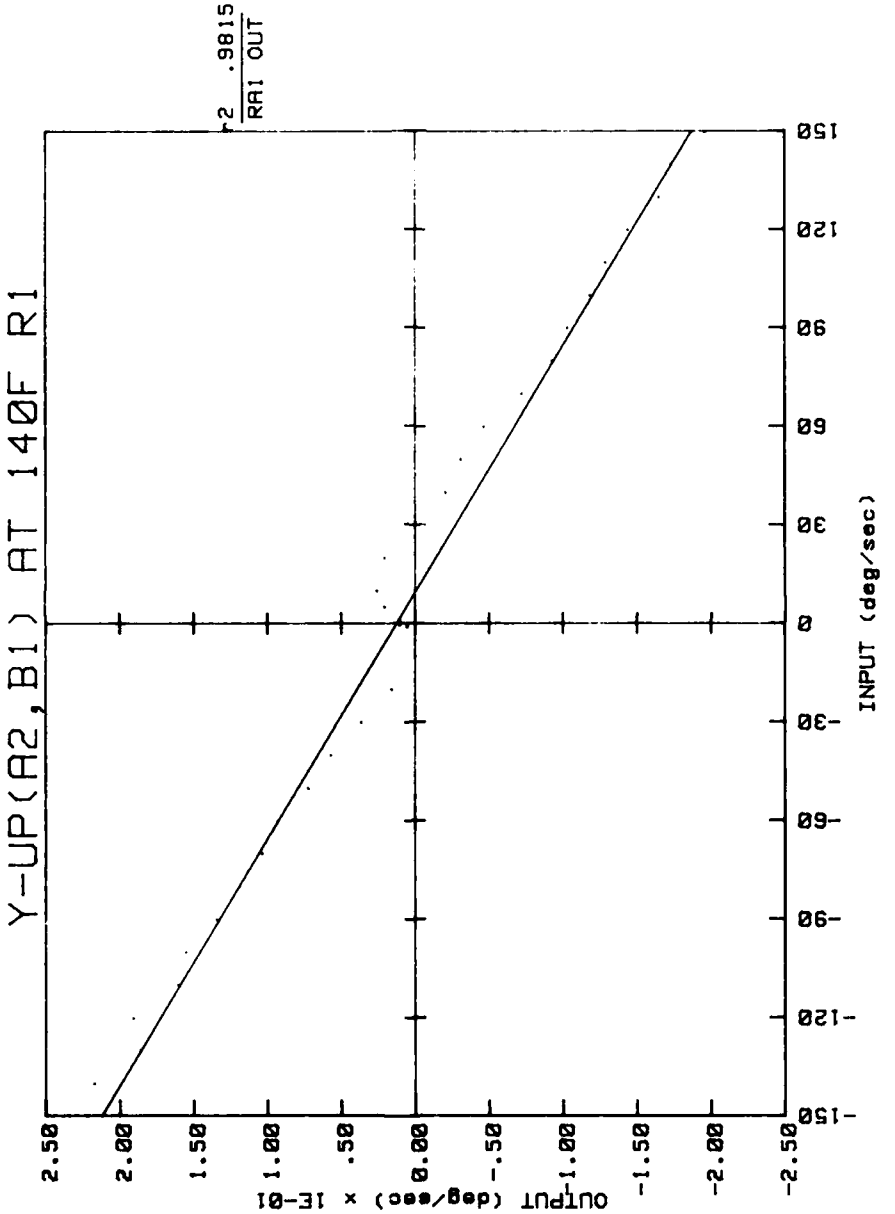

Figure 110. Input-output characteristics for repeat test R1.

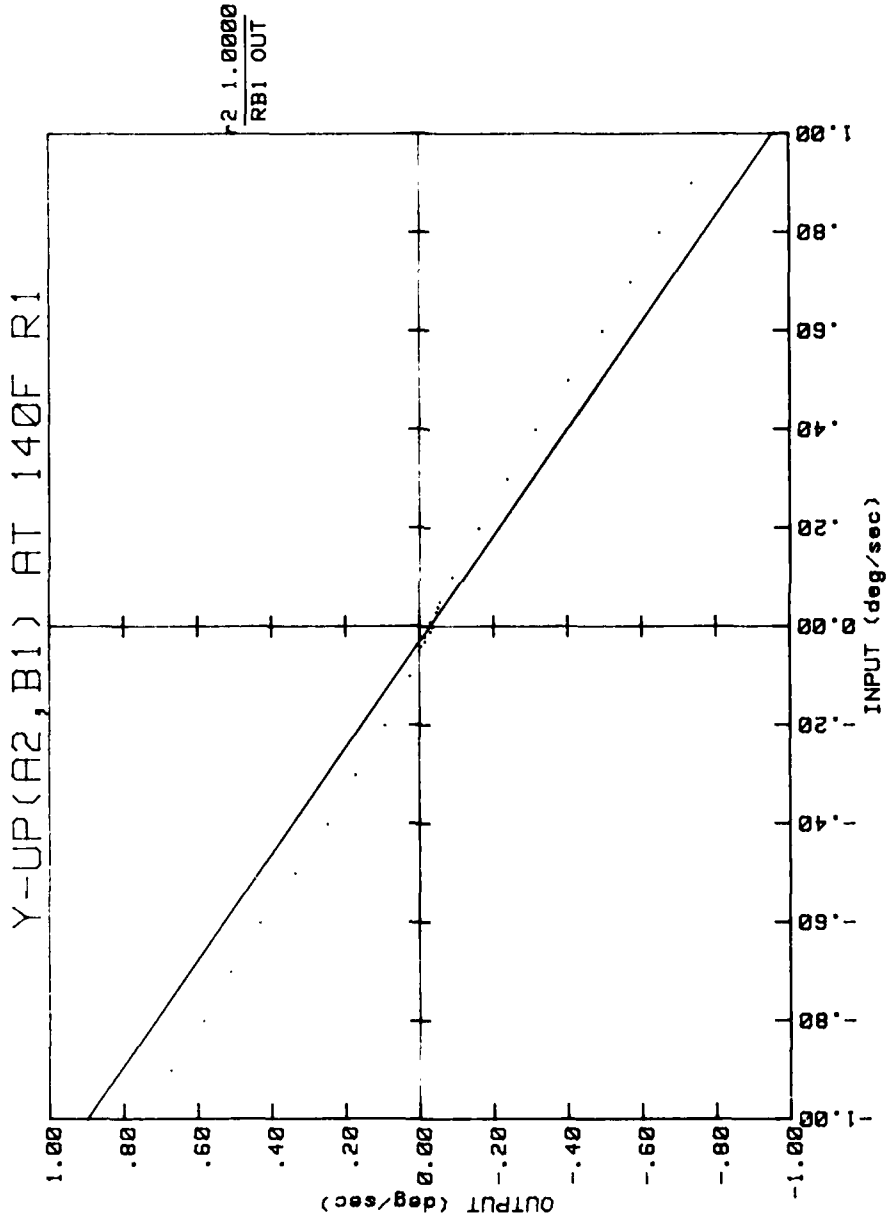

Figure 109. Input-output characteristics for repeat test R1.

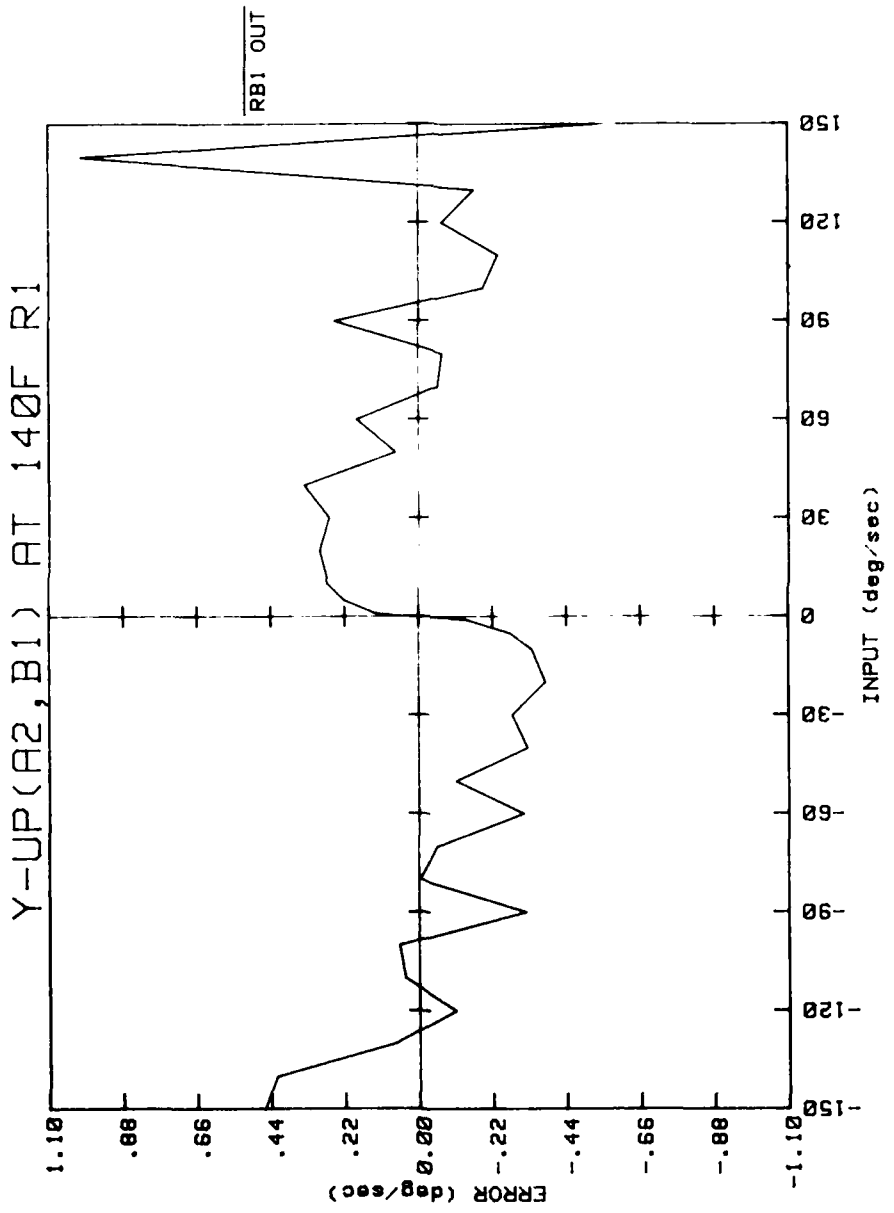

Figure 108. Input-output characteristics.for repeat test R1.

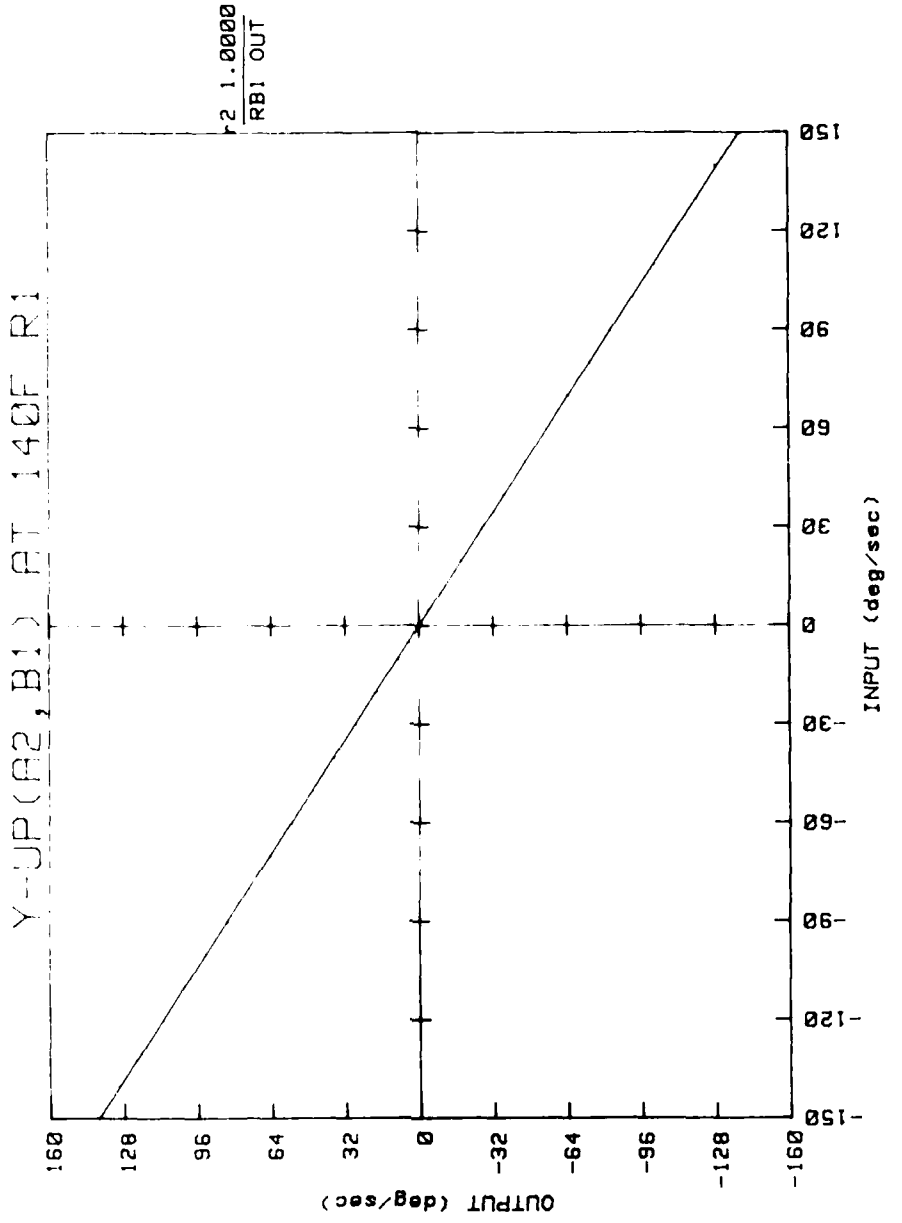

Figure 107. Input-output characteristics for repeat test R1.

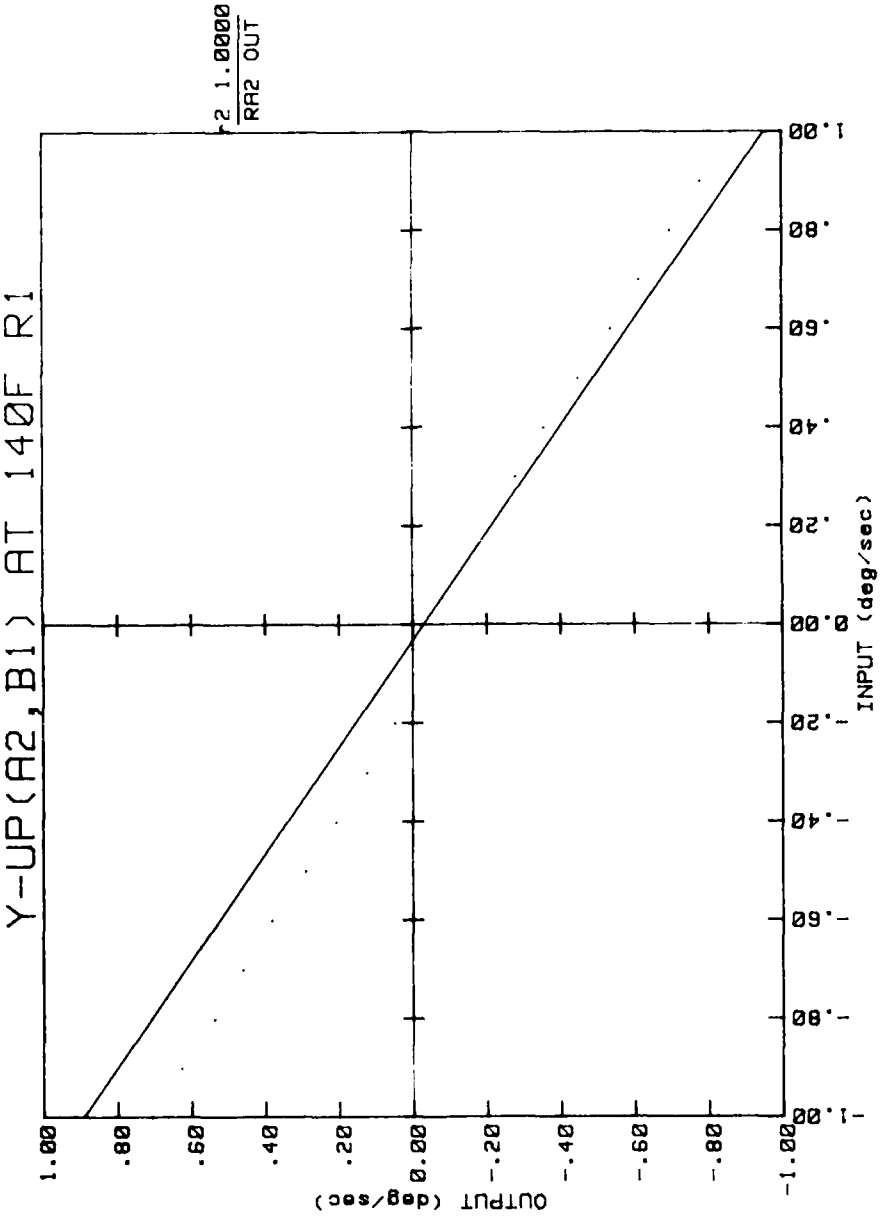

Figure 106. Input-output characteristics for repeat test R1.

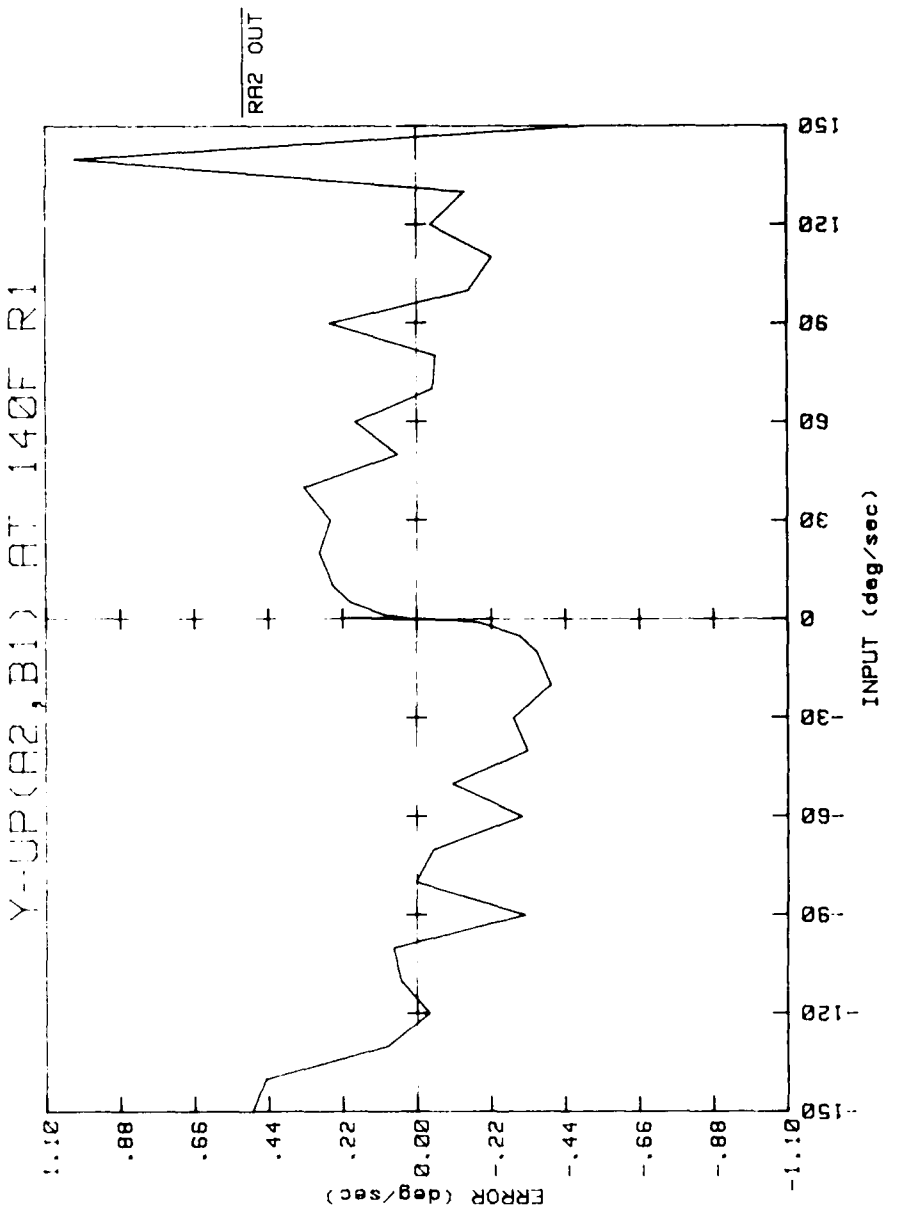

Figure 105. Input-output characteristics for repeat test R1.

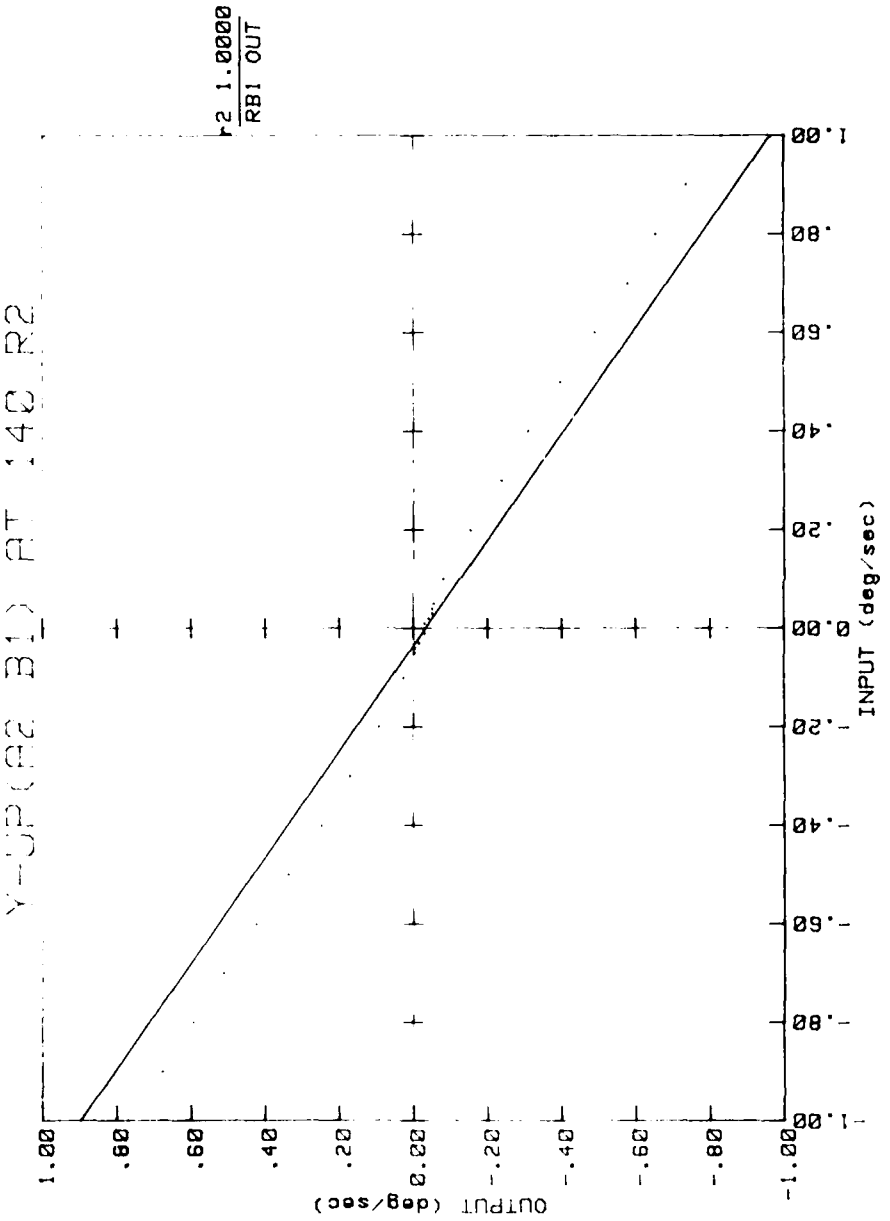

Figure 119. Input-output characteristics for repeat test R2.

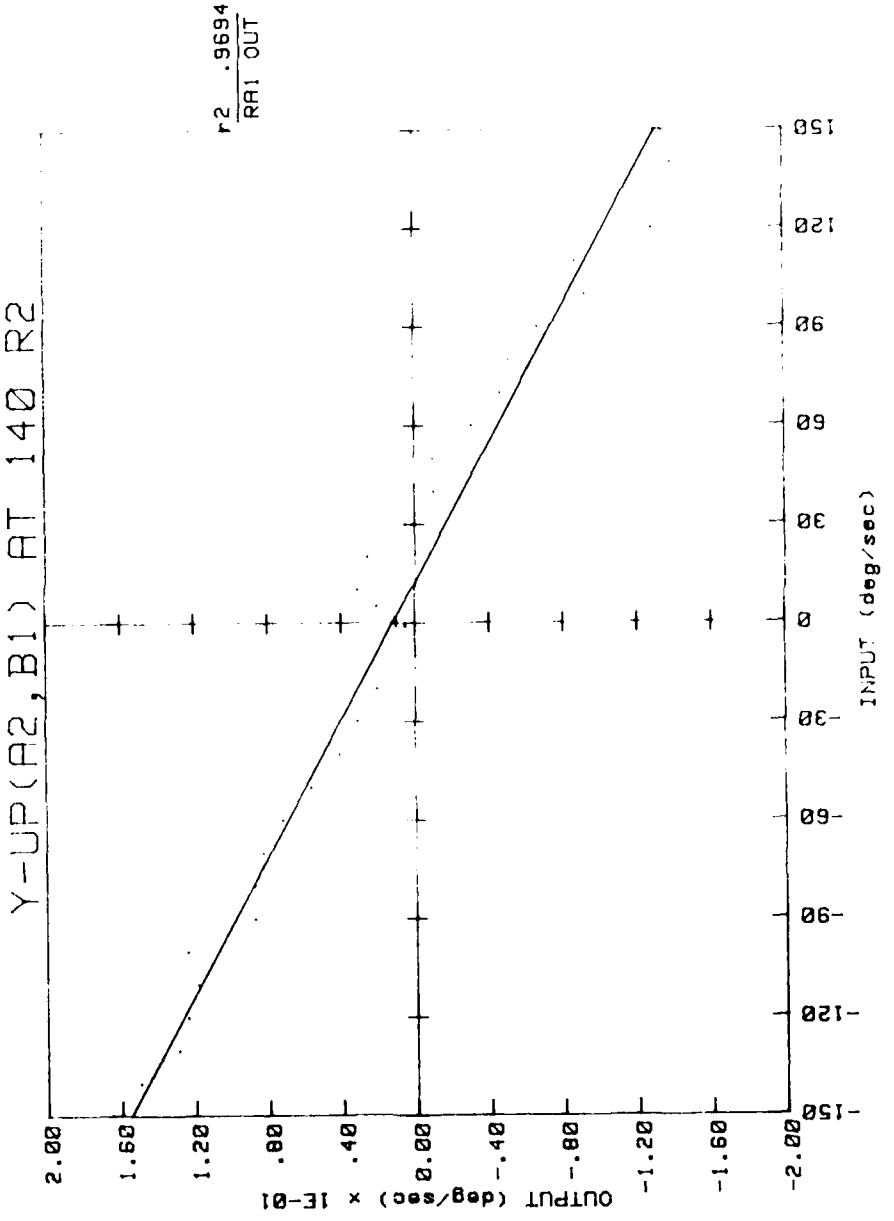

Figure 120. Input-output characteristics for repeat test R2.

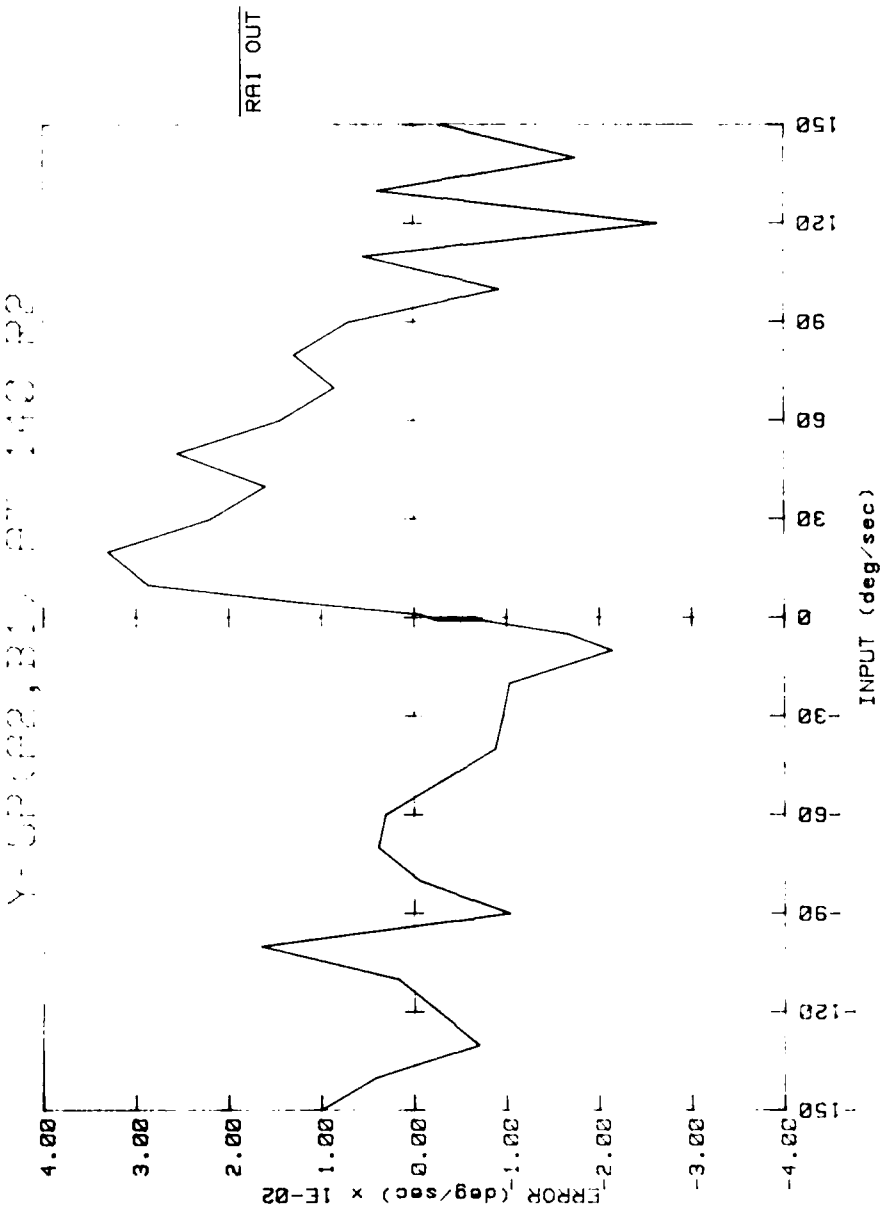

Figure 121. Input-output characteristics for repeat test R2.

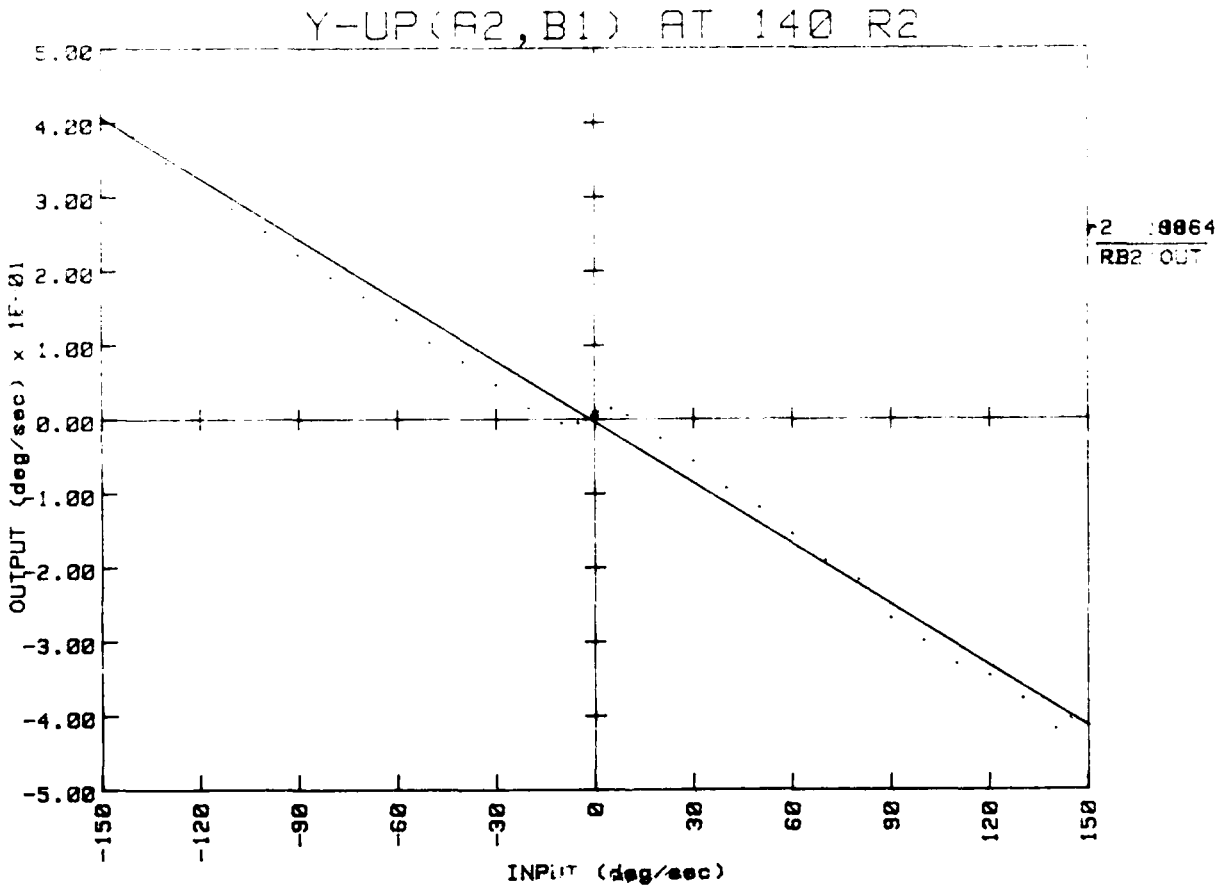

Figure 122. Input-output characteristics for repeat test R2.

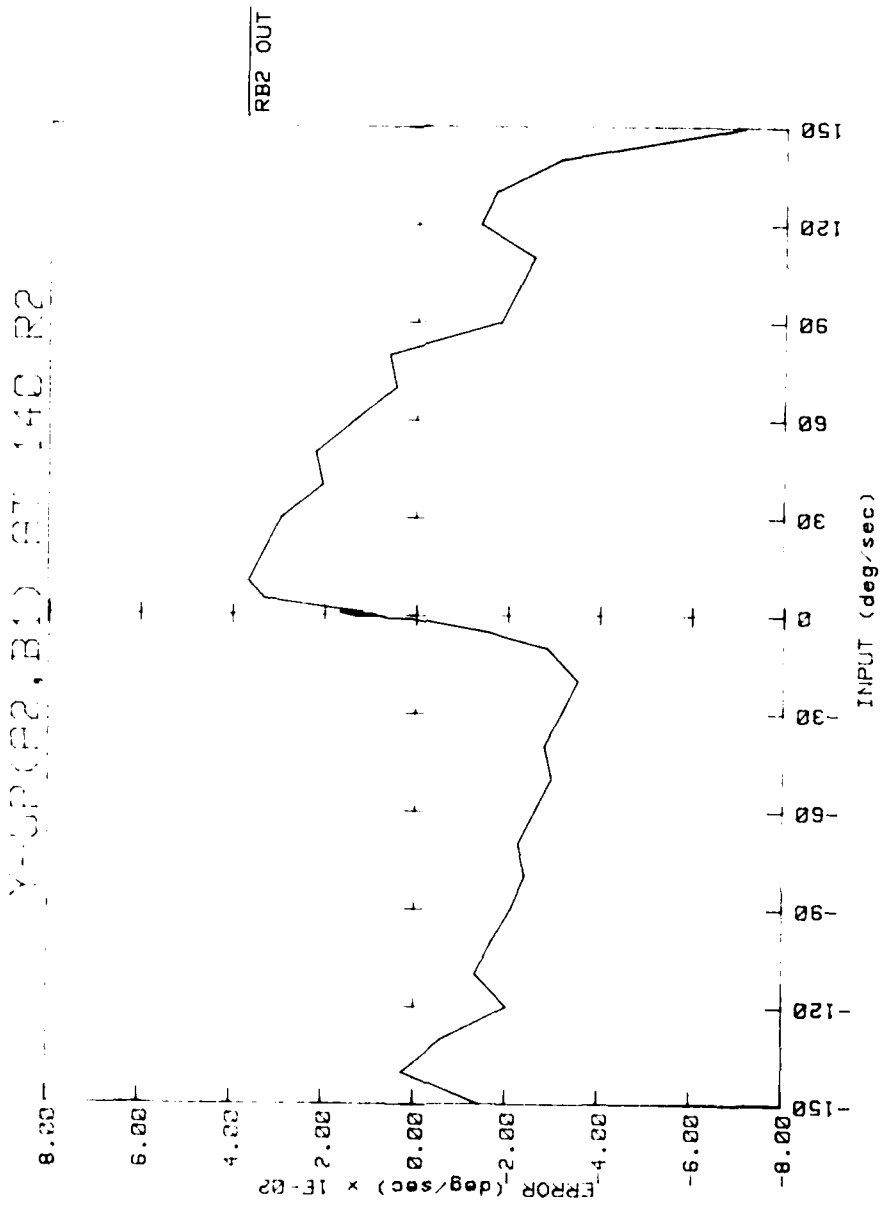

Figure 123. Input-output characteristics for repeat test R2.

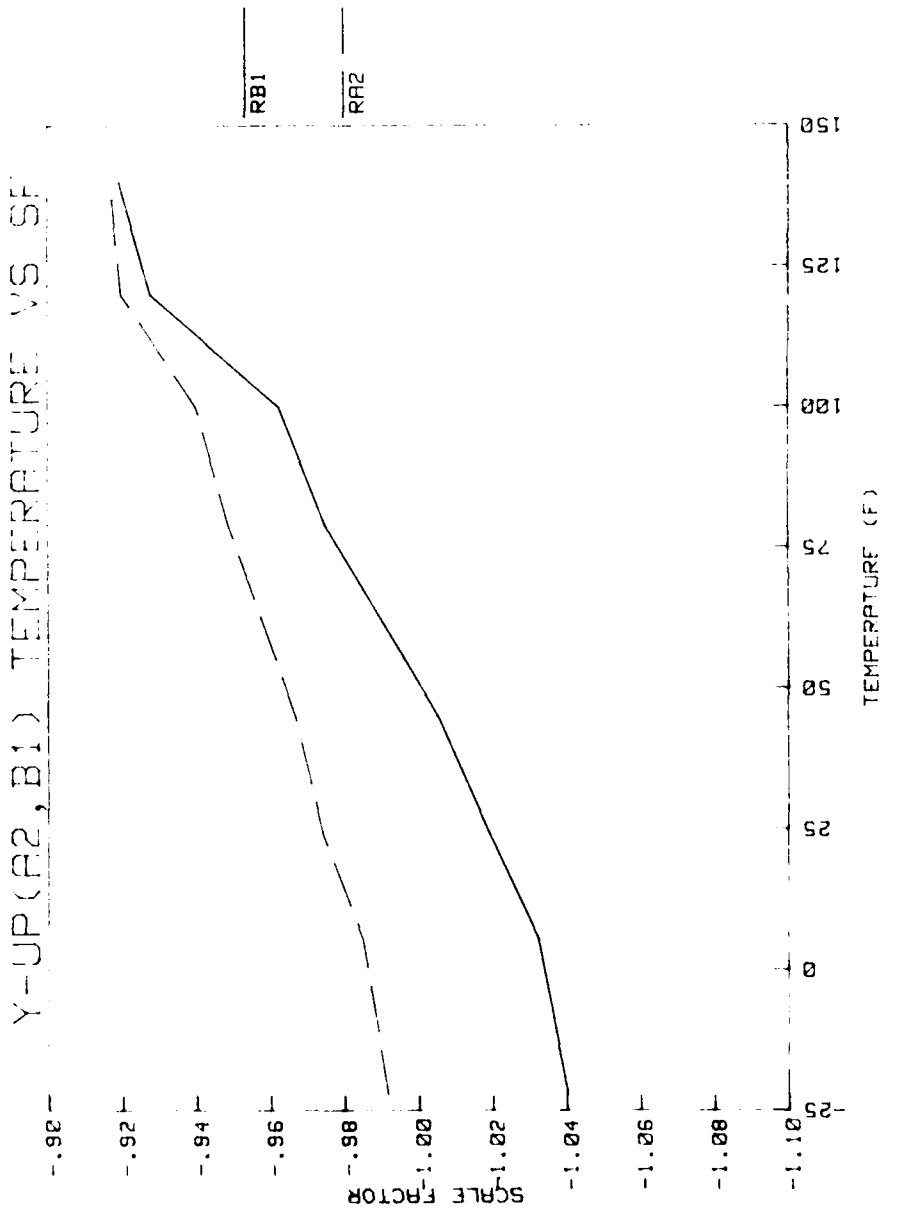

Figure 124. Gyro scale factor thermal sensitivity.

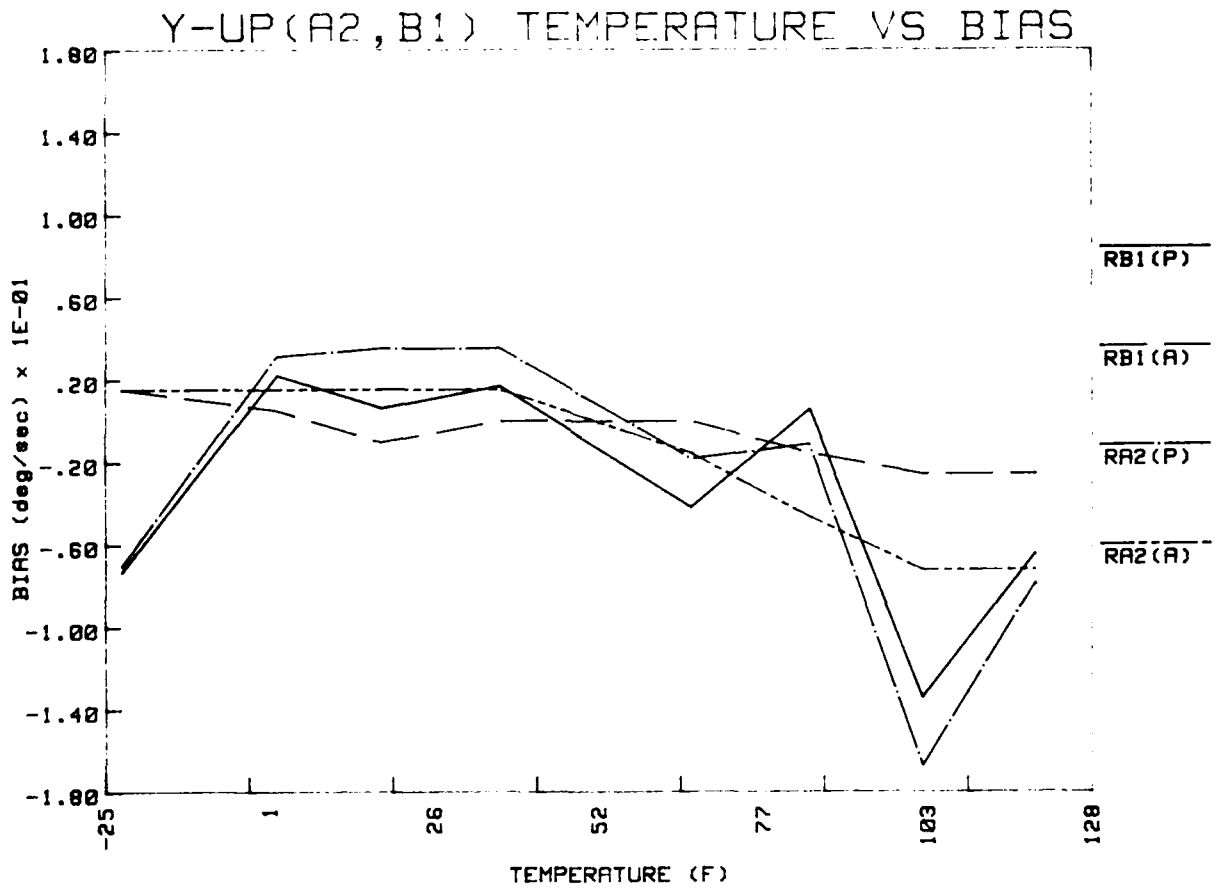

Figure 125. Zero offset (bias) thermal sensitivity.

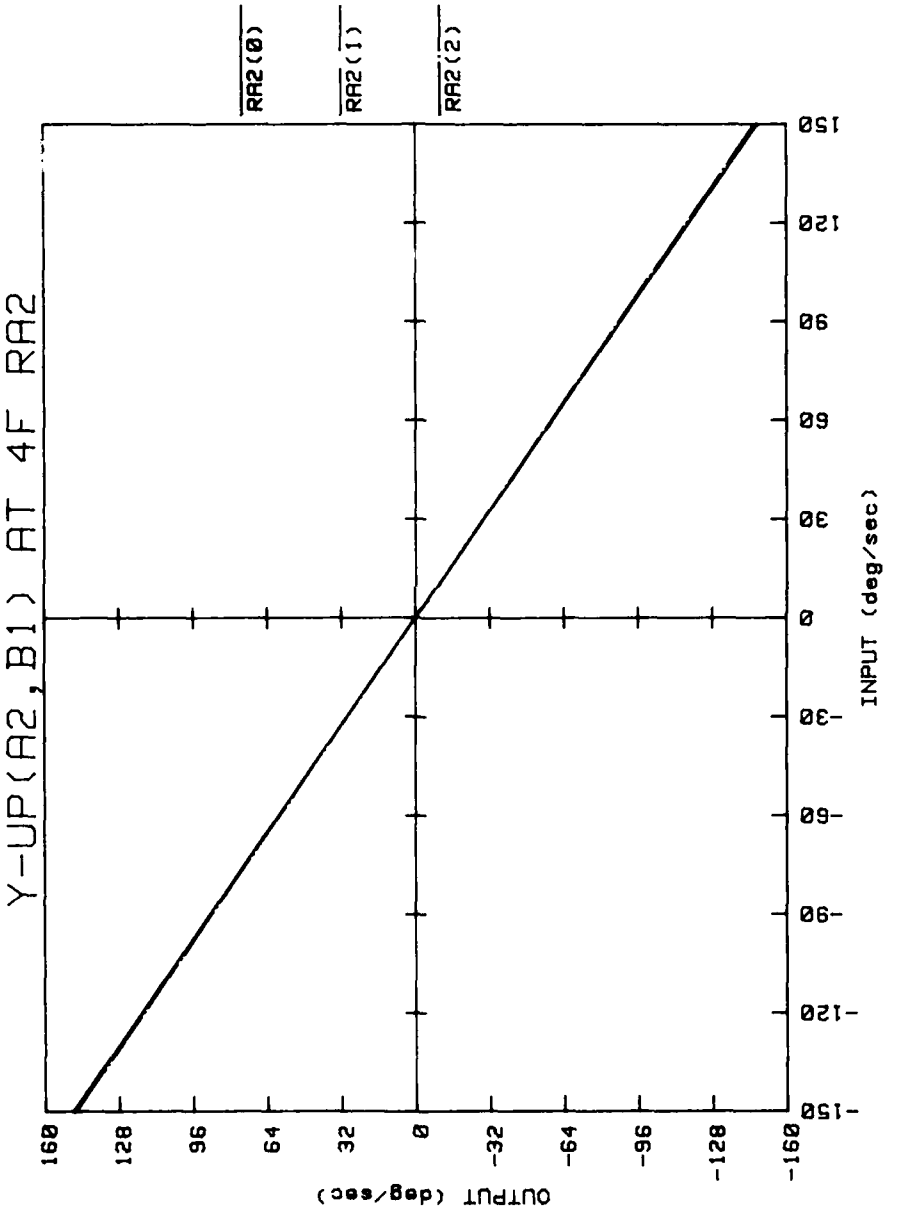

Figure 126. Input-output characteristics for repeat tests R1 and R2.

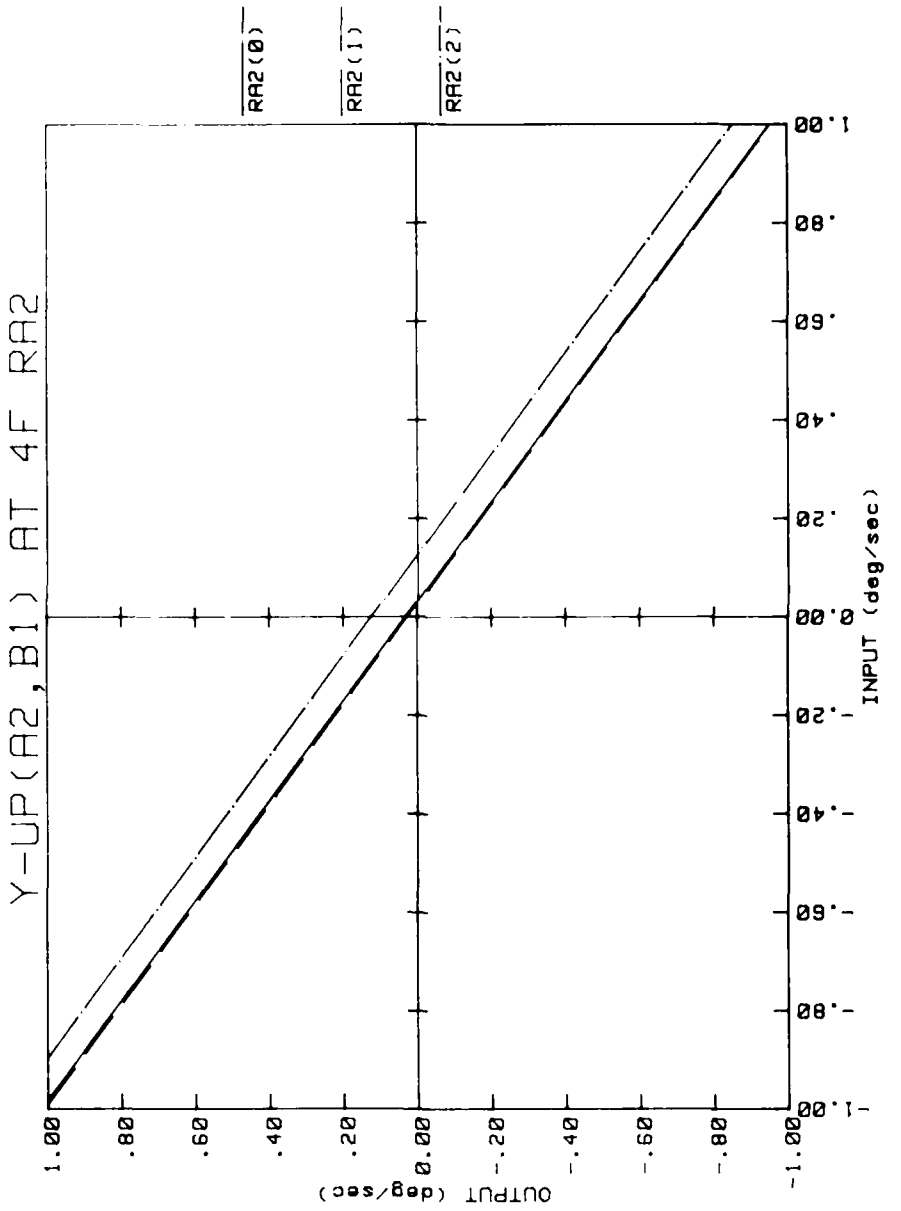

Figure 127. Input-output characteristics for repeat tests R1 and R2.

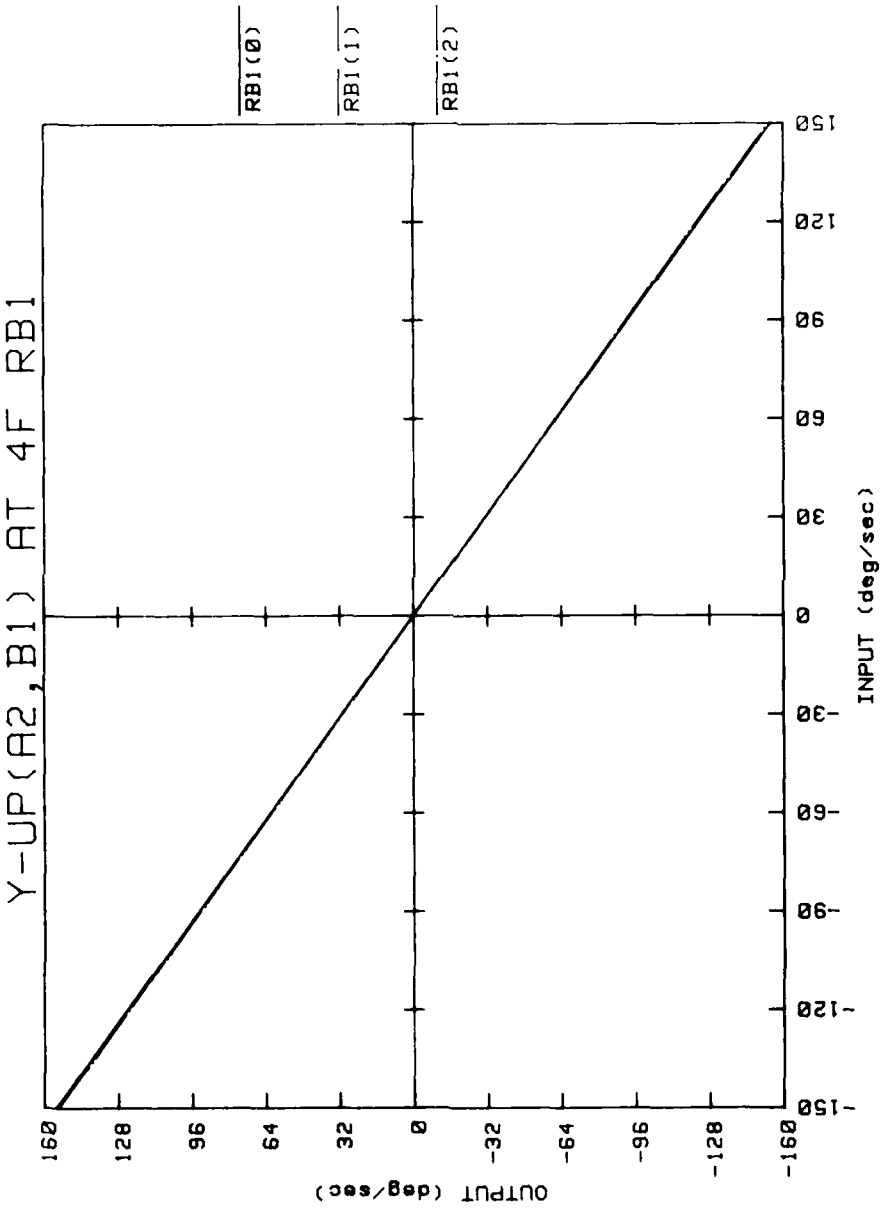

Figure 128. Input-output characteristics for repeat tests R1 and R2.

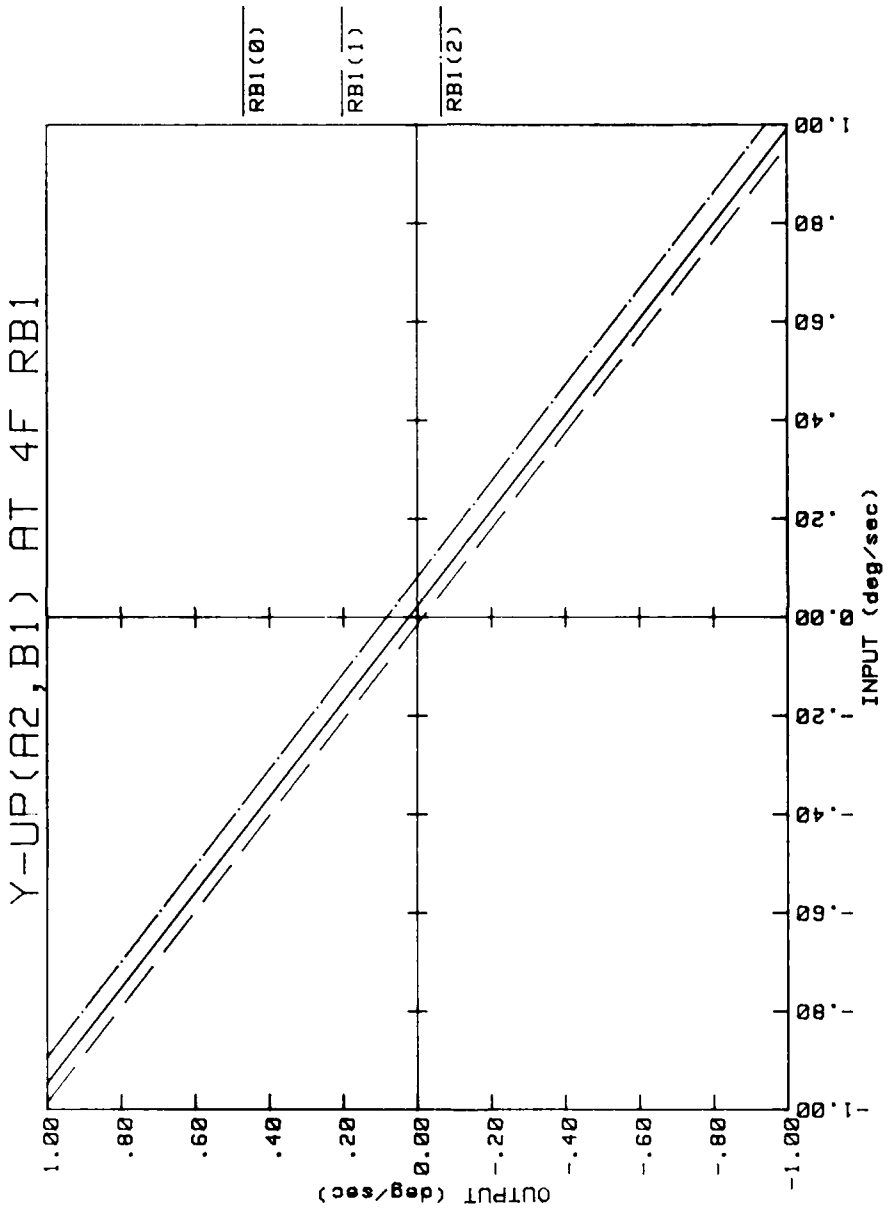

Figure 129. Input-output characteristics for repeat tests R1 and R2.

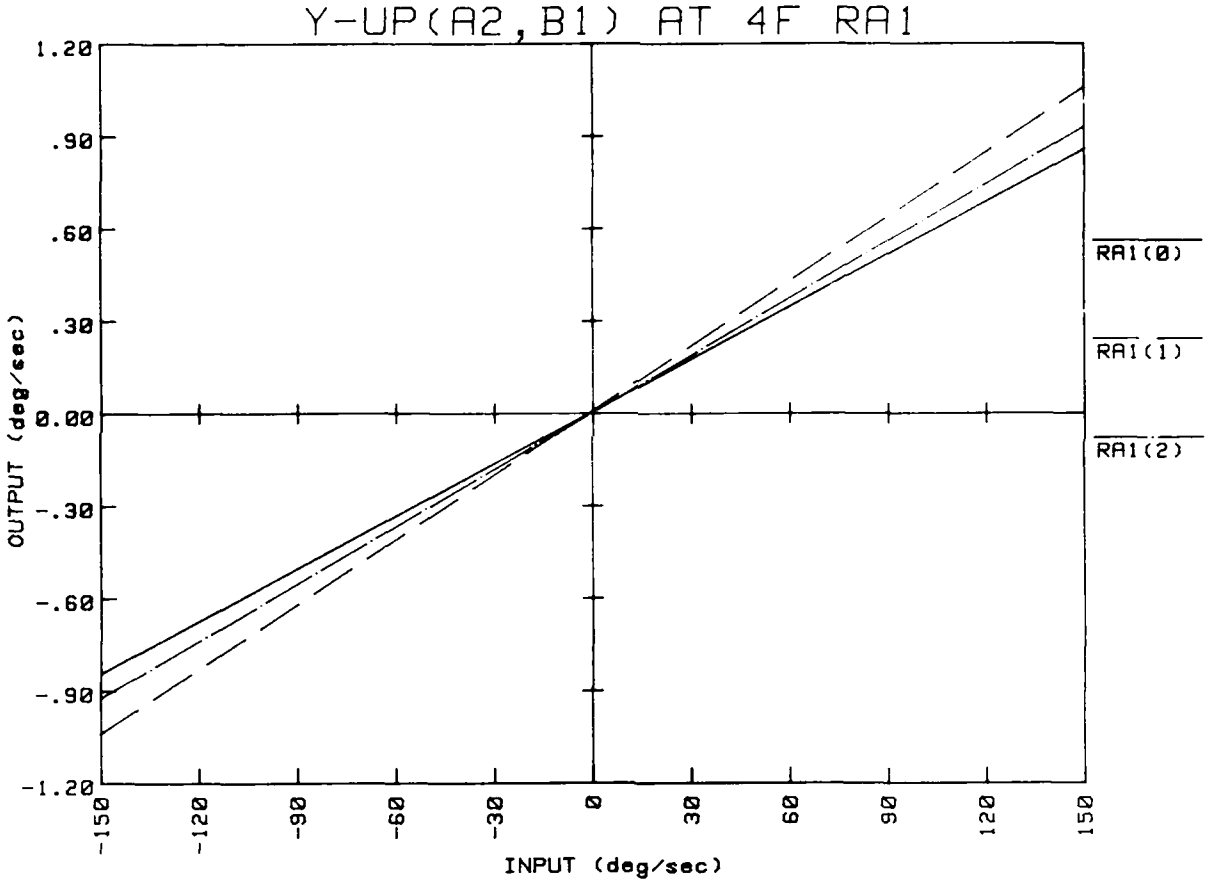

Figure 130. Input-output characteristics for repeat tests R1 and R2.

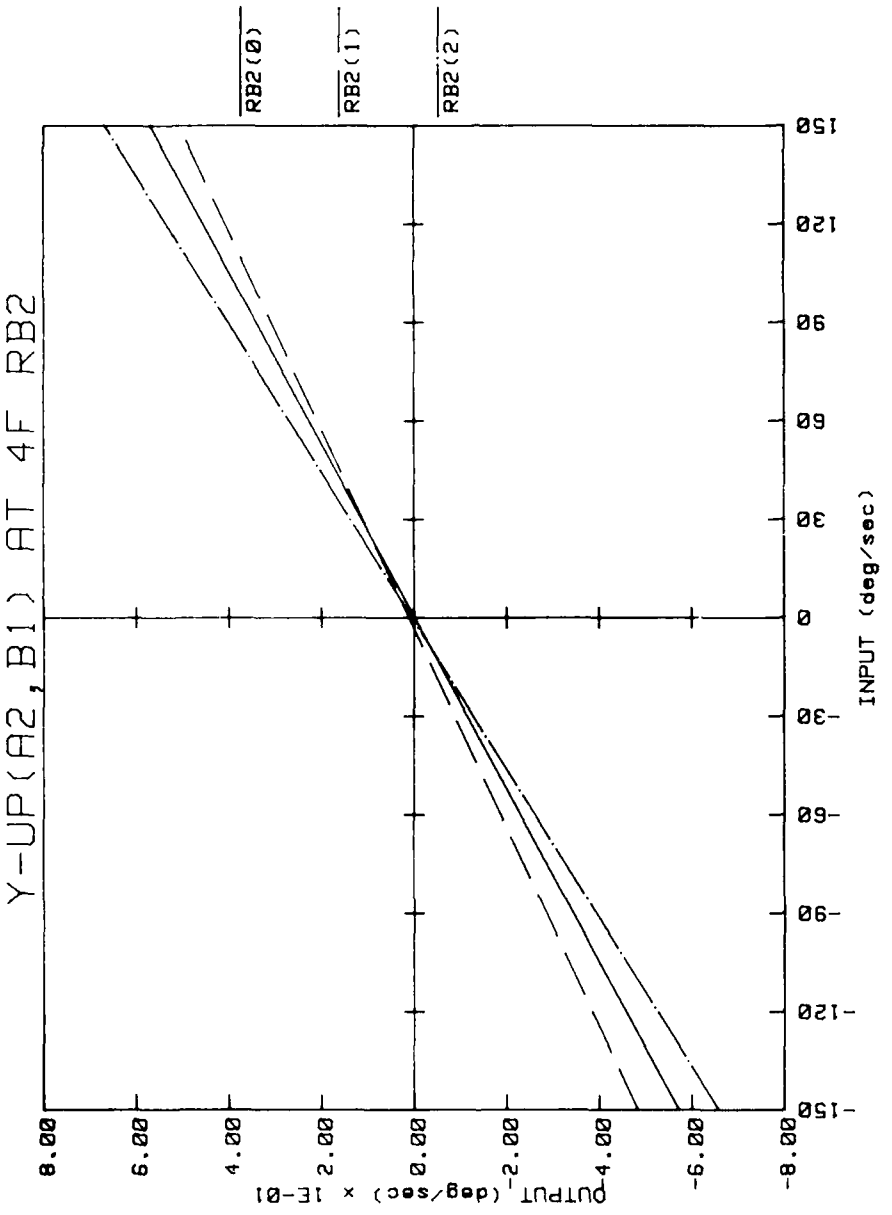

Figure 131. Input-output characteristics for repeat tests R1 and R2.

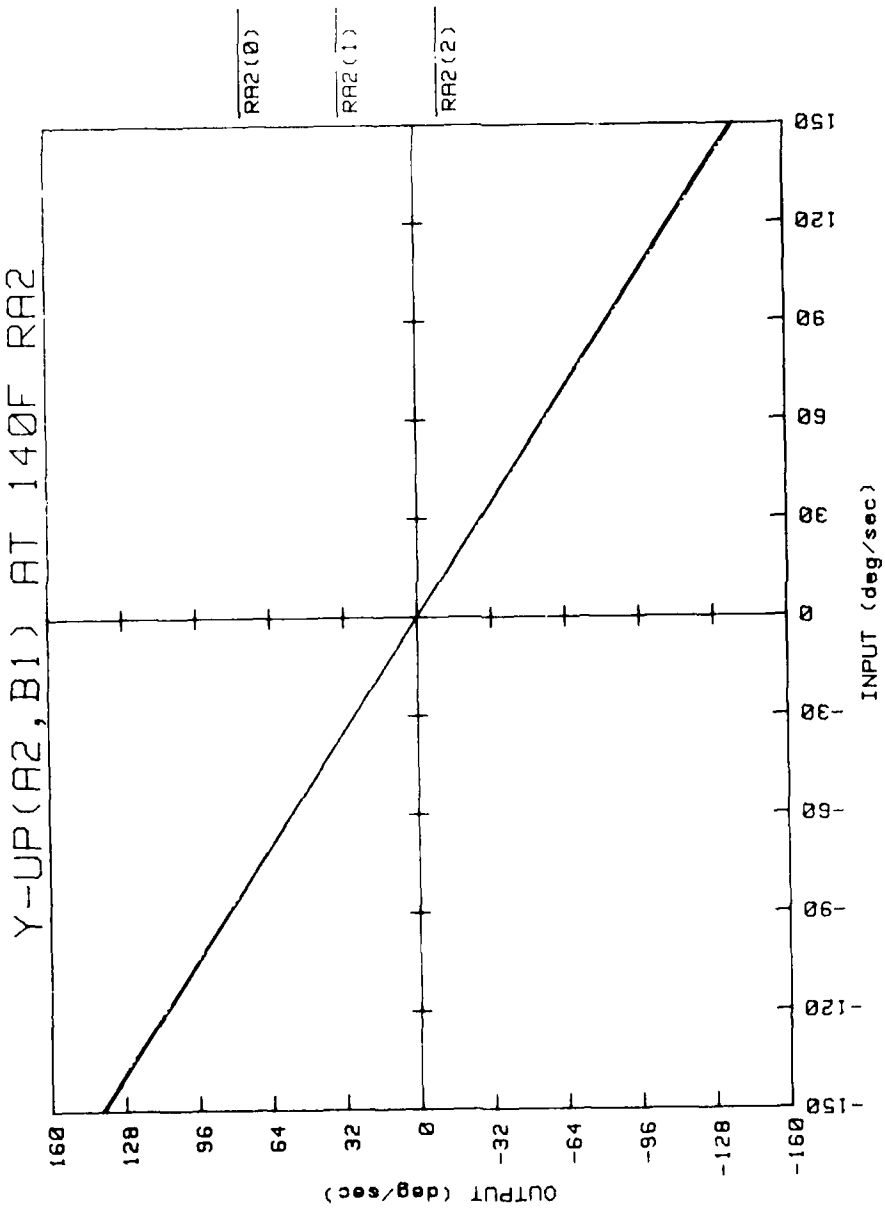

Figure 132. Input-output characteristics for repeat tests R1 and R2.

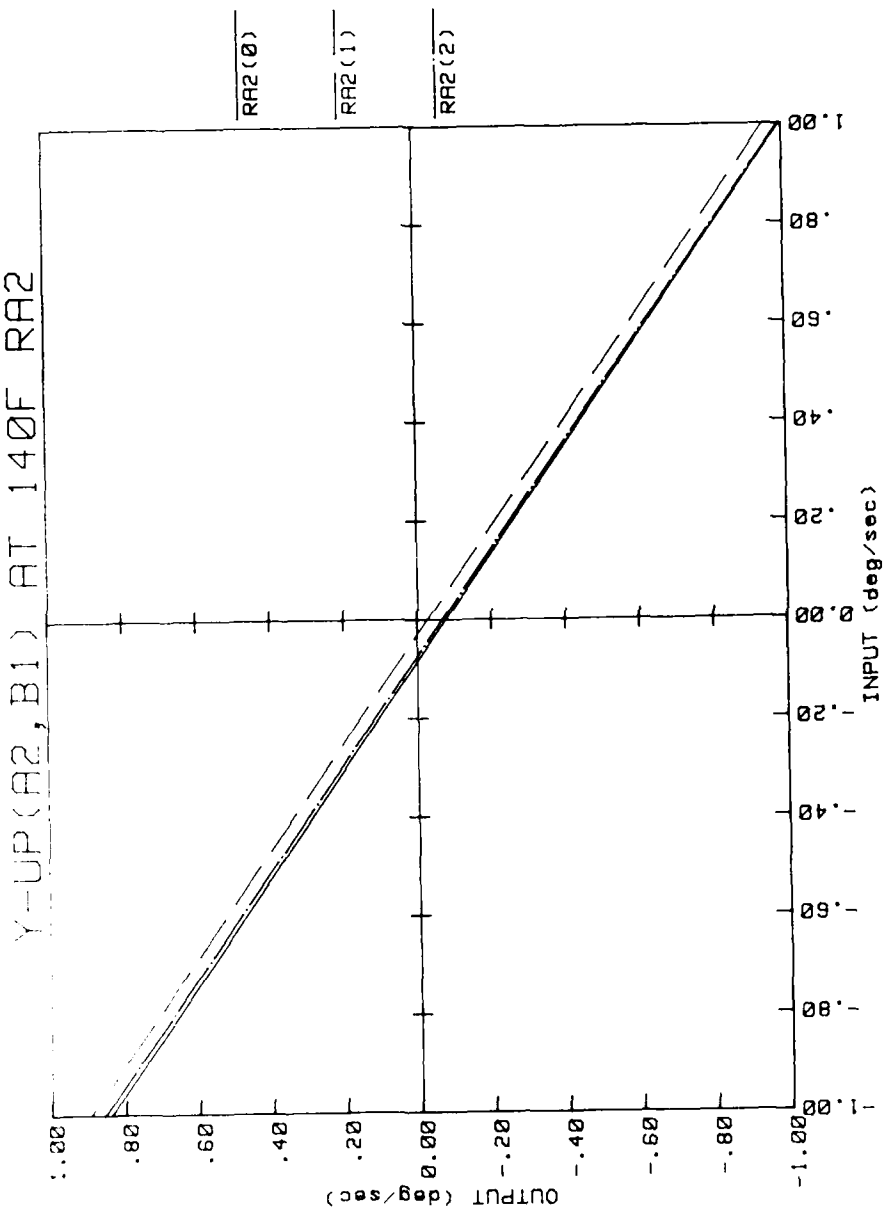

Figure 133. Input-output characteristics for repeat tests R1 and R2.

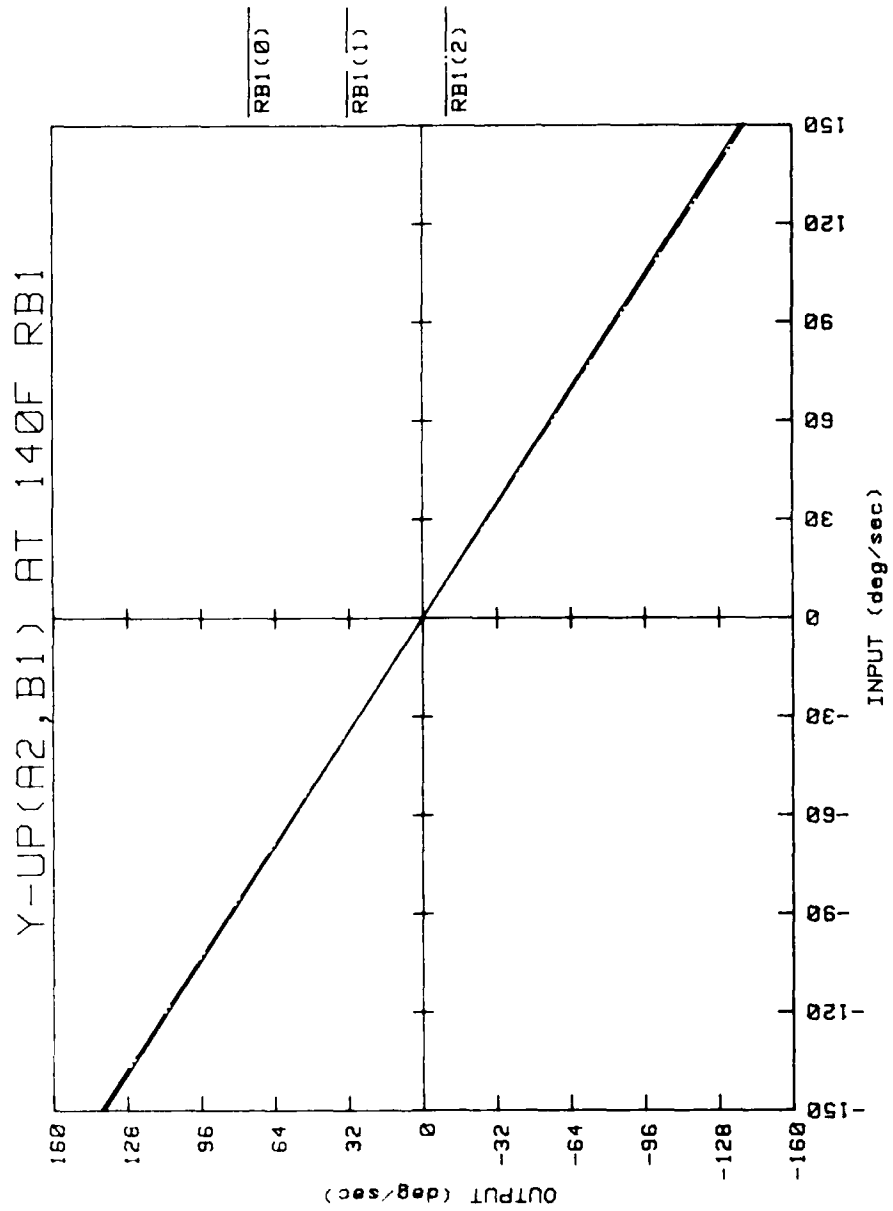

Figure 134. Input-output characteristics for repeat tests R1 and R2.

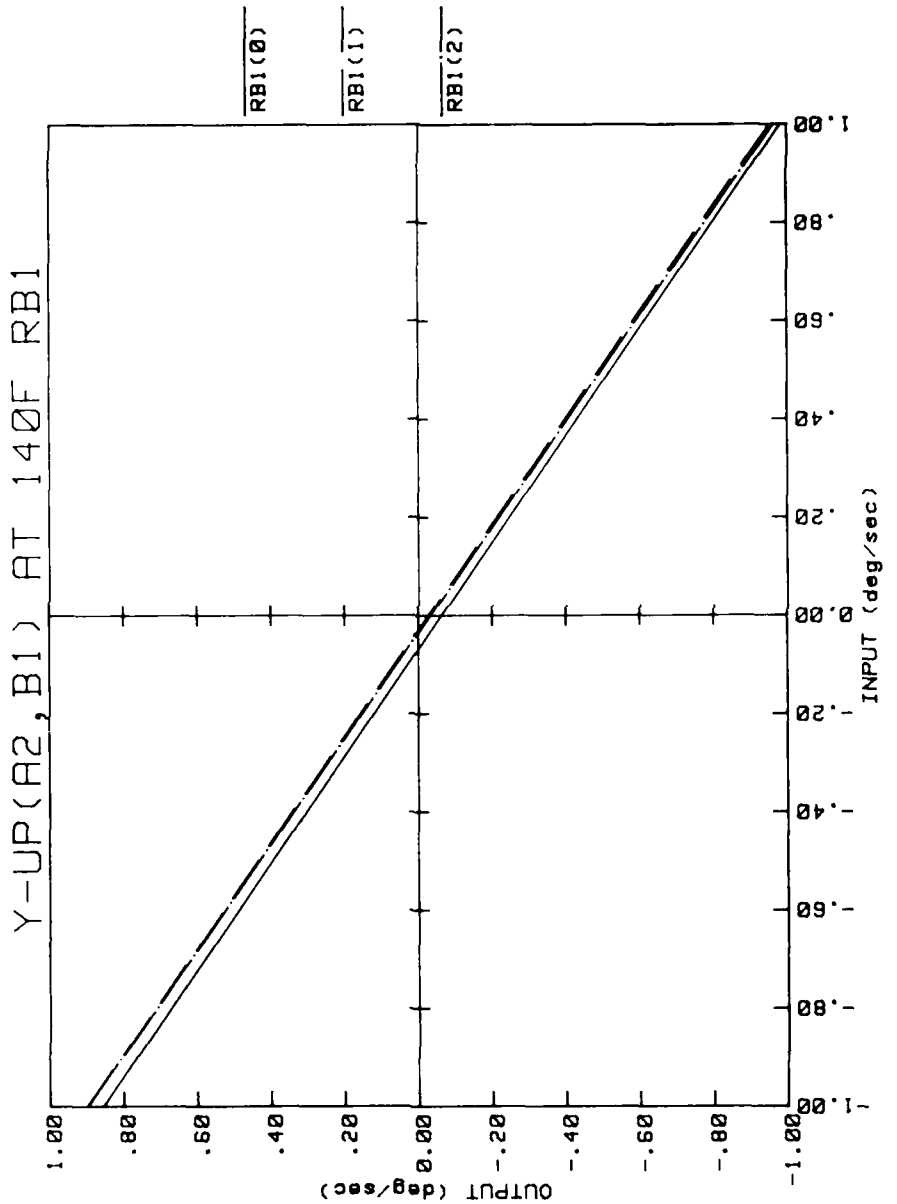

Figure 135. Input-output characteristics for repeat tests R1 and R2.

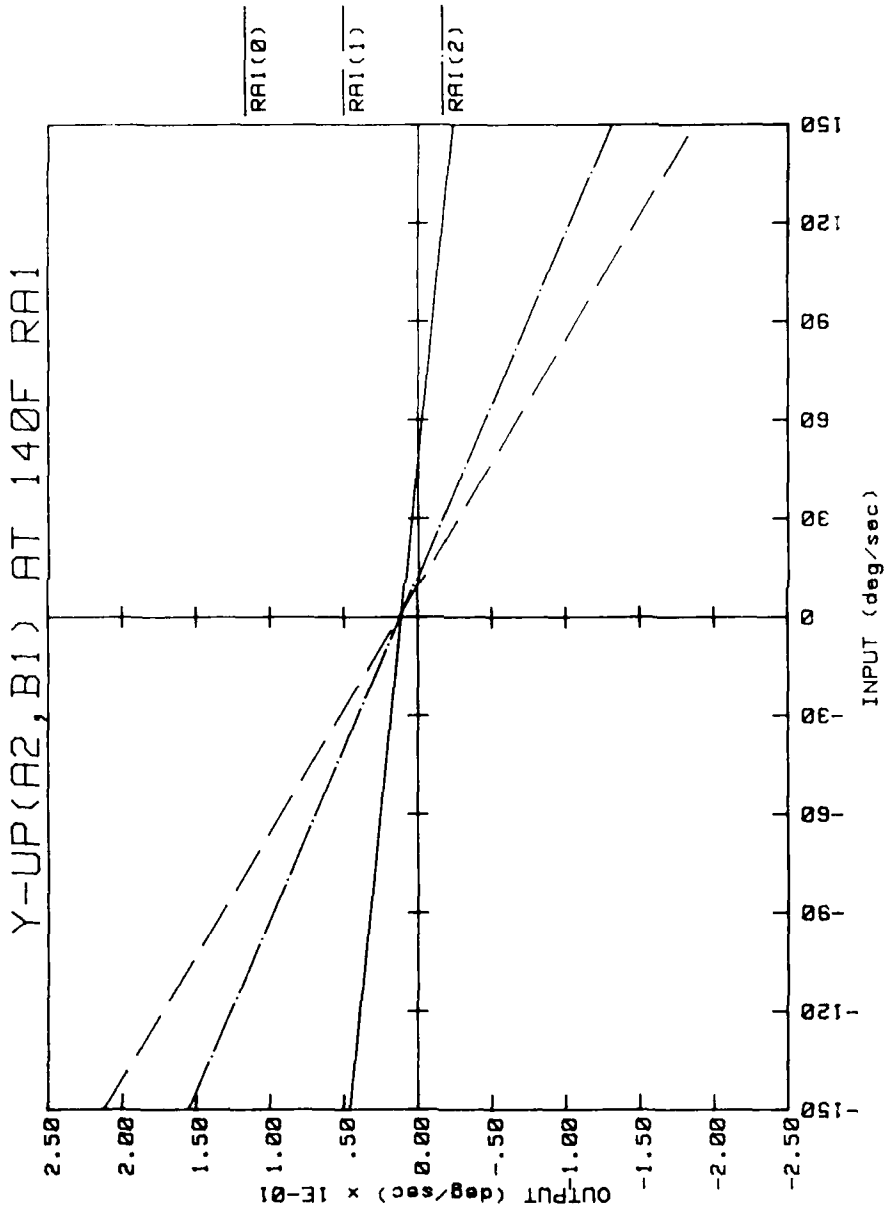

Figure 136. Input-output characteristics for repeat tests R1 and R2.

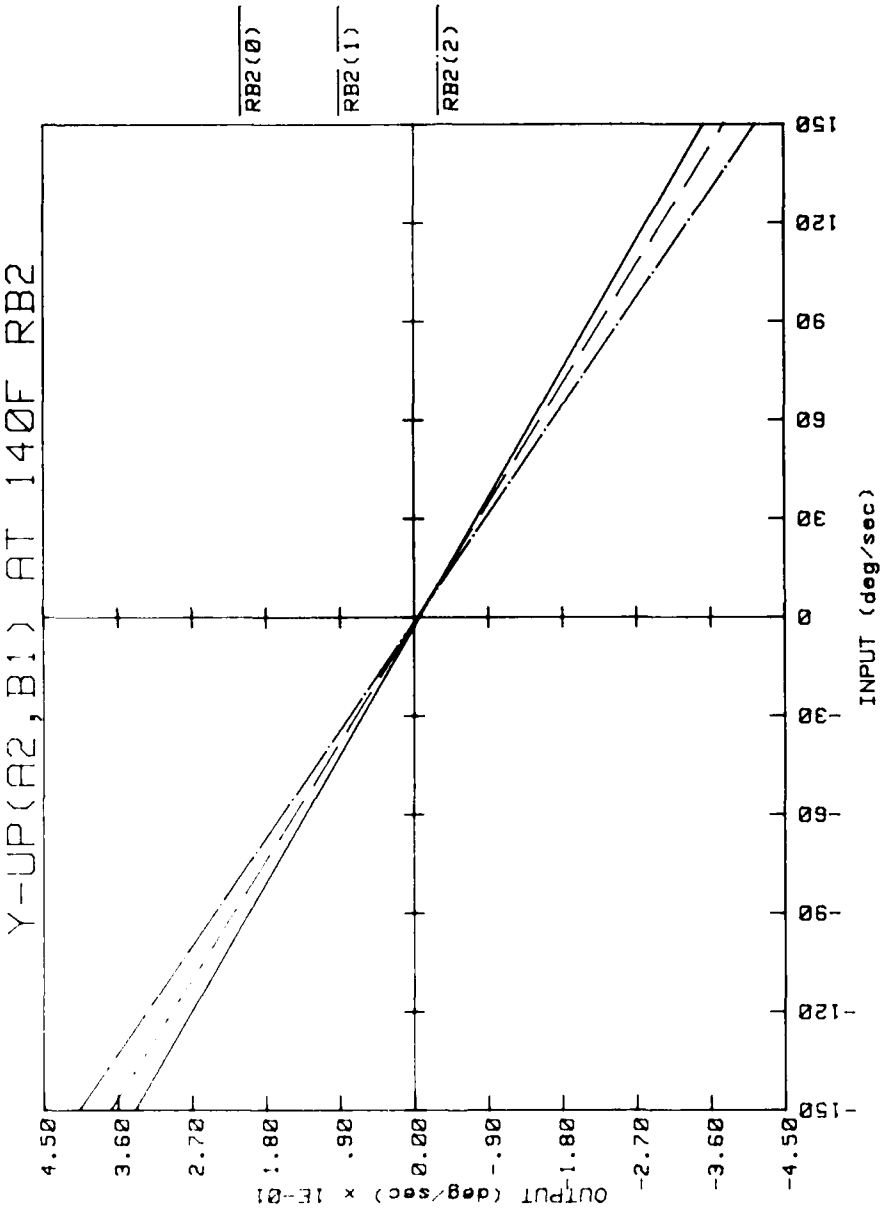

Figure 137. Input-output characteristics for repeat tests R1 and R2.

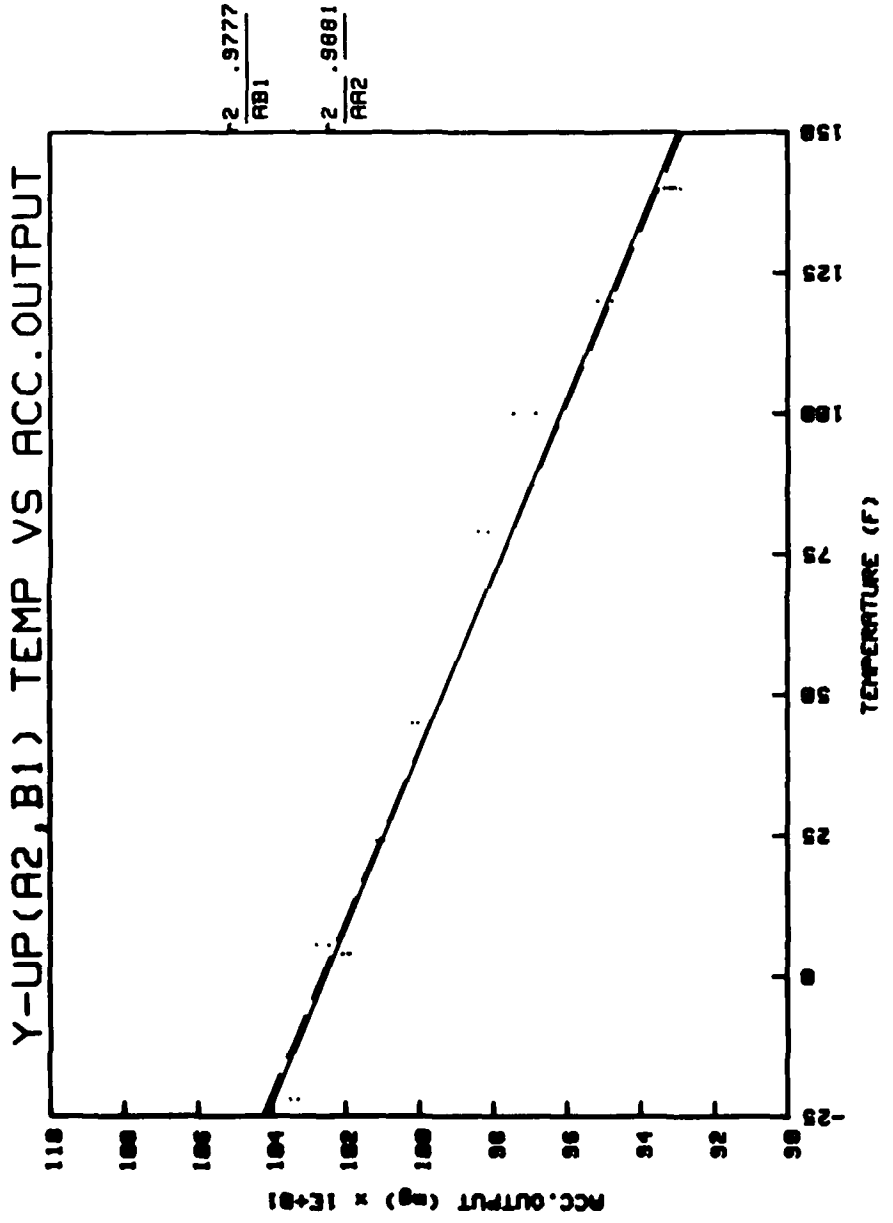

Figure 138. Accelerometer output thermal sensitivity.

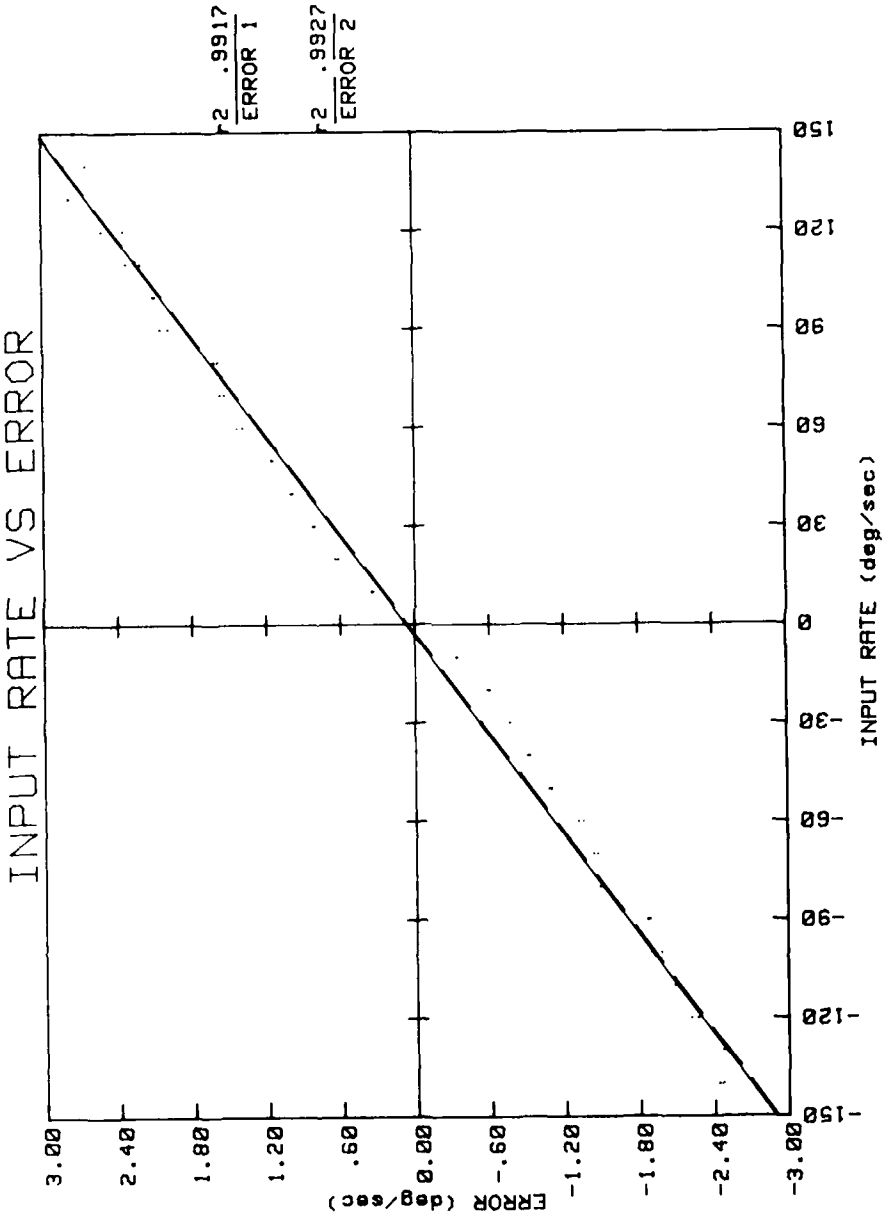

Figure 139. Rate table calibration results for test 1 and repeat test 2.

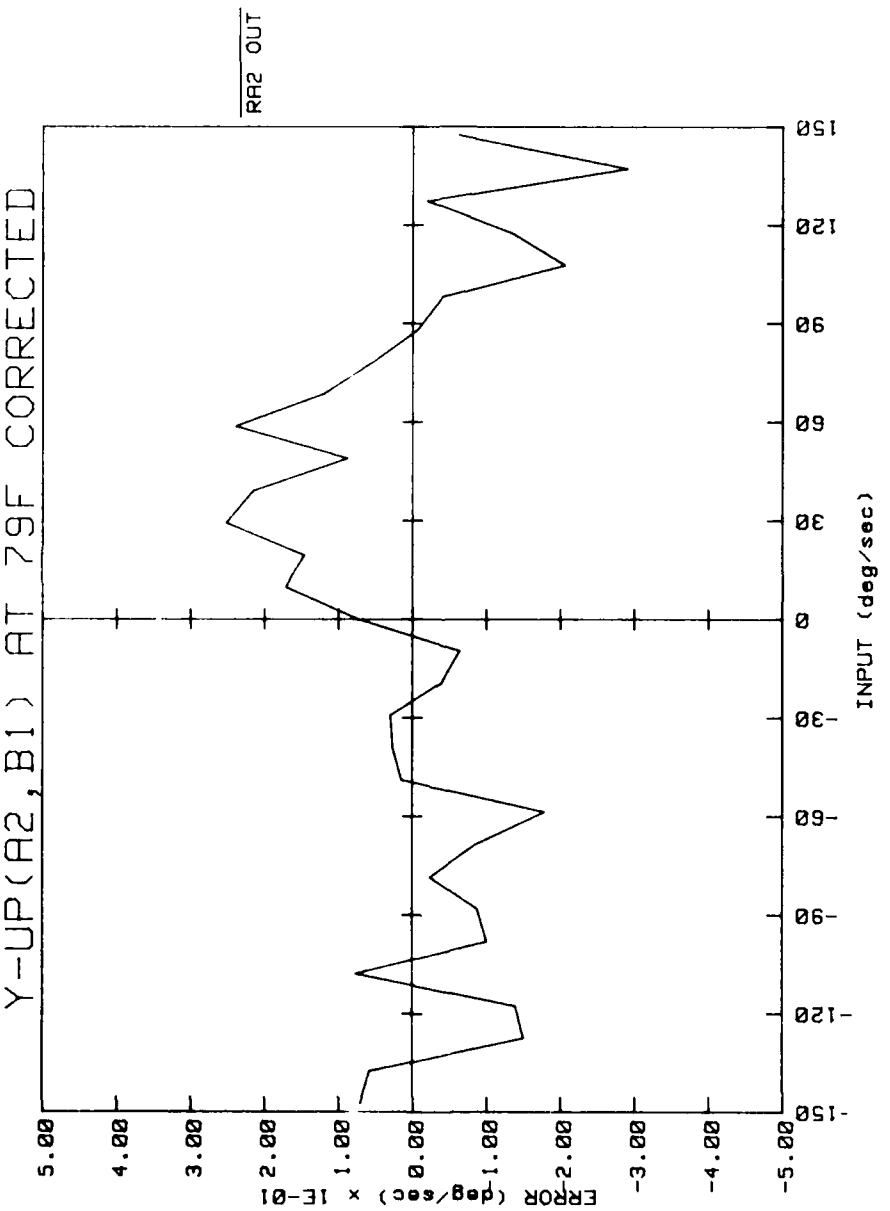

Figure 140. Corrected input-output characteristics for figure 45.

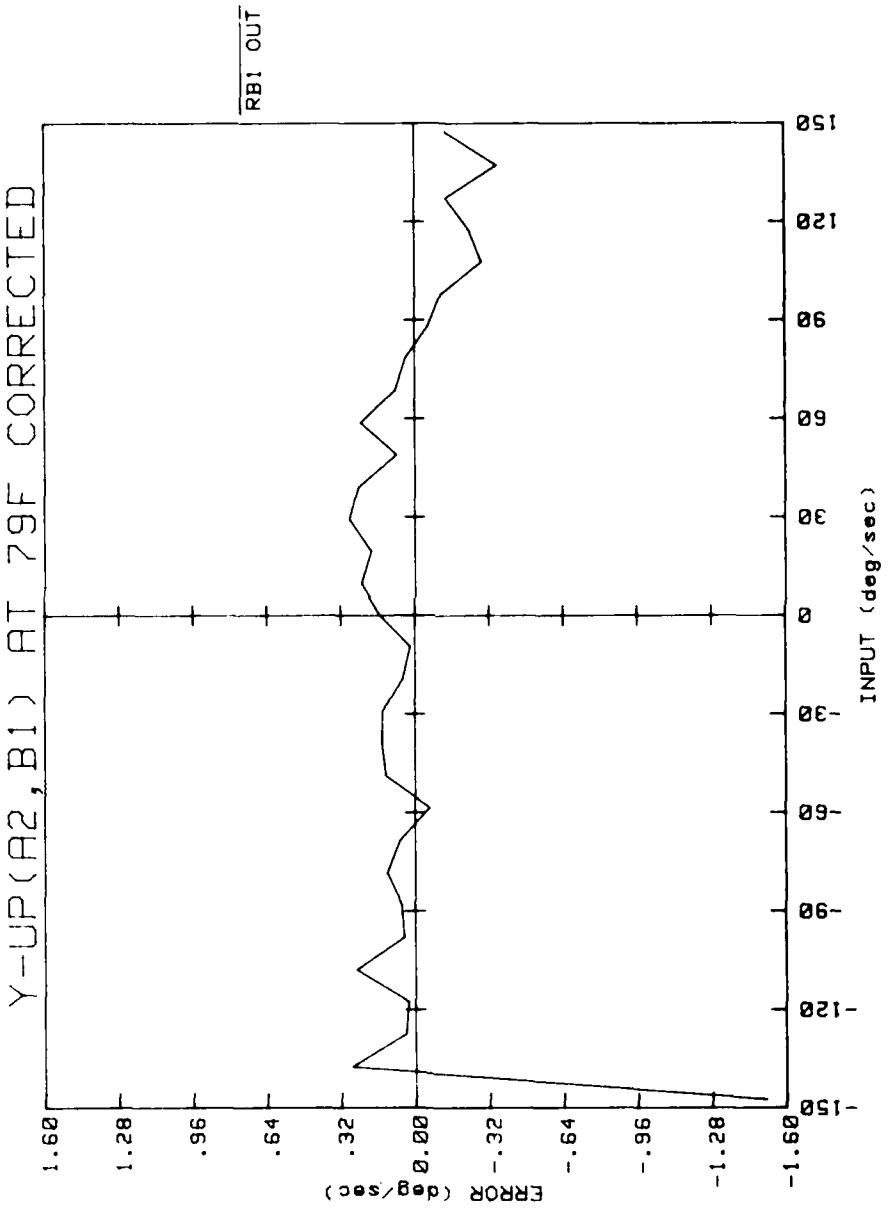

Figure 141. Corrected input-output characteristic for figure 45.

DISTRIBUTION

	Copies
US Army Materiel Analysis Activity ATTN: AMXSY-MP Aberdeen Proving Ground, MD 21005	1
AMSMI-R, Dr. McCorkle	1
Dr. Rhoades	1
-RG, Dr. Yates	1
Mr. Aubrey Rodgers	1
-RGL, Mr. Clayton	40
-RPR	15
-RPT	1

END

FILMED

8-85

DTIC